

AN ABSTRACT OF THE DISSERTATION OF

Yonggang He for the degree of Doctor of Philosophy in Chemistry
presented on January 27, 2005.

Title: Electronic Spectroscopy of Biological Relevant Species and their Complexes with Solvent Molecules.

Redacted for Privacy

Abstract approved: _____
Wei Kong

In this dissertation, I present electronic spectroscopy of a few biologically relevant species and their complexes with solvent molecules in the gas phase using a variety of techniques, including resonantly enhanced multiphoton ionization (REMPI), laser induced fluorescence (LIF), and zero kinetic energy (ZEKE) photoelectron spectroscopy. My work on several methylated uracils and thymines and thymine-water complexes alludes to a new interpretation with regard to the origin of the photostability of our genetic code. I believe that it is the water solvent that stabilizes the photophysical and photochemical behavior of these bases under UV irradiation. For systems that demonstrate vibrational resolution in the first electronically excited state (S_1) and the cationic state, I performed vibrational analysis of both states with the aid of *ab initio* and density functional calculations. These observations are explained in terms of the structural changes from the ground state to S_1 and further to the cation. To bridge results from the gas phase to the solution phase, I also report studies of supersonically cooled water complexes of the three isomers of aminobenzoic acid. Density functional theory calculations

are carried out to identify structural minima of water complexes in the ground state. The solvation mechanism is investigated based on vibrational analysis of the S_1 state of the neutral complex and the shift of ionization thresholds with increasing water content.

Electronic Spectroscopy of Biological Relevant Species
and their Complexes with Solvent Molecules

by
Yonggang He

A DISSERTATION

submitted to

Oregon State University

in partial fulfillment of
the requirements for the
degree of

Doctor of Philosophy

Presented January 27, 2005
Commencement June 2005

Doctor of Philosophy dissertation of Yonggang He presented on January 27, 2005

APPROVED:

Redacted for Privacy

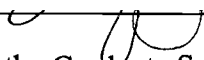


Major Professor, representing Chemistry

Redacted for Privacy

Chair of the Department of Chemistry

Redacted for Privacy



Dean of the Graduate School

I understand that my dissertation will become part of the permanent collection of Oregon State University Libraries. My signature below authorizes release of my dissertation to any reader upon request.

Redacted for Privacy

Yonggang He, Author

TABLE OF CONTENTS

	<u>Page</u>
1. Introduction.....	1
2. Decay pathways of thymine and methyl substituted uracil and thymine in the gas phase.....	7
2.1. Abstract.....	8
2.2. Introduction.....	9
2.3. Experiment.....	9
2.4. Results.....	10
2.5. Discussion.....	14
2.6. Conclusion.....	18
2.7. Acknowledgement.....	18
2.8. References.....	18
3. Photophysics of methyl substituted uracils and thymines and their water complexes in the gas phase.....	21
3.1. Abstract.....	22
3.2. Introduction.....	22
3.3. Experimental details.....	25
3.4. Results.....	26
3.4.1. Bare compounds.....	26
3.4.2. Hydrated clusters.....	37
3.5. Discussion.....	41
3.5.1. Decay mechanism of the pyrimidine bases.....	41
3.5.2. Hydration effect on the photophysics of the excited state.....	44
3.6. Conclusions.....	47
3.7. Acknowledgement.....	48
3.8. References.....	49
4. Resonantly enhanced two photon ionization and ZEKE spectroscopy of jet-cooled 4-aminopyridine.....	51
4.1. Abstract.....	52

TABLE OF CONTENTS (Continued)

	<u>Page</u>
4.2. Introduction.....	53
4.3. Experimental section.....	53
4.4. Results.....	54
4.4.1. Two-color 1+1' REMPI spectrum.....	54
4.4.2. ZEKE spectra.....	58
4.4.2.1. Transitions associated with the inversion mode I.....	60
4.4.2.2. Transitions associated with mode 12.....	62
4.4.2.3. Transitions associated with mode 6a.....	62
4.4.2.4. Transitions associated with mode 1.....	65
4.4.2.5. Other bands and summary of the ZEKE spectra.....	65
4.5. Discussion.....	69
4.6. Conclusion.....	76
4.7. Acknowledgements.....	77
4.8. References.....	77
5. Two-color two-photon REMPI and ZEKE photoelectron spectroscopy of jet-cooled 2-chloropyrimidine.....	79
5.1. Abstract.....	80
5.2. Introduction.....	81
5.3. Experimental setup.....	82
5.4. Results.....	84
5.4.1. REMPI spectrum.....	84
5.4.2. ZEKE spectra.....	88
5.5. Discussion.....	92
5.6. Conclusions.....	95
5.7. Acknowledgements.....	96
5.8. References.....	97

TABLE OF CONTENTS (Continued)

	<u>Page</u>
6. Zero kinetic energy photoelectron spectroscopy (ZEKE) of <i>p</i> -amino benzoic acid (PABA).....	98
6.1. Abstract.....	99
6.2. Introduction.....	100
6.3. Experimental setup.....	101
6.4. Results.....	103
6.4.1. One-color 1+1 REMPI spectrum.....	103
6.4.2. ZEKE spectra.....	106
6.5. Discussion.....	113
6.6. Conclusion.....	118
6.7. Acknowledgements.....	118
6.8. References.....	119
7. Observation of rotamers of <i>m</i> -aminobenzoic acid (MABA): ZEKE and hole-burning REMPI spectroscopy.....	121
7.1. Abstract.....	122
7.2. Introduction.....	123
7.3. Experimental section.....	125
7.4. Results.....	126
7.4.1. Two-color 1+1' REMPI and UV-UV hole-burning spectroscopy....	126
7.4.2. ZEKE spectra.....	131
7.4.2.1. Conformer I.....	132
7.4.2.2. Conformer II.....	138
7.5. Discussion.....	138
7.6. Conclusion.....	144
7.7. Acknowledgements.....	144
7.8. References.....	145
8. Cation vibrational energy levels of 1,3-benzodioxole obtained via zero kinetic energy photoelectron spectroscopy.....	146

TABLE OF CONTENTS (Continued)

	<u>Page</u>
8.1. Abstract.....	147
8.2. Introduction.....	148
8.3. Experimental setup.....	150
8.4. Results.....	151
8.4.1. Two-color 1+1' REMPI spectrum.....	151
8.4.2. ZEKE spectra.....	153
8.5. Discussion.....	157
8.6. Acknowledgement.....	159
8.7. References.....	160
9. Structure of gas phase radical cation of 1,3,6,8-tetraazatricyclo[4.4.1.1 ^{3,8}] dodecane determined from zero kinetic energy photoelectron spectroscopy.....	161
9.1. Abstract.....	162
9.2. Introduction.....	163
9.3. Experiment.....	164
9.4. Discussion.....	169
9.5. Acknowledgement.....	169
9.6. References.....	170
10. A theoretical and experimental study of water complexes of <i>m</i> -aminobenzoic acid MABA·(H ₂ O) _n (<i>n</i> = 1 and 2).....	172
10.1. Abstract.....	173
10.2. Introduction.....	174
10.3. Experimental details.....	176
10.4. Calculations.....	176
10.5. Results.....	177
10.5.1. Theoretical calculations.....	177
10.5.2. Experimental results.....	181
10.6. Discussion.....	189
10.7. Conclusions.....	193

TABLE OF CONTENTS (Continued)

	<u>Page</u>
10.8. Acknowledgement.....	194
10.9. References.....	195
11. Theoretical and experimental studies of water complexes of <i>p</i> - and <i>o</i> -aminobenzoic acid.....	196
11.1. Abstract.....	197
11.2. Introduction.....	198
11.3. Experimental setup and calculation method.....	199
11.4. Results.....	200
11.4.1. Theoretical calculations.....	200
11.4.2. Experimental results.....	206
11.5. Discussion.....	220
11.6. Conclusion.....	222
11.7. Acknowledgements.....	224
11.8. References.....	224
12. Observing microsolvation by adding one water molecule at a time: Electronic spectroscopy of water complexes of <i>p</i> -aminobenzoic acid.....	226
12.1. Abstract.....	227
12.2. Introduction.....	228
12.3. Results.....	229
12.3.1. REMPI spectrum.....	229
12.3.2. Photoionization spectroscopy.....	235
12.4. Discussion.....	238
12.5. References and Notes.....	239
13. Concluding remarks and future work.....	242
13.1. Summary.....	242
13.2. Future Work.....	242
13.3. References.....	243

LIST OF FIGURES

<u>Figure</u>	<u>Page</u>
2.1 Effect of the pump laser at 250 nm with a time advance of 10 ns on the 1+1 REMPI of the probe laser	11
2.2 Pump-probe transient ionization signal of 1,3-DMU in the gas phase with the pump and probe wavelengths at 251 nm and 220 nm respectively.....	13
2.3 Lifetimes of 1-methyl uracil, 1,3-dimethyl uracil, 1,3-dimethyl thymine, and thymine at different excitation wavelengths.....	15
3.1 1+1 REMPI, 1+1' REMPI and UV absorption spectra of 1,3-DMU.....	28
3.2 Effect of the pump laser at 250 nm with a time advance of 10 ns on the one laser REMPI of the probe laser.....	29
3.3 Pump-probe transient ionization signal of 1,3-DMU in the gas phase with the pump and probe wavelengths at 265 and 248 nm, respectively.....	30
3.4 Pump-probe transient ionization signal of 1,3-DMU in the gas phase with the pump and probe wavelengths at 251 and 220 nm, respectively.....	32
3.5 Pump-probe transients of 1,3-DMU in the gas phase at different excitation wavelengths.....	33
3.6 Lifetimes of 1-methyl uracil, 1,3-dimethyl uracil, 1,3-dimethyl thymine, and thymine at different excitation wavelengths.....	35
3.7 Fluorescence signal of 1,3-DMU in the gas phase at different excitation wavelengths.....	36
3.8 One-color REMPI mass spectra of hydrated thymine clusters, obtained at the excitation wavelengths of 229 nm (a) and 268 nm (b) respectively.....	38
3.9 Ratios of ion intensities between the hydrated clusters $T(H_2O)_n$ and bare thymine as a function of the excitation wavelength.....	39
3.10 pump-probe transients of bare thymine and $T(H_2O)_1$ in the gas phase with the pump and probe wavelengths at 267 and 220 nm, respectively.....	40
3.11 Proposed potential energy surfaces and processes for the pyrimidine bases.....	42
4.1 (1+1') REMPI spectrum of jet-cooled 4-AP.....	56

LIST OF FIGURES (Continued)

<u>Figure</u>	<u>Page</u>
4.2 Two-color ZEKE spectra of 4-AP recorded via the following vibrational levels of the S_1 state as intermediate states: (a) 0^0 , (b) I_1^1 , (c) I^2 , (d) $I^1 12^1$	59
4.3 Two-color ZEKE spectra of 4-AP recorded via the following vibrational levels of the S_1 state as intermediate states: (a) 12^1 , (b) $I^1 12^1$, (c) $16a^1 12^1$, (d) $6a^1 12^1$	61
4.4 Two-color ZEKE spectra of 4-AP recorded via the following vibrational levels of the S_1 state as intermediate states: (a) $6a^1$, (b) $6a^2$, (c) $6a^1 1^1$, (d) $6a^1 12^1$	63
4.5 Two-color ZEKE spectra of 4-AP recorded via the following vibrational levels of the S_1 state as intermediate states: (a) 1^1 , (b) $6a^1 1^1$, (c) 1^2	64
4.6 Two-color ZEKE spectra of 4-AP recorded via the intermediate vibrational levels (a) $10b^2$ and (b) $9b^1$ of the S_1 state.....	66
4.7 Resonance structures of 4-AP, 3-AP, 2-AP and aniline in the S_1 state.....	72
5.1 (1+1') REMPI spectrum of jet-cooled 2-CIP.....	83
5.2 Pump-probe transient ionization signal of 2-CIP in the gas phase with the pump and probe wavelengths at 318.5 and 218 nm, respectively.....	87
5.3 Two-color ZEKE spectra of 2-CIP recorded via the following vibrational levels of the S_1 state as intermediate states: (a) 0_0^0 , (b) $6a_0^1$, (c) $7a_0^1$, (d) $6a_0^2$, (e) 1_0^1	89
6.1 (1+1) REMPI spectrum of jet-cooled PABA.....	102
6.2 Normal modes in the S_1 state of PABA corresponding to a) mode A at 185 cm^{-1} , b) mode D at 459 cm^{-1} , and c) mode E at 564 cm^{-1}	105
6.3 Two-color ZEKE spectra of PABA recorded via the following vibrational levels of the S_1 state as intermediate states: (a) 0^0 , (b) A^1 , and (c) D^1	107
6.4 Two-color ZEKE spectra of PABA recorded via the following vibrational levels of the S_1 state as intermediate states: (a) $6b^1$, (b) E^1 , and (c) I^1	111
7.1 Structures of conformers A and B of MABA.....	124

LIST OF FIGURES (Continued)

<u>Figure</u>	<u>Page</u>
7.2 Two-color two-photon REMPI spectrum of jet-cooled MABA (a) and UV-UV hole-burning spectra with the hole-burning laser fixed at the I (30479 cm ⁻¹ , b) and II (30506 cm ⁻¹ , c) positions.....	127
7.3 Displacement vectors of a) mode <i>D</i> at 377 cm ⁻¹ , b) mode <i>E</i> at 486 cm ⁻¹ , and c) mode <i>F</i> at 585 cm ⁻¹ , of the S ₁ state for conformer A.....	129
7.4 Two-color ZEKE spectra of conformer I recorded via the following vibrational levels of the S ₁ state as intermediate states: (a) 0 ⁰ , (b) 6b ¹ , (c) <i>E</i> ¹ , and (d) 6a ¹	133
7.5 Two-color ZEKE spectra of conformer I recorded via the following vibrational levels of the S ₁ state as intermediate states: (a) <i>D</i> ¹ , (b) <i>F</i> ¹ , and (c) 12 ¹	134
7.6 Two-color ZEKE spectra of conformer II recorded via the following vibrational levels of the S ₁ state as intermediate states: (a) 0 ⁰ , (b) <i>E</i> ¹ , and (c) 6a ¹	136
8.1 Structure of BDO.....	149
8.2 Two-color two-photon REMPI spectra of jet-cooled BDO.....	152
8.3 Two-color ZEKE spectra of BDO recorded via the following vibronic transitions of Figure 2: (a) 0, (b) 102, (c) 204, (d) 93, (e) 180, and (f) 54 cm ⁻¹ ...	154
9.1 ZEKE spectra of TTD taken via the $\nu = 0 - 8$ levels of mode 20 (<i>a - i</i>) of the S ₁ state.....	166
9.2 Franck-Condon factors from the S ₁ to the D ₀ state of TTD.....	168
10.1 Structural conformers of MABA.....	175
10.2 Optimized geometries of the 1:1 water complex of the two conformers of MABA at the B3LYP/6-31+G(d) level.....	178
10.3 Optimized geometries of the 1:2 water complex of conformer I of MABA at the B3LYP/6-31+G(d) level.....	179
10.4 Two most stable structures for the 1:2 water complex of conformer II of MABA at the B3LYP/6-31+G(d) level.....	180

LIST OF FIGURES (Continued)

<u>Figure</u>	<u>Page</u>
10.5 Two-color two-photon REMPI spectrum of jet-cooled $\text{MABA} \cdot (\text{H}_2\text{O})_1$ (trace <i>a</i>) and UV-UV hole-burning spectra with the hole-burning laser fixed at the Ia (30365 cm^{-1} , trace <i>b</i>) and IIa (30373 cm^{-1} , trace <i>c</i>) positions.....	182
10.6 Two-color two-photon REMPI spectrum of jet-cooled $\text{MABA} \cdot (\text{H}_2\text{O})_2$ (trace <i>a</i>) and UV-UV hole-burning spectra with the hole-burning laser fixed at the Ia (30414 cm^{-1} , trace <i>b</i>) and IIa (30486 cm^{-1} , trace <i>c</i>) positions.....	186
10.7 REMPI spectra of the 1:1 and 1:2 complexes of MABA.....	188
10.8 Frequency shifts of a few observed normal modes in $\text{MABA} \cdot (\text{H}_2\text{O})_1$ relative to the bare compound. The uncertainty for all the values is 3 cm^{-1}	191
11.1 Optimized geometries of 1:1 water complex of PABA at the B3LYP/6-31+G(d) level.	201
11.2 Optimized geometries of 1:2 water complex of PABA at the B3LYP/6-31+G(d) level.....	202
11.3 Optimized geometries of 1:1 water complex of OABA at the B3LYP/6-31+G(d) level.....	204
11.4 Two most stable geometries of the 1:2 water complex of OABA at the B3LYP/6-31+G(d) level.....	205
11.5 (1+1) REMPI spectrum of jet-cooled $\text{PABA}(\text{H}_2\text{O})_n$ ($n = 0 - 2$) plotted with respect to the origin of the $S_1 \leftarrow S_0$ transition of bare PABA at 34185 cm^{-1}	207
11.6 Frequency shifts of a few observed normal modes in $\text{PABA}(\text{H}_2\text{O})_n$ ($n = 1$ and 2) relative to the bare compound.....	210
11.7 Two-color PIE spectra of jet-cooled $\text{PABA}(\text{H}_2\text{O})_n$ ($n = 0 - 2$).....	211
11.8 (1+1') REMPI spectrum of jet-cooled $\text{OABA}(\text{H}_2\text{O})_n$ ($n = 0 - 2$) plotted with respect to the origin of the $S_1 \leftarrow S_0$ transition of bare OABA at 28594 cm^{-1}	213
11.9 Frequency shifts of a few observed normal modes in $\text{OABA}(\text{H}_2\text{O})_n$ ($n = 1$ and 2) relative to the bare compound.....	218
11.10 Two-color PIE spectra of jet-cooled $\text{OABA}(\text{H}_2\text{O})_n$ ($n = 0 - 2$).....	219
12.1 REMPI spectra of PABA•water complexes.....	230

LIST OF FIGURES (Continued)

<u>Figure</u>	<u>Page</u>
12.2 Frequency shifts of a few observed normal modes in PABA(H ₂ O) _n (<i>n</i> = 1 and 2) complexes.....	231
12.3 The most stable structures of PABA(H ₂ O) _n (<i>n</i> = 1 - 6) complexes obtained from our density functional calculation at the B3LYP/6-31g* level.....	233
12.4 Time-of-flight mass spectra of PABA(H ₂ O) _n (<i>n</i> = 0 - 40) at six different excitation wavelengths.....	236
12.5 Ionization thresholds of PABA•water complexes.....	237
13.1 1+1 REMPI spectrum of laser-desorbed and jet-cooled guanine.....	244
13.2 1+1 REMPI spectrum of laser-desorbed and jet-cooled PABA near the origin of the S ₁ state.....	245

LIST OF TABLES

<u>Table</u>	<u>Page</u>
4.1 Observed vibrational frequencies and assignments for the S_1 state of 4-AP.....	57
4.2 Observed vibrational frequencies and assignments in the ZEKE spectra of 4-AP.....	67
4.3 Energy levels of the inversion mode for the S_0 , S_1 and D_0 states.....	70
4.4 Average values of the observed fundamental and higher harmonics of the cation.....	71
4.5 Molecular geometry parameters of 4-AP in the S_0 , S_1 , and D_0 states.....	74
4.6 Measured electronic transitions and adiabatic ionization potentials of aniline, 2-AP, 3-AP, and 4-AP.....	75
5.1 Observed vibrational frequencies and assignments for the S_1 state of 2-CIP.....	85
5.2 Observed vibrational frequencies and assignments in the ZEKE spectra of 2-CIP.....	90
5.3 Molecular geometry parameters of 2-CIP in the S_0 , S_1 , and D_0 states.....	91
5.4 Observed vibrational frequencies of 2-CIP and pyrimidine in the S_1 and the D_0 states.....	93
6.1 Observed vibrational frequencies and assignments for the S_1 state of PABA.....	104
6.2 Observed vibrational frequencies and assignments in the ZEKE spectra of PABA.....	108
6.3 Molecular geometry parameters of PABA in the S_0 , S_1 , and D_0 states.....	114
6.4 Mulliken charge distributions of PABA in the S_0 , S_1 , and D_0 states.....	115
7.1 Observed vibrational frequencies and assignments for the S_1 state of MABA.....	130
7.2 Observed vibrational frequencies and assignments in the ZEKE spectra of MABA (conformer I).....	135
7.3 Observed vibrational frequencies and assignments in the ZEKE spectra of MABA (conformer II).....	137
7.4 Molecular geometry parameters of MABA in the S_0 , S_1 , and D_0 states.....	140
7.5 Mulliken charge distributions of MABA in the S_0 , S_1 , and D_0 states.....	141

LIST OF TABLES (Continued)

<u>Table</u>	<u>Page</u>
8.1 Observed vibrational frequencies and assignments in the ZEKE spectra of BDO.....	155
8.2 Molecular geometry parameters of BDO in the ground state of the neutral molecule (S_0) and the cation (D_0).....	156
9.1 Observed vibrational levels of mode 20 of TTD^{*+} (cm^{-1}).....	167
10.1 Observed vibrational frequencies and assignments for the S_1 state of the 1:1 water complex of MABA.....	183
10.2 Observed vibrational frequencies and assignments for the S_1 state of the 1:2 water complex of MABA.....	187
11.1 Observed vibrational frequencies and assignments for the S_1 state of $PABA(H_2O)_{0-2}$	208
11.2 Observed vibrational frequencies and assignments for the S_1 state of $OABA(H_2O)_{0-2}$	215
11.3 Calculated hydrogen bond lengths in the 1:1 complex of PABA and OABA upon electronic excitation.....	221

1. Introduction

The overall objective of my research project is to study photochemistry and photophysics of biologically relevant species. The approach includes linear and nonlinear ultraviolet (UV) spectroscopy of supersonically cooled gas phase species. Two different scenarios are encountered during this course of study. For molecules that are unstable in the upper excited state and the ground cationic state, we use a variety of pump-probe techniques to investigate the decay mechanisms after photoexcitation. A case study that will be discussed in this thesis is methylated pyrimidine bases. For molecules that are stable in the upper states, we use high resolution spectroscopic techniques to study their vibrational signatures of both the neutral excited states and ground ionic species. Several molecular systems will be presented in this thesis, such as substituted aromatic systems including 4-aminopyridine (4-AP), 2-chloropyrimidine (2-ClP), two isomers of amino benzoic acids; a cage-adamanzane named 1,3,6,8-tetraazatricyclo[4.4.1.1^{3,8}] dodecane (TTD); and an indan-like benzene-fused ring 1,3-benzodioxole (BDO). The spectroscopic techniques used in this type of studies include resonantly enhanced multiphoton ionization (REMPI), laser induced fluorescence (LIF), and zero kinetic energy (ZEKE) photoelectron spectroscopy. In addition, to bridge our observation from the gas phase to the solution phase, we have also succeeded in generating water complexes of several solute molecules. The results on the microsolvation mechanism of substituted aromatic molecules obtained using gas phase spectroscopic techniques will also be presented.

The first two manuscripts (Chapter 2 and 3) relate to the photophysics of methyl-substituted uracils and thymines and their water complexes in the gas phase. This study of the nucleic acid bases bears direct relevance to carcinogenic mutations of DNA under UV irradiation. Prior to our work, a general perception based on efforts from both the gas phase and the solution phase was that the fast internal population conversion between the first excited state (S_1) and the ground state (S_0) was an intrinsic property of the bases.¹⁻⁹ This property was suggested to be the reason for the adoption of these bases as

the building blocks of the genetic code during the early stages of life's evolution.⁸ Results from our two different REMPI experiments, however, provided strong evidence that the decay pathways of bare molecules were quite different from those in solutions: bare molecules from the excited state were largely funneled into and trapped in a dark state via fast internal conversion. Lifetimes of this dark state were determined to be tens to hundreds of nanoseconds, depending on the internal energy and the degree of methyl substitution. In addition, our investigation on the water complexes of thymine showed that the lifetime of the dark state decreased gradually as the bases became more hydrated. We thus further proposed that it was the environment that modified the decay pathway in the solution phase and quenched the dark state. Our work thus revealed that the photostability was not an intrinsic property of the pyrimidine bases. Rather, it was the solution environment that stabilized the photophysical and photochemical behavior of the bases under UV irradiation.

Chapters 4 to 9 present our high resolution studies of a few non-volatile biologically relevant species. Our goal is to understand the geometric and electronic structural change upon photoexcitation and ionization. Chapters 4 and 5 present results of 4-AP and 2-ClP, both containing an electron rich group. Our work reveals that substitution with an electron rich group reduces the electron deficiency of the ring through increased conjugation between the ring and the substitute. The integrity of the molecular frame is therefore largely intact even after photoionization. In this sense, the electron rich group acts as an electron donating group in the cationic state. In the ZEKE spectrum, the rigidity of the ring structure during ionization manifests as a propensity of maintaining the vibrational excitation of the intermediate state. As a result, the normal coordinates of the S_1 and the ground cationic state (D_0) states are essentially identical. In contrast, previous studies have shown that without the availability of an electron rich group in the side chain, excitation and ionization create a substantial change in the molecular frame, which further induces rich vibronic activities in the ZEKE spectrum.¹⁰⁻¹²

Chapters 6 and 7 extend this investigation to molecules with both an electron withdrawing and an electron donating group in the side chain of the aromatic ring. Our

goal is to observe the “push” or “pull” effect of each substituent on the charge distribution. Consistent with our previous conclusion on mono-substituted aromatic systems, in *p*-amino benzoic acid (PABA, Chapter 6), *m*-amino benzoic acid (MABA, Chapter 7), and *o*-amino benzoic acid (OABA, not presented in this thesis), the rigidity of the ring structure was also maintained upon electronic excitation and ionization. The distance between the two substituents, on the other hand, affects the relative contribution of electron back donation. On the basis of the changes in geometry and charge distribution upon electronic excitation and ionization, we deduce that in the S_1 and D_0 states, the *ortho* and the *meta* compounds are similar in terms of electron back donation, while they are considerably different from the *para* compound. This conclusion is different from the general belief in organic chemistry, which typically concerns the similarity between the *ortho* and the *para* isomers in the ground state.¹³

The study presented in chapter 8 stems from a controversy over the assignment of the vibrational structure of 1,3-benzodioxole (BDO).¹⁴⁻¹⁷ Although we make no formal attempt to resolve the issue with regard to the vibrational energy levels of the S_1 state, as will become clear from our results, we provide evidence that the cationic state is planar and therefore has no tunneling splitting, unlike the puckered ground state and the neutral electronically excited state. Assignment of the vibrational levels of the cation is therefore independent of the identity of the intermediate level. Moreover, from the ZEKE spectra obtained via different vibrational levels of the S_1 state, we can derive some inspiration with regard to the assignment of the REMPI spectrum and thereby the vibrational levels of the S_1 state.

Chapter 9 attempts to resolve a debate on the symmetry of the cation of a cage molecule TTD. Nelsen and Buschek first alluded to the potential effect of solvent on the location of the charge, either localized on one of the NCH_2CH_2N bridges with a C_{2v} symmetry, or totally delocalized throughout the whole molecular frame with a D_{2d} symmetry.^{18,19} With more advanced technology including Electron-Nuclear Double Resonance (ENDOR) spectroscopy and a variety of deuterated compounds, the most recent work by Zwier, *et al.* concluded that there was a single energy minimum with D_{2d}

symmetry.²⁰ However, the ENDOR experiment was performed in the solution phase in the presence of strong oxidizing agents. Moreover, the limited time resolution of the ENDOR experiment can only provide a time-averaged “effective” symmetry. In this work, we report gas phase studies of TTD⁺⁺ using two-color two-photon zero kinetic energy (ZEKE) photoelectron spectroscopy. From the distribution of active vibrational modes and comparisons between the experiment and theoretical simulation, we offer direct proof that the D_0 state do have the same D_{2d} symmetry as the S_1 state.

Chapters 10, 11 and 12 are related to the study of water complexes of aminobenzoic acids. Our ultimate goal is to bridge our observation from the gas phase to the solution phase by looking at the change in physical and chemical properties of the solute as a function of the number of solvent molecules. Aminobenzoic acids are multifunctional hydrogen bonding molecules. In protic solvents, they can act both as H acceptors at the O atom of the $-C=O$ group and the N atom of the $-NH_2$ group, and as H donors at the $-OH$ group and the $-NH_2$ group. They can also form hydrogen bonds through their aromatic π electrons. The existence of multiple hydrogen bonding sites makes these molecules ideal models for studying the interaction between water and aromatic chromophors. In chapter 10, we present our investigation on the structural and spectroscopic properties of $MABA \cdot (H_2O)_n$ complexes with $n = 1$ and 2. We have also performed quantum mechanical calculations to obtain structures and binding energies for a few possible isomers in the ground state, and vibrational frequencies of these species in the first electronically excited state. Chapter 11 extends our study to water complexes of the other two isomers of aminobenzoic acid. Assisted by quantum mechanical calculations, we present detailed vibrational assignment of the REMPI spectra of $PABA(H_2O)_n$ and $OABA(H_2O)_n$ complexes with n from 0 to 2. Chapter 12 further extends this study to $PABA(H_2O)_n$ complexes containing up to 40 water molecules. This systematic study alludes to a microsolvation process of PABA. The shifts in the observed vibrational frequencies of the S_1 state for complexes with $n = 1$ and 2 provide the evidence that solvation in water begins with the carboxylic group. The similarity among all the REMPI spectra with $n \leq 6$ further suggests that addition of more water molecules simply expands the water cluster within the complex, without a major modification of the PABA

molecular frame. The smooth drop in the ionization threshold with increasing solvent molecules demonstrates that closure of the solvation shell is unidirectional. When there are more than twenty solvent molecules in the vicinity, the ionization threshold of the complexes approaches the value of the corresponding liquid solution.

Reference

1. Daniels, M.; Hauswirth, W. *Science* 1971, 171, 675.
2. Callis, P. R. *Annu. Rev. Phys. Chem.* 1983, 34, 329.
3. Nikogosyan, D. N.; Angelov, D.; Soep, B.; Lindqvist, L. *Chem. Phys. Lett.* 1996, 252, 322.
4. Häupl, T.; Windolph, C.; Jochum, T.; Brede, O.; Hermann, R. *Chem. Phys. Lett.* 1997, 280, 520.
5. Reuther, A.; Nikogosyan, D. N.; Laenen, R.; Laubereau, A. *J. Phys. Chem.* 1996, 100, 5570.
6. Reuther, A.; Iglev, H.; Laenen, R.; Laubereau, A. *Chem. Phys. Lett.* 2000, 325, 360.
7. Pecourt, J.-M. L.; Peon, J.; Kohler, B. *J. Am. Chem. Soc.* 2000, 122, 9348.
8. Pecourt, J.-M. L.; Peon, J.; Kohler, B. *J. Am. Chem. Soc.* 2001, 123, 10370.
9. Gustavsson, T.; Sharonov, A.; Markovitsi, D. *Chem. Phys. Lett.* 2002, 351, 195.
10. S.-I. Sato, K. Omiya, K. Kimura, *J. Electron Spectrosc.* 1998, 97, 121.
11. X. Zhang, J. M. Smith, J. L. Knee, *J. Chem. Phys.* 1992, 97, 2843.
12. X. Song, M. Yang, E. R. Davidson, J. P. Reilly, *J. Chem. Phys.* 1993, 99, 3224.
13. A. Streitwieser, Jr., C.H. Heathcock, *Introduction to Organic Chemistry* (3rd edition), Macmillan Publishing Company, New York, 1989.
14. A.C.P. Alves, J.M. Hollas, B.R. Midmore, *J. Mol. Spectrosc.* 1979, 77, 124.
15. K.H. Hassan, J.M. Hollas, *Chem. Phys. Lett.* 1989, 157, 183.
16. J. Laane, E. Bondoc, S. Sakurai, K. Morris, N. Meinander, J. Choo, *J. Am. Chem. Soc.* 2000, 122, 2628.

17. G. Pietraperzia, A. Zoppi, M. Becucci, E. Droghetti, E. Castellucci, *Chem. Phys. Lett.* 2004, 385, 304.
18. Nelsen, S. F.; Buschek, J. M. *J. Am. Chem. Soc.* 1974, 96, 6424.
19. Nelsen, S. F.; Haselbach, E.; Gschwind, R.; Klemm, U.; Lanyova, S. *J. Am. Chem. Soc.* 1978, 100, 4367.
20. Zwier, J. M.; Brouwer, A. M.; Keszthelyi, T.; Balakrishnan, G.; Offersgaard, J. F.; Wilbrandt, R.; Barbosa, F.; Buser, U.; Amaudrut, J.; Gescheidt, G.; Nelsen, S. F.; Little, C. D. *J. Am. Chem. Soc.* 2002, 124, 159.

Decay pathways of thymine and methyl substituted uracil and thymine in the
gas phase

*Yonggang He, Chengyin Wu, and Wei Kong**

Department of Chemistry, Oregon State University, Corvallis, Oregon 97331-4003.

Journal of Physical Chemistry, A
PO Box 3337, Columbus, OH, 43210, USA
2004, 107, 5145-5148

* To whom correspondence should be addressed.
E-mail: kongw@chem.orst.edu. Phone: 541-737-6714. Fax: 541-737-2062.

2. Decay pathways of thymine and methyl substituted uracil and thymine in the gas phase

2.1. Abstract

We report observations of a dark state in the decay pathways of thymine, 1,3-dimethyl thymine, 1,3-dimethyl uracil, and 1-methyl uracil in the gas phase. After initial excitation by a nanosecond laser, the excited molecules failed to return to the ground state, but rather, were trapped in a dark state for tens to hundreds of nanoseconds. This result contradicts those reported in water solutions. We therefore propose that the photochemistry of these pyrimidine bases is different in the gas phase from that in the liquid phase, and that the dark state is effectively quenched in water solutions. Although we do not have a quantitative measure of the yield of this dark state, the fact that further ionization from this dark state has a high yield in the deep UV makes this pathway important in the chemistry of nucleic acid bases. The photostability of our genetic code could then be a result of the water solvent rather than an inherent property of the bases themselves.

2.2. Introduction

One of the important risk factors to living organisms is ultraviolet (UV) induced carcinogenesis from sunlight; the two major cellular targets are DNA and RNA because of their strong absorption in the 200-300 nm range.¹ Fortunately, stratospheric ozone and our own self defense and enzymatic repair systems offer the necessary protection. However, ozone depletion caused by the buildup of man-made chemicals in the atmosphere has led to increased UV radiation at the earth's surface and consequently a rising rate of skin cancer.² In general, two photo-induced processes are believed to trigger lethal mutagenesis and carcinogenesis: one is photoionization of the bases via the absorption of two photons and the other is formation of cyclobutane dimers between adjacent pyrimidine bases via a long lived intermediate state.^{3,4} Over the past two decades, efforts have been made in the study of the relaxation dynamics of excited-state nucleic acid bases. The lifetimes of the first electric dipole allowed state (S_1) have been observed to be generally short (around 1 ps), and fast decay to the ground state via internal conversion (IC) has been proposed.⁵⁻¹³ However, this decay mechanism is far from certain, and other possibilities have also been suggested.¹⁴⁻¹⁶ In this paper, we present evidence of an alternative decay path for isolated species in the gas phase. We observed a dark state in methyl substituted uracil and thymine bases with lifetimes of 23-209 ns, depending on the excess energy and methyl substitution. Enhanced ion yield in the deep UV region centered at 220 nm from molecules in this dark state manifests the significance of this channel in the photostability of these nucleic acid bases.

2.3. Experiment

Three types of measurements were carried out in this study. In the 1+1' resonantly enhanced multiphoton ionization (REMPI) experiment, a Nd:YAG pumped dye laser was used to pump the molecules to the S_1 state, while a Nd:YAG pumped OPO laser was used to probe the excited species. Without the pump laser, the probe laser alone generated a 1+1 REMPI signal, and the net 1+1' REMPI spectrum was obtained by removing the one-laser signal from the two-laser signal. Lifetime measurements were performed by varying the delay of the probe laser relative to the pump laser. In the time-resolved fluorescence measurement, the signal was detected by a photomultiplier tube through two

collection lenses. The wavelength region of the fluorescence signal was determined using long pass filters. Great care was taken to avoid any saturation effect in the 1+1' experiment and the fluorescence experiment by recording a linear power dependence of the ion and fluorescence signal on the energy of the pump and probe laser. In the case of the one laser 1+1 REMPI experiment, a second order power dependence was indeed observed. The samples 1,3-dimethyl uracil (DMU), 1-methyl uracil, and thymine were purchased from Aldrich Co. and used without further purification. 1,3-dimethyl thymine (DMT) was synthesized from thymine,¹⁷ and its purity was checked by nuclear magnetic resonance (NMR) and infrared absorption (IR) spectra. The powder sample was heated directly inside the pulsed valve to temperatures ranging from 120°C (DMU) to 240°C (thymine) and was supersonically expanded into the interaction region. Limited by the performance of our pulsed valve, we were unsuccessful in conducting the same measurement on uracil, but the resemblance of 1-methyl uracil and uridine, and the consistency of our results for all four compounds, including thymine and 1,3-dimethyl thymine, should make our results directly relevant to the photochemistry of DNA.

2.4. Results

Figure 1 compares the intensity of the ion signal in the net 1+1' experiment and the 1+1 experiment. Neither spectrum was normalized by the intensity of the scanning laser, rather, they were smoothed to eliminate structures caused by the fluctuating laser power. The energy of the scanning OPO laser decreased at the blue edge of the spectrum, and this resulted in the missing S_2 state in the 1+1 experiment. The rise in the 1+1' spectrum in the same energy region, on the other hand, emphasizes the dramatic increase in the total ion signal when the probe laser was in the deep UV. The only difference between the two experiments was an advanced pump beam at 250 nm in the 1+1' experiment, and the advance time was 10 ns. When the probe laser was at a wavelength between 245 and 280 nm, the early arrival of the pump laser caused a depletion of the ion signal from the probe laser alone, but when the probe laser scanned between 217 and 245 nm, a several fold increase in the overall ion signal was observed. The maximum depletion observed under the same intensity for the probe laser was 25% of the 1+1 laser signal.

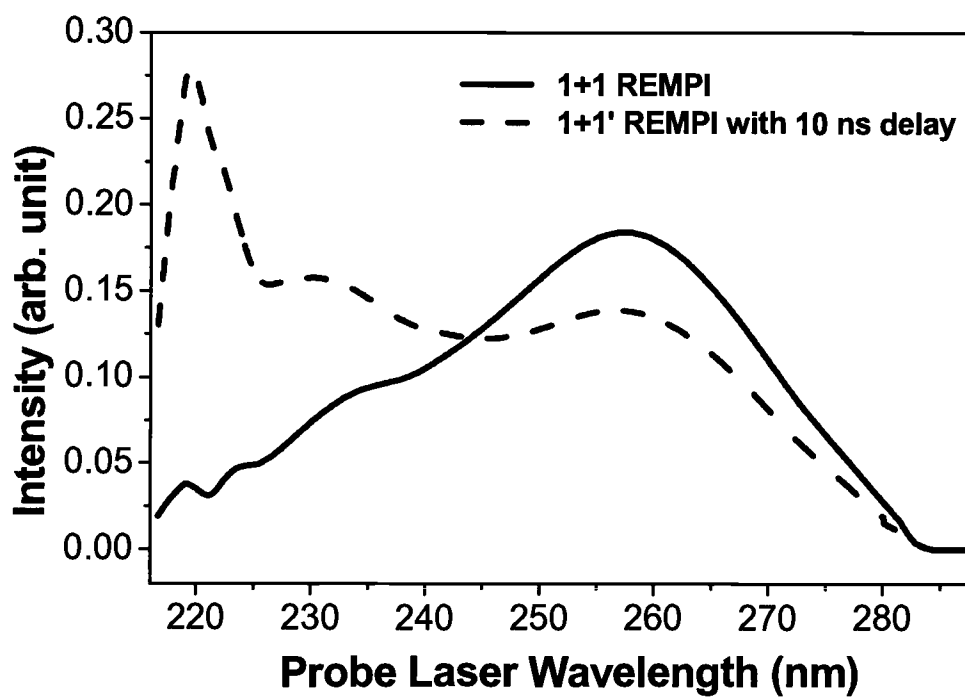


Figure 1. Effect of the pump laser at 250 nm with a time advance of 10 ns on the 1+1 REMPI of the probe laser. The spectra were recorded using the same intensity for the probe laser, and the maximum depletion was 20 – 25% across the region between 245 and 280 nm

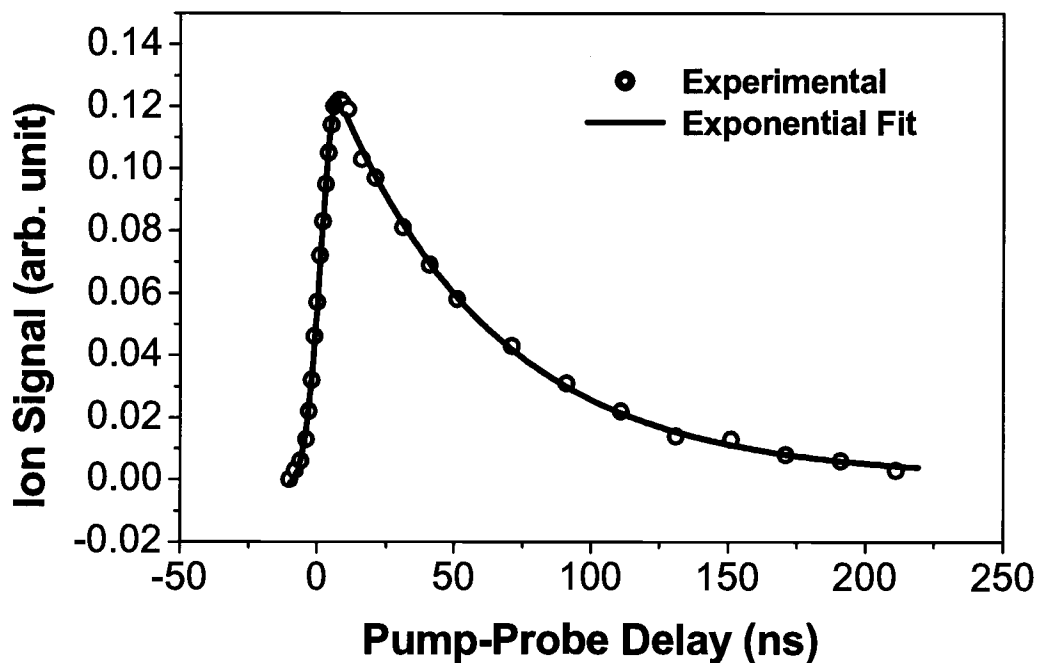


Figure 2. Pump-probe transient ionization signal of 1,3-DMU in the gas phase with the pump and probe wavelengths at 251 nm and 220 nm respectively. The exponential decay constant was determined to be 56 ns. abbreviations in the caption agree with those in the figure itself and in the text and that the figure is already sized appropriately.

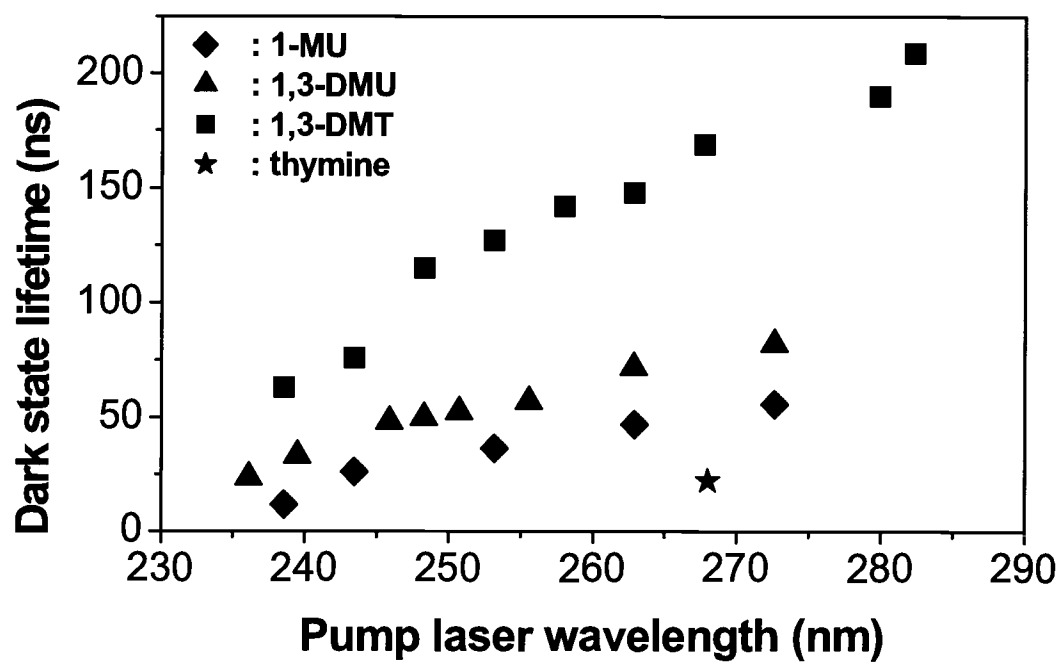


Figure 3. Lifetimes of 1-methyl uracil, 1,3-dimethyl uracil, 1,3-dimethyl thymine, and thymine at different excitation wavelengths.

Figure 2 shows the pump-probe transient of 1,3-DMU with the probe wavelength at 220 nm. A single exponential decay function convoluted with a Gaussian function representing the response of the laser system was used to fit the decay constant. The fitting errors were limited by the time resolution of our laser system to 5 ns. The resulting decay time is dependent on the degree of methyl substitution and the excitation wavelength. The general trend is that the lower the excitation energy and the more substituted the ring, the slower the decay process.

To further assess the fate of the molecules in the excited state, we attempted to observe the fluorescence signal, but the signal strength was so low that a quantitative measurement of the fluorescence spectrum was impossible with our existing setup. Qualitatively, the fluorescence lifetime agreed with the decay rate of the REMPI signal, ranging from 18 ns when pumped at 236 nm to 54 ns when pumped at 260 nm for DMU. Using long pass filters, we determined that the peak of the radiation was centered between 370 and 440 nm. In contrast, the fluorescence peak of the S_1 state was measured to be around 300 nm,¹⁸ significantly different from this result.

2.5. Discussion

Based on these observations, we propose that after initial excitation to the S_1 state, a significant fraction of the gas phase molecules decay to a dark state with lifetimes of tens to hundreds of nanoseconds. This dark state does not absorb in the range of 245 – 280 nm, but instead, in a much higher energy region from 217 – 240 nm. In the REMPI experiment of Figure 1, this absence of absorption causes the depletion of the two laser signal when the probe wavelength is between 245 and 280 nm. When the probe laser scans into the absorption region of this dark state, an enhanced ion yield is observable. The decay process in Figure 2 corresponds to the decay of this dark state, and the fluorescence of this state is centered between 370 and 440 nm. Methyl substitution seems to stabilize this dark state, while more vibrational energy obtained from the initial excitation step destabilizes this state by opening more decay channels.

In Figure 2, the time scale of the decay suggests that the probe beam is not sensing the decay of the highly vibrationally excited states populated from fast IC_0 and intramolecular vibrational redistribution (IVR) in the dark state.¹⁹ Rather, it should be

representative of a different electronic state than S_0 and S_1 . It is worth noting that in this gas phase experiment, molecules in the reaction region can be regarded as collision free and immobile within the time frame of several hundred nanoseconds. Moreover, with our nanosecond laser systems, we are insensitive to the fast initial steps involving IC_0 and IVR. Therefore, the decay constants in Figure 2 cannot be attributed to the loss of population from S_1 , which is known to be several picoseconds.¹³ Instead, we should be sensitive to processes after the completion of population redistribution. The decay of the “rediscovered” molecules when the probe beam was between 217 and 240 nm is on a time scale of tens to hundreds of nanoseconds. These constants are much smaller than those from the decay of hot vibrational levels after IVR under collision free conditions.¹⁹ Thus Figure 2 should be regarded as characteristic of the dark state, rather than that of vibrationally excited ground state species in the molecular beam.

Perhaps the most convincing evidence for the existence of the dark state is the similar decay constants of the ion signal and the fluorescence signal. Although qualitative, the matching of the two decay constants identifies both channels as having the same origin. The possibility for such a fluorescing state to be a manifold of a vibrationally excited ground state populated from IC_0 and IVR is highly unlikely.

At first glance, our gas phase results contradict those from the liquid phase. Kohler’s group observed red shifted absorption of the nucleoside in water solutions after excitation to the S_1 state.¹⁰ This spectroscopic shift was regarded as an indication of internal conversion to the ground state (denoted as IC_0 in the following), and the absorption was due to the hot bands generated from the IC_0 and IVR. In the gas phase, we failed to observe such an effect, and there was no enhanced ion signal at the red edge of the absorption band. Instead, Figure 1 shows a more or less uniform depletion of the ion signal due to the pump beam across the region between 245 and 280 nm. We attribute this difference to the effect of water solvent on the lifetime of the dark state, and our future report will detail this issue.²⁰

A quantitative assessment of the yield of the dark state is impossible without knowledge of the absorption cross section, but an estimate can be obtained from Figure 1. The depletion between 245 and 280 nm should be a result of population loss from the ground state. If we eliminate the possibility of IC_0 , and we have neither experimental nor

theoretical evidence with regard to dissociation from the S_1 state, the only contributing factor is therefore trapping of the dark state. Assuming an excitation probability of 100% by the pump beam at 250 nm (an over estimate!), a depletion of 20% represents a lower limit for the yield of the dark state. Unfortunately, we were unable to probe the S_1 state and the dark state under saturation conditions, so the enhancement factor at 220 nm cannot be used for a similar estimate.

These states are readily coupled to the $1\pi\pi^*$ state by out-of-plane vibrational modes via conical intersections (CI). This type of fast state switch has been invoked to explain the extremely low quantum yield of fluorescence from the $1\pi\pi^*$ state. Based on our assessment of the low fluorescence quantum yield of this $1\pi\pi^*$ state, however, we further propose that there exists a weak conical intersection between this $1\pi\pi^*$ state and the ground state, and an energy barrier on the $1\pi\pi^*$ surface that hinders effective population relaxation. The fact that the lifetime of the dark state dropped continuously with increasing pump photon energy offers supporting evidence. A recent calculation by Sobolewski et al. showed that conical intersections between the $1\pi\pi^*$ state and nearby $1\sigma\pi^*$ states in aromatic biomolecular systems are ubiquitous.¹⁶ However, the authors stressed that this intersection relies on the polarizability of the NH or OH bond. It is therefore unclear to us whether the same mechanism would be applicable to N-methyl substituted compounds. The multiplicity of the dark state is certainly a point of debate, although we tentatively believe that a triplet state is unlikely because the lifetime of a triplet state in pyrimidine bases has been measured to be on the order of millisecond to second in the condensed phase.²²⁻²⁴ Moreover, our recent work on water complexes of thymine demonstrates strong quenching effect on the lifetime of the dark state with the addition of just one or two water molecules.²⁰ Such a strong effect is unexpected if the involved state is triplet in nature. Although a triplet state for the corresponding nucleosides in solutions is known to be within the same energy region as this dark state,²⁵ a few theoretical calculations also reported simultaneous existence of a singlet state.²⁶⁻²⁸

The decay mechanism proposed above is consistent with several literature reports.^{13, 28} The work on cytosine in the gas phase by De Vries' group also reported a long lived dark state,²⁸ with a lifetime of nearly 300 ns. Based on the scale of the lifetime, however, the authors suspected the involvement of a triplet state. Kang et al. measured the lifetime of

the S_1 state of all purine and pyrimidine bases in the gas phase using femtosecond pump-probe ionization.¹³ The authors observed fast disappearance of the S_1 state within a few picoseconds, but the wavelength of their probe laser at 800 nm was mostly insensitive to the dark state we observed: a three photon process corresponds to ionization at 267 nm, while a four photon process corresponds to 200 nm. In both cases, the ionization cross section was unfavorable for the dark state as seen from Figure 1. Interestingly, the authors reported two decay components in the case of thymine. The longer one with an estimated lifetime of more than 100 ps was suggested to be from a triplet state based on energetic analysis. However, knowing that the $1n\pi^*$ state in thymine falls in the same energy region as its triplet state,²⁶⁻²⁸ the identity of this component should be considered uncertain. The lifetime measurement of more than 100 ps could simply be a reflection of the time limit in such a femtosecond laser experiment.

Theoretical studies also support our proposal.³⁰ A recent investigation on cytosine showed the existence of a state switch between $\pi\pi^*$ and $n_O\pi^*$ (the lone pair electron on the oxygen atom) states.³⁰ The crossing between the two states is weakly avoided and there exists a small energy barrier between the equilibrium position of the $1n_O\pi^*$ state and its intersection with the ground state. This barrier might be the very reason that the majority of the molecules were trapped in the dark state after the $^1\pi\pi^* \rightarrow ^1n\pi^*$ internal conversion. More detailed calculations of the decay process from the $1n_O\pi^*$ state to the ground state will be revealing, as suggested by the authors.

This revelation on the pyrimidine bases parallels that of the purine bases.^{10, 13, 31} In water solutions, purine bases were also determined to exhibit fast internal conversion to the ground state with similar time constants as the pyrimidine bases.¹⁰ In the gas phase, Kang et al. did not observe any evidence of a long lived dark state.¹³ However, Chin et al. attributed the featureless red shifted fluorescence of four guanine tautomers with lifetimes of tens of nanoseconds to a $n\pi^*$ state.³¹ Although the authors cautiously pointed out the lack of direct proof for this claim, previous calculations did reveal such a state for all the purines.³²

2.6. Conclusion

In summary, we present here evidence for a new decay mechanism of uracil and thymine bases in the gas phase. Our results differ from those of the liquid phase, where fast internal conversion to the ground state dominates the decay path. Instead, the excited-state molecules are funneled into and trapped in a dark state with a lifetime of tens to hundreds of nanoseconds. Ionization from this dark state by deep UV radiation has a substantially high yield, making this channel dangerous in life's early evolution on earth. The very existence of this dark state in isolated molecules further suggests that the photostability of our genetic code may not be an inherent property of the bases themselves. Rather, it could be the water solvent that effectively quenches the potentially harmful photochemistry of the dark state. A future report on water complexes of these bases and more extended systems is under preparation.

2.7. Acknowledgement

This work was supported by the National Science Foundation, the Petroleum Research Foundation, and the Alfred P. Sloan Foundation. The authors are grateful for discussions with Professor Bern Kohler from Ohio State University and Professor Charlie Parmenter from Indiana University. The skillful synthesis of 1,3-DMT by T. Suyama is deeply appreciated..

2.8. REFERENCES

- (1) Craighead, J. E. Pathology of environmental and occupational disease, Mosby-Year book, Inc., 1995.
- (2) McKenzie, R.; Connor, B.; Bodeker, G. *Science* 1999, 285, 1709-1711.
- (3) Becker, D.; Sevilla, M. D. In *Advances in Radiation Biology* Vol. 17; Lett, J. T., Adler, H., Eds.; Academic Press: New York, 1993; pp. 121-180.
- (4) Brash, D. E. *Photochem. Photobiol.*, 1988, 48, 59-66.
- (5) Daniels, M.; Hauswirth, W. *Science* 1971, 171, 675-677.
- (6) Callis, P. R. *Annu. Rev. Phys. Chem.* 1983, 34, 329-357.

- (7) Nikogosyan, D. N.; Angelov, D.; Soep, B.; Lindqvist, L. *Chem. Phys. Lett.* 1996, 252, 322-326.
- (8) Reuther, A.; Iglev, H.; Laenen, R.; Laubereau, A. *Chem. Phys. Lett.* 2000, 325, 360-368.
- (9) Pecourt, J.-M. L.; Peon, J.; Kohler, B. *J. Am. Chem. Soc.* 2000, 122, 9348- 9349.
- (10) Pecourt, J.-M. L.; Peon, J.; Kohler, B. *J. Am. Chem. Soc.* 2001, 123, 10370-10378.
- (11) Peon, J.; Zewail, A. H. *Chem. Phys. Lett.* 2001, 348, 255-262.
- (12) Gustavsson, T.; Sharonov, A.; Markovitsi, D. *Chem. Phys. Lett.* 2002, 351, 195-200.
- (13) Kang, H.; Lee, K. T.; Jung, B.; Ko, Y. J.; Kim, S. K. *J. Am. Chem. Soc.* 2002, 124, 12958-12959.
- (14) Broo, A. *J. Phys. Chem. A* 1998, 102, 526-531
- (15) Mennucci, B.; Toniolo, A.; Tomas, J. *J. Phys. Chem. A* 2001, 105, 4749-4757.
- (16) Sobolewski, A. L.; Domcke, W.; Dedonder-Lardeux, C.; Jouvet, C. *Phys. Chem. Chem. Phys.* 2002, 4, 1093-1100.
- (17) Hedayatullah, M. *J. Heterocyclic Chem.* 1981, 18, 339-342.
- (18) Becker, R. S.; Kogan, G. *Photochem. Photobiol.* 1980, 31, 5-13.
- (19) Hold, U.; Lenzer, T.; Luther, K.; Reihs, K.; Symonds, A. C. *J. Chem. Phys.* 2000, 112, 4076-4089.
- (20) He, Y.; Wu, C.; Kong, W. *J. Phys. Chem. A* (in preparation, 2003).
- (21) Lim, E. C. *J. Phys. Chem.* 1986, 90, 6770-6777.
- (22) Salet, C.; Bensasson, R. *Photochem. Photobiol.*, 1975, 22, 231-235.
- (23) Hønnås, P. I.; Steen, H. B. *Photochem. Photobiol.*, 1970, 11, 67-76.
- (24) Görner, H. *J. Photochem. Photobiol, B*, 1990, 5, 359-377.
- (25) Wood, P. D.; Redmond, R. W. *J. Am. Chem. Soc.* 1996, 118, 4256-4263.
- (26) Lorentzon, J.; Fülischer, M. P.; Roos, B. O. *J. Am. Chem. Soc.* 1995, 117, 9265-9273.
- (27) Baraldi, I.; Bruni, M. C.; Costi, M. P.; Pecorari, P. *Photochem. Photobiol.* 1990, 52, 361-374.
- (28) Broo, A.; Pearl, G.; Zerner, M. C. *J. Phys. Chem. A* 1997, 101, 2478-2488.

- (29) Nir, E.; Müller, M.; Grace, L. I; de Vries, M. S. *Chem. Phys. Lett.* 2002, 355, 59-64.
- (30) Ismail, N.; Blancafort, L.; Olivucci, M.; Kohler, B.; Robb, A. J. *Am. Chem. Soc.* 2002, 124, 6818-6819.
- (31) Chin, W.; Mons, M.; Dimicoli, I.; Piuze, F.; Tardivel, B.; Elhanine, M. *Eur. Phys. J. D* 2002, 20, 347-355.
- (32) Lipinski, J. *Spectrosc. Acta Pt. A-Molec. Biomolec. Spectr.* 1989, 45, 557-559.

Photophysics of methyl substituted uracils and thymines and their water
complexes in the gas phase

*Yonggang He, Chengyin Wu, and Wei Kong**

Department of Chemistry, Oregon State University, Corvallis, Oregon 97331-4003.

Journal of Physical Chemistry, A
PO Box 3337, Columbus, OH, 43210, USA
2004, 108, 943-949

* To whom correspondence should be addressed.
E-mail: kongw@chem.orst.edu. Phone: 541-737-6714. Fax: 541-737-2062.

3. Photophysics of methyl substituted uracils and thymines and their water complexes in the gas

3.1. ABSTRACT

We report studies on several methylated uracils and thymines and thymine-water complexes in the gas phase using resonantly enhanced multiphoton ionization (REMPI) and laser induced fluorescence (LIF) spectroscopy. Results from two different REMPI experiments provided strong evidence that after photoexcitation to the S_1 state, bare molecules were funneled into and trapped in a dark state via fast internal conversion. Lifetimes of this dark state were determined to be tens to hundreds of nanoseconds, depending on the internal energy and the degree of methyl substitution. The mass spectra of hydrated thymine clusters demonstrated dependence on the excitation wavelength, and the gradual loss of the ion signal with increasing water content across the absorption region of the S_1 state indicated a reduced lifetime of the S_1 state by the water solvent. In addition, the lifetime of the dark state also decreased gradually as thymine became more hydrated. Based on these results, we conclude that in water solutions, the decay from the S_1 state should be essentially fast internal conversion to the ground state, in agreement with studies from the liquid phase. Our work reveals that the photostability is not an intrinsic property of these pyrimidine bases. Rather, it is the water solvent that stabilizes the photophysical and photochemical behavior of these bases under UV irradiation.

3.2. Introduction

The photophysical and photochemical properties of electronically excited states of nucleic acids are crucial to the understanding of the mechanism of DNA photodamage. During the past four decades, efforts have been made in the study of the relaxation dynamics of excited nucleic acid bases. In the condensed phase, the lifetimes of the first electric dipole allowed excited state (S_1) of the nucleic acid bases are generally short, on the order of one picosecond.¹⁻⁹ This ultrashort lifetime has been suggested to be the

reason for the adoption of these bases as the building blocks of the genetic code during the early stages of life's evolution.⁸ The mechanism of the fast decay process has been proposed to be internal conversion (IC) to the ground state.^{5,8,10} In the gas phase, however, we observed a dark state in the decay of several methyl substituted pyrimidine bases. We then proposed that instead of internal conversion to the ground state, the majority of the pyrimidine bases were actually trapped in this dark state for several tens of nanoseconds.¹¹ Most of the studies in the condensed phase were conducted in water solutions. It is therefore unclear whether the conclusions from the condensed phase referred to the intrinsic properties of these molecules or a result of their interaction with the water solvent. In this report, we present our gas phase observations of the decay pathways of several methyl substituted pyrimidine bases and their water complexes. This work will bridge the observations in the two different phases and reveal the role of the solvent in modifying the photophysics of these bases.

Studies on isolated nucleic acid bases in the gas phase have been limited mainly due to the difficulties associated with vaporization of these non-volatile compounds. Work on the purine bases reported obvious discrepancies with those from the condensed phase. Using laser desorption, Nir *et al.* probed the first excited state of guanine.¹² The authors showed evidence that internal conversion was not the dominant decay channel at low temperatures and in the absence of solvent interactions. Piuze *et al.* carried out more detailed studies using IR-UV hole burning.¹³ For all of the four tautomers of guanine in the gas phase, the decay lifetimes were observed to be in the nanosecond range. Instead of direct internal conversion to the ground state, decay to a nearby $^1n\pi^*$ state via strong vibronic mixing was therefore tentatively proposed. This photophysical model involving two interacting electronic states was also evoked by Kim and co-workers and de Vries and co-workers in their own studies of adenine.^{14,15} Using picosecond time resolved 1+1' photoionization, the lifetime of the first electronically excited state of adenine was determined by Lühres *et al.*¹⁶ The authors also cast doubt on the generally believed model that involved direct IC to the ground state after photoexcitation. The possibility of either to a low lying $n\pi^*$ state through IC or to a triplet state via intersystem crossing (ISC) was suggested.

The existence of a dark state in the decay pathway of the nucleic acid bases has been proposed in several theoretical studies.^{17, 18} Broo suggested that in adenine, a strong mixing between the lowest $n\pi^*$ and $\pi\pi^*$ states via the out-of-plane vibrational modes could lead to increased overlap with the vibrational states of the ground state.¹⁷ This “proximity effect”, as suggested by Lim,¹⁹ was used in the past to explain the ultra short lifetimes of the DNA bases. A more recent work by Sobolewski *et al.* proposed that it was the lowest $\sigma\pi^*$ state that was responsible for the fast internal conversion of nitrogen-heterocyclic compounds.¹⁸ However, to the authors knowledge, there is no available calculation on the lifetime of the dark state and the related quantum yields.

In contrast to the purine bases, experimental studies on the pyrimidine bases are even more limited. However, indications of different decay pathways from that of the condensed phase also exist. The possibility of a low lying state that couples with the S_1 state was suggested by Levy and co-workers to explain the broad featureless spectra of uracil and thymine in jet-cooled gas phase experiments.²⁰ The work on cytosine by De Vries’ group reported a long lived dark state with a lifetime of nearly 300 ns.²¹ The authors attributed this state to a triplet state only accessible in the gas phase. Recently, Kang *et al.* measured the lifetimes of all five nucleic acid bases using the pump-probe technique in the femtosecond regime.²² In addition to a fast component with a decay time of 6.4 ps, a relatively long-lived state (longer than 100 ps) was observed in thymine, indicating the existence of an alternative pathway. Based on energetic analysis, they also attributed this channel to a triplet state. Our previous study on methyl substituted uracil and thymine confirmed the existence of such a long-lived dark state.¹¹ However, just based on the energetics and the scale of the lifetime, we were unsure of the multiplicity of the dark state. In fact, we suspected a singlet $n\pi^*$ state instead of a triplet state.

Several attempts have been made to decipher the effect of hydration on the photophysics of nucleic acid bases. Experimental efforts include mass spectroscopy and ionization potential measurements of gas phase hydration complexes of thymine and adenine,²³ fragmentation pattern analysis of hydrated adenine and thymine,^{24,25} UV spectroscopy of hydrated guanine formed in a supersonic jet,¹³ and femtosecond pump-probe ionization mass spectroscopy of hydrated adenine clusters.²⁶ Theoretical studies on the interaction between these bases with water molecules have also been performed.²⁷⁻²⁹

Despite of these efforts, however, the effect of hydration on the relaxation dynamics of electronically excited states remains unclear. This understanding is crucial not only in terms of revealing the true origin of the photostability of nucleic acid bases, but also in reconciling the differences between results from the gas phase and those from the condensed phase. In this article, we report investigations of hydrated clusters of thymine using resonantly enhanced multiphoton ionization (REMPI). Similar to bare molecules, hydrated clusters also decay via a dark state, although the lifetime of this dark state decreases gradually as thymine becomes more hydrated. An interesting observation is that in the REMPI experiment, there was almost no signal from hydrated clusters when the excitation laser scanned across the entire absorption region of the S_1 state. We suspect that in these complexes, the interaction between thymine and water greatly enhances the corresponding conical intersections and consequently, the lifetime of the S_1 state becomes too short to sustain a detectable population using our nanosecond laser system.

3.3. Experimental Details

The experimental apparatus was a standard molecular beam machine with a time of flight mass spectrometer (TOF-MS) and a pulsed valve for supersonic cooling. The sample was housed and heated in the nozzle to obtain sufficient vapor pressure, and the operational temperature was 130°C for 1,3-dimethyluracil (DMU), 150°C for 1-methyluracil (MU), 180°C for 1,3-dimethylthymine (DMT), and 220°C for thymine. No indication of thermal decomposition was observed at these temperatures. The vapor was seeded in 2 atm of helium gas, and the gaseous mixture was expanded into a vacuum chamber at a 10 Hz repetition rate through a 1 mm orifice. Water complexes were formed by bubbling the carrier gas through a room temperature water reservoir (vapor pressure: ~23 mbar) before being routed to the heated sample. The sample 1-MD, 1,3-DMU and thymine were purchased from Aldrich Co. and used without further purification. 1,3-DMT was synthesized from thymine,³⁰ and its purity was checked by nuclear magnetic resonance (NMR) and infrared absorption (IR) spectra.

A Nd:YAG (Continuum, Powerlite 7010) pumped OPO laser (Continuum, Panther) and a Nd:YAG (Spectra Physics GCR 230) pumped dye laser (LAS, LDL 2051) were used in these experiments. In the REMPI experiment, the two lasers were set to

counterpropagate; and the light path, the flight tube, and the molecular beam were mutually perpendicular. The delay time between the two lasers was controlled by a delay generator (Stanford Research, DG535). Two different types of 1+1' REMPI experiments were performed, by either scanning the resonant or the ionization laser. In the laser induced fluorescence (LIF) experiment, the molecular beam was intercepted by the laser beam from the OPO laser; and the signal was detected by a photomultiplier tube (PMT, Thorn EMI 9125B) through two collection lenses in the direction opposite the molecular beam. In order to reject the scattered light, masks were used to cover all the windows and lenses, and cut-off filters were inserted in front of the PMT. Using a Tektronix TDX350 digital oscilloscope, the time resolution of the fluorescence signal was essentially limited by the width of the laser pulse (~ 5 ns). The wavelength region of the fluorescence signal was determined using long pass filters.

3.4. Results

3.4.1. Bare compounds

Figure 1 shows the 1+1 (one color) REMPI and 1+1' (two color) REMPI spectra together with the gas phase UV absorption spectrum of 1,3-DMU. In the one color experiment, a second order dependence of the ion signal on the laser intensity was observed, while in the two color experiment, the single photon nature of each excitation step was confirmed from a linear dependence of the ion signal on both laser beams. The delay between the pump and the probe laser was 10 ns, and the probe laser was set at 220 nm in the 1+1' experiment. The two features in the UV absorption spectrum were assigned as the first and second excited singlet state, S_1 and S_2 , and both were believed to have $\pi\pi^*$ characters.³¹ The one color REMPI spectrum more or less traces the absorption curve for the S_1 feature, while the missing S_2 feature is solely a result of the low output power of the OPO laser. Limited by the non-flat tuning curve of the OPO laser, artificial structures caused by the scanning laser were observed and smoothed out. For this very reason, neither REMPI spectrum was normalized by the intensity of the OPO laser. When divided by the square of the laser power, the one color REMPI spectrum indeed peaked up again in the vicinity of the S_2 feature. The absorption spectrum was taken at 140°C, while the REMPI spectra were obtained from a supersonic jet with the pulsed valve

heated to the same temperature. Supersonic cooling might be the reason for the slightly higher energy onset of the 1+1 spectrum. The 1+1' REMPI spectrum, on the other hand, shows clear discrepancies compared with the one color spectrum. It has a much narrower feature between 285 nm and 240 nm, and its center for the S_1 feature is slightly shifted to a lower energy. Under the same experimental conditions, no two color signal was obtained when the resonant laser scanned further into the S_2 region, even after taking into account the low output power of the OPO laser. Since the only difference between the two REMPI experiments is the delayed ionization (10 ns) by another laser beam at 220 nm, this result is a manifestation of the dynamical behaviors of the excited states.

Figure 2 shows the result of a different REMPI experiment: the first pump laser was set at 250 nm, while the delayed (10 ns) ionization laser scanned through the UV region. The spectra are composites of seven segments, each spanning an adjacent wavelength region of 5 nm. For each segment, we first scanned the OPO laser to obtain the one color REMPI spectrum (dashed curve), and the two photon nature of this measurement was confirmed from a power dependent study. Then with the dye laser beam set at 250 nm and fired 10 ns before the arrival of the OPO laser, we scanned the same wavelength region again using the same OPO laser with **the same power** to obtain the two laser spectrum (solid curve). The power of the dye laser was carefully controlled so that it generated no ion signal. It is worth noting that this two laser experiment is not a typical 1+1' REMPI experiment, and it is referred to as a “two laser” experiment in this following. When the OPO scanned through the region between 240 and 217 nm, a first order dependence of the two laser ion signal on the power of the dye laser was obtained. Quite opposite to the one color spectrum, the two laser spectrum shows a sharp rise at the blue edge despite of the drop in the power of the OPO laser. Qualitatively, a thirty-fold increase in the ion signal at 220 nm was observed. In contrast, when the OPO laser was at a wavelength between 245 and 280 nm, the early arrival of the pump laser caused a depletion of ~25% of the one color ion signal. Deviation of the pump wavelength from 250 nm did not result in any difference in the degree of depletion, so long as the pump wavelength was within the absorption profile of the S_1 state. Similar to Figure 1, neither spectrum was normalized by the power of the OPO laser, and the precise shapes of the observed features are unimportant to the present discussion. The major issue is that if the

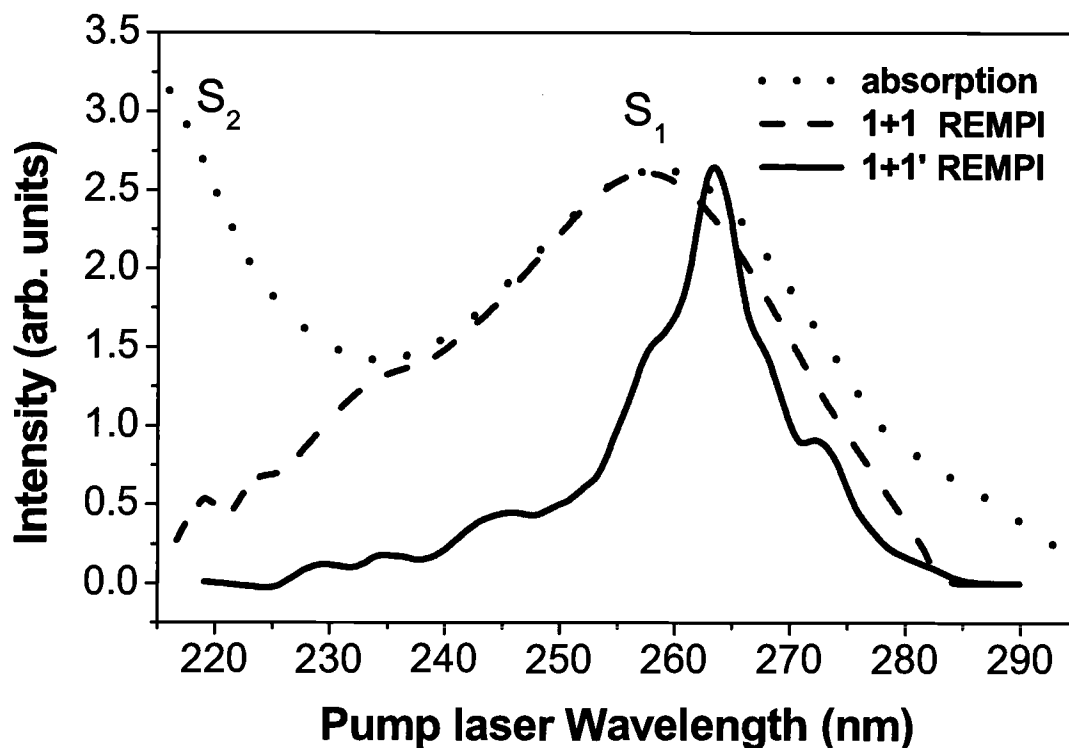


Figure 1. 1+1 REMPI, 1+1' REMPI and UV absorption spectra of 1,3-DMU. The 1+1' REMPI spectrum was obtained by scanning the pump laser and setting the probe laser at 220 nm with a delay time of 10 ns. Neither REMPI spectrum was normalized by the laser power, and at the blue edge of the figure, the low output power of the OPO laser resulted in the missing S_2 feature in the 1+1 spectrum. The absorption spectrum was taken at 140°C, the same temperature of the pulsed valve during the REMPI experiments.

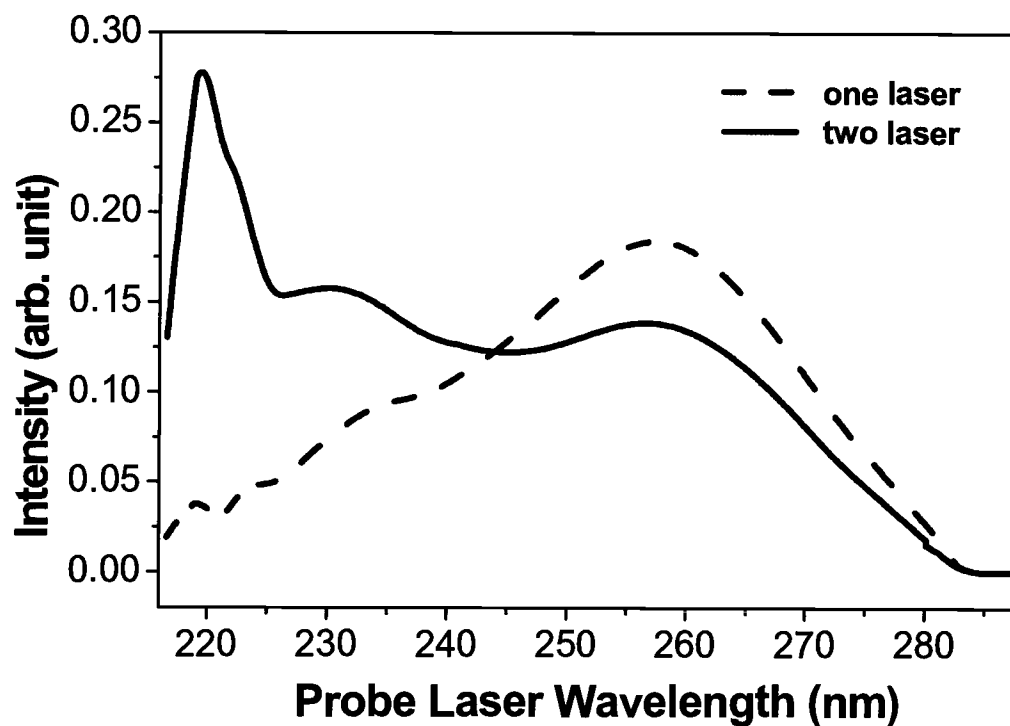


Figure 2. Effect of the pump laser at 250 nm with a time advance of 10 ns on the one laser REMPI of the probe laser. Both spectra were recorded using the same intensity for the probe laser. The pump laser in the two laser experiment resulted in a maximum depletion of 20-25% in the region between 245 and 280 nm, and an enhancement of three decades at 220 nm. See text for a detailed explanation of the experimental method and the implications of this result.

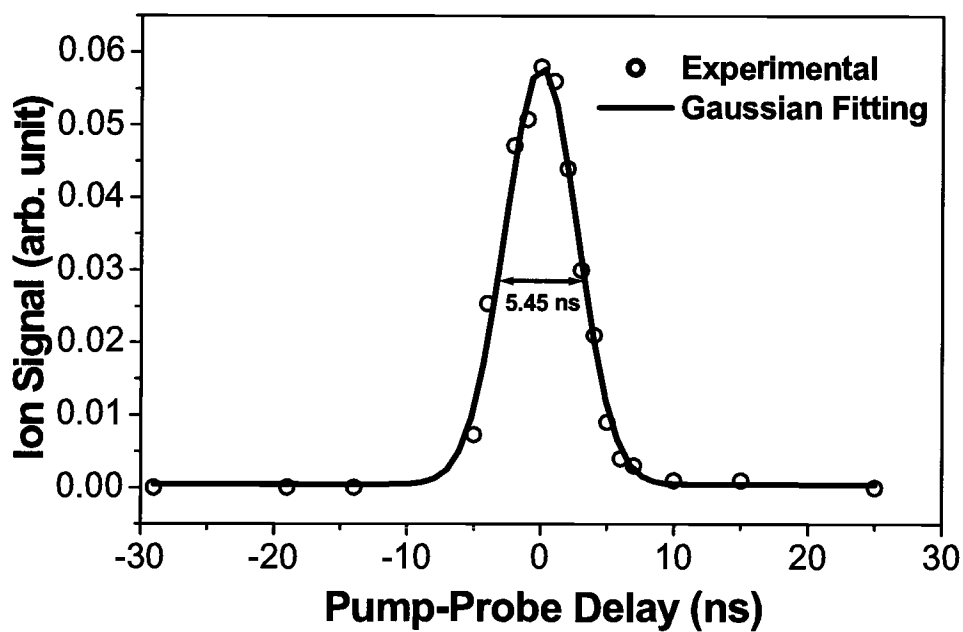


Figure 3. Pump-probe transient ionization signal of 1,3-DMU in the gas phase with the pump and probe wavelengths at 265 and 248 nm, respectively. The time constant (full width at half maximum) for the Gaussian function is 5.45 ns.

S_1 state were short-lived and could decay to the ground state through fast IC, 10 ns after excitation, a full recovery of the ground state population would be expected, and the pump laser should have no effect on the two laser signal. The depletion effect in Figure 2 manifests the existence of a population trap in the decay pathway of the S_1 state, while the enhancement further indicates that the trap can be illuminated under a higher excitation energy.

In the two types of REMPI experiment of Figure 1 and Figure 2, dependence of the signal strength on the delay time between the pump and the probe lasers has been observed. Figure 3 shows a pump-probe transient of 1,3-DMU with both laser beams in the S_1 region: the pump beam at 265 nm, while the probe beam at 248 nm. The profile is fitted by a Gaussian function with a time constant (full width at half maximum) of 5.54 ns. Kang *et al.* reported the lifetimes of the S_1 state of the pyrimidine bases to be in the range of several picoseconds using their femtosecond laser system.²² Thus we believe that the time constant of 5.54 ns reflects the response time of our instrument.

Figure 4 shows the pump-probe transient of 1,3-DMU with the pump wavelength at 251 nm and the probe wavelength at 220 nm. On the scale of the figure, the ion signal due to either one laser alone was insignificant, and the overall signal intensity showed linear dependence on the power of each laser. The signal reached its maximum at a delay time of 8 ns between the two beams, and then it decayed to the background level exponentially. Obviously the decay process in this figure is different from that in Figure 3, and the involvement of another totally different state, i.e., a dark state, is implied. Under this assumption, we would expect that the observed time evolution should contain two components: one exponential component corresponding to the decay of the population from the dark state, and the other Gaussian component corresponding to the decay of the S_1 state together with the instrumental response. However, decomposition of the decay profile indicated that the weight of the Gaussian component was negligible compared with that of the exponential component. In other words, the decay curve showed a single-exponential property.

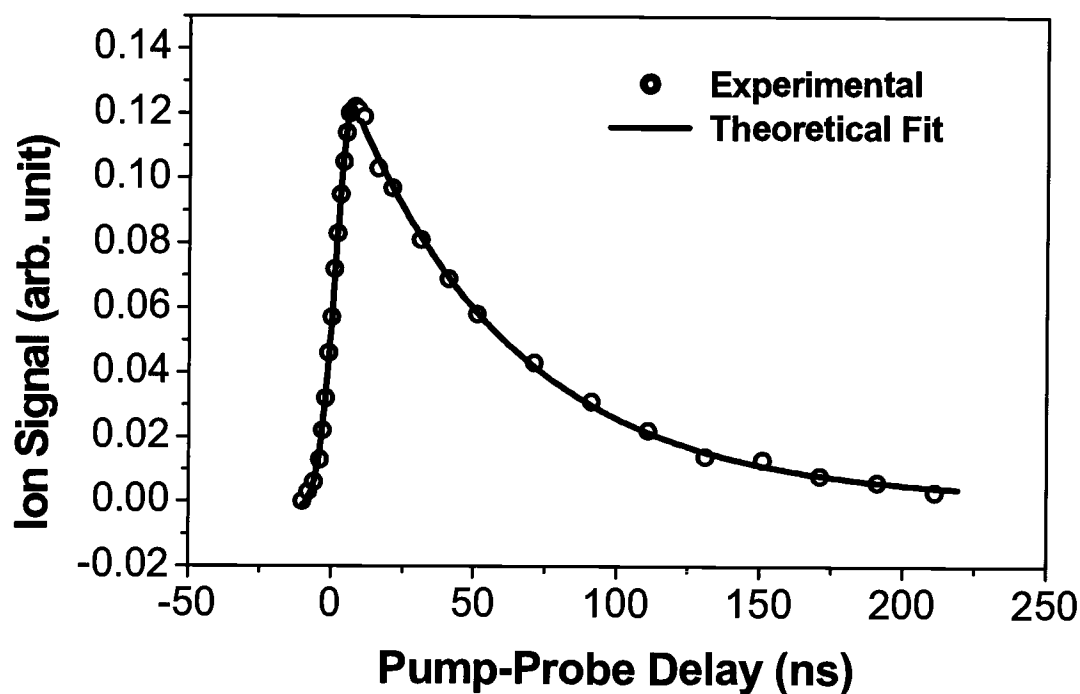


Figure 4. Pump-probe transient ionization signal of 1,3-DMU in the gas phase with the pump and probe wavelengths at 251 and 220 nm, respectively. Hollow circles represent experimental data, and the solid line is a theoretical fit including a single exponential decay convoluted with the instrumental response obtained from Figure 3. The exponential decay constant is 56 ns.

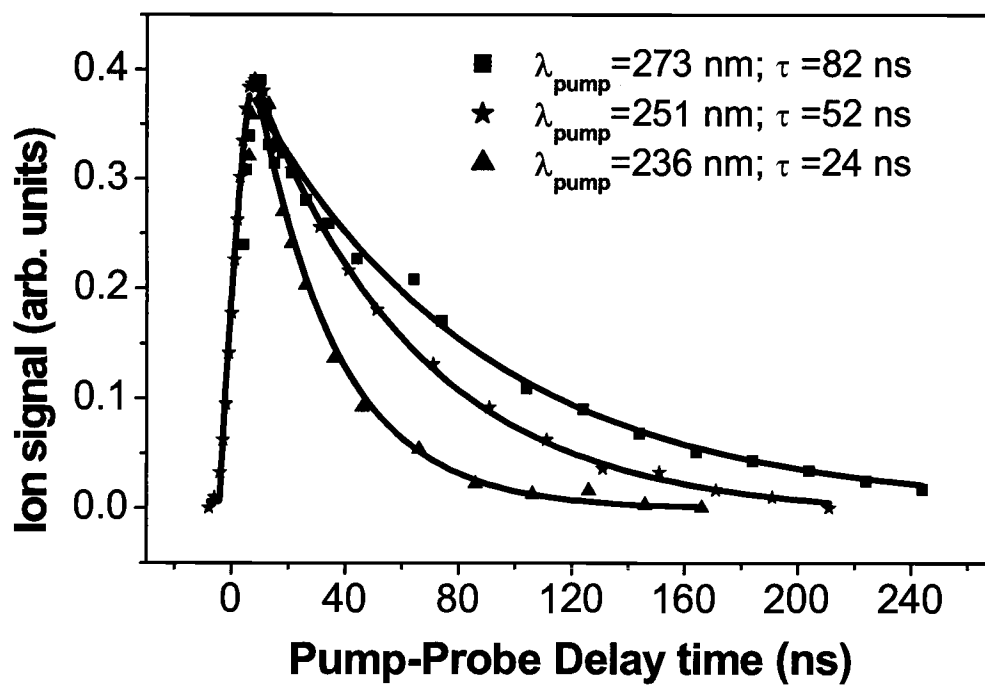


Figure 5. Pump-probe transients of 1,3-DMU in the gas phase at different excitation wavelengths.

The lifetime of this dark state demonstrates explicit dependence on the wavelength of the pump beam. With the probe laser fixed at 220 nm, the lifetime of the dark state at different pump wavelengths ranging from 236 nm to 273 nm is shown in Figure 5. All decay curves have been normalized to have the same amplitude, and the solid lines represent the best fits to the recorded data. The lifetime of the dark state increases gradually as the pump wavelength is increased. For 1,3-DMU, this value ranges from 23 ns at 236 nm to 82 ns at 273 nm. It is worth noting that although the lasers propagate normal to the jet expansion axis, drifting of the molecular beam within a delay time of 300 ns between the two lasers is still negligible. The decay constants in Figure 5 are therefore not contaminated by this instrumental effect.

The number and position of substituted methyl groups on the uracil ring also affect the lifetime of this dark state. Figure 6 summarizes the results on the four pyrimidine bases investigated in this work. The general trend is that the more substituted the ring and the longer the pump wavelength, the longer the lifetime of the dark state. Moreover, substitution at the -1 position is more effective than at the -5 position in stabilizing the dark state.

To further assess the fate of the molecules in the excited state, we attempted to observe the fluorescence signal, but the signal was so weak that a quantitative measurement of the spectrum was impossible with our existing setup. However, by recording the decay profile, the fluorescence lifetimes were obtained at different pump wavelengths. Figure 7 shows two typical fluorescence decay curves. The oscillations in these profiles were caused by an electrical problem of our detection system. All decays could be fitted to single-exponential functions, with constants ranging from 18 ns at 236 nm to 54 ns at 260 nm for 1,3-DMU. These values were obtained without corrections of the instrumental response, so they should be regarded as qualitative rather than quantitative. Nevertheless, these fluorescence lifetimes are in good agreement with the decay time of the REMPI signals of Figure 6. Using long pass filters, we determined that the peak of the radiation was centered between 370 and 440 nm.

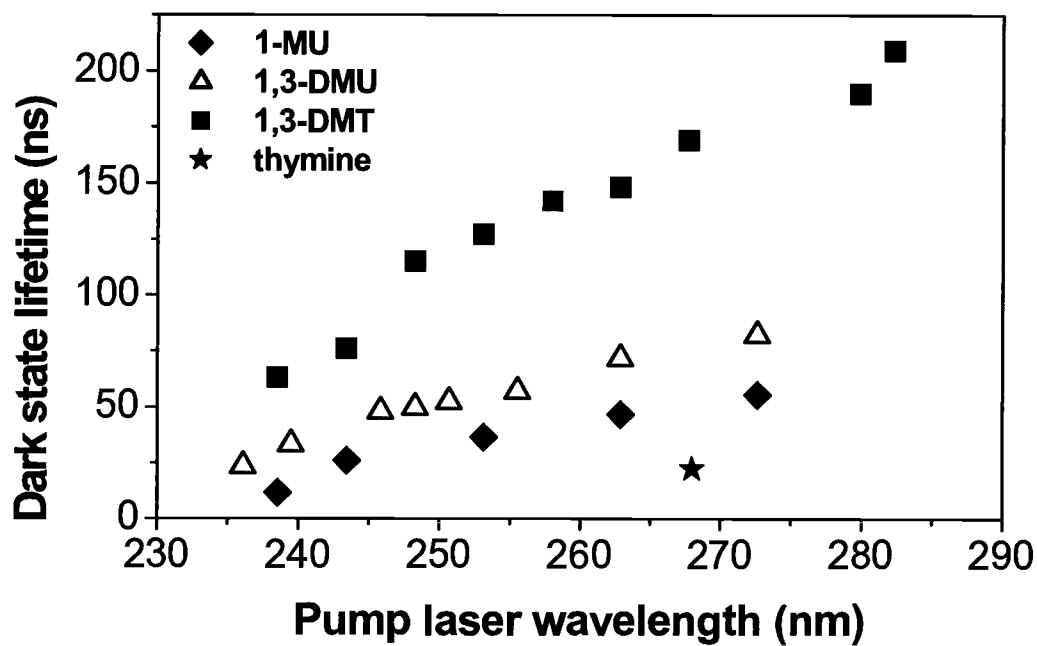


Figure 6. Lifetimes of 1-methyl uracil, 1,3-dimethyl uracil, 1,3-dimethyl thymine, and thymine at different excitation wavelengths.

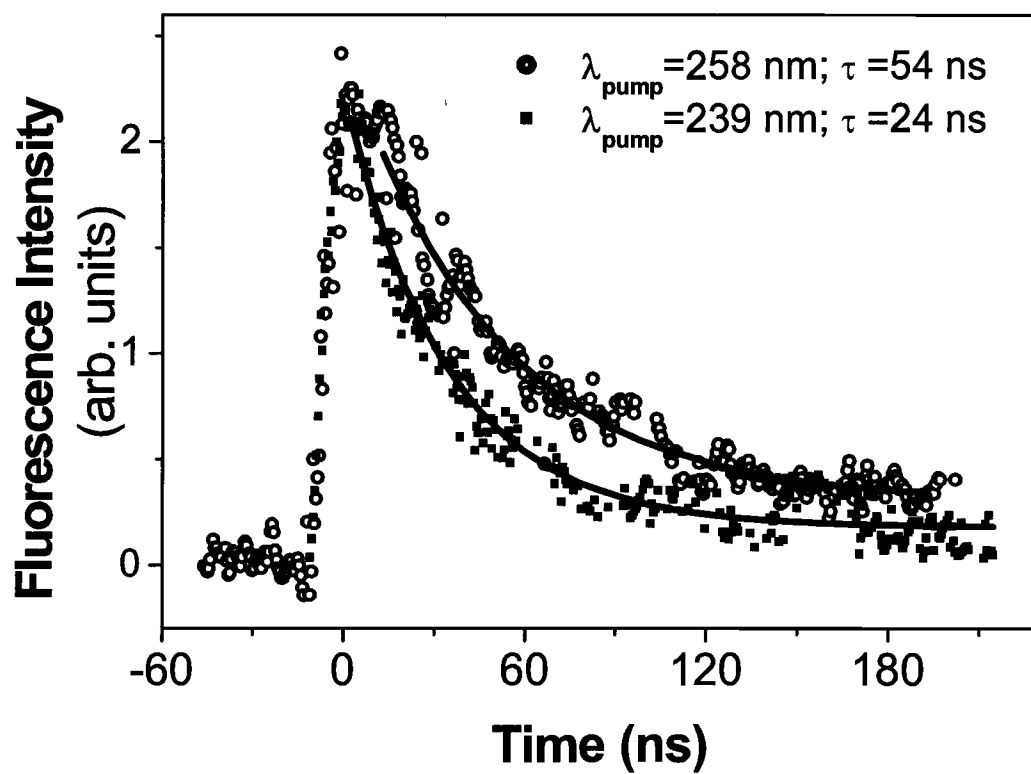


Figure 7. Fluorescence signal of 1,3-DMU in the gas phase at different excitation wavelengths. Solid curves are best fits to the experimental data. The oscillations in the decay curves were caused by an electrical problem in our detection system.

3.4.2. Hydrated clusters

To investigate the hydration effect on the properties of the excited states of these bases, we attempted similar experiments on solvated water clusters. However, because a few H-bonding sites were occupied by methyl groups in 1-MU, 1,3-DMU and 1,3-DMT, we were only successful in generating sufficient thymine-water complexes $T(H_2O)_n$ in our molecular beam. During this experiment, the heating condition and helium stagnation pressure were carefully adjusted to minimize the formation of thymine dimer. At a typical laser intensity of 1 MW/cm^2 (OPO laser), the one color two photon mass spectrum demonstrated dependence on the excitation wavelength as shown in Figure 8. These spectra were obtained at the excitation wavelengths of 229 nm (a) and 268 nm (b) respectively. From 220 nm to 240 nm (the absorption region of the S_2 state of the bare molecule), small water clusters with n up to 4 were readily observable, while in the region of 240 to 290 nm (the absorption region of the S_1 state of the bare molecule), these hydrated cluster ions were conspicuously missing or barely detectable.

The ratios of ion intensities between hydrated clusters $T(H_2O)_n$ and bare thymine as a function of the excitation wavelength are displayed in Figure 9. These ratios are normalized at 220 nm (S_2 state) to highlight the dynamics at the S_1 state. At 220 nm, all cluster ions with $n \leq 5$ can be clearly seen, suggesting the existence of the corresponding neutral clusters in our source. In the absorption region of the S_1 state, however, the attachment of one water molecule decreases the ion signal to half of its value compared with that of the bare molecule. Additional attachment of one or two water molecules has a similar effect. When four or more water molecules are attached, the S_1 state is no longer observable from the ionization spectra. Since the ionization potential (IP) of thymine is 9.15 eV, corresponding to 271 nm in this one laser experiment, and $T(H_2O)_n$ clusters are believed to have even lower IPs,²³ the lack of heavy ions in the S_1 region cannot be attributed to the insufficiency of the excitation photon energy. This dramatic loss of heavy ions in the S_1 region should therefore be a result of a loss during excitation or ionization. It is worth noting that although fragmentation has been known to be a recalcitrant problem in studies of clusters, fortunately in this case, it has no effect on our conclusion.

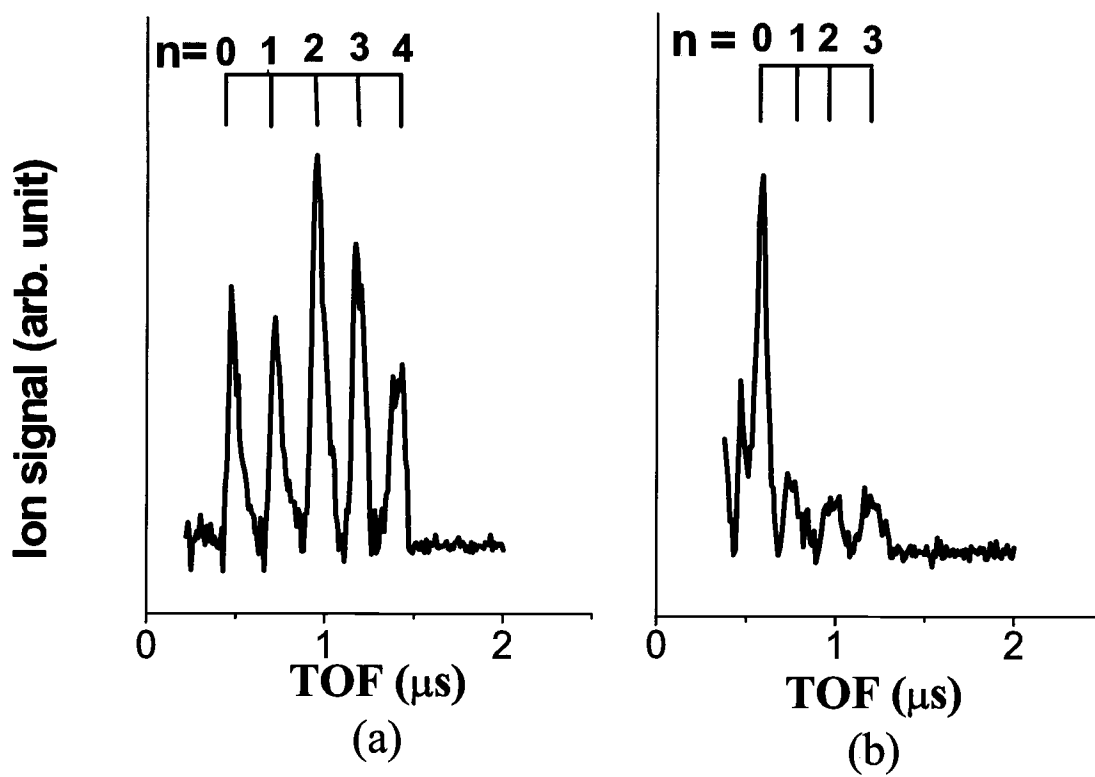


Figure 8. One-color REMPI mass spectra of hydrated thymine clusters, obtained at the excitation wavelengths of 229 nm (a) and 268 nm (b) respectively.

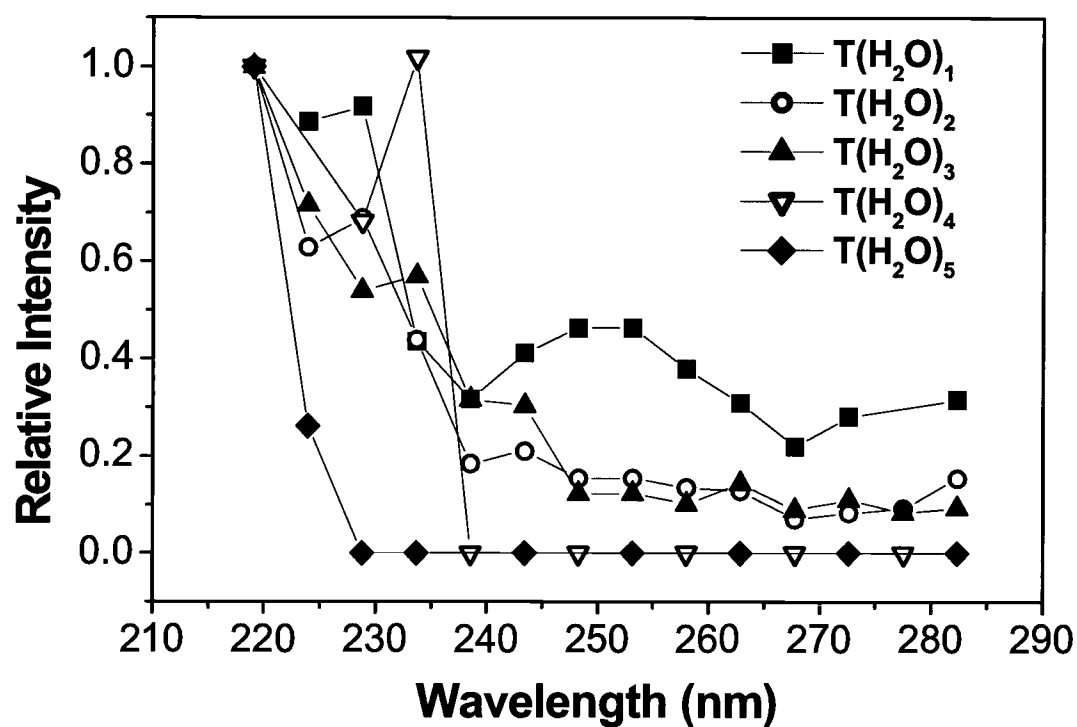


Figure 9. Ratios of ion intensities between the hydrated clusters $T(H_2O)_n$ and bare thymine as a function of the excitation wavelength. The ratios were normalized at 220 nm (S_2 state) to highlight the dynamics at the S_1 state.

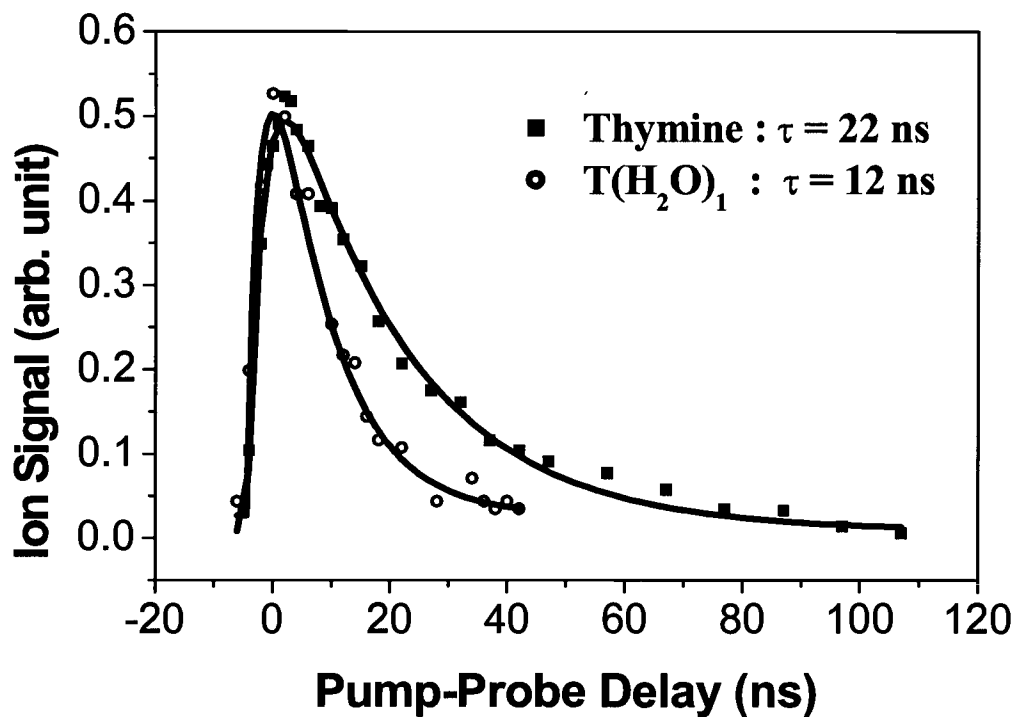


Figure 10. Pump-probe transients of bare thymine and $T(H_2O)_1$ in the gas phase with the pump and probe wavelengths at 267 and 220 nm, respectively.

Figure 10 compares the transients of thymine and $T(H_2O)_1$ obtained from a two color 1+1' experiment. With the pump wavelength set at 267 nm and the ionization wavelength at 220 nm, the lifetimes of the dark state of thymine and $T(H_2O)_1$ were measured to be 22 ns and 12 ns respectively. The fact that the decay profile of $T(H_2O)_1$ contains only a single exponential decay function is evidence that this measurement was not contaminated by dissociative products of larger complexes. For clusters with two or three water molecules attached, the two color signals were too weak to accurately determine the decay constants. However, as we increased the delay time between the pump and the probe laser, we observed that heavier clusters disappeared faster than lighter ones. We therefore conclude that this decrease in lifetime with increasing water content is gradual in complexes with $n < 5$. No two color ion signals were observable for clusters with four or more water molecules.

3.5. Discussion

3.5.1. Decay mechanism of the pyrimidine bases

Our results provide concrete evidence that the decay mechanism of methyl substituted uracil and thymine bases relies heavily on the environment. Figure 11 shows the proposed energy levels and processes for the pyrimidine bases in the gas phase. After initial excitation to the S_1 state, we believe that a significant fraction of the gas phase molecules decay to a dark state S_d . While the lifetime of the S_1 state is shorter than our instrumental response, the lifetime of the dark state is in the range of tens to hundreds of nanoseconds, depending on the degree of methylation and the amount of excess energy. The nature of this dark state is most likely a low lying $^1n\pi^*$ state, and further ionization from this dark state requires a much higher excitation energy. Although we are unable to provide a precise estimate of the quantum yield for this decay channel, based on our previous estimate, the lower limit should be 20% in bare molecules.¹¹ Water molecules, on the other hand, can significantly reduce the lifetime of the S_1 state and enhance the IC from the dark state to the ground state. As a result, in aqueous solutions, the dark state becomes essentially undetectable. The S_2 state, on the other hand, follows an entirely different pathway, as indicated by the lack of two laser signals for the bare compound in Figure 1 and the existence of all four water complexes in Figure 8. It is worth noting that

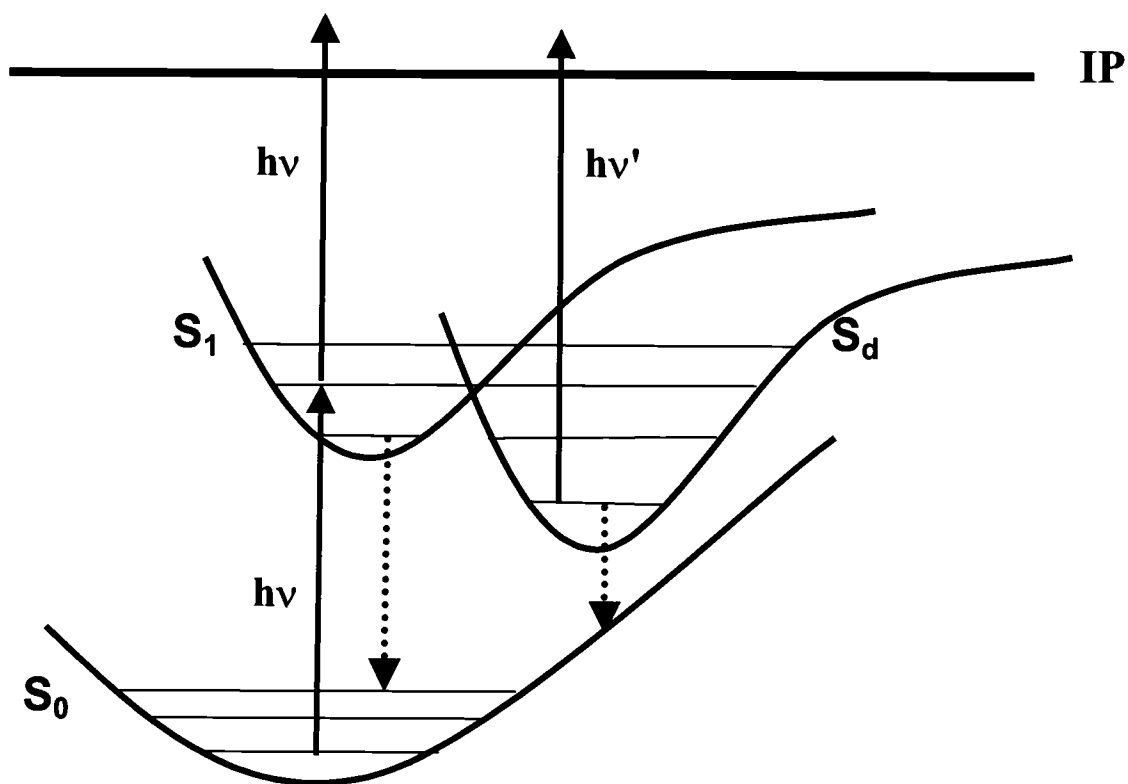


Figure 11. Proposed potential energy surfaces and processes for the pyrimidine bases. Ionization from the S_1 state and the dark state S_d samples a different Franck-Condon region of the ionic state, resulting in a different ionization energy from these two states.

this model should be applicable to all pyrimidine bases given their similar behaviors in the gas phase and in the liquid phase, despite the fact that we were only successful in studies of thymine-water complexes.

This model can provide a consistent explanation of our experimental observations. The 1+1' REMPI signal in Figure 1 (solid line) is from ionization of this dark state, while the one color signal is from ionization of the molecules initially populated in the S_1 state. The narrower width of the 1+1' spectrum compared with that of the one color spectrum reflects the limited energy range for effective overlap between the dark state and the S_1 state. This dark state does not absorb in the region of 245 – 280 nm, rather, it absorbs in a much higher energy region from 217 to 245 nm. Relaxation of the molecular frame in the dark state could result in a different Franck-Condon region for vertical ionization, thereby increasing the ionization energy from the dark state. In the REMPI experiment of Figure 2, this shift in absorption profile of the excited species causes the depletion of the two laser signal when the probe wavelength is between 245 and 280 nm. When the probe laser scans into the absorption region of this dark state, an enhanced ion yield is observable. The decay process in Figure 4 corresponds to the decay of this dark state. Fluorescence from this dark state should take place in a red-shifted region, i. e., 370-440 nm from this study, compared with that of the S_1 state (300 nm).³² The similarity of the decay constants of the fluorescence (Figure 7) and the 1+1' REMPI signal (Figures 4 and 5) confirms that in both experiments, we are probing the same dark state. Methyl substitution stabilizes this dark state as shown in Figure 6, while more vibrational energy obtained from the initial excitation step destabilizes this state by opening more decay channels (Figures 5 and 6). The loss of ion signal in the S_1 region of Figure 9 with the addition of water molecules is caused by the decreased lifetime of the S_1 state. This decrease is a result of enhanced vibronic coupling between the S_1 state and the dark state or the ground state, due to the presence of H_2O molecules.

The existence of the dark state and the above decay mechanism are also supported by previous experimental and theoretical results. The work on cytosine in the gas phase by De Vries' group also reported a long lived dark state with a lifetime of nearly 300 ns.²¹ Based on the scale of the lifetime, however, the authors suggested the involvement of a triplet state. Kang *et al.* reported two decay components for thymine in the gas phase

using the femtosecond pump-probe ionization technique.²² The slower component with an estimated lifetime of more than 100 ps corresponded to a state within the same energy region as our dark state, though the authors also suspected the involvement of a triplet state based on energetic analysis. Brady *et al.* observed the broad and diffusive feature of the S_1 state in their gas phase study of uracil and thymine.²⁰ The authors attributed the featureless spectrum to either mixing of electronic states or a large geometry change between the ground and excited electronic states. A recent theoretical investigation on cytosine showed the existence of a state switch between $\pi\pi^*$ and $n_o\pi^*$ (the lone pair electron on the oxygen atom) states.³³ The crossing between the two states was weakly avoided and there existed a small energy barrier between the equilibrium position of the $^1n_o\pi^*$ state and its intersection with the ground state. This barrier might be the very reason that the majority of the molecules are trapped in the dark state after the $^1\pi\pi^* \rightarrow ^1n\pi^*$ internal conversion. More detailed calculations of the decay process from the $^1n_o\pi^*$ state to the ground state will be revealing, as suggested by the authors.

3.5.2. Hydration effect on the photophysics of the excited state

The reduction or complete loss of one color ion signal for hydrated clusters near the absorption region of the S_1 state (Figure 9) signifies a reduction of lifetime for these clusters. Under our experimental conditions using a nanosecond laser system, the failure to accumulate a population at the S_1 state for further ionization can only be attributed to fast depopulation from the initially prepared state, through internal conversion, intersystem crossing, or dissociation. Kim and co-workers studied hydrated adenine clusters in the gas phase.^{24,26} Using a nanosecond laser, they observed a near complete loss of hydrated adenine ions in the S_1 region, while using a femtosecond laser, all hydrated clusters were observable. They also measured the lifetime of the S_1 state to be 230 fs for $A(H_2O)_1$ and 210 fs for $A(H_2O)_2$, while the lifetime of the S_1 state of bare adenine was 1 ps. This five fold change in lifetime was apparently sufficient to cause a qualitatively different behavior under femtosecond or nanosecond excitation.

Lifetime reduction upon hydration should be no surprise based on studies in the gas phase and the liquid phase. For thymine, the lifetime of the S_1 state was reported to be 6.4 ps in the gas phase²² and 1.2 ps in the liquid phase.⁶ Similarly, for the other two

pyrimidine bases, uracil and cytosine, the lifetimes of the S_1 states were measured to be 2.4 ps and 3.2 ps respectively in the gas phase,²² while these values decreased to 0.9 ps and 1.1 ps in the liquid phase.⁶ The measurement related to Figure 9 further confirms that this lifetime reduction is a gradual process with increasing water content. When four or more water molecules are in the vicinity, we suspect that the behavior of thymine is essentially the same as that in the liquid phase, i. e., on the picosecond time scale. Further experiments in the femtosecond regime is under preparation.

The reason for the lifetime reduction of the S_1 state should be faster internal conversion upon hydration. In the work of Wanna *et al.* on pyrazine and pyrimidine, a similar loss of ion signal from hydrated clusters was observed,³⁴ and an increased rate of internal conversion upon solvation was proposed. In the case of the pyrimidine bases, however, we could not distinguish the destination of the increased IC either being the dark state or the ground state, although indications from our experimental data, including the faster decay of the dark state upon hydration in Figure 10, favor the dark state as the destination. Typically in a $n\pi^*$ transition, solvation by a proton donor such as water causes a blue shift; while in a $\pi\pi^*$ transition, this effect is a slight red shift.³⁵ The energy gap between the initially accessed $\pi\pi^*$ (S_1) and the $n\pi^*$ dark state can thus be reduced in the presence of water, and subsequently a better vibronic coupling between the two states can occur. On the other hand, we cannot exclude the possibility that IC directly to the ground state might still be somewhat competitive with IC to the dark state even in the gas phase. In the presence of water, the balance between the two decay pathways could shift, and a faster direct IC process to the ground state could also reduce the lifetime of the S_1 state.

The weak two color ion signal and the reduced lifetime of the dark state in Figure 10 further indicate a faster decay process of the dark state for hydrated clusters. Limited by the signal to noise ratio in our experiment, we could not extract the lifetimes of larger clusters. However, as we increased the delay time between the pump and the probe laser, we observed that heavier clusters disappeared faster than lighter ones. We therefore conclude that with increasing water content, the lifetime of the dark state should also demonstrate a gradual decrease. In the liquid phase, it is likely that the dark state is so short-lived that it is beyond detection using typical femtosecond pump-probe techniques.

We propose that the reason for this lifetime reduction is a decrease in the barrier for the conical intersection between the dark state and the ground state. In the gas phase,¹¹ this conical intersection is thought to be responsible for the low fluorescence quantum yield of the $^1n\pi^*$ dark state, and the barrier effectively blocks this intersection from easy access. However, solute-solvent interactions can shift the relative positions of the involved states and therefore lower the barrier to the intersection.

This observation on the effect of hydration can reconcile the differences between results from the gas phase and those from the liquid phase. In the liquid phase, the dark state is no longer as stable as in the gas phase, and a fast cascade from the S_1 state via the dark state to the ground state becomes essentially indistinguishable from a direct IC process to the ground state. Alternatively, one could also interpret the lifetime reduction of the S_1 state as an indication of increased yield of the IC process directly to the ground state due to the presence of water. In either explanation, the photophysics of the pyrimidine bases is significantly affected by the water solvent. The origin of the photostability of the pyrimidine bases therefore lies in the environment, not in the intrinsic property of these bases.

In Figure 9, the total loss of cluster ions in the S_1 region for $T(H_2O)_n$ when $n \geq 4$ and the failure to observe any two color signal for these ions suggest the completion of the first solvation shell with four water molecules. This result is consistent with a previous study by Kim *et al.*²⁵ Based on the fragmentation pattern of hydrated thymine clusters, the authors deduced a well-defined hydration shell structure, and the first hydration shell was composed of only four water molecules. It is this first solvation shell that dramatically changes the photophysical property of thymine. In this sense, four water molecules are sufficient to capture the essence in modeling these pyrimidine bases in a solution environment.

Our conclusion on the hydration of thymine molecules is different from that of adenine. In the study of $A(H_2O)_n$, a complete loss of cluster ions, including those with $n < 4$, was observed for all sized clusters in the S_1 region. The authors attributed this loss to the dissociative $^1n\pi^*$ state upon hydration.²⁴ The basis of this statement was that according to their preliminary calculation and a theoretical result,³⁶ solvent water molecules preferred to form a water cluster before solvating the adenine molecule. The

severance of one water-adenine bond was therefore sufficient to eliminate all the solvent molecules. For the pyrimidine bases, however, theoretical studies showed that water molecules bind to the pyrimidine ring at three different primary sites in a shell like structure.^{37,38} In Figure 9, the signal loss for $T(H_2O)_n$ displayed a clear n -dependence; and the total loss of cluster ions only occurred when $n \geq 4$. This result is clearly different from that of $A(H_2O)_n$.

3.6. Conclusions

We present here evidence for a decay mechanism of uracil and thymine bases in the gas phase and the strong effect of solvation by water molecules. After photoexcitation to the S_1 state, a bare molecule is funneled into and trapped in a dark state with a lifetime of tens to hundreds of nanoseconds. The nature of this dark state is most likely a low lying $^1n\pi^*$ state. Solvent molecules affect the decay pathways by increasing IC from the S_1 to the dark state or to the ground state and from the dark state to the S_0 state. The lifetimes of the S_1 state and the dark state are decreased with the addition of only one or two water molecules. When more than four water molecules are attached, the photophysics of these hydrated clusters should rapidly approach that in the condensed phase. We are currently in preparation of a femtosecond experiment to further elucidate the energetics and lifetimes of the dark state.

Our gas phase results reveal an important function of water in protecting our genetic code from photodamage. The high ionization yield of bare base molecules from the dark state by deep UV radiation, as shown in Figure 2, indicates that the photostability of our genetic code is not an intrinsic property of the bases themselves. Rather, the interaction of these bases with water molecules provides the necessary relaxation mechanism for the excited species. Quenching by solvent molecules may be the key for the photostability of the pyrimidine bases in DNA and RNA.

Our work on hydrated clusters manifests the value of gas phase experiments. Condensed phase studies reveal the properties of the bulk system. However, it is difficult to distinguish intrinsic vs. collective properties of a system. Gas phase studies, on the other hand, directly provide information on bare molecules. Moreover, the investigation of size selected water complexes can mimic the transition from an isolated molecule to

the bulk. The comparison of gas phase experimental results with theoretical calculations can also provide a direct test of theoretical models.

3.7. ACKNOWLEDGMENT

This work was supported by the National Science Foundation, the Petroleum Research Foundation, and the Alfred P. Sloan Foundation. The skillful synthesis of 1,3-DMT by T. Suyama is deeply appreciated.

3.8. REFERENCES

1. Daniels, M.; Hauswirth, W. *Science* 1971, 171, 675-677.
2. Callis, P. R. *Annu. Rev. Phys. Chem.* 1983, 34, 329-357.
3. Nikogosyan, D. N.; Angelov, D.; Soep, B.; Lindqvist, L. *Chem. Phys. Lett.* 1996, 252, 322-326.
4. Häupl, T.; Windolph, C.; Jochum, T.; Brede, O.; Hermann, R. *Chem. Phys. Lett.* 1997, 280, 520-524.
5. Reuther, A.; Nikogosyan, D. N.; Laenen, R.; Laubereau, A. *J. Phys. Chem.* 1996, 100, 5570-5577.
6. Reuther, A.; Iglev, H.; Laenen, R.; Laubereau, A. *Chem. Phys. Lett.* 2000, 325, 360-368.
7. Pecourt, J.-M. L.; Peon, J.; Kohler, B. *J. Am. Chem. Soc.* 2000, 122, 9348-9349.
8. Pecourt, J.-M. L.; Peon, J.; Kohler, B. *J. Am. Chem. Soc.* 2001, 123, 10370-10378.
9. Gustavsson, T.; Sharonov, A.; Markovitsi, D. *Chem. Phys. Lett.* 2002, 351, 195-200.
10. Andréasson, J.; Holmén, A.; Albinsson, B. *J. Phys. Chem. B* 1999, 103, 9782-9789.
11. He, Y.; Wu, C.; Kong, W. *J. Phys. Chem. A* 2003, 107, 5145-5148.
12. Nir, E.; Grace L.; Brauer, B.; de Vries, M. S. *J. Am. Chem. Soc.* 1999, 121, 4896-4897.
13. Piuze, F.; Mons, M.; Dimicoli, I.; Tardivel, B.; Zhao, Q. *Chem. Phys.* 2001, 270, 205-214.
14. Kim, N. J.; Jeong, G.; Kim, Y. S.; Sung, J.; Kim, S. K. *J. Chem. Phys.* 2000, 113, 10051-10055.
15. Nir, E.; Kleinermanns, K.; Grace L.; de Vries, M. S. *J. Phys. Chem. A* 2001, 105, 5106-5110.
16. Lührs, D. C.; Viallon, J.; Fischer, I. *Phys. Chem. Chem. Phys.* 2001, 3, 1827-1831.
17. Broo, A. *J. Phys. Chem. A* 1998, 102, 526-531.
18. Sobolewski, A. L.; Domcke, W.; Dedonder-Lardeux, C.; Jouvet, C. *Phys. Chem. Chem. Phys.* 2002, 4, 1093-1100.
19. Lim, E. C. *J. Phys. Chem.* 1986, 90, 6770-6777.
20. Brady, B. B.; Peteanu, L. A.; Levy, D. H. *Chem. Phys. Lett.* 1988, 147, 538-543.
21. Nir, E.; Müller, M.; Grace, L. I.; de Vries, M. S. *Chem. Phys. Lett.* 2002, 355, 59-64.

22. Kang, H.; Lee, K. T.; Jung, B.; Ko, Y. J.; Kim, S. K. *J. Am. Chem. Soc.* 2002, *124*, 12958-12959.
23. Kim, S. K.; Lee, W.; Herschbach, D. R. *J. Phys. Chem.* 1996, *100*, 7933-7937.
24. Kim, N. J.; Kang, H.; Jeong, G.; Kim, Y. S.; Lee, K. T.; Kim, S. K. *J. Phys. Chem. A* 2000, *104*, 6552-6557.
25. Kim, N. J.; Kim, Y. S.; Jeong, G.; Ahn, T. K.; Kim, S. K. *Int. J. Mass Spec.* 2002, *219*, 11-12.
26. Kang, H.; Lee, K. T.; Kim, S. K. *Chem. Phys. Lett.* 2002, *359*, 213-219.
27. Del Bene, J. E. *J. Comp. Chem.* 1981, *2*, 200-206.
28. Marian, C. M.; Schneider, F.; Kleinschmidt, M.; Tatchen, J. *Eur. Phys. J. D* 2002, *20*, 357-367.
29. Sobolewski, A. L.; Domcke, W.; Dedonder-Lardeux, C.; Jouvet, C. *Phys. Chem. Chem. Phys.* 2002, *4*, 1093-1100.
30. Hedayatullah, M. J. *Heterocyclic Chem.* 1981, *18*, 339-342.
31. Clark, L. B.; Peschel, G. G.; Tinoco, Jr., I. *J. Phys. Chem.* 1965, *69*, 3615-3618.
32. Becker, R. S.; Kogan, G. *Photochem. Photobiol.* 1980, *31*, 5-13.
33. Ismail, N.; Blancafort, L.; Olivucci, M.; Kohler, B.; Robb, M. A. *J. Am. Chem. Soc.* 2002, *124*, 6818-6819.
34. Wana, J.; Menapace, J. A.; Bernstein, E. R. *J. Chem. Phys.* 1986, *85*, 1795-1805.
35. Brealey, G. J.; Kasha, M. *J. Am. Chem. Soc.* 1955, *77*, 4462-4468.
36. Périquet, V.; Moreau, A.; Carles, S.; Schermann, J. P.; Desfrancois, C. *J. Electron. Spectrosc.* 2000, *106*, 141-151.
37. Gageot, M-P.; Ghomi, M. *J. Phys. Chem. B* 2001, *105*, 5007-5017.
38. Marian, C. M.; Schneider, F.; Kleinschmidt, M.; Tatchen, J. *Eur. Phys. J. D* 2002, *20*, 357-367.

**Resonantly enhanced two photon ionization and ZEKE spectroscopy of
jet-cooled 4-aminopyridine**

Yonggang He, Chengyin Wu, and Wei Kong*

Department of Chemistry, Oregon State University, Corvallis, Oregon

97331-4003

Journal of Chemical Physics, **2004**, *120*, 7497-7504
American Institute of Physics, Suite 1NO1, 2 Huntington Quadrangle
Melville, NY 11747-4502, USA

* Corresponding author, Kongw@chem.orst.edu, fax: 541-737-2062

4. Resonantly enhanced two photon ionization and ZEKE spectroscopy of jet-cooled 4-aminopyridine

4.1. Abstract

We report studies of supersonically cooled 4-aminopyridine (4-AP) using two-color resonantly enhanced multiphoton ionization (REMPI) and two-color zero kinetic energy (ZEKE) photoelectron spectroscopy. With the aid of *ab initio* and density functional calculations, vibrational modes of the first electronically excited state (S_1) of the neutral species and those of the cation have been assigned, and the adiabatic ionization potential has been determined to be $62291 \pm 6 \text{ cm}^{-1}$. The REMPI spectrum of the S_1 state is dominated by ring deformation modes and the inversion mode of the amino group, while the ZEKE spectra demonstrate a strong propensity of $\Delta v = 0$, where v is the vibrational quantum number of the intermediate vibronic state from S_1 . In addition, the ZEKE spectra obtained via different vibrational levels of the S_1 state contain four common features, corresponding to the activation of four different vibrational modes of the cation. These observations are explained in terms of the structural changes from the ground state to S_1 and further to the cation. The vibrational mode distributions in both the REMPI and the ZEKE spectra, the excitation energy of the S_1 state, and the ionization potential of 4-AP, are remarkably similar to those of aniline, suggesting that the electronic activity is centered on the ring.

4.2. Introduction

As model compounds of the pyrimidine bases, aminopyridines (AP) have had many biochemical applications.¹⁻³ Investigations of their electronic structures will help clarify the origin of the photochemical and photophysical properties of the nucleic acid bases. Among the three isomers of AP, the ortho- and meta-isomers have low melting points, 57 °C and 64 °C respectively, while para-aminopyridine (4-AP) has a much higher melting point of 157 °C.⁴ The relative ease in vaporization of 2-AP and 3-AP has rendered gas phase spectroscopic studies possible, and detailed descriptions of the ground and excited electronic states of the neutral and the cationic species are now available.⁵⁻¹³ In contrast, investigations on 4-AP in the gas phase have been limited. Christen *et. al.* recorded the microwave spectrum and determined that similar to the other two isomers, 4-AP is non-planar in the S_0 state.¹⁴ Kydd studied the amino inversion vibration via far IR absorption spectroscopy.¹⁵ Based on his assignment, the author concluded that the barrier to the amino inversion vibration was similar for 2- and 4-AP, while the barrier for 3-AP was substantially higher. The ionization potential (*I.P.*) of 4-AP in the gas phase was measured by several groups in the 60's and 70's using electron-impact mass spectrometry and photoelectron spectrometry.¹⁶⁻²⁰ Due to the limit of their experimental setups, conflicting data was obtained.

In this paper, we report studies of two-color two-photon resonantly enhanced multiphoton ionization (REMPI) as well as zero kinetic energy (ZEKE) photoelectron spectroscopy of 4-AP. Detailed spectroscopic analysis for the vibrational levels of the S_1 state and the ground cationic state (D_0) will be performed, with the assistance of *ab initio* and density functional calculations. From the distribution of active vibrational modes and comparisons between the ZEKE and REMPI spectra, conclusions on the structural changes upon electronic excitation and ionization will be obtained.

4.3. Experimental Section

The experimental apparatus was a standard molecular beam machine with a time of flight mass spectrometer (TOF-MS) and a pulsed valve for supersonic cooling.²¹ 4-AP was purchased from Aldrich Co. and used without further purification. The sample was housed and heated to 160 °C in the nozzle to obtain sufficient vapor pressure. The vapor

was seeded into ~ 2 atm of argon and expanded into the vacuum through a pulsed valve with a 1 mm diameter orifice. The pump laser in the 280 - 296 nm range with a pulse energy of ~ 1 mJ/pulse was generated by frequency doubling of the output from a dye laser (LAS, LDL 2051) pumped by a Nd:YAG laser (Spectra Physics GCR 230). The ionization laser in the 332-362 nm region was generated by frequency doubling of the laser output from a dye laser (LAS, LDL 20505) pumped by another Nd:YAG laser (Spectra Physics GCR 190). The absolute wavelength of each laser was calibrated using an iron hollow-cathode lamp filled with neon. The two laser beams were set to counterpropagate; and the light path, the flight tube, and the molecular beam were mutually perpendicular. The relative timing between the two laser pulses was controlled by a delay generator (Stanford Research, DG535), and the optimal signal was obtained under exact temporal overlap between the two lasers. In the ZEKE experiment, corresponding changes in the voltages of the electrodes of the mass spectrometer and the detector were made for electron detection.²² Molecules excited to the long lived Rydberg states were allowed to stay for 500 – 600 ns in the presence of a spoiling field of ~ 1 V/cm, and ionization and extraction was achieved by a pulsed electric field of ~ 16 V/cm. ZEKE electrons were then accelerated to a field-free region and detected by a chevron microchannel plate detector.

In order to assign the observed vibronic structures in both the REMPI and ZEKE spectra, we used the Gaussian 98 suite²³ to calculate the geometry and vibrational frequencies for all the involved electronic states. Density functional theory (DFT) calculations using the Becke 3LYP functional were carried out with the 6-311G++(d,p) basis set for the ground state of the neutral molecule and the cation. The calculation for the first excited state was performed at the CIS level using the same basis set. Good agreement between experimental and theoretical results was obtained when a scaling factor of 0.9 for the calculated frequencies of the S_1 state was used. No scaling factor for the cationic state was used.

4.4. Results

4.4.1. Two-color 1+1' REMPI spectrum

The two-color 1+1' REMPI spectrum of 4-AP near the origin of the $S_1 \leftarrow S_0$ electronic transition is displayed in Figure 1. The ionization laser was set at 340 nm and was temporally overlapped with the scanning resonant laser. Limited by the linewidth of the excitation laser ($\sim 3 \text{ cm}^{-1}$), we could not definitively resolve the rotational profiles of the observed features, and the resulting linewidths of most transitions are on the order of 5 cm^{-1} .

In Figure 1, the most intense peak at 34040 cm^{-1} is assigned as the band origin, and the higher energy features are assigned as transitions to excited vibrational levels of the S_1 state as listed in Table 1. The labeling of each vibrational mode is based on Varsanyi's nomenclature,²⁴ which was derived from the normal modes of benzene. However, in some instances, strong coupling between the ring and the $-\text{NH}_2$ moiety renders this type of assignment only an approximation. There are 33 normal modes in 4-AP, among which, 27 are associated with the aromatic ring and 6 are associated with the amino moiety. The stretching modes involving N-H and C-H bonds are on the order of 3000 cm^{-1} , and are therefore not observable in Figure 1. The S_1 state of 4-AP is believed to be $\pi\pi^*$ in nature (see Section 4 for further discussion), and the direction of the transition dipole moment should be in the plane of the aromatic ring. Thus only in-plane or even quanta of out-of-plane vibrational modes are symmetry allowed. To further assist assignment, we performed *ab initio* calculations on the CIS/6-311++G(d,p) level and used a scaling factor of 0.9 to compare with the experimental spectrum. However, limited by the harmonic oscillator approximation in the calculation, we could not obtain the correct value for the inversion mode I associated with the amino nitrogen. The assignment of this mode is therefore based on previous studies on aniline.^{25, 26} The shoulder on the lower energy side of the origin band by $\sim 40 \text{ cm}^{-1}$ is regarded as a hot band of this mode designated as I_1^0 . The bands at 293 and 760 cm^{-1} are assigned as allowed transitions of I_1^1 and I_0^2 with changes of even quanta. Higher harmonics of this mode are even more difficult to assign due to changes in the tunneling probability, and we make no attempt to identify the weak peaks around 1100 cm^{-1} , which might contain I_1^3 . In addition to this inversion mode, the only other observed out-of-plane vibrational mode is 10b at 350 cm^{-1} and 701 cm^{-1} with changes of even quanta.

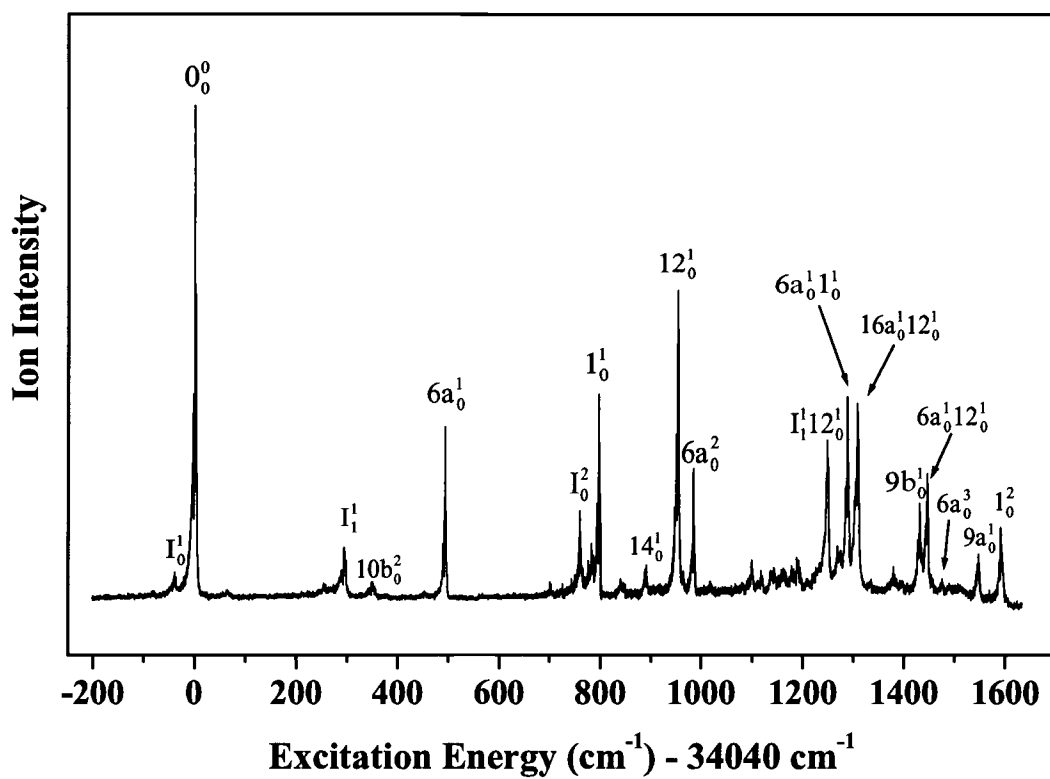


Figure 1 (1+1') REMPI spectrum of jet-cooled 4-AP.

Table 1. Observed vibrational frequencies and assignments for the S_1 state of 4-AP.

Exp.	Calc.*	Assignment and approx. description [#]
	184	$10b_0^1$, γ (ring) and NH_2 wag
	351	$16a_0^1$, γ (ring)
	437	$16b_0^1$, γ (ring) and CN wag
- 40		I_1^0 , NH_2 inversion
293		I_1^1 , NH_2 inversion
350		$10b_0^2$, γ (ring) and NH_2 wag
493	499	$6a_0^1$, β (ring)
701	697	$10b_0^4$, γ (ring) and NH_2 wag
760		I_0^2 , NH_2 inversion
797	804	1_0^1 , ring breathing
891	860	14_0^1 , ν (ring)
953	962	12_0^1 , β (ring)
984		$6a_0^2$, β (ring)
1249		$I_1^1 12_0^1$
1288		$6a_0^1 1_0^1$
1308		$16a_0^1 12_0^1$
1431	1482	$9b_0^1$, ν (ring) and β CH
1446		$6a_0^1 12_0^1$
1479		$6a_0^3$, β (ring)
1548	1567	$9a_0^1$, ν (ring) and β CH
1592		1_0^2

* The values include a scaling factor of 0.9.

[#] ν , β , and γ represent stretching, in-plane bending, and out-of-plane bending vibrations.

The REMPI spectrum in Figure 1 is dominated by three in-plane ring deformation modes of 6a, 1 and 12, their higher harmonics, and their combination bands. From comparisons with calculation results, the three strong bands below 1000 cm^{-1} can be assigned without any difficulty, and the weak peak at 891 cm^{-1} is assigned as 14_0^1 . Modes with higher fundamental frequencies are overlapped with combination bands and higher order harmonics, and assignments of these bands are assisted by correlations with the corresponding ZEKE spectra. As will be seen in the next section, with the exception of only four weak bands, we were able to obtain ZEKE spectra via fourteen of the features in Figure 1. For example, the ZEKE spectrum in Figure 4c was obtained via the excitation of the $6a_0^1 1_0^1$ band, and the resulting cation spectrum contained higher harmonics of each mode, such as $6a_0^2 1_0^1$ and $6a_0^1 1_0^2$. The assignment of the combination band at 1288 cm^{-1} in Figure 1 is therefore confirmed. In addition to combination bands, Figure 1 contains two vibrational series involving modes 6a and 1, and the Franck-Condon profiles favor the lowest vibrational level in both cases.

4.4.2. ZEKE spectra

By scanning the ionization laser while setting the resonant laser at one of the intermediate states identified in the above REMPI experiment, we obtained pulsed field ionization zero kinetic energy photoelectron spectra. In Figures 2-6, the data will be presented according to the vibrational modes of the intermediate states, and in Table 2, these observations are summarized in comparison with our calculation results. The same labeling scheme as that of the S_1 state is used in the assignment of the cationic state, and no distinction is made to explicitly represent the vibrational modes of the cation or those of the S_1 state. The identity of the intermediate level for each ZEKE spectrum is marked on the corresponding figure by a black dot. To avoid clutter, only the vibrational quantum numbers of the cationic state are labeled in the figures and tables. Limited by the linewidth of each resonant transition, unfortunately, the error in the experimental values of the ZEKE spectra is 6 cm^{-1} . No scaling factor for the vibrational frequencies of the cation in the calculation is used, and the agreement is reasonable.

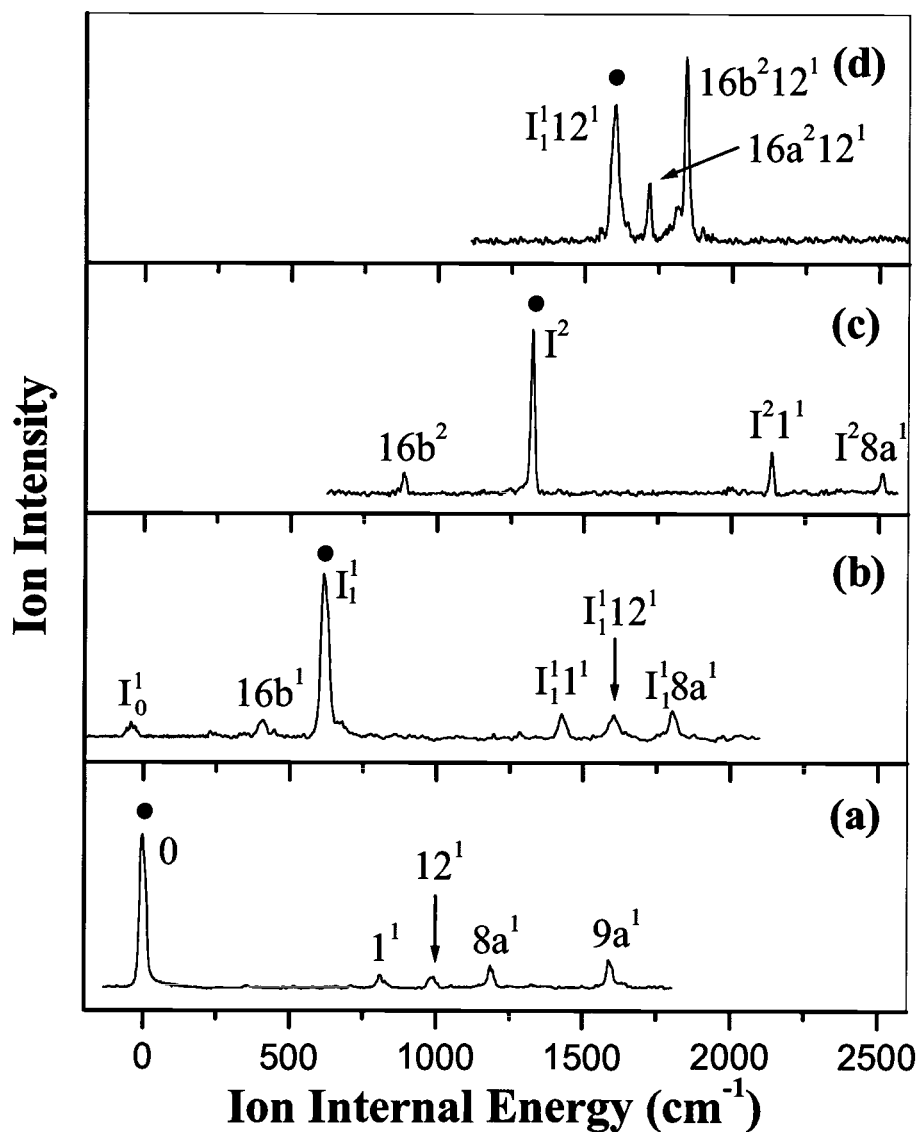


Figure 2 Two-color ZEKE spectra of 4-AP recorded via the following vibrational levels of the S_1 state as intermediate states: (a) 0^0 , (b) I_1^1 , (c) I^2 , (d) $I_1^1 12^1$. The energy is relative to the ionization threshold at 62291 cm^{-1} . The assignment in the figure refers to the vibrational levels of the cation, and the corresponding vibrational level of the intermediate state is labeled by a black dot in each panel.

Figure 2a shows the ZEKE spectrum of 4-AP recorded via the origin of the S_1 state, and the most intense peak in the spectrum corresponds to the origin of the cation. The resulting adiabatic $I.P.$, including a correction due to field ionization,²⁷ is $62291 \pm 6 \text{ cm}^{-1}$ ($7.7231 \pm 0.0007 \text{ eV}$). In contrast, the $I.P.$ value of 4-AP was first determined to be 8.97 eV in 1963 by Basila *et. al.* using electron-impact spectrometry. About ten years later, different $I.P.$ values of 9.27 eV and 8.8 eV were obtained by Groenneberg *et. al.*¹⁷ and Stefanovic *et. al.*¹⁸ using similar method. The $I.P.$ of 4-AP was also measured by Ramsey *et. al.*²⁰ using photoelectron spectrometer, and their measured value was 8.77 eV. In addition to the origin of the cation, a few weak transitions also appear in the ZEKE spectrum, corresponding to excitations of mode 1, 12, 8a, and 9a. As will be seen in the following, these modes constitute the majority of the active modes in the rest of the ZEKE spectra.

4.4.2.1. Transitions associated with the inversion mode I

Three transitions in Figure 1 are identified to be associated with the inversion mode, and their ZEKE spectra are shown in the top three panels of Figure 2. Figure 2b and 2c have remarkable resemblance, including the activation of mode 16b, mode 1, and mode 8a. This consistency further supports the present assignment. In comparison, Figure 2d has a quite different pattern; although the assignment of the $I_1^1 12^1$ band can be confirmed from the position of the same transition in Figure 2b, assignments of the other two peaks at 1718 and 1846 cm^{-1} are tentative. The supporting evidence for the present assignment is the observation of Figure 3 where the intermediate state contains one quanta of mode 12, and in all cases, no de-excitation of mode 12 is observed.

The present assignment provides information on the tunneling splittings of 4-AP. The hot band transition I_1^0 in Figure 1 is believed to originate from the higher energy component of the tunneling doublet in the ground state. In Figure 2b, this value can be further confirmed from the I_1^0 band of the cation. In contrast, Kydd reported a much higher value of 93.6 cm^{-1} based on his far IR absorption spectrum from 50 to 665 cm^{-1} .¹⁵ If our value of 36 cm^{-1} is correct, the transition between the doublet should be out of the range of the far IR experiment. Moreover, although studies of the other two isomers of AP did not directly report the values of the inversion doublets, judging from the

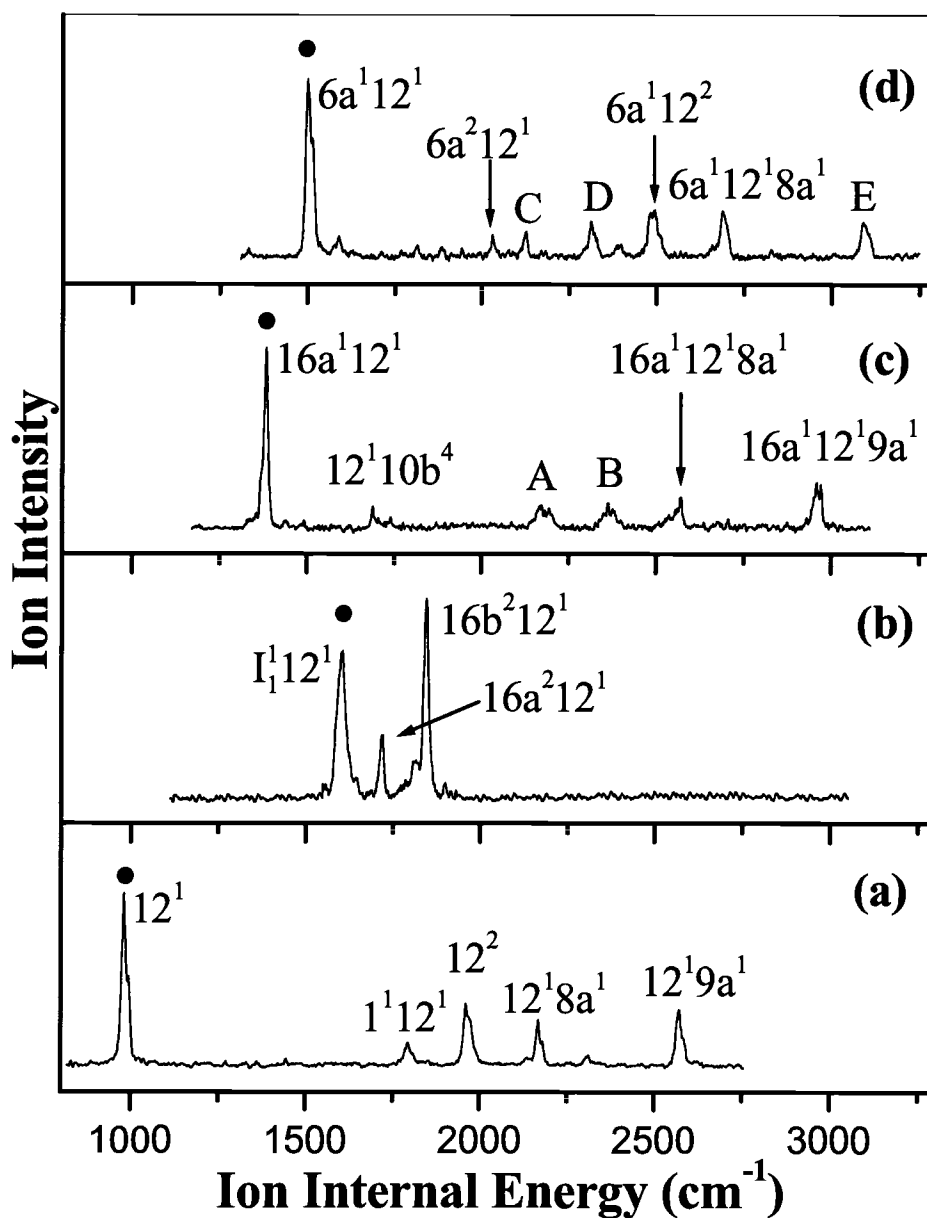


Figure 3 Two-color ZEKE spectra of 4-AP recorded via the following vibrational levels of the S_1 state as intermediate states: (a) 12^1 , (b) I^112^1 , (c) $16a^112^1$, (d) $6a^112^1$. Labels A, B, C, D, and E represent transitions $16a^112^11^1$, $16a^112^2$, $6a^1I^112^1$, $6a^11^112^1$, and $6a^112^19a^1$ respectively. Panel b is a reproduction of Figure 2d.

appearance of the hot bands in the reported spectra,^{12, 13} we believe that all three isomers have similar inversion splittings, and they are on the order of $30 - 50 \text{ cm}^{-1}$.

This new value of doublet splitting for the neutral ground state can be used to obtain the corresponding values for the S_1 and D_0 states, and to correct the vibrational frequencies of the observed bands in Table 2. The vibrational frequencies for the inversion mode of all three electronic states are compiled in Table 3. It is interesting to notice that other than the ground state, both the S_1 and the D_0 state have negative anharmonicity with no clear indications of doublet splittings. The lack of inversion splittings is a sign of planarity for the amino group, as will be discussed in Section 4.

4.4.2.2. *Transitions associated with mode 12*

Figure 3a shows the ZEKE spectrum of 4-AP taken via mode 12 of the S_1 state. The fundamental frequency of this mode for the cation is therefore determined to be 984 cm^{-1} , in agreement with the observation of Figure 2a and the calculation result. A Franck-Condon progression can be observed, although the transition to 12^3 is out of the range of this scan. In addition, excitation of mode 12 in the S_1 state activates mode 1, 8a and 9a of the cation.

Other ZEKE spectra involving mode 12 of the S_1 state are obtained via the combination bands $1^1 12^1$, $16a^1 12^1$, and $6a^1 12^1$, as shown in the top three panels of Figure 3. Assignments of the strongest features in the latter two panels are corroborated by the assignment of Figure 4a (another independent observation of the transition $6a^1 12^1$) and 6a (the frequency of mode 16a). Similar to the above case of Figure 3a, in Figure 3c and 3d, a progression of mode 12 is also observable. It is interesting to notice that the pattern for the last four features in Figure 3a, 3c, and 3d are similar, corresponding to the activation of modes 1, 12, 8a, and 9a, and this pattern is essentially a repeat of Figure 2a.

4.4.2.3. *Transitions associated with mode 6a*

Mode 6a is quite active in the REMPI spectrum, and four different intermediate states involving this mode have been chosen in the ZEKE experiment. The calculation result for this mode agrees with the experimental data remarkably well, and there is essentially no anharmonicity associated with this mode from the observed $6a^2$ transition (Table 2).

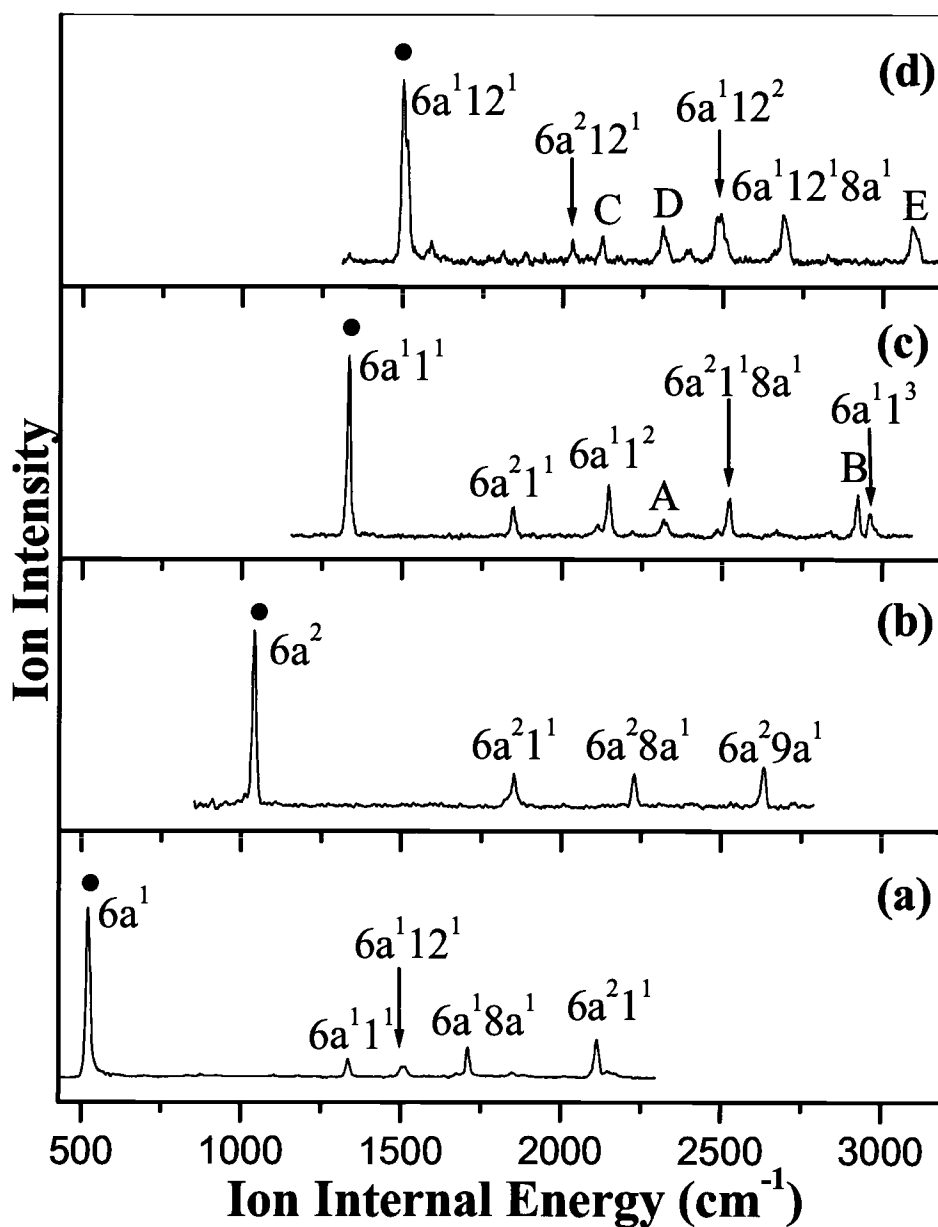


Figure 4 Two-color ZEKE spectra of 4-AP recorded via the following vibrational levels of the S_1 state as intermediate states: (a) $6a^1$, (b) $6a^2$, (c) $6a^11^1$, (d) $6a^112^1$. Labels A, B, C, D, and E represent $6a^11^112^1$, $6a^11^19a^1$, $6a^11^112^1$, $6a^11^112^1$, and $6a^112^19a^1$ respectively. Panel d is a reproduction of Figure 3d.

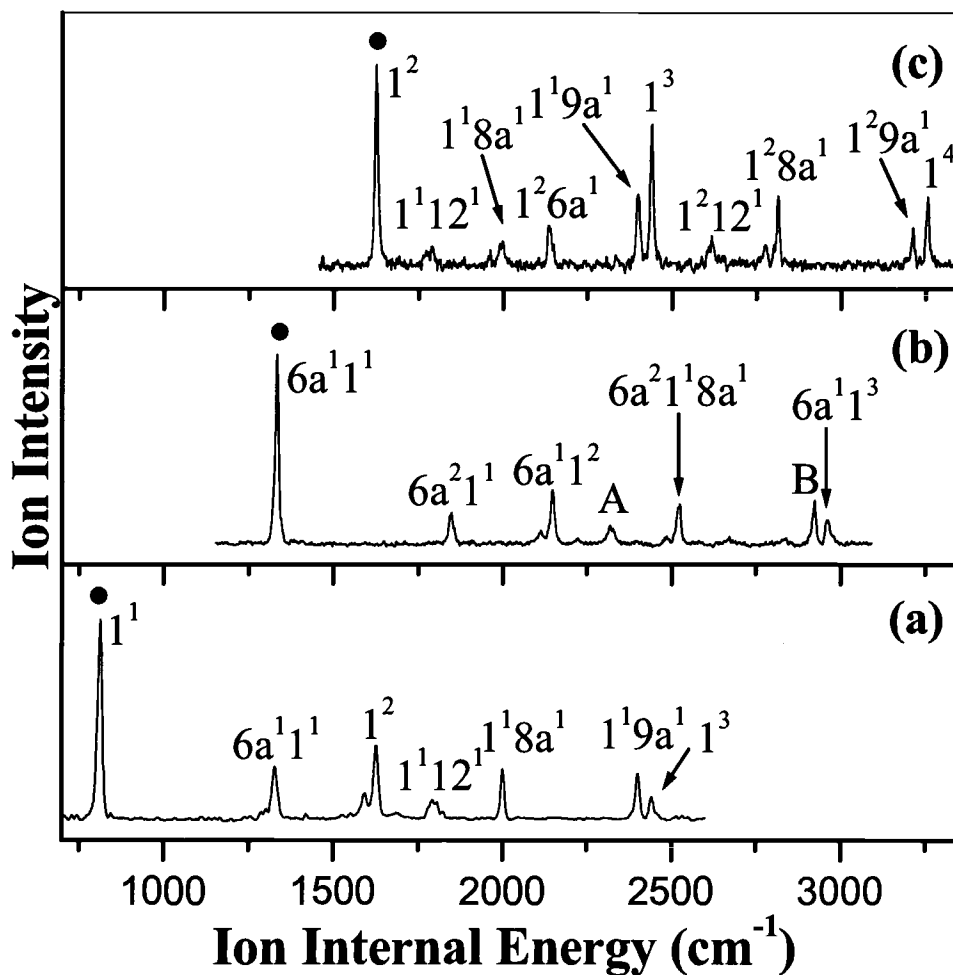


Figure 5 Two-color ZEKE spectra of 4-AP recorded via the following vibrational levels of the S_1 state as intermediate states: (a) 1^1 , (b) $6a^11^1$, (c) 1^2 . Labels A and B represent transitions $6a^11^112^1$, and $6a^11^19a^1$ respectively. Panel b is a reproduction of Figure 4c.

Although in the REMPI spectrum of Figure 1, a vibrational progression involving three members of this mode is clearly observable, the ZEKE spectra of Figure 4a and 4b do not exhibit similar progressions. The normal coordinates of this mode for the S_1 and the D_0 states must be essentially identical, resulting in a strong propensity for $\Delta\nu = 0$. The ZEKE spectra obtained via the combination bands in Figure 4c and 4d, however, do contain higher harmonics of the 6a mode in the combination bands of the cation. Anharmonic coupling with other modes seems necessary to provoke higher members of the 6a mode.

In three of the four panels of Figure 4, a common pattern involving the activation of modes 1, 12, 8a, and 9a can be observed, while in panel b, the missing $6a^212^1$ transition could be a result of our limited sensitivity. This pattern is again remarkably similar to that of Figure 3 and Figure 2a. The similarity between the spectra associated with mode 6a (Figure 4) and 12 (Figure 3) should not be a result of accidental degeneracy, since the frequency for mode 12 differs from twice the frequency of mode 6a by $\sim 60\text{ cm}^{-1}$.

4.4.2.4. *Transitions associated with mode 1*

The ring breathing mode 1 is not only active in the REMPI spectrum, but also observable in twelve of the fourteen ZEKE spectra reported here. Assignments of the spectra in all three panels of Figures 5 are straightforward, with each containing a vibrational progression of mode 1 and demonstrating a propensity of $\Delta\nu = 0$. Our calculation result of 810 cm^{-1} agrees remarkably well with the experimental observation. From the values of the higher harmonics (Table 2), essentially no anharmonicity is observable. In addition, all three spectra show similar patterns with regard to the activation of other modes, including mode 6a, 12, 8a, and 9a. In Figure 5c, some of the vibrational energy in mode 1 of the S_1 state is lost to modes 12, 8a, and 9a of the cation.

4.4.2.5. *Other bands and summary of the ZEKE spectra*

A consistent theme among the ZEKE spectra emerges from the above analysis. All spectra obey the propensity for $\Delta\nu = 0$, and in some cases, this propensity is manifested in its extreme form with only the harmonics satisfying $\Delta\nu = 0$ observable. Moreover,

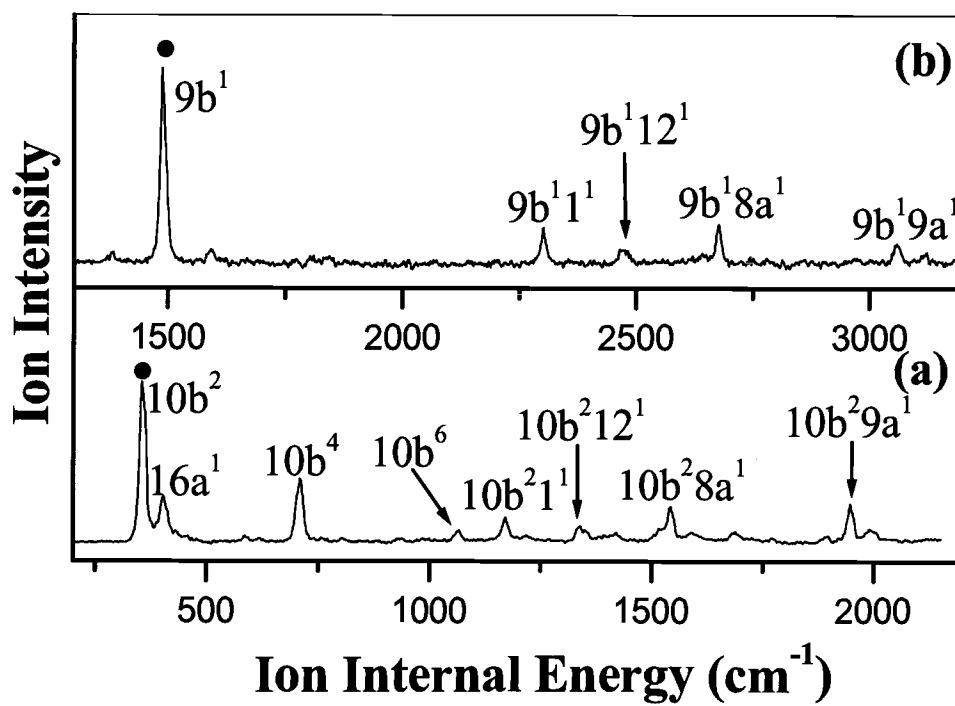


Figure 6 Two-color ZEKE spectra of 4-AP recorded via the intermediate vibrational levels (a) $10b^2$ and (b) $9b^1$ of the S_1 state.

Table 2. Observed vibrational frequencies and assignments in the ZEKE spectra of 4-AP.

Intermediate level in the S ₁ state							Assignment
0 ₀ ⁰	I ₁ ¹	10b ₀ ²	6a ₀ ¹	I ₀ ²	1 ₀ ¹	12 ₀ ¹	
0							origin
		355					10b ²
		404					16a ¹
	408*						16b ¹
			521				6a ¹
	616*						I ¹
		708					10b ⁴
809					814		1 ¹
				886			16b ²
987						981	12 ¹
		1064					10b ⁶
		1171					10b ² 1 ¹
1186							8a ¹
				1324			I ²
			1332		1326		6a ¹ 1 ¹
		1339					10b ² 12 ¹
	1427						I ¹ 1 ¹
		1514					6a ¹ 12 ¹
		1542					10b ² 8a ¹
1587					1592		9a ¹
	1604						I ¹ 12 ¹
					1629		1 ²
		1689					10b ⁴ 12 ¹
		1708					6a ¹ 8a ¹
					1792	1793	1 ¹ 12 ¹
	1800						I ¹ 8a ¹
		1847					6a ² 1 ¹
		1949					10b ² 9a ¹
						1961	12 ²
		1992					10b ² 1 ²
					2001		1 ¹ 8a ¹
			2113				6a ¹ 9a ¹
				2138			I ² 1 ¹
						2168	12 ¹ 8a ¹
						2311	6a ¹ 1 ¹ 12 ¹
					2400		1 ¹ 9a ¹
					2444		1 ³
				2514			I ² 8a ¹
						2573	12 ¹ 9a ¹

* The corresponding vibrational frequencies for these peaks should be 440 and 648 cm⁻¹ taking into account the contribution of the hot band.

Table 2. Observed vibrational frequencies and assignments in the ZEKE spectra of 4-AP.
(continued)

Intermediate level in the S ₁ state							Cal.	Assignment
6a ₀ ²	I ₁ ¹ 12 ₀ ¹	6a ₀ ¹ 1 ₀ ¹	16a ₀ ¹ 12 ₀ ¹	9b ₀ ¹	6a ₀ ¹ 12 ₀ ¹	1 ₀ ²		
1040								6a ₀ ²
		1332						6a ₀ ¹ 1 ₀ ¹
			1385					16a ₀ ¹ 12 ₀ ¹
				1489			1491	9b ₀ ¹
					1500			6a ₀ ¹ 12 ₀ ¹
	1604							I ₁ ¹ 12 ₀ ¹
						1624		1 ₀ ²
			1691					12 ₀ ¹ 10b ₀ ⁴
	1718*							16a ₀ ² 12 ₀ ¹
						1788		1 ₀ ¹ 12 ₀ ¹
						2000		1 ₀ ¹ 8a ₀ ¹
	1846*							16b ₀ ² 12 ₀ ¹
1853		1844						6a ₀ ² 1 ₀ ¹
					2030			6a ₀ ² 12 ₀ ¹
		2113						6a ₀ ¹ 9a ₀ ¹
					2127			6a ₀ ¹ I ₁ ¹ 12 ₀ ¹
						2134		1 ₀ ² 6a ₀ ¹
		2148						6a ₀ ¹ 1 ₀ ²
			2173					12 ₀ ¹ 8a ₀ ¹
2225								6a ₀ ² 8a ₀ ¹
				2300				9b ₀ ¹ 1 ₀ ¹
		2318			2313			6a ₀ ¹ 1 ₀ ¹ 12 ₀ ¹
			2363					16a ₀ ¹ 12 ₀ ²
						2397		1 ₀ ¹ 9a ₀ ¹
						2440		1 ₀ ³
				2483				9b ₀ ¹ 12 ₀ ¹
					2495			6a ₀ ¹ 12 ₀ ²
		2526						6a ₀ ¹ 1 ₀ ¹ 8a ₀ ¹
			2574					16a ₀ ¹ 12 ₀ ¹ 8a ₀ ¹
						2616		1 ₀ ² 12 ₀ ¹
2632								6a ₀ ² 9a ₀ ¹
				2677				9b ₀ ¹ 8a ₀ ¹
					2687			6a ₀ ¹ 12 ₀ ¹ 8a ₀ ¹
						2812		1 ₀ ² 8a ₀ ¹
	2922							6a ₀ ¹ 1 ₀ ¹ 9a ₀ ¹
		2958						16a ₀ ¹ 12 ₀ ¹ 9a ₀ ¹
	2964							6a ₀ ¹ 1 ₀ ³
				3063				9a ₀ ¹ 9b ₀ ¹
					3088			6a ₀ ¹ 12 ₀ ¹ 9a ₀ ¹
						3213		1 ₀ ² 9a ₀ ¹
						3256		1 ₀ ⁴

regardless of the vibrational excitation in the S_1 state, only four additional modes are activated in the ZEKE spectra, and they are modes 1, 12, 8a, and 9a.

As further illustrations of these two general features, Figure 6 shows two ZEKE spectra via the $10b^2$ and the $9b$ vibrational levels. In Figure 6a, a progression with an increment of two quanta of the $10b$ mode is observable, while in Figure 6b, only the $9b^1$ band exists, with no higher harmonics of the $9b$ mode. The rest of the features in the two figures are essentially identical, containing activations of modes 1, 12, 8a, and 9a. In Figure 6a, the optically inactive out-of-plane bending mode $16a$ is also observed, and its appearance might be related to its close proximity with $10b^2$.

Table 4 lists the average values for all the observed fundamental and higher harmonics of the cation. Given the experimental accuracy of 6 cm^{-1} , the agreement between the calculation results and our experimental values is impressive. Other than the inversion mode, the rest of the modes show little anharmonicity, implying high rigidity in the structure of the cation.

4.5. Discussion

In Table 3, only the ground electronic state demonstrates clear tunneling splitting with respect to the amino nitrogen, while both the S_1 and D_0 states seem to be of planar symmetry. To confirm this speculation, we performed DFT calculations on the B3LYP level for the S_0 and D_0 states, and *ab initio* calculations at the CIS level for the S_1 state. The resulting geometry parameters are listed in Table 5 and the numbering scheme is shown in Figure 7. In the S_0 state, the angle between the amino group and the ring plane is calculated to be 32.25° , which agrees with the X-ray crystallography study,²⁸ while the corresponding values for the S_1 and D_0 states are close to zero. The symmetry of 4-AP is therefore changed from C_s for the puckered ground state to C_{2v} for the planar S_1 state. For the cation, the pyridine nitrogen protrudes slightly out of the plane, suggesting a loss of aromaticity for the D_0 state. Our CIS calculation shows $\pi\pi^*$ character for the S_1 state. Moreover, the nonbonding electron of the amino nitrogen participates in the conjugation with the aromatic ring, inducing a double-bond character between C4 and N7. In Table 5, the most prominent change during the $S_1 \leftarrow S_0$ transition is the large decrease of the C4-N7 bond length. In addition, the bond length for C2-C3 is slightly decreased while the

Table 3. Energy levels of the inversion mode for the S_0 , S_1 and D_0 states.

State	Vibrational Quanta	
	1	2
S_0	40	
S_1	333	760
D_0	648	1324

Table 4. Average values of the observed fundamental and higher harmonics of the cation.

mode	Calc.	Vibrational quanta					
		1	2	3	4	5	6
10b			355		708		1064
16a	340	404					
16b	385	440	886				
6a	519	521	1040				
I	655	648	1324				
1	810	812	1626	2442	3256		
12	942	984	1961				
8a	1214	1186					
9b	1491	1489					
9a	1566	1590					

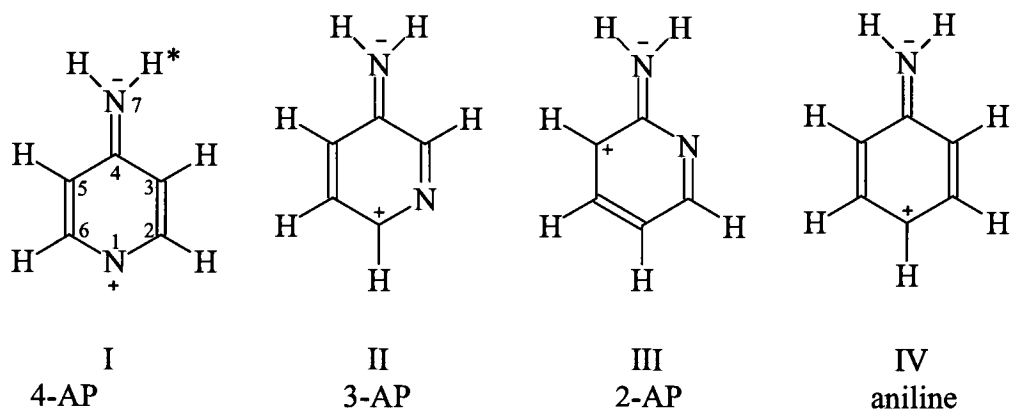


Figure 7 Resonance structures of 4-AP, 3-AP, 2-AP and aniline in the S_1 state.

bond length for C3-C4 is slightly increased. These changes in the ring structure are responsible for the activation of the ring breathing mode 1 and the in-plane bending modes 6a and 12. The change in planarity upon photoexcitation is responsible for the observation of the inversion mode and the out of plane bending mode 10b in Figure 1. For both the planar S_1 and the near planar D_0 states, Table 3 shows unusual (negative) anharmonicity. The increased spacing between adjacent vibrational levels of this mode in these two electronic states should be related to the essentially flat potential surfaces with respect to the puckering of the amino moiety. This anharmonic potential should be a direct result of the diminished barrier for inversion and thereby the flattened and widened bottom of the potential well. It is worth noting that in the studies of 2-AP and 3-AP, weak hot bands were also observed in the corresponding REMPI spectra.^{12, 13} Although these hot bands were not assigned in the initial reports, their similarities to our results on 4-AP indicate that they were due to the same inversion mode with similar inversion splittings.

The $D_0 \leftarrow S_1$ ionization involves the removal of the π^* electron. While the amino group remains planar in both states, a slight nonplanarity with the ring nitrogen atom bending out of the plane by about 5° occurs in the D_0 state. The reduction in the degree of conjugation for the π electron cloud of the pyridine ring has apparently resulted in a change in the hybridization of the ring nitrogen. From Table 5, however, this change is so insignificant that it barely affects the geometry of the molecular frame, hence a strong propensity for $\Delta v = 0$ is observed in all ZEKE spectra. The activation of the in-plane ring deformation modes in the ZEKE spectra is a result of the slightly elongated molecular frame upon ionization.

The experimental transition energies for $S_1 \leftarrow S_0$ and the adiabatic *I.P.* of 4-AP, 3-AP, 2-AP and aniline are listed in Table 6. The origin of the $S_1 \leftarrow S_0$ transition of 4-AP is higher by 569 and 992 cm^{-1} than that of 2-AP and 3-AP,¹¹⁻¹³ while it is close to that of aniline.^{25, 26} Moreover, both the observed active vibrational modes and their frequencies in the S_1 and the D_0 states of 4-AP correspond well to those of aniline. This comparison further confirms that the $S_1 \leftarrow S_0$ transition mostly involves ring electrons, i. e., $\pi\pi^*$ in nature, while the lone pair electrons of the ring nitrogen are inconsequential. Based on Mulliken population analysis,²⁹ the total atomic charge on the amino nitrogen atom is

Table 5. Molecular geometry parameters of 4-AP in the S_0 , S_1 , and D_0 states.

	S_0	S_1	D_0
<i>Bond length (Å)</i>			
N1-C2	1.338	1.329	1.346
C2-C3	1.389	1.373	1.377
C3-C4	1.403	1.429	1.431
C4-N7 (C-NH ₂)	1.383	1.311	1.333
<i>dihedral angle (°)</i>			
H*N7C4C3	-20.332	-0.012	-0.222
N1C2C3C4	0.025	-0.013	-4.924
angle between the ring and -NH ₂	32.25	0.02	1.33

Table 6. Measured electronic transitions and adiabatic ionization potentials of aniline, 2-AP, 3-AP, and 4-AP.

	$S_1 \leftarrow S_0$ (cm ⁻¹)	Adiabatic I.P. (cm ⁻¹)
Aniline ^{25, 26}	34029	62271
2-AP ^{11, 13}	33471	65411
3-AP ¹²	33048	65229
4-AP	34040	62291

changed from -0.294 in the S_0 state to -0.600 in the S_1 state for 4-AP, while the ring nitrogen is positively charged in the S_1 state. In contrast, for 2-AP and 3-AP, it is the ring carbon atoms that are electron deficient. Figure 7 shows the most stable resonance structures of the three isomers and that of aniline. This difference in the charge distribution of the S_1 state might be related to the difference in the excitation energy of the $S_1 \leftarrow S_0$ transition. A higher energy is likely required to place a positive charge on the more electrophilic nitrogen atom than on a carbon atom.

While the excitation energies to the S_1 states of 4-AP and aniline are higher than those of 2- and 3-AP, the opposite is true for the ionization energies.²⁵ Lin *et. al.* compared the *I.P.* values of 3-AP, 2-AP and aniline,¹² and they attributed the difference in ionization energy to the difference in electron density around the N atom of the amino group for the neutral ground state. However, our Mulliken population analysis does not support this argument. It is worth noting that due to the method for electron partition in the Mulliken analysis, the net charge distribution is skewed towards the nucleophilic atom. The above charge analysis should be treated with caution. Nevertheless, the similarity in the transition energy of $S_1 \leftarrow S_0$ and the adiabatic *I.P.* of 4-AP with aniline indicates that the replacement of the para-carbon atom on the ring by a nitrogen atom only slightly affects the electronic property of the molecule.

4.6. Conclusion

We report spectroscopic information on the first electronically excited state and the ground state of the cation of 4-AP obtained using two-color REMPI and ZEKE techniques. Our observation includes in-plane vibrational modes, one out of plane vibrational mode, and the inversion mode for both the S_1 and the D_0 states. Overall, these assignments are in good agreement with *ab initio* and DFT calculations. The electronic excitation to the S_1 state and further ionization to D_0 involve a π electron on the aromatic ring, and the resulting systems demonstrate increased conjugation with the amino group. The similarity in geometry for S_1 and D_0 results in a strong propensity for ionization from the S_1 state, i. e., the dominant feature in the ZEKE spectrum obtained via an intermediate vibrational level of the S_1 state corresponds to the same vibrational level of the cation. The adiabatic ionization energy of 4-AP in the gas phase is determined to be

$62291 \pm 6 \text{ cm}^{-1}$ ($7.7231 \pm 0.0007 \text{ eV}$). This value is close to that of aniline, while it is substantially different from those of the other two isomers of AP. A similar result of comparison exists for the excitation energy of the S_1 state and for the vibrational mode distribution. Analysis of charge distributions of the ground state for the three isomers of AP and aniline does not provide a clear clue as to the origin of this similarity with aniline.

4.7. Acknowledgements

This work was supported by the National Science Foundation, Division of Chemistry. Acknowledgment is made to the Donors of The Petroleum Research Fund, administered by the American Chemical Society, for partial support of this research. Wei Kong is an Alfred P. Sloan research fellow.

4.8. References

- ¹ R. Llinas, K. Walton, and V. Bohr, *Biophys. J.*, **16**, 83 (1976).
- ² A. Kon, K. Takagaki, H. Kawasaki, T. Nakamura, and M. Endo, *J. Biochem.*, **110**, 132 (1991).
- ³ D. Agoston, P. Hargittai, and A. Nagy, *J. Neurochem.*, **41**, 745 (1983).
- ⁴ Z. Eckstein, E. Lipczynska-Kochany, and J. Krzeminski, *Heterocycles* **20**, 1899 (1983).
- ⁵ J. M. Hollas, H. Musa, and T. Ridley, *J. Mol. Spectrosc.* **104**, 89 (1984).
- ⁶ R. D. Gordon, D. Clark, J. Crawley, and R. Mitchell, *Spectrochim. Acta A*, **40**, 657 (1984).
- ⁷ J. W. Hager, G. W. Leach, D. R. Demmer, and S. C. Wallace, *J. Phys. Chem.* **91**, 3750 (1987).
- ⁸ P. Carmona, M. Molina, R. Escobar, *Spectrochim. Acta A*, **49**, 1 (1993).
- ⁹ B. Kim, C. P. Schick, and P. M. Weber, *J. Chem. Phys.* **103**, 6903 (1995).
- ¹⁰ S. Akyuz, *J. Mol. Spectrosc.* **449**, 23 (1998).
- ¹¹ J. L. Lin, R. H. Wu, and W. B. Tzeng, *Chem. Phys. Lett.* **353**, 55 (2002).
- ¹² J. L. Lin, R. H. Wu, and W. B. Tzeng, *Chem. Phys.* **280**, 191 (2002).
- ¹³ S. J. Baek, K-W. Choi, Y. S. Choi, and S. K. Kim, *J. Chem. Phys.* **117**, 2131 (2002).
- ¹⁴ D. Christen, D. Norbury, and D. Lister, and P. Palmieri, *J.C.S. Faraday II*, **71**, 438 (1975).
- ¹⁵ R. A. Kydd, *Spectrochim. Acta*, **35A**, 409 (1979).
- ¹⁶ M. R. Basila, and D. J. Clancy, *J. Phys. Chem.* **67**, 1551 (1963).
- ¹⁷ T. Groenneberg, and K. Undhaim, *Tetrahedron Lett.* **31**, 3193 (1972).
- ¹⁸ D. Stefanovic, and H. F. Gruetzmacher, *Organic Mass Spectrometry* **9**, 1052 (1974).
- ¹⁹ T. Kobayashi, and S. Nagakura, *Journal of Electron Spectroscopy and Related Phenomena* **4**, 207 (1974).

- ²⁰ B. G. Ramsey, and F. A. Walker, *J. Am. Chem. Soc.* **96**, 3314 (1974).
- ²¹ Y. He, C. Wu, and W. Kong, *J. Phys. Chem. A* **107**, 5145 (2003).
- ²² X. Peng and W. Kong, *J. Chem. Phys.* **117**, 9306 (2002).
- ²³ GAUSSIAN 98, Revision A. 7, M. J. Frisch, G. W. Trucks, H. B. Schlegel, G. E. Scuseria, M. A. Robb, J. R. Cheeseman, V. G. Zakrzewski, J. A. Montgomery, Jr., R. E. Stratmann, J. C. Burant, S. Dapprich, J. M. Millam, A. D. Daniels, K. N. Kudin, M. C. Strain, O. Farkas, J. Tomasi, V. Barone, M. Cossi, R. Cammi, B. Mennucci, C. Pomelli, C. Adamo, S. Clifford, J. Ochterski, G. A. Petersson, P. Y. Ayala, Q. Cui, K. Morokuma, D. K. Malick, A. D. Rabuck, K. Raghavachari, J. B. Foresman, J. Cioslowski, J. V. Ortiz, A. G. Baboul, B. B. Stefanov, G. Liu, A. Liashenko, P. Piskorz, I. Komaromi, R. Gomperts, R. L. Martin, D. J. Fox, T. Keith, M. A. Al-Laham, C. Y. Peng, A. Nanayakkara, C. Gonzalez, M. Challacombe, P. M. W. Gill, B. Johnson, W. Chen, M. W. Wong, J. L. Andres, C. Gonzalez, M. Head-Gordon, E. S. Replogle, and J. A. Pople, Gaussian, Inc., Pittsburgh, Pennsylvania, 1998.
- ²⁴ G. Varsanyi, *Assignment of Vibrational Spectra of Seven Hundred Benzene Derivatives* (Wiley, New York, 1974).
- ²⁵ X. Song, M. Yang, E. R. Davidson, and J. P. Reilly, *J. Chem. Phys.* **99**, 3224 (1993).
- ²⁶ J. L. Lin, and W. B. Tzeng, *J. Chem. Phys.* **115**, 743 (2001).
- ²⁷ E. W. Schlag, *ZEKE Spectroscopy* (Cambridge University Press, Cambridge, 1998).
- ²⁸ M. Chao, and E. Schempp, *Acta Crystallogr. B* **33**, 1557 (1977).
- ²⁹ R. S. Mulliken, *J. Chem. Phys.* **23**, 1833 (1955).

**Two-color two-photon REMPI and ZEKE photoelectron spectroscopy
of jet-cooled 2-chloropyrimidine**

Yonggang He, Chengyin Wu, and Wei Kong*

*Department of Chemistry, Oregon State University,
Corvallis, Oregon 97331-4003*

Chemical Physics Letters, **2004**, *391*, 38-43

* Corresponding author, email: wei.kong@oregonstate.edu, fax: 541-737-2062

5. Two-color two-photon REMPI and ZEKE photoelectron spectroscopy of jet-cooled 2-chloropyrimidine

5.1. Abstract

We report studies of supersonically cooled 2-chloropyrimidine (2-CIP) using two-color resonantly enhanced multiphoton ionization (REMPI) and two-color zero kinetic energy (ZEKE) photoelectron spectroscopy. With the aid of *ab initio* and density functional calculations, vibrational modes of the first electronically excited state (S_1) of the neutral species and those of the ground state cation (D_0) have been assigned, and the adiabatic ionization potential has been determined to be $77106 \pm 4 \text{ cm}^{-1}$ ($9.5600 \pm 0.0005 \text{ eV}$). These results will be discussed in comparison with pyrimidine and other related compounds. Although the rate of intersystem crossing is affected by halosubstitution, 2-CIP and pyrimidine have qualitatively similar photophysical behaviors.

5.2. Introduction

Diazines, in particular pyrimidine, have attracted considerable attention in recent years due to their importance in biological science [1] - [11]. The photochemistry and photophysics of these species and their derivatives are of direct relevance to the photostability of nucleic acid bases. Halogenated pyrimidines, in particular, can undergo photochemical hydration and dimerization accompanied by dehalogenation under UV irradiation [12] - [14]. Information on electronic excitation and ionization, both in terms of spectroscopic data and dynamical behavior, is therefore of fundamental value to the understanding of photoreaction mechanisms of these species. However, gas phase experimental data that are pertinent to the intrinsic properties of these species are rather limited. In this work, we chose to investigate 2-chloropyrimidine (2-ClP) using mature gas phase spectroscopic techniques, such as resonantly enhanced multiphoton ionization (REMPI) and zero kinetic energy photoelectron spectroscopy (ZEKE) [15]. A chlorine atom is generally believed to be a strong electron-withdrawing group through σ bonding, while it can also donate an electron to the aromatic ring by forming a conjugated π bond. The effect of chlorine substitution will manifest from the changes in energy levels, vibrational frequencies and other spectroscopic and dynamic behaviors. Our analysis will be placed in the context of a series of polar aromatic compounds, so that generalization on the electronic excitation and photochemical behavior can be achieved.

We report two-color two-photon REMPI and ZEKE spectroscopy of 2-ClP via five intermediate vibronic states. To assist spectroscopic assignments, we have also performed *ab initio* and density functional theory (DFT) calculations. Essentially all the observed vibrational modes in both the first excited electronic state (S_1) and the ground cationic state (D_0) are assigned without ambiguity. The adiabatic ionization energy is determined from the ZEKE spectra. Our analysis of the vibronic structures of both the REMPI and the ZEKE spectra reinforces our previous observation in 4-aminopyridine [16], i. e., the molecular frame remains largely intact from the ground electronic state to S_1 and further to D_0 . The propensity for maintaining the vibrational excitation of the intermediate state is again illustrated.

5.3. Experimental Setup

The experimental apparatus has been reported in a previous publication [16]. Briefly, it consisted of a pulsed molecular beam source for supersonic cooling and a time-of-flight mass spectrometer (TOF-MS), which could be converted into a pulsed field ionization (PFI) zero kinetic energy photoelectron spectrometer. The sample 2-CIP was purchased from Aldrich Co. and used without further purification. A small amount of the sample was housed and heated to 50 °C in the nozzle, and the stagnation pressure of the argon carrier gas was 2 atm. The pulsed valve had an orifice of 1 mm in diameter, and the repetition rate was 10 Hz. The two tunable UV laser beams were generated by two sets of Nd:YAG pumped dye lasers equipped with frequency doubling crystals (Spectra Physics GCR 230 and GCR 190; Laser Analytical Systems, LDL 2051 and LDL 20505). The absolute wavelength of each laser was calibrated using an iron hollow-cathode lamp filled with neon. The relative timing between the two lasers was controlled by a delay generator (Stanford Research, DG535), and the temporal overlap was confirmed from a photodiode with a subnanosecond response time. The two laser beams were set to counterpropagate; and the light path, the flight tube, and the molecular beam were mutually perpendicular. In the REMPI experiment, ionization occurred in the presence of an extraction electric field, and potential power saturation was monitored by checking the power dependence of the overall ion signal. In the ZEKE experiment, molecules excited to the ZEKE states experienced a delay of 500 – 600 ns in the presence of a spoiling field of ~ 1 V/cm, and the ionization pulse was ~ 16 V/cm.

All calculations were carried out using the Gaussian 98 suit [17]. For the ground state of both the neutral species and the cation, density functional theory calculations using the Becke 3LYP function at the 6-311G++(d,p) level were carried out for structural optimization and harmonic frequencies. The excited state geometry and harmonic frequencies were obtained at the CIS level using the same basis set, and a scaling factor of 0.91 was used for the assignment of the vibrational modes of the S_1 state.[18]

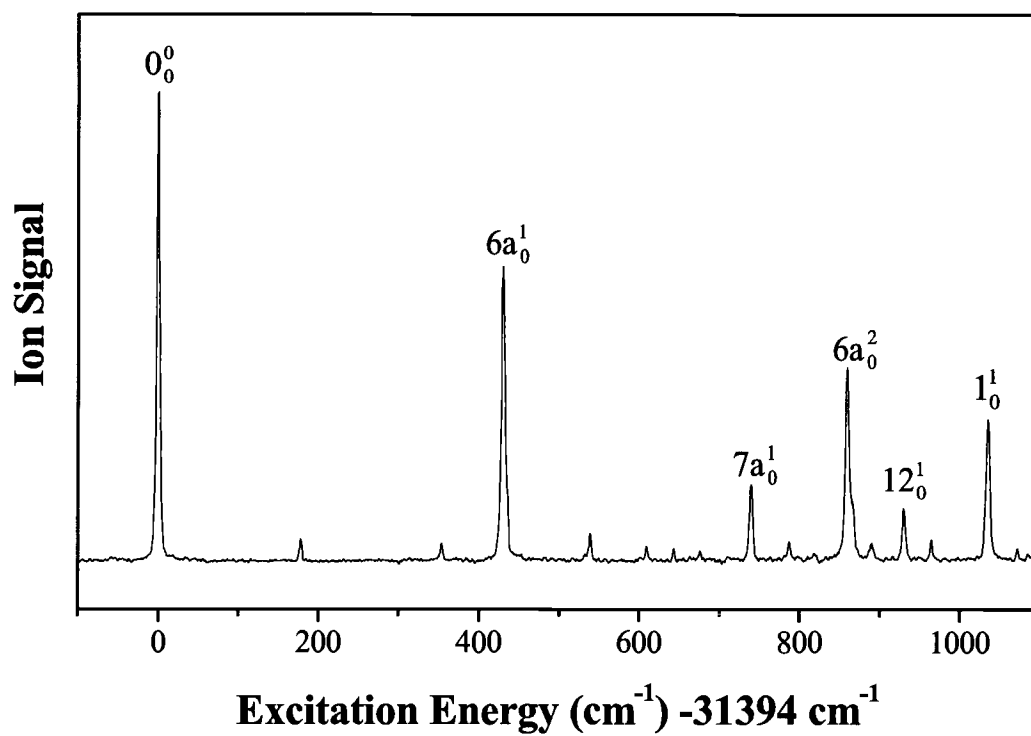


Figure 5.1 $(1+1')$ REMPI spectrum of jet-cooled 2-ClP.

5.4. Results

5.4.1. REMPI spectrum

Fig. 1 shows the two-color two-photon REMPI spectrum of 2-CIP near the origin of the $S_1 \leftarrow S_0$ electronic transition. In this experiment, the ionization laser was set at 218 nm and was temporally overlapped with the scanning resonant laser. The two isotopes of chlorine were observable from the mass spectrum of the parent ions, and only the ^{35}Cl parent ion was monitored by setting the time gate on the corresponding mass peak. Among all the observed vibronic transitions, only one feature demonstrated clear isotope effect, and the result will be presented in the next section. The linewidth of each vibronic transition is on the order of 3 - 5 cm^{-1} , although the linewidth of the excitation lasers were no more than 0.2 cm^{-1} . Unresolved rotational profiles are suspected. In Fig. 1, the most prominent peak at 31393.8 cm^{-1} is assigned as the origin of the S_1 state. Higher energy bands are transitions to excited vibrational levels in the S_1 state.

Table I summarizes the observed vibronic transitions together with our assignment. Following the study on pyrimidine [1][9], we adopted Varsanyi's nomenclature in the labeling of the normal modes [19]. Our *ab initio* and DFT calculations indicate that 2-CIP is planar and belongs to the C_{2v} point group in both the S_0 and the S_1 state. Similar to pyrimidine, the $S_1 \leftarrow S_0$ transition is electric dipole allowed with a transition dipole perpendicular to the molecular plane, i. e., ${}^1B_1 \leftarrow {}^1A_1$ (π^*n) in nature. Among the 24 normal modes, only totally symmetric vibrational modes that involve in-plane ring deformation or even-quanta of out-of-plane modes are symmetry allowed. Moreover, high frequency vibrations involving C-H stretching motions are not observable within the range of our spectrum. In Table 1, the vibrational frequencies for the S_1 state from calculation include a scaling factor of 0.91, and the comparison between theory and experiment is remarkable. The intense bands at 430, 740, 930, and 1035 cm^{-1} are assigned as in-plane ring vibrations $6a_0^1$, $7a_0^1$, 12_0^1 , and 1_0^1 . Weak transitions at 354 and 539 cm^{-1} are due to out-of-plane modes $10b_0^2$ and $16a_0^2$ respectively. This vibronic pattern is similar to that of 4-aminopyridine [16], with modes 6a, 12, and 1 being the most active in the REMPI spectrum. It is interesting to notice that in Table 1, some low

Table 5.1. Observed vibrational frequencies and assignments for the S_1 state of 2-ClP.

Exp.	Calc.*	Assignment and approx. description #
0		0_0^0 , band origin
178	178	$10b_0^1$, γ (ring)
	262	$16a_0^1$, γ (ring)
354		$10b_0^2$, γ (ring)
430	426	$6a_0^1$, β (ring)
539		$16a_0^2$, γ (ring)
610		$6a_0^1 10b_0^1$
740	732	$7a_0^1$, ν (ring) + σ (C-Cl)
788		$6a_0^1 10b_0^2$
860		$6a_0^2$, β (ring)
890		$16a_0^2 10b_0^2$
930	931	12_0^1 , ν (ring)
965	978	$19b_0^1$, ν (ring)
1035	1021	1_0^1 , ring breathing

* The values include a scaling factor of 0.91.

ν , β , and γ represent stretching, in-plane bending, and out-of-plane bending vibrations, respectively.

frequency symmetry forbidden bands, such as $10b_0^1$ and its combination bands, are also observable. Weak vibronic coupling is therefore suspected.

The two isotopomers associated with ^{35}Cl and ^{37}Cl are mostly indistinguishable in vibrational frequency, except for the 6a mode. This result should be attributed partially to the relatively low resolution of our experiment and, more importantly, to the nature of the observed vibrational modes. The transition $6a_0^1$ occurs at 430 cm^{-1} for ^{35}Cl and at 424 cm^{-1} for the ^{37}Cl isotopomer, while the corresponding second harmonic occurs at 860 cm^{-1} and 847 cm^{-1} . This change in vibrational frequency corresponds to a change in effective mass of 2.8 %. If we assume that mode 6a involves only Cl-ring stretch, the change in the effective mass should be 3.7 %. Mode 6a is therefore dominated by Cl-ring stretch, coupled with ring deformation. Based on our calculation, the fundamental frequency of the 6a mode should be 6 cm^{-1} lower than that of the ^{37}Cl isotopomer, and the difference is in excellent agreement with the experimental observation. The 7a mode, however, should only have a shift of 2 cm^{-1} , thus it is indistinguishable under our resolution. For the other observed modes, including mode 12, 19b, and 1, our calculation shows no isotope shift at all. In the works of Tzeng's group, isotope effects involving chlorine and bromine atoms on the vibrational frequencies of the S_1 state of aniline were investigated [20][21]. The authors observed small isotope shifts, on the order of several wavenumbers, in the REMPI spectra for all of the active fundamental modes, in agreement with our general conclusion.

To investigate the dynamics of the S_1 state, we recorded the transient of the parent ion by setting the pump laser at the origin of the S_1 state and the probe laser at 218 nm. Fig. 2 shows the experimental data with a fitting result including a biexponential function. All the reported REMPI and the following ZEKE spectra in this work were recorded under exact temporal overlap, which was the condition for maximal signal strength. Limited by the pulse width of our laser system (5 ns), the faster component in Fig. 2 could not be determined quantitatively. The lifetime of the slower component was measured to be 200 ns. It must be noted that the laser beams propagated normal to the jet expansion axis, so drifting of the molecular beam during delay times longer than a few hundred nanoseconds was a contributing factor to the decay of the slow component. The measured lifetime of 200 ns should thus be considered a lower limit. According to a

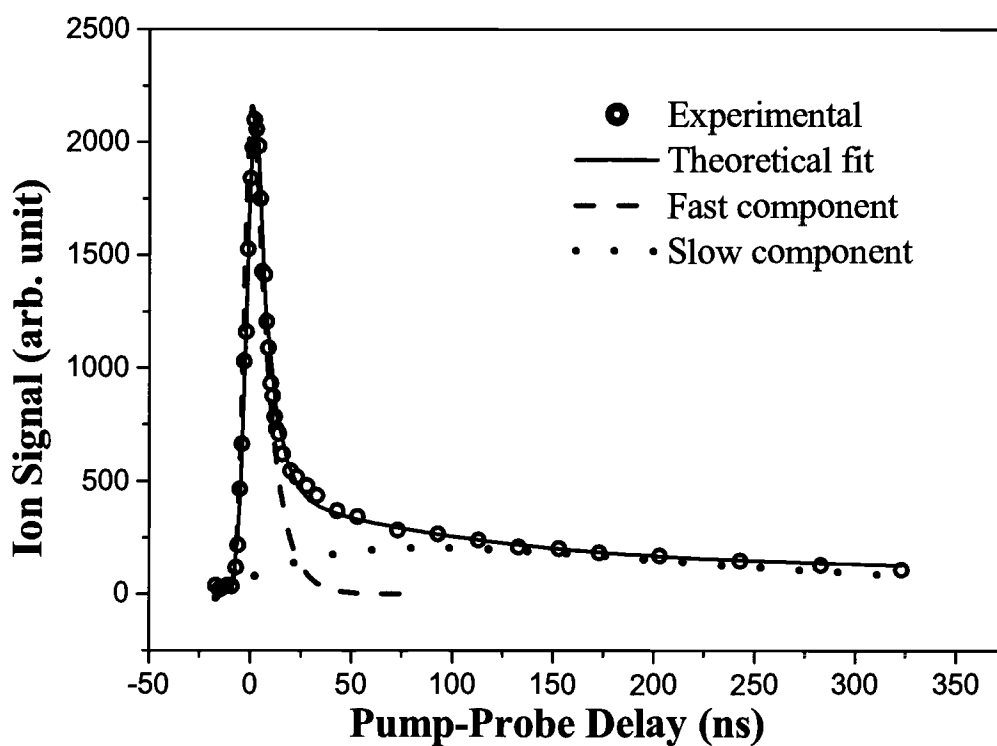


Figure 5.2 Pump-probe transient ionization signal of 2-ClP in the gas phase with the pump and probe wavelengths at 318.5 and 218 nm, respectively. Hollow circles represent experimental data, and the solid line is a theoretical fit including a bi-exponential decay (dashed and dotted lines) convoluted with the instrumental response (not shown).

previous study on the phosphorescence of 2-CIP, this long-lived component should be attributed to a nearby triplet state $^3A_1(\pi^*\pi)$ [22]. Biexponential decay has been extensively studied in pyrimidine, and the participation of a nearby triplet state has also been evoked [2][3][6]. However, in pyrimidine, the slower component dominated the decay profile, while the fast component was difficult to detect. This difference in the yield of intersystem crossing (ISC) between 2-CIP and pyrimidine cannot be explained from the heavy atom effect of chlorine, which would increase the yield of ISC while decrease the lifetime of the triplet state. Our CIS calculation shows that halosubstitution by a chlorine atom induces a blue shift for the $^1n\pi^*$ state by 566 cm^{-1} , while the energy level for the $^3\pi\pi^*$ state is only changed by 332 cm^{-1} . Perhaps it is this change in the energy gap of 234 cm^{-1} between the two coupling states that modifies the yield of ISC.

5.4.2. ZEKE spectra

Using five of the vibronic transitions labeled in Figure 1 as intermediate states, we recorded the ZEKE spectra, and the results are shown in Figure 3. In the following, vibrational levels of the cationic state are labeled by an additional “+” sign in the superscript to distinguish them from those of the S_1 state. The strong feature in the spectrum obtained via the origin band of the S_1 state (trace a) is assigned the origin band of the cation 0^{+0} . This assignment is also supported by the appearance of this band in other traces when vibrationally excited levels of the S_1 state were used as intermediate states (traces c and e). The adiabatic ionization potential for 2-CIP is therefore determined to be $77106 \pm 4\text{ cm}^{-1}$ ($9.5600 \pm 0.0005\text{ eV}$), including a correction due to the pulsed ionization field [15]. To the authors knowledge, this is the first report on the ionization potential of 2-CIP. Although mode 6a is sensitive to the isotope effect in the S_1 state, the overall ionization potentials of the two isotopomers are identical within our experimental uncertainty.

The spectra in Figure 3 are remarkably simple, which can be partially attributed to state selection achieved in typical REMPI experiments. Each spectrum is dominated by a single strong transition, and in all cases, this transition can be assigned the same vibrational level of the corresponding S_1 state. This strong correlation between the intermediate level and the final vibrational level of the ion has been reported in our

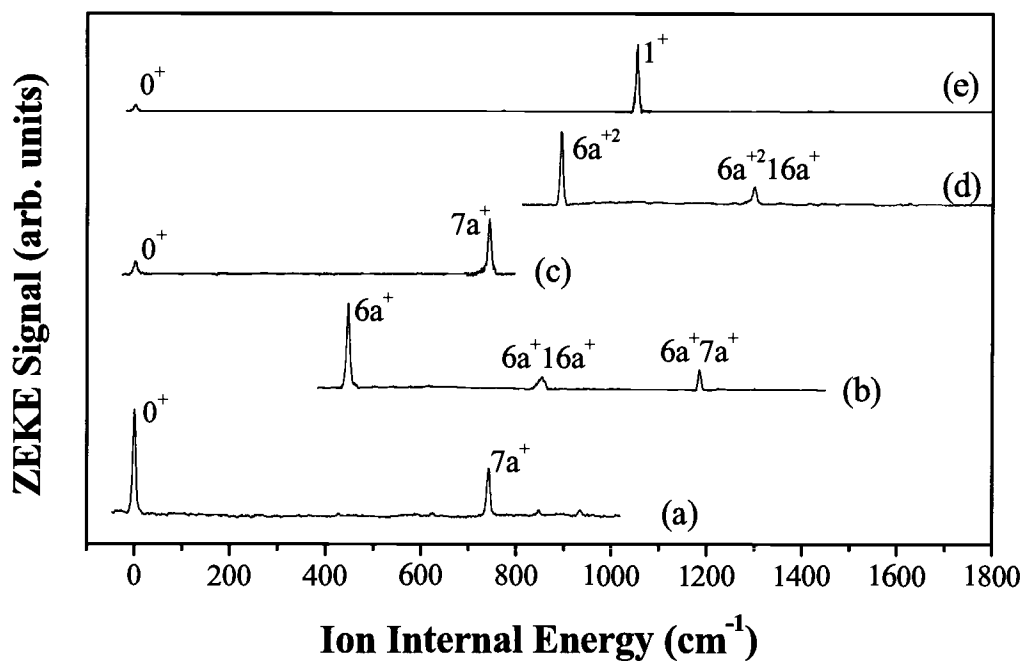


Figure 5.3 Two-color ZEKE spectra of 2-CIP recorded via the following vibrational levels of the S_1 state as intermediate states: (a) 0_0^0 , (b) $6a_0^1$, (c) $7a_0^1$, (d) $6a_0^2$, (e) 1_0^1 .

Table 5.2. Observed vibrational frequencies and assignments in the ZEKE spectra of 2-CIP.

Intermediate level in the S_1 state						Assignment
0_0^0	$6a_0^1$	$7a_0^1$	$6a_0^2$	1_0^1	Calc.	
0		0		0		0^+
	447				450	$6a^+$
742		743			757	$7a^+$
	854					$6a^+16a^+$
			894			$6a^{+2}$
934					964	12^+
				1055	1073	1^+
	1185					$6a^+7a^+$
			1301			$6a^{+2}16a^+$

Table 5.3. Molecular geometry parameters of 2-ClP in the S_0 , S_1 , and D_0 states.

	S_0	S_1	D_0
Bond length (Å)			
C ₂ -Cl	1.751	1.710	1.683
N ₁ -C ₂	1.325	1.292	1.323
N ₁ -C ₆	1.337	1.363	1.318
C ₄ -C ₅	1.390	1.384	1.397

previous studies of 4-aminopyridine [16]. We also derived a propensity rule of $\Delta\nu = 0$ to describe this effect, where ν is the vibrational quantum number of the intermediate state. Other features of the sparse spectra are relatively easy to assign. Table 2 lists the observed vibrational modes of the cation along with our calculation results. No scaling factors were used, and the agreement is impressive. Ionization via mode 7a (trace c) and mode 1 (trace e) of the S_1 state does not activate any other vibrational modes of the cation, but ionization via mode 6a shows weak signs of combination bands in the ZEKE spectra (traces b and d). Nevertheless, mode 6a demonstrates no anharmonicity, and the molecular frame remains rigid throughout the excitation and further ionization processes.

5.5. Discussion

We performed DFT calculations at the B3LYP level for the S_0 and D_0 states, and *ab initio* calculations at the CIS level for the S_1 state. The resulting geometry parameters are listed in Table 3. Our calculation indicates that 2-ClP remains planar with C_{2v} symmetry in all three states. Excitation to the S_1 state is of $\pi\pi^*$ character, while ionization involves removal of the π^* electron. In the S_1 state, the nonbonding electron of the chlorine atom participates in the conjugation with the aromatic ring, inducing a double-bond character between C_2 and Cl. This resonant effect results in the decrease of the C_2 -Cl bond length. As a result, based on our Mulliken population analysis,[23] the atomic charge on the Cl atom decreases from +0.507 in the S_0 state to +0.411 in the S_1 state. In addition, the polar ends of the molecular frame become more compact, while the bonds connecting the two ends (N1-C6) are elongated. These geometry changes may indicate that a partial delocalization of π electrons takes place following the $S_1 \leftarrow S_0$ transition. These changes in the ring structure are responsible for the activation of the ring breathing mode 1 and the in-plane bending modes 6a, 7a, and 12.

The back-donation of electrons from the chlorine atom to the aromatic ring is even more intensified in the D_0 state. The C_2 -Cl bond is further decreased, and according to our Mulliken population analysis, 71% of the positive charge is located on the chlorine atom. The ring structure, on the other hand, more or less recovers back to the geometry of the S_0 state. Apparently, the cation is stabilized by the formation of the “seven-center six-electron” π conjugation system. Nevertheless, these geometry changes are

Table 5.4. Observed vibrational frequencies of 2-ClP and pyrimidine in the S_1 and the D_0 states.

	2-ClP ^a	Pyrimidine ^b	Ratio
mode (S_1)			
6a	430	614	0.70
12	930	941	0.99
1	1035	1014	1.02
7a	740		
mode (D_0)			
6a	450	636	0.71
12	964	954	1.01
1	1073	1038	1.03
7a	757		

^a Experimental values from this work.

^b Ref. [9], with the values of mode 1 and 12 exchanged, see text for details.

insufficient to result in a large shift of the normal coordinates, and similar to the case of 4-aminopyridine, a strong propensity for $\Delta\nu = 0$ is still observed in the ZEKE spectra of Fig. 3.

It is interesting to compare the vibronic activities of 2-ClP in both the S_1 and the D_0 states with those of pyrimidine. Table 4 lists some observed vibrational modes of 2-ClP and pyrimidine in both the S_1 state and the D_0 state. Modes 6a, 1, and 12 are in-plane ring deformation modes involving the motion of the hydrogen or chlorine atom, thus differences in vibrational frequencies are expected. In Table 4, the variation in frequency between the two species is consistent for both electronic states, but the magnitude of change is quite different for mode 6a from those of the other two modes. An exceedingly high sensitivity to halosubstitution is demonstrated in mode 6a. This result is consistent with our observation of the high sensitivity of this mode to isotope substitution. It is worth noting that in our assignment of pyrimidine, mode 12 and mode 1 are exchanged from that of Knight *et al.* [1] and Sato *et al.* [9]. This revision is based on our high level CIS calculation, where the vibrational frequency of mode 12 is predicted to be lower than that of mode 1 by 68 cm^{-1} . Our DFT calculation for the cationic state is also consistent with this change. The listed experimental values for pyrimidine in Table 4 are therefore revised from the original report.

The observation of mode 7a in Fig. 1 differs from that of the REMPI spectrum of pyrimidine.[1],[9] In the studies of pyrimidine, mode 7a was not observed despite of intensive efforts, while at 740 cm^{-1} in Fig. 1, it is one of the most salient features. This discrepancy is similar to that of aniline and p-chloroaniline. Lin *et al.* recorded the one-color REMPI spectrum of p-chloroaniline [20]. The authors assigned the intense transition at 360 cm^{-1} as mode 7a. However, in all studies of aniline using REMPI [24][25], no indication of mode 7a was ever reported even when the pump laser was scanned to 1310 cm^{-1} above the origin band. Similar to mode 6a, mode 7a also involves C-Cl stretch and ring vibration. The differences between the two modes are the direction and the amplitude of the displacement vector for the C-H or C-Cl motion. It is therefore reasonable to assume that the decrease in the $C_2\text{-Cl}$ bond length upon excitation leads to the activation of mode 7a. Incidentally in p-chloroaniline [20], excitation to the S_1 state also induced a decrease of the C-Cl bond length from 1.746 \AA to 1.714 \AA . Without

halosubstitution, however, the change in the C-H bond length must be too small to activate this mode. Unlike mode 6a, mode 7a does not demonstrate clear isotope effect, and we attribute this phenomenon to the smaller amplitude of the displacement vector for the Cl-ring stretch in mode 7a.

Using REMPI and ZEKE spectroscopic methods, a wide variety of aromatic compounds and their complexes have been investigated in detail.[15] In particular, work on the pyrimidine and aniline series has provided a road map in understanding the photochemical and photophysical behaviors of these systems.[9],[20],[21],[24],[25] In this context, we comment on the stability of the aromatic ring during electronic excitation and further ionization. Without the availability of an electron withdrawing group in the side chain, excitation and ionization create a substantial change in the molecular frame [9][24][25]. As a result, rich vibronic activities in the ZEKE spectrum have been reported. However, substitution with an electron withdrawing group reduces the electron deficiency of the ring through increased conjugation between the ring and the substitute [20][21][26]. The integrity of the molecular frame is therefore largely intact even after photoionization. In this sense, the electron withdrawing group acts as an electron donating group in the cationic state. In the ZEKE spectrum, the rigidity of the ring structure during ionization manifests as a propensity of maintaining the vibrational excitation of the intermediate state. The normal coordinates of the S_1 and the D_0 states are essentially identical.

5.6. Conclusion

We report spectroscopic investigations on the first electronically excited state of 2-ClP and the ground state of its cation using two-color REMPI and ZEKE techniques. The adiabatic ionization threshold is determined to be $77106 \pm 4 \text{ cm}^{-1}$ ($9.5600 \pm 0.0005 \text{ eV}$). Most observed vibrational modes in both the S_1 and D_0 states are in-plane ring deformation modes, and our assignment is in good agreement with results from *ab initio* and DFT calculations. Mode 6a demonstrates clear isotope effect, and the nature of this mode is also consistent with our assignment. Similar to the case of aminopyridine, a propensity for maintaining the vibrational excitation of the intermediate state upon ionization is observed. Electronic excitation to the S_1 state involves a non-bonding

electron on the nitrogen atom to a π^* orbital, and further ionization removes this electron. The resulting system from each step of excitation demonstrates increased conjugation between the aromatic ring and the chlorine atom. This change is responsible for the activation of mode 7a in 2-CIP and in other halosubstituted aromatic compounds. The photophysics of the S_1 state of 2-CIP is similar to that of pyrimidine, though the probability of intersystem crossing is lower in 2-CIP.

5.7. Acknowledgements

This work was supported by the National Science Foundation, Division of Chemistry. Acknowledgment is made to the Donors of The Petroleum Research Fund, administered by the American Chemical Society, for partial support of this research. Wei Kong is an Alfred P. Sloan research fellow.

5.8. References

- [1] A. E. W. Knight, C. M. Lawburgh, C. S. Parmenter, *J. Chem. Phys.* 63 (1975) 4336.
- [2] D. M. Bartels, K. G. Spears, *J. Phys. Chem.* 86 (1982) 5180.
- [3] T. G. Dietz, M. A. Duncan, A. C. Pulu, R. E. Smalley, *J. Phys. Chem.* 86 (1982) 4026.
- [4] A. E. W. Knight, J. T. Jones, C. S. Parmenter, *J. Phys. Chem.* 87 (1983) 973.
- [5] G. M. Nathanson, G. M. McClelland, *J. Chem. Phys.* 84 (1986) 3170.
- [6] P. U. de Haag, W. Leo Meerts, *Chem. Phys.* 156 (1991) 197.
- [7] R. T. Carter, H. Bitto, J. R. Huber, *J. Chem. Phys.* 102 (1995) 5890.
- [8] P. N. Wang, H. Liu, E. C. Lim, *J. Chem. Phys.* 105 (1996) 5697.
- [9] S.-I. Sato, K. Omiya, K. Kimura, *J. Electron Spectrosc.* 97 (1998) 121.
- [10] K. J. Franks, H. Li, W. Kong, *J. Chem. Phys.* 110 (1999) 11779.
- [11] W. Kong, J. Bulthuis, *J. Phys. Chem. A* 104 (2000) 1055.
- [12] R. A. F. Deeelman, H. C. Van der Plas, A. Koudijs, Mrs. P. S. Darwinkel-Risseeuw, *Tetrahedron Lett.* 44 (1971) 4159.
- [13] J. Nasielski, A. Kirsch-Demesmaeker, R. Nasielski-Hinkens, *Tetrahedron* 28 (1972) 3767.
- [14] L. Lindqvist, B. Czochralska, M.-P. Fontaine-Aupart, W. Kawczynski, F. Tfibel, T. Douki, *Photochem. Photobiol. Sci.* 1 (2002) 600.
- [15] E. W. Schlag, *ZEKE Spectroscopy* (Cambridge University Press, Cambridge, 1998).
- [16] Y. He, C. Wu, W. Kong, *J. Chem. Phys.* 120 (2004) 7497.
- [17] GAUSSIAN 98, Revision A. 7, M. J. Frisch, *et al*, Gaussian, Inc., Pittsburgh, Pennsylvania, 1998.
- [18] M. E. Casida, C. Jamorski, K. C. Casida, and D. R. Sulahub, *J. Chem. Phys.* 108 (1998) 4439.
- [19] G. Varsanyi, *Assignment of Vibrational Spectra of Seven Hundred Benzene Derivatives* (Wiley, New York, 1974).
- [20] J. L. Lin, W. B. Tzeng, *J. Chem. Phys.* 113 (2000) 4109.
- [21] J. L. Lin, S. C. Yang, Y. C. Yu, W. B. Tzeng, *Chem. Phys. Lett.* 356 (2002) 267.
- [22] N. Nishi, R. Shimada, Y. Kanda, *Bull. Chem. Soc. Jpn.* 43 (1970) 41.
- [23] R. S. Mulliken, *J. Chem. Phys.* 23 (1955) 1833.
- [24] X. Zhang, J. M. Smith, J. L. Knee, *J. Chem. Phys.* 97 (1992) 2843.
- [25] X. Song, M. Yang, E. R. Davidson, J. P. Reilly, *J. Chem. Phys.* 99 (1993) 3224.
- [26] W. B. Tzeng, J. L. Lin, *J. Phys. Chem. A* 103 (1999) 8612.

Zero kinetic energy photoelectron spectroscopy (ZEKE) of
p-amino benzoic acid (PABA)

Yonggang He, Chengyin Wu, and Wei Kong*

*Department of Chemistry, Oregon State University,
Corvallis, Oregon 97331-4003*

Journal of Chemical Physics, **2004**, *121*, 3533-3539
American Institute of Physics, Suite 1NO1, 2 Huntington Quadrangle
Melville, NY 11747-4502, USA

* Corresponding author, email: wei.kong@oregonstate.edu, fax: 541-737-2062

6. Zero kinetic energy photoelectron spectroscopy (ZEKE) of *p*-amino benzoic acid (PABA)

6.1. Abstract

We report studies of supersonically cooled *p*-amino benzoic acid (PABA) using one-color resonantly enhanced multiphoton ionization (REMPI) and two-color zero kinetic energy (ZEKE) photoelectron spectroscopy. With the aid of *ab initio* and density functional calculations, vibrational modes of the first electronically excited state (S_1) of the neutral species and those of the cation have been assigned, and the adiabatic ionization potential has been determined to be $64540 \pm 5 \text{ cm}^{-1}$. A common pattern involving the activation of five vibrational modes of the cation is recognizable among all the ZEKE spectra. A propensity of $\Delta v = 0$, where v is the vibrational quantum number of the intermediate vibronic state from S_1 , is confirmed, and the origin of this behavior is discussed in the context of electron back donation from the two substituents in the excited state and in the cationic state. A puzzling observation is the doublet splitting of 37 cm^{-1} in the ZEKE spectrum obtained via the inversion mode of the S_1 state. This splitting cannot be explained from our density functional calculations.

6.2. Introduction

The interest in *p*-amino benzoic acid (PABA) arises from both its biological importance and its chemical properties.¹⁻¹⁰ It is a doubly substituted electron push-pull aromatic system with the donor (-NH₂) and the acceptor (-COOH) groups connected by the π -ring. Upon electronic excitation, however, both electron rich substituents can back donate to the electron deficient ring through hyper conjugation. On the biological aspect, PABA is an antimetabolite of sulfanilamide and was once widely used as an active ingredient in sunscreen and as a photodegradation inhibitor.

Several investigations of the photochemical and photophysical properties of PABA have been reported over the past,¹¹⁻¹⁵ including spectroscopic studies in the gas phase.¹⁶⁻²⁷ Using laser desorption, Meijer, *et al.* have recorded the resonantly enhanced multiphoton ionization (REMPI) spectra of the PABA monomer, its dimer, and its complexes with argon, methanol and water molecules.¹⁶ Tang, *et al.* have examined the gas-phase basicity of the three isomers of amino benzoic acids in a quadrupole ion trap.¹⁷ Mass selective gas-phase infrared (IR) spectroscopy of PABA has been studied by Putter, von Helden, and Meijer via infrared and vacuum ultraviolet (VUV) double resonance ionization.¹⁸ In a very recent study, Compagnon, *et al.* have measured the permanent electric dipole moment of isolated PABA in the ground state by coupling a matrix-assisted laser desorption source to an electric beam deflection setup.¹⁹ Using supersonic expansion from a heated source, Castaño's group has studied the first excited state of both methyl-*p*-aminobenzoate and ethyl-*p*-aminobenzoate and their water and ammonia complexes.²⁰⁻²⁶

So far studies on the cationic states of these molecules have been rare. To our knowledge, the only published work on cations of PABA is the mass-selective IR multiple photon dissociation spectroscopy by Oomens, *et al.*²⁷ The electronic activity of PABA upon photoexcitation and ionization is particularly intriguing in the context of our investigations of substituted aromatic systems. Our previous studies of 4-aminopyridine²⁸ (4-AP) and 2-chloropyrimidine²⁹ (2-CIPM) have concluded that upon excitation and ionization, the substituent would back donate to the aromatic ring, ensuring the integrity of the ring structure. As a result, in two photon zero kinetic energy photoelectron spectroscopy (ZEKE) experiments, a strong propensity has been observed

where the vibrational excitation of the intermediate state was largely preserved upon ionization. PABA contains two substituents, and it would be interesting to observe the “push” or “pull” effect of each substituent on the charge distribution.

In this paper we report studies of the one-color two-photon REMPI as well as the two-color ZEKE spectroscopy of PABA via six different intermediate states. Detailed analysis of the vibrational levels of the S_1 state and the ground cationic state (D_0) will be performed, with the assistance of *ab initio* and density functional calculations. The adiabatic ionization energy will be determined from analysis of the ZEKE spectra. From the distribution of active vibrational modes and comparisons between the ZEKE and REMPI spectra, conclusions on the structural changes upon electronic excitation and ionization will be obtained. Implications of these structural changes, particularly on the charge distribution among the ring and the substituents, will be discussed.

6.3. Experimental Setup

The experimental apparatus is a standard molecular beam machine with a time of flight mass spectrometer (TOF-MS) and a pulsed valve for supersonic cooling.³⁰ PABA was purchased from Aldrich Co. and used without further purification. The sample was housed and heated to 165 °C in the nozzle to obtain sufficient vapor pressure. The vapor was seeded into ~ 2 atm of argon and expanded into vacuum through a pulsed valve with a 1 mm diameter orifice. The pump laser in the 282 - 296 nm range with a pulse energy of ~ 1 mJ/pulse was generated by frequency doubling of the output from a dye laser (Laser Analytical Systems, LDL 2051) pumped by a Nd:YAG laser (Spectra Physics GCR 230). The ionization laser in the 332-362 nm region was generated by frequency doubling of the output from a dye laser (Laser Analytical Systems, LDL 20505) pumped by another Nd:YAG laser (Spectra Physics GCR 190). The absolute wavelength of each laser was calibrated using an iron hollow-cathode lamp filled with neon. The two laser beams were set to counterpropagate; and the light path, the flight tube, and the molecular beam were mutually perpendicular. The relative timing between the two laser pulses was controlled by a delay generator (Stanford Research, DG535), and the optimal signal was obtained under temporal overlap between the two lasers. In the ZEKE experiment, molecules excited to ZEKE states were allowed to stay for 1-2 μ s in the presence of a

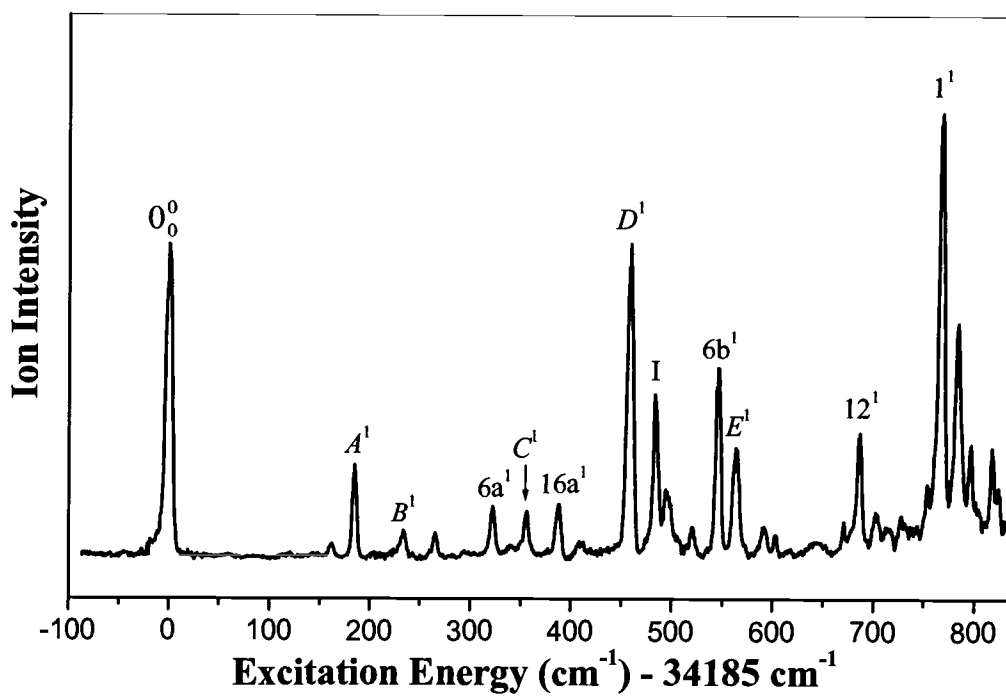


Figure 6.1 (1+1) REMPI spectrum of jet-cooled PABA. The spectrum is shifted by 34185 cm^{-1} (the origin of the $S_1 \leftarrow S_0$ transition) to emphasize the frequencies of the different vibrational modes of the S_1 state.

spoiling field of ~ 1 V/cm, and ionization and extraction was achieved by a pulsed electric field of ~ 16 V/cm.

In order to assign the observed vibronic structures in both the REMPI and ZEKE spectra, we used the Gaussian 98 suite³¹ to perform a series of calculations. For the ground state of the neutral and the cation, density functional theory (DFT) calculations using the Becke 3LYP functional were carried out with the 6-31G+(d) basis set. The excited state geometry and harmonic frequencies were calculated at the CIS level using the 6-31G(d) basis set. Good agreement between experimental and theoretical results was obtained when a scaling factor of 0.9 for the calculated frequencies of the S_1 state was used.³² No scaling factor for the cationic state was used.

6.4. Results

6.4.1. One-color 1+1 REMPI spectrum

The one-color 1+1 REMPI spectrum of PABA near the origin of the $S_1 \leftarrow S_0$ electronic transition is displayed in Figure 1. This spectrum is similar to that reported by Meijer, *et al.* using a laser desorption source.¹⁶ The intense peak at 34185 cm^{-1} is assigned as the origin band, and other vibronic transitions are listed in Table 1. There are 45 normal modes in PABA, among which 30 are associated with the aromatic ring, 6 are associated with the amino moiety, and 9 are associated with the carboxylic acid moiety. The seven stretching modes involving N-H, O-H, and C-H bonds are on the order of 3000 cm^{-1} , and are therefore not observable in Figure 1. Our CIS calculation shows $\pi\pi^*$ character for the S_1 state, and that the direction of the transition dipole moment should be in the plane of the aromatic ring. Only in-plane or even quanta of out-of-plane vibrational modes are symmetry allowed. In both Table 1 and Figure 1, modes that are associated with the motion of the aromatic ring are labeled using the convention of Varsanyi's nomenclature.³³ Other modes that mainly involve motions of $-\text{NH}_2$ and $-\text{COOH}$ moieties are named with letters from *A* to *G* in the order of increasing frequency. However, in some instances, strong coupling between the ring and the substituent renders this type of assignment only an approximation. For example, based on the displacement vectors from our own calculation, mode 6b highly couples with the $-\text{NH}_2$ inversion mode, and similarly, mode 12 and mode *E* ($-\text{COOH}$ scissoring motion) also demonstrate strong

Table 6.1. Observed vibrational frequencies and assignments for the S_1 state of PABA.

Exp.	Calc.*	Assignment and approx. description [#]
185	149	A_0^1 , β (-COOH) and C-NH ₂ torsion
233	209	B_0^1 , β (-COOH) and C-NH ₂ torsion
322	323	$6a_0^1$, β (ring)
357	329	C_0^1 , β (-NH ₂)
388	376	$16a_0^1$, γ (ring)
459	466	D_0^1 , β (-COOH) and β (-NH ₂)
483	512	I_0^1 , NH ₂ inversion
546	543	$6b_0^1$, β (ring)
564	564	E_0^1 , -COOH scissoring
592	591	F_0^1 , γ (-OH)
670	697	$10a_0^1$, γ (ring)
687	694	12_0^1 , β (ring)
768	767	I_0^1 , ring breathing
784	762	$17b_0^1$, γ (ring)
857	906	$17a_0^1$, γ (ring)
876		$A_0^1 12_0^1$
893	936	$19a_0^1$, β (ring)

* The values include a scaling factor of 0.9.

[#] ν , β , and γ represent stretching, in-plane bending, and out-of-plane bending vibrations.

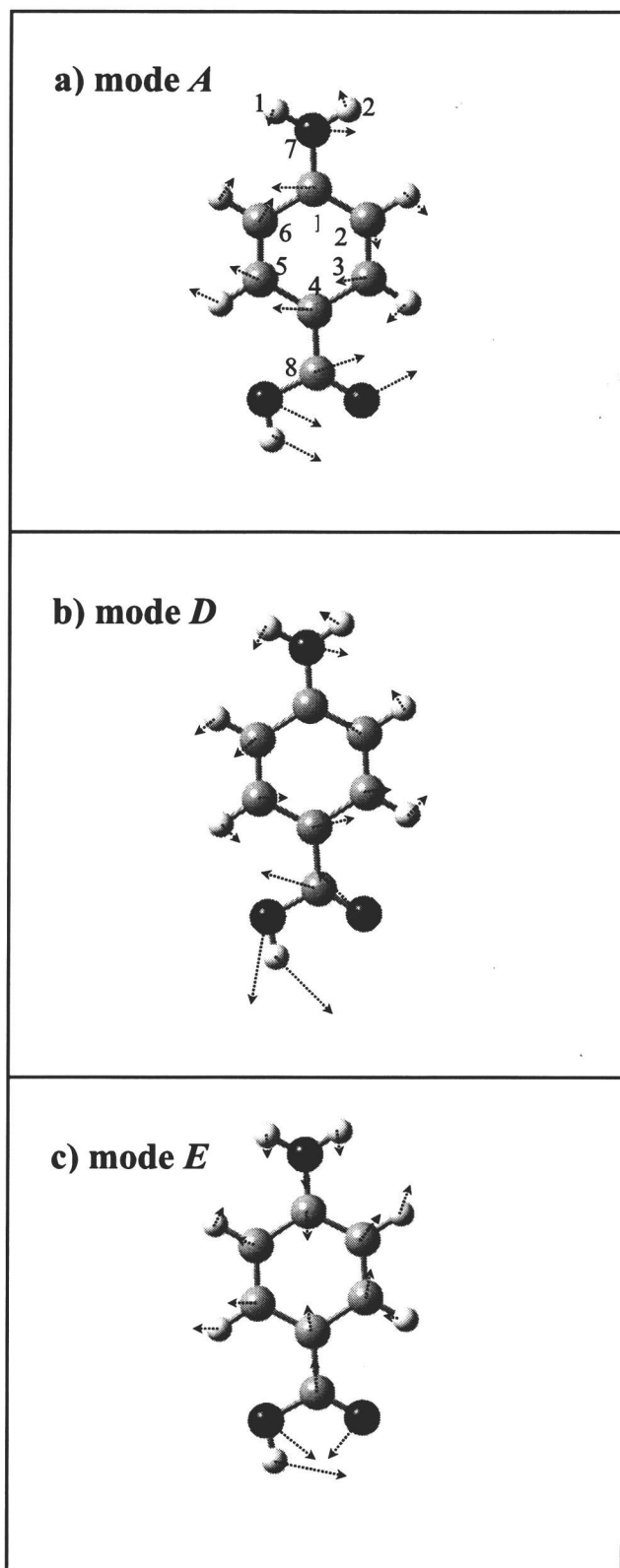


Figure 6.2 Normal modes in the S_1 state of PABA corresponding to a) mode *A* at 185 cm^{-1} , b) mode *D* at 459 cm^{-1} , and c) mode *E* at 564 cm^{-1} .

mixing. To assist assignment, we performed *ab initio* calculations on the CIS/6-31G(d) level and used a scaling factor of 0.9 to compare with the experimental result. An overall agreement between the calculation and the experiment was obtained. In the work of Meijer, *et al.*, the transition at 461.2 cm^{-1} was assigned as mode 6a.¹⁶ In Figure 1, this transition occurs at 459 cm^{-1} and is reassigned as mode *D* based on our own CIS calculation (Table 1). According to our calculation, mode 6a should be at a much lower frequency of 323 cm^{-1} , so the observed transition at 322 cm^{-1} is believed to be mode 6a.

One of the interesting features in the REMPI spectrum is the high activity of several in-plane bending modes involving mainly the motions of either the carboxylic group or the amino group (modes *A* through *G*). Three of these in-plane modes with high transition intensities were chosen as intermediate states to record the ZEKE spectra, which will be discussed in the next section. The displacement vectors of these normal modes are shown in Figure 2. All three modes involve the distortion of the phenyl ring. Mode *A* mainly involves the in-plane bending of the carboxylic group, but it also couples to the ring-NH₂ torsion. Mode *D* mainly involves the in-plane bending motion of the carboxylic group and the amino group. Mode *E* can be described as the scissoring motion of the carboxylic group.

6.4.2. ZEKE spectra

By scanning the ionization laser while setting the resonant laser at one of the intermediate states identified in the above REMPI experiment, we obtained pulsed field ionization ZEKE spectra. In Figures 3 and 4, the data will be presented according to the modes of the intermediate states. The same labeling scheme as that of the *S*₁ state is used in the assignment of the vibrational modes of the cationic state *D*₀. In the following, vibrational levels of the cationic state are labeled by an additional “+” sign in the superscript to distinguish them from those of the *S*₁ state. The identity of the intermediate level for each ZEKE spectrum is marked on the figure by a black dot. Table 2 summarizes these observations, including our calculation results on the B3LYP/6-31G+(d) level. No scaling factor for the vibrational frequencies of the cation in the calculation is used, and the agreement seems to be quite reasonable. Limited by the linewidth of each resonant transition, unfortunately, the error in the experimental values

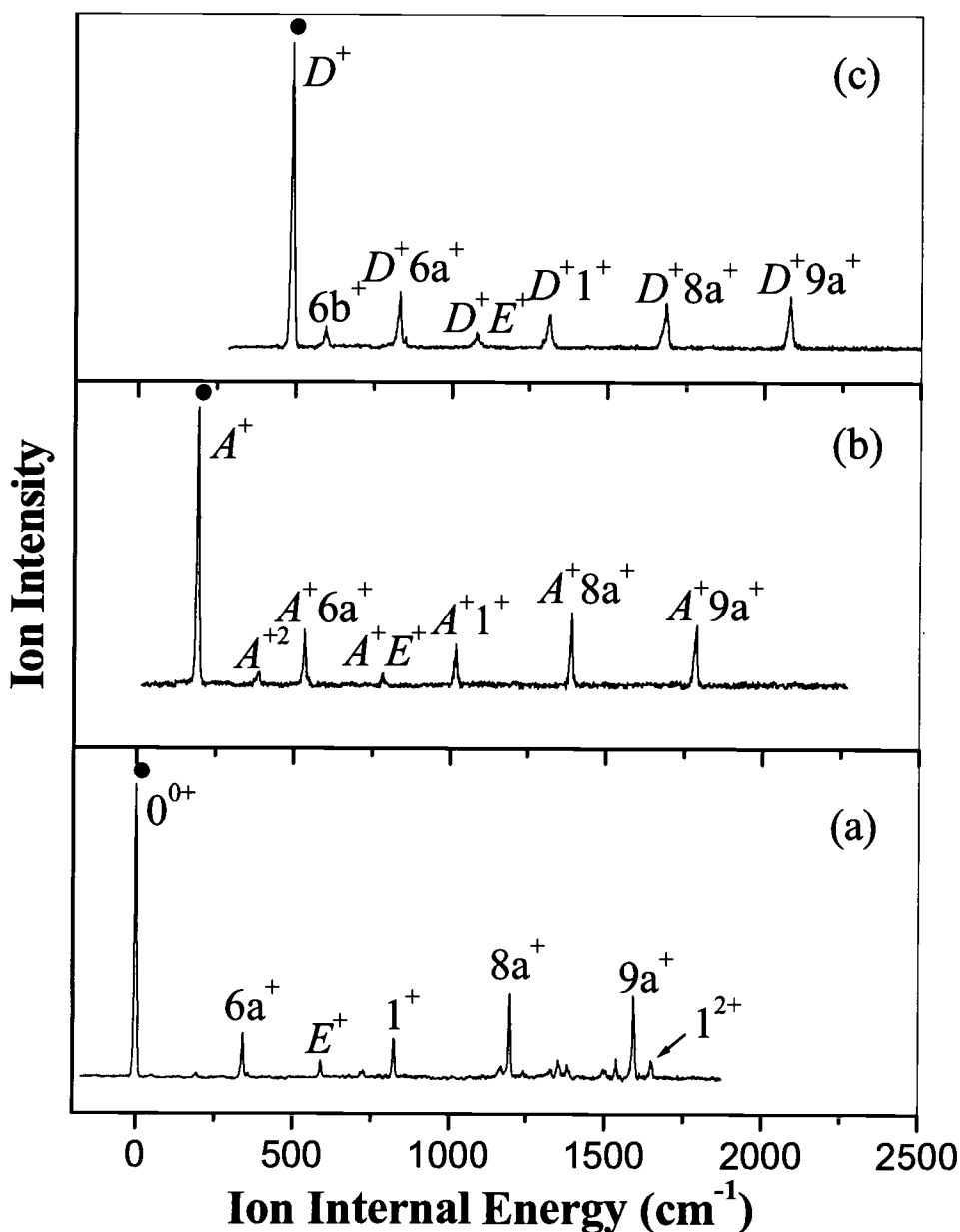


Figure 6.3 Two-color ZEKE spectra of PABA recorded via the following vibrational levels of the S_1 state as intermediate states: (a) 0^0 , (b) A^1 , and (c) D^1 . The energy in the abscissa is relative to the ionization threshold at 64540 cm^{-1} . The assignment in the figure refers to the vibrational levels of the cation, and the corresponding vibrational level of the intermediate state is labeled by a black dot in each panel.

Table 6.2. Observed vibrational frequencies and assignments in the ZEKE spectra of PABA.

Intermediate level in the S_1 state							Assignment
0_0^0	A_0^1	D_0^1	I_0^1	$6b_0^1$	E_0^1	Cal.	
0						0	origin
194	193					192	A^+
343						345	$6a^+$
	388						A^{+2}
			482				α^+
		490		491		503	D^+
			519				β^+
	533						A^+6a^+
590					587	596	E^+
		597		597		610	$6b^+$
724						730	12^+
	785						A^+E^+
				789			A^+6b^+
			822				α^+6a^+
823						835	1^+
		832					D^+6a^+
			858				β^+6a^+
				908		872	$17b^+$
				936	939		$6a^+6b^+$
	1017						A^+1^+
		1077					D^+E^+
1168						1166	$19b^+$
				1185			$6b^+E^+$
1197						1228	$8a^+$
				1251			$17b^+6a^+$
					1283		$6a^{+2}6b^+$
			1304				α^+1^+
		1315					D^+1^+
			1338				β^+1^+
	1389						A^+8a^+
				1416			$6b^+1^+$
1500						1517	$9b^+$
1538						1536	G^+
1592						1639	$9a^+$
1647							1^{+2}
			1681				α^+8a^+
		1685					D^+8a^+
			1715				β^+8a^+
					1765		$6a^+6b^+1^+$
					1785		E^+8a^+

1788			A^+9a^+
		1793	$6b^+8a^+$
	2073		α^+9a^+
2082			D^+9a^+
		2105	$17b^+8a^+$
	2108		β^+9a^+
		2181	E^+9a^+
		2188	$6b^+9a^+$
		2507	$17b^+9a^+$
		2531	$6a^+6b^+9a^+$

is 5 cm^{-1} . Among the six ZEKE spectra, a clear propensity of $\Delta\nu = 0$ can be identified; i.e., the vibrational quantum number ν of each mode is directly transferred from the intermediate state to the cationic state, with little vibrational relaxation or mode mixing. This strong correlation between the intermediate level and the final vibrational level of the cation has also been reported in our previous studies of 4-aminopyridine²⁸ and 2-chloropyrimidine²⁹.

Figure 3a shows the ZEKE spectrum recorded via the origin of the S_1 state. The most intense peak in the spectrum corresponds to the origin of the cation. The resulting adiabatic ionization potential including a correction due to field ionization,³⁴ is $64540 \pm 5\text{ cm}^{-1}$ ($8.0020 \pm 0.0006\text{ eV}$). Our value is 33 cm^{-1} higher than that reported by Meijer, *et al.*¹⁶ in their two-color photoionization experiment. This discrepancy between the two values could be related to the extrapolation method used for threshold ions in the earlier report. Other transitions with medium intensities in the ZEKE spectrum of Figure 3a correspond to excitations of modes $6a^+$, E^+ , 1^+ , $8a^+$, and $9a^+$. As will be seen in the following, these modes constitute the majority of the active modes in the ZEKE spectra. It is interesting to notice that the ring breathing mode 1 is the most intense in the REMPI spectrum, and it is also active in the ZEKE spectrum, with a Franck-Condon progression containing a weak 1^{+2} band.

The other two ZEKE spectra in Figure 3 (the top two panels) are associated with the in-plane bending modes A and D . As shown in the previous section, mode A and mode D are two similar vibrational modes that both involve the motion of the carboxylic group. The ZEKE spectra obtained via these two modes also show remarkable resemblance, including the activation of modes $6a^+$, E^+ , 1^+ , $8a^+$, and $9a^+$, and this pattern is essentially a repeat of that of Figure 3a. The fundamental frequencies of these two modes for the cation are determined to be 193 and 490 cm^{-1} , in agreement with our calculation results. In the ZEKE spectrum taken via mode A , a higher harmonic A^{+2} is also weakly observable. Ionization via mode D activates the ring deformation mode $6b^+$. It is interesting to note that in Figure 4a, the reverse is also true; i.e., ionization via mode $6b$ results in the activation of mode D^+ . This result indicates a strong coupling between these two vibrational modes.

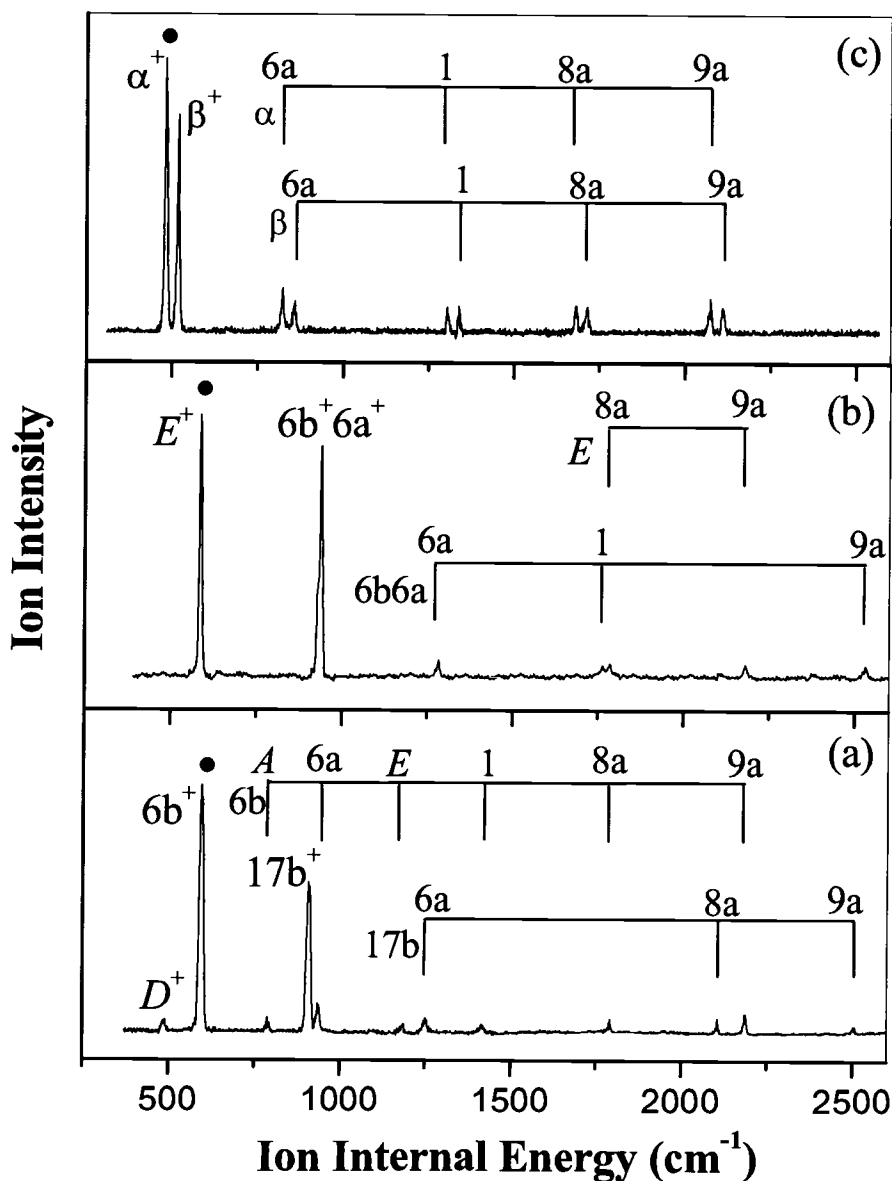


Figure 6.4 Two-color ZEKE spectra of PABA recorded via the following vibrational levels of the S_1 state as intermediate states: (a) $6b^1$, (b) E^1 , and (c) I^1 . The combination bands associated with the major band (labeled beside the ticks) of each spectrum are marked by guide lines and labeled above the ticks. The “+” sign in the labeling of the combination bands is omitted to avoid clutter.

The ZEKE spectrum taken via mode 6b of the S_1 state (Figure 4a) shows the strongest transition at 597 cm^{-1} , asserting its identity as the $6b^+$ mode of the cation. In comparison, the *ab initio* value for the same mode is 610 cm^{-1} . The spectrum shows a similar pattern as those in Figure 3 with regard to the activation of other modes, including modes $6a^+$, E^+ , 1^+ , $8a^+$, and $9a^+$. A combination band of $6b^+$ with mode A^+ is also observable at 789 cm^{-1} . The assignment for the strong band at 908 cm^{-1} is tentative. Interestingly, this band has a series of combination bands of its own, with a similar pattern as that of the $6b^+$ mode. This band could be a combination of mode A^+ and mode 12^+ , which should occur at 918 cm^{-1} , since mode A^+ is observed in the combination band with mode $6b^+$, and mode 12^+ is observed in Figure 3a as an extremely weak transition. However, both transitions to A^+ and 12^+ are weak; thus, it is difficult to explain the exceptionally strong intensity of this combination band. According to our DFT calculation, the closest vibrational mode in frequency to this band at 908 cm^{-1} is $17b^+$ at 872 cm^{-1} . However, mode $17b^+$ is out-of-plane and therefore largely symmetry forbidden, and it has no obvious association with mode $6b^+$.

Figure 4b shows the ZEKE spectrum of PABA taken via mode E of the S_1 state. The most intense feature at 587 cm^{-1} corresponds to mode E^+ . This assignment is consistent with our *ab initio* value of 596 cm^{-1} . Compared with the pattern observed in Figure 3, Figure 4b only shows the combination bands of mode E^+ with modes $8a^+$ and $9a^+$, while combinations with modes $6a^+$ and 1^+ are probably too weak for our sensitivity. An interesting feature of this spectrum is the intense $6a^+6b^+$ band, which has its own combinations with other modes and follows a similar pattern as those of Figure 3. The observation of this intense $6a^+6b^+$ band via mode E of the S_1 state is a surprise. However, a careful examination of the displacement vectors of mode E in Figure 2 reveals that in the S_1 state, this scissoring motion of the $-\text{COOH}$ moiety strongly couples with the ring deformation mode 6b, while in the D_0 state, it couples with $6a^+$. This type of cross link makes it quite possible for the observation of the combination band in the ionization spectrum.

The ZEKE spectrum via the $-\text{NH}_2$ inversion mode, shown in Figure 4c, is the most intriguing. Each feature is split into two, with a spacing of $\sim 37\text{ cm}^{-1}$. The overall pattern in terms of combination bands is the same as those shown in the other ZEKE spectra. We

denote the two intense peaks around 500 cm^{-1} as α^+ and β^+ , and we tentatively assign them as transitions to the doublet of the $-\text{NH}_2$ inversion mode in the D_0 state. However, as will become clear in the next section, a close scrutiny of the nonplanarity of the amino group in the D_0 state is needed to confirm this assignment.

6.5. Discussion

We performed DFT calculations on the B3LYP level for the S_0 and D_0 states, and *ab initio* calculations at the CIS level for the S_1 state. The resulting geometry parameters are listed in Table 3 and the numbering scheme is shown in Figure 2. Our CIS calculation shows $\pi\pi^*$ character for the S_1 state. During the $\text{S}_1 \leftarrow \text{S}_0$ transition, the molecular frame becomes more compact along the main axis (N7-C1-C4-C8). The decreases of the C1-N7 and the C4-C8 bond lengths indicate the participation of both polar ends in the conjugation with the aromatic ring, and the resulting chemical bonds between the adjacent moieties take on partial double-bond characters. In the meantime, according to Table 3, the pseudo symmetry with respect to the main axis is severely distorted, both in terms of the ring structure and the twist of the amino group. These changes are responsible for the activation of the ring breathing mode 1, the ring deformation modes 6a, 12 and 19a, and the in-plane bending modes *A* through *G*. In our previous observations of 4-aminopyridine²⁸ and 2-chlorophyrimidine²⁹, we reported similar changes in the bonding between the ring and the polar group. We concluded that whenever there was an electron rich group, upon $\pi\pi^*$ transition, the substituent would back donate to the ring and form a partial double bond with the ring. Although 4-AP, 2-CIPM, and PABA belong to different symmetry groups, just from the electron withdrawing effect of the substituent, the conclusion seems to remain essentially the same. With the availability of two polar groups in PABA, both substituents participate in back donation.

The internal rotation of the amino group around the C1-N7 bond upon photoexcitation (Table 3) breaks the symmetry of the two N-H bonds with respect to the main molecular axis. Typically, this type of twist hinders effective charge transfer of π electrons between the two adjacent moieties.³⁵ On the other hand, the carboxylic group remains planar in both states, permitting facile charge transfer between the ring and the carboxylic group.

Table 6.3. Molecular geometry parameters of PABA in the S_0 , S_1 , and D_0 states.

	S_0	S_1	D_0
<i>Bond length (Å)</i>			
N7-C1	1.387	1.367	1.335
C1-C2 (C1-C6)	1.410 (1.410)	1.421 (1.447)	1.438 (1.438)
C2-C3 (C5-C6)	1.387 (1.389)	1.364 (1.355)	1.342 (1.374)
C3-C4 (C4-C5)	1.405 (1.406)	1.450 (1.442)	1.421 (1.420)
C4-C8	1.475	1.443	1.502
C=O	1.220	1.208	1.211
C-O(H)	1.365	1.346	1.342
<i>dihedral angle (°)</i>			
H1N7C1C2	-21.462	-15.437	-0.007
H2N7C1C6	21.525	26.452	0.009

Table 6.4. Mulliken charge distributions of PABA in the S_0 , S_1 , and D_0 states.

	S_0	S_1	D_0
-NH ₂	+0.108	-0.146	+0.127
-COOH	-0.121	-0.074	+0.307
Benzene ring	+0.011	+0.219	+0.568
C4	+0.721	-0.229	+0.357

In the REMPI spectrum of Figure 1, modes associated with the carboxylic group are particularly active. We suspect that during this $S_1 \leftarrow S_0$ transition, part of the electron deficiency on the ring due to excitation is alleviated by electron back donation from the carboxylic group to the ring. In Table 4, we list the Mulliken charge population³⁶ on the three functional groups and the carbon atom connected to the carboxylic group (C4). Upon $S_1 \leftarrow S_0$ excitation, the net charge on the carboxylic group is decreased from -0.121 to -0.074, while a net negative charge, from +0.721 in S_0 to -0.229 in S_1 , builds up at the C4 atom. The resulting permanent dipole of the S_1 state is higher than that of the ground state by ~ 1 Debye. The amino group, though rich with electrons, can only achieve some of its electron donating potential in this twisted geometry. Its charge is actually increased from +0.108 to -0.146 in the S_1 state. Although one needs to exercise caution when dealing with Mulliken charge distributions, the trend in the change of charge distributions within the same molecule should be reliable.

The $D_0 \leftarrow S_1$ ionization process involves the removal of the π^* electron. The subsequent major change is flattening of the amino group, making it conducive to charge transfer. In addition, the bond length for C1-N7 is further decreased, while the bond length for C4-C8 increases to a maximum value of 1.5 Å in Table 3. According to our Mulliken population analysis (Table 4), the atomic charge on the amino group is changed from -0.146 in the S_1 state to +0.127 in the D_0 state. This additional effective back-donation of electrons from the amino group to the aromatic ring greatly alleviates the electron-deficiency of the ring in the D_0 state. As a result, the rigidity of the ring structure remains throughout the ionization process. The normal coordinates are largely unchanged upon ionization, and similar to the cases of 4-aminopyridine and 2-chloropyrimidine,^{28,29} a strong propensity for $\Delta\nu = 0$ is observed in the ZEKE spectra of Figures 3 and 4.

It is interesting to compare the different behaviors of the two substituents upon excitation and ionization. While the bond length for C1-N7 becomes progressively shorter with successive excitation, the bond length for C4-C8 first decreases in the S_1 state and then increases to a maximum value in the D_0 state. The electron donating role of the amino group is realized to its maximum degree in the cation. The carboxylic group, on the other hand, maintains its electron donating role throughout the whole excitation

process with a charge of +0.307 in the D_0 state, although upon ionization, conjugation with the ring is removed.

The value of the vibrational frequency is reflective of the rigidity of the chemical bond involved in the corresponding normal mode. The ring deformation modes 6a, 6b, 1, and 12 all have higher frequencies in the cationic state than in the S_1 state, indicating stronger bond strengths for the ring in the D_0 state. Mode D involves in-plane bending of the $-NH_2$ moiety. Our experiment shows that the vibrational frequency of this mode increases by 31 cm^{-1} upon ionization. This result is in agreement with the observation that the C-N bond length is decreased in the cation, as shown in Table 3.

The ZEKE spectrum obtained via the $-NH_2$ inversion mode in Figure 4c implies a non-planar geometry for the ground ionic state, with a doublet splitting of 37 cm^{-1} . However, our DFT calculation did not support such a conclusion. Previous studies of a series of amino-substituted aromatic compounds all concluded on a planar geometry for the related cations.^{28,37-40} We then investigated the likelihood of proton tunneling within the $-COOH$ group and eventually ruled out this possibility. The estimated barrier for tunneling in the D_0 state is higher than 15000 cm^{-1} . If tropolone can be used as a reference, which has a barrier height of 5890 cm^{-1} and a doubling splitting of 0.97 cm^{-1} ,⁴¹ the splitting in PABA, if any, should not exceed 1 cm^{-1} . Furthermore, although Figure 4c was obtained via the amino inversion mode of the S_1 state, there is no indication of any coupling between the out-of-plane bending mode in the D_0 state at 648 cm^{-1} (based on our calculation) and the $-COOH$ scissoring mode E^+ at 590 cm^{-1} . In the S_1 state, the inversion mode I is coupled to mode 6b, and it is 24 cm^{-1} apart from mode D (Table 1). In the D_0 state, mode D^+ at 490 cm^{-1} is in between the doublet α^+ and β^+ . This triangular relationship between modes 6b, D , and I could result in strong anharmonic behaviors. However, we fail to see a direct link between this anharmonicity and the observed doublet feature in Figure 4c. In the work of Yan and Spangler on p-methylaniline,⁴² coupling between the motions of the amino group and torsion of the methyl group was demonstrated. The authors stated that the methyl group makes the “up” and “down” NH_2 conformations different in energy, leading to a quartet splitting in the inversion mode and the torsional mode of the amino group. In our case, however, the first excitation laser has achieved selectivity in the S_1 state, and any splitting has to be associated with the planar

D₀ state. Based on our calculation, the torsional mode for the amino group should be at 572 cm⁻¹, and the torsional mode of the carboxylic group should be at 53 cm⁻¹. It is possible that these two modes would couple and result in a 37 cm⁻¹ splitting. However, as Yan and Spangler pointed out,⁴² the mechanism of this type of coupling remains a mystery. Moreover, the shortened C1-N7 bond and the lengthened C4-C8 bond upon ionization both favor a higher torsional barrier for the amino group than for the carboxylic group. At present, we do not have an explanation for this splitting in the ZEKE spectrum.

6.6. Conclusion

Spectroscopic properties of the excited and ionic states of PABA have been studied using one-color REMPI and two-color ZEKE spectroscopy. Many in-plane and out-of-plane vibrational modes and combination bands in both states have been identified. The adiabatic ionization energy of PABA in the gas phase is determined to be 64540 ± 5 cm⁻¹ (8.0020 ± 0.0006 eV). The similarity in geometry between S₁ and D₀ results in a strong propensity for ionization from the S₁ state; i.e., the ZEKE spectrum obtained via a vibrational level of the S₁ state features a dominant transition to the same vibrational level of the cation. The origin of this rigidity can be traced to the electron back donation of the carboxylic group in the S₁ state and to both polar groups in the cationic state. This observation is consistent with our previous conclusion on polar substituted aromatic compounds. The electron withdrawing group in the ground state behaves as an electron donating group upon electronic excitation and ionization. *Ab initio* and DFT calculations are found to be largely consistent with the experimental observations. However, the origin of the doublet splitting in the ZEKE spectrum taken via the inversion mode of S₁ remains a mystery.

6.7. Acknowledgements

This work was supported by the National Science Foundation, Division of Chemistry. Acknowledgment is made to the Donors of The Petroleum Research Fund, administered by the American Chemical Society, for partial support of this research. Wei Kong is an Alfred P. Sloan research fellow.

6.8. References

- ¹ P. R. Srinivasan and B. Weiss, *Biochim. Biophys. Acta* **51**, 597 (1961).
- ² H. H. Thijssen, *J. Med. Chem.* **20**, 233 (1977).
- ³ J. K. Seydel and W. Butte, *J. Med. Chem.* **20**, 439 (1977).
- ⁴ F. Mandelbaum-Shavit and S. H. Blondheim, *Biochem. Pharmacol.* **30**, 65 (1981).
- ⁵ H. Verweij and J. van Steveninck, *Biochem. Pharmacol.* **30**, 1033 (1981).
- ⁶ W. M. Watkins, D. G. Sixsmith, J. D. Chulay, and H. C. Spencer, *Mol. Biochem. Parasit.* **14**, 55 (1985).
- ⁷ T. Gichner, J. Veleminsky, I. A. Rapoport, and S. V. Vasilieva, *Mutat. Res.* **192**, 95 (1987).
- ⁸ C. E. Rutherford, L. F. Salter, and R. C. Thomas, *J. Photoch. Photobio. A* **52**, 337 (1990).
- ⁹ J. M. Allen, S. Engenolf, and S. K. Allen, *Biochem. Bioph. Res. Co.* **212**, 1145 (1995).
- ¹⁰ A. Kluczyk, T. Popek, T. Kiyota, P. de Macedo, P. Stefanowicz, C. Lazar, and Y. Konishi, *Curr. Med. Chem.* **9**, 1871 (2002).
- ¹¹ F. P. Gasparro, *Photodermatology* **2**, 151 (1985).
- ¹² H. Flindt-Hansen, C. J. Nielsen, and P. Thune, *Photodermatology* **5**, 257 (1988).
- ¹³ A. A. Shaw, L. A. Wainschel, and M. D. Shetlar, *Photochem. Photobiol.* **55**, 647 (1992).
- ¹⁴ A. M. Halpern and B. R. Ramachandran, *Photochem. Photobiol.* **62**, 686 (1995).
- ¹⁵ S. A. Langford, J. K. Sugden, and R. W. Fitzpatrick, *J. Pharmaceut. Biomed.* **14**, 1615 (1996).
- ¹⁶ G. Meijer, M. S. de Vries, H. E. Hunziker, and H. R. Wendt, *J. Chem. Phys.* **92**, 7625 (1990).
- ¹⁷ M. Tang, J. Isbell, B. Hodges, and J. Brodbelt, *J. Mass Spectrom.* **30**, 977 (1995).
- ¹⁸ M. Putter, G. von Helden, and G. Meijer, *Chem. Phys. Lett.* **258**, 118 (1996).
- ¹⁹ I. Compagnon, R. Antoine, D. Rayane, M. Broyer, and P. Dugourd, *J. Phys. Chem. A* **107**, 3036 (2003).
- ²⁰ A. Longarte, J. A. Fernandez, I. Unamuno, and F. Castano, *Chem. Phys. Lett.* **308**, 516 (1999).
- ²¹ A. Longarte, J. A. Fernandez, I. Unamuno, and F. Castano, *J. Chem. Phys.* **112**, 3170 (2000).
- ²² J. A. Fernandez, A. Longarte, I. Unamuno, and F. Castano, *J. Chem. Phys.* **113**, 5804 (2000).
- ²³ A. Longarte, J. A. Fernandez, I. Unamuno, and F. Castano, *Chem. Phys.* **260**, 83 (2000).
- ²⁴ J. A. Fernandez, A. Longarte, I. Unamuno, and F. Castano, *J. Chem. Phys.* **113**, 8531 (2000).
- ²⁵ J. A. Fernandez, A. Longarte, I. Unamuno, and F. Castano, *J. Chem. Phys.* **113**, 8541 (2000).
- ²⁶ A. Longarte, J. A. Fernandez, I. Unamuno, and F. Castano, *J. Chem. Phys.* **113**, 8549 (2000).

- ²⁷ J. Oomens, D. T. Moore, G. Meijer, G. von Helden, *Phys. Chem. Chem. Phys.* **6**, 710 (2004).
- ²⁸ Y. He, C. Wu, and W. Kong, *J. Chem. Phys.* **120**, 7497 (2004).
- ²⁹ Y. He, C. Wu, and W. Kong, *Chem. Phys. Lett.* (in press, 2004).
- ³⁰ Y. He, C. Wu, and W. Kong, *J. Phys. Chem. A* **107**, 5145 (2003).
- ³¹ GAUSSIAN 98, Revision A. 7, M. J. Frisch, *et al.*, Gaussian, Inc., Pittsburgh, Pennsylvania, 1998.
- ³² M. E. Casida, C. Jamorski, K. C. Casida, and D. R. Sulahub, *J. Chem. Phys.* **108**, 4439 (1998).
- ³³ G. Varsanyi, *Assignment of Vibrational Spectra of Seven Hundred Benzene Derivatives* (Wiley, New York, 1974).
- ³⁴ E. W. Schlag, *ZEKE Spectroscopy* (Cambridge University Press, Cambridge, 1998).
- ³⁵ H. Suzuki, *Electronic Absorption Spectra and Geometry of Organic Molecules* (Academic Press, New York, 1967).
- ³⁶ R. S. Mulliken, *J. Chem. Phys.* **23**, 1833 (1955).
- ³⁷ X. Song, M. Yang, E. R. Davidson, and J. P. Reilly, *J. Chem. Phys.* **99**, 3224 (1993).
- ³⁸ J. L. Lin, R. H. Wu, and W. B. Tzeng, *Chem. Phys. Lett.* **353**, 55 (2002).
- ³⁹ J. L. Lin, R. H. Wu, and W. B. Tzeng, *Chem. Phys.* **280**, 191 (2002).
- ⁴⁰ S. J. Baek, K-W. Choi, Y. S. Choi, and S. K. Kim, *J. Chem. Phys.* **117**, 2131 (2002).
- ⁴¹ Y. Tomioka, M. Ito, and N. Mikami, *J. Phys. Chem.* **87**, 4401 (1983).
- ⁴² S. Yan and L. H. Spangler, *J. Chem. Phys.* **96**, 4106 (1992).

**Observation of rotamers of *m*-aminobenzoic acid (MABA):
ZEKE and hole-burning REMPI spectroscopy**

Yonggang He, Chengyin Wu, and Wei Kong*

*Department of Chemistry, Oregon State University,
Corvallis, Oregon 97331-4003*

Journal of Chemical Physics, **2004**, *121*, 8321-8328
American Institute of Physics, Suite 1NO1, 2 Huntington Quadrangle
Melville, NY 11747-4502, USA

* Corresponding author, email: wei.kong@oregonstate.edu, fax: 541-737-2062

7. Observation of rotamers of *m*-aminobenzoic acid (MABA): ZEKE and hole-burning REMPI spectroscopy

7.1. Abstract

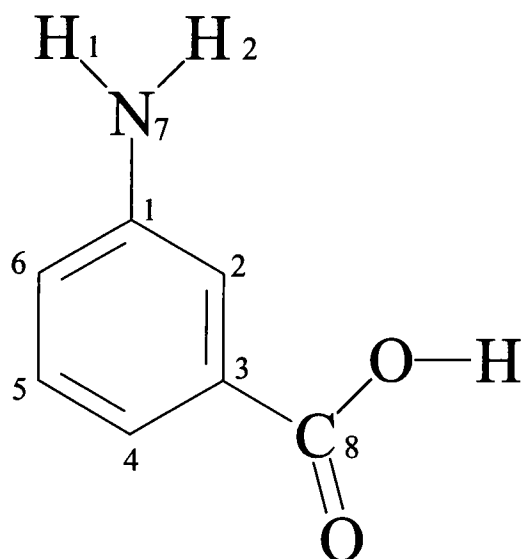
We report studies of supersonically cooled *m*-aminobenzoic acid (MABA) using two-color resonantly enhanced multiphoton ionization (REMPI) and two-color zero kinetic energy (ZEKE) photoelectron spectroscopy. Two conformers have been identified and characterized using the hole-burning method in the REMPI experiment. With the aid of *ab initio* and density functional calculations, vibrational modes of the first electronically excited state (S_1) of the neutral species and those of the ground state cation (D_0) have been assigned, and the adiabatic ionization potentials have been determined for both conformers. The REMPI spectra are dominated by in-plane motions of the substituents and ring deformation modes. A propensity of $\Delta\nu = 0$, where ν is the vibrational quantum number of the intermediate vibronic state from S_1 , is observed in the ZEKE spectra. The origin of this behavior is discussed in the context of electron back donation from the two substituents in the excited state and in the cationic state. Comparisons of these results with those of *p*-aminobenzoic acid will be analyzed.

7.2. Introduction

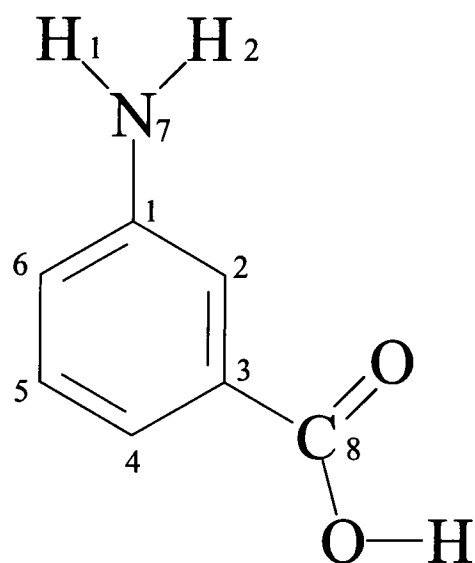
The interest in *m*-aminobenzoic acid (MABA) arises from both its biological importance and its chemical properties.¹²³⁴⁵ Like *p*-aminobenzoic acid (PABA), MABA is a doubly substituted electron push-pull aromatic system with the donor (-NH₂) and the acceptor (-COOH) groups connected by the π -ring. Due to the resonant effect, however, the electron-attracting inductive effect of the carboxylic group in MABA is slightly smaller than that in PABA. Upon electronic excitation or ionization, both electron rich substituents can back donate to the electron deficient ring through hyper conjugation. In non-polar solvents, MABA exists predominantly as a neutral molecule. In the solid state or in aqueous solutions, interestingly, it exists as a zwitterion, unlike *o*-aminobenzoic acid (OABA) and PABA.^{6,7} MABA is also of great importance in pharmaceutical and chemical industries. For example, it is used in synthesis of analgesics, antihypertensives and vasodilators.⁸

Several investigations of the chemical and physical properties of MABA have been reported over the past.⁸⁻¹⁴ From X-ray photoelectron spectroscopy, Yoshida and Sawada have concluded that MABA exists in a dipolar form in the solid state.¹⁰ Both theoretical and crystallographic studies have confirmed that ground state MABA exists in two conformations as shown in Figure 1.^{8,9} Infrared spectroscopy of MABA has been reported both in the solid state and in the gas phase,^{6,11} however, neither investigated the existence of conformational isomers. More recently, using inelastic neutron scattering (INS), Raman spectroscopy, IR spectroscopy, and density functional (DFT) calculations, Pawlukojc and Leciejewicz have confirmed the presence of molecular dimers in the crystal.¹² The ionization potential (*I.P.*) of MABA in the gas phase has been measured by Benoit using electron-impact mass spectrometry¹³ and Meeks, *et al.* using photoelectron spectroscopy¹⁴. In both cases, the uncertainty was on the order of tens to hundreds of millielectron Volts. To the best of our knowledge, gas phase spectroscopic studies of MABA in the first electronically excited (*S*₁) and cationic state (*D*₀) are still unavailable.

Recently, we have investigated spectroscopic properties of the first excited electronic state and the cationic ground state of a series of substituted aromatic systems. In monosubstituted systems such as 4-aminopyridine¹⁵ and 2-chloropyrimidine¹⁶, we have concluded that upon excitation and ionization, the substituent would back donate to the



Structure A



Structure B

Figure 7.1 Structures of conformers A and B of MABA.

aromatic ring, ensuring the integrity of the ring structure. In the bi-substituted system of PABA¹⁷, we have learned that in the S_1 state, due to a twist of the amino group around the C-N bond, the carboxylic group plays an important role in electron back donation. Upon further excitation to the D_0 state, on the other hand, the amino group demonstrates strong hyper conjugation with the ring. For all the substituted systems we have investigated, due to this type of back donation, a propensity has been observed in the two photon zero kinetic energy (ZEKE) photoelectron spectroscopy experiment, i.e., the vibrational excitation of the intermediate state is largely preserved upon ionization. Further extended studies to MABA and OABA can reveal the effect of the internal interaction between the functional groups and the site of substitution.

In this work, we report two-color two-photon resonantly enhanced multiphoton ionization (REMPI) and ZEKE spectroscopy of MABA. To identify and characterize each conformer, the hole-burning method is used in the REMPI experiment. Detailed spectroscopic analysis for the vibrational levels of the S_1 state and the D_0 state is performed, with the assistance of *ab initio* and density functional calculations. Adiabatic ionization energies of the two conformers are also determined. From the distribution of active vibrational modes and comparisons between the ZEKE and REMPI spectra, conclusions on the structural changes upon electronic excitation and ionization will be obtained. Implications of these structural changes, particularly in the charge distribution among the ring and the substituents, will be discussed. Comparisons of these observations with those of PABA will be analyzed.

7.3. Experimental Section

The experimental apparatus is a standard molecular beam machine with a time of flight mass spectrometer (TOF-MS) and a pulsed valve for supersonic cooling.¹⁸ MABA was purchased from Aldrich Co. and used without further purification. The sample was housed and heated to 165°C in the nozzle to obtain sufficient vapor pressure. The vapor was seeded in ~ 2.5 atm of argon and expanded into vacuum through a pulsed valve with a 1 mm diameter orifice.

Two different experiments were performed to investigate the spectroscopy of the S_1 state. The two-color two-photon REMPI spectrum was recorded by scanning the pump

laser (Laser Analytical Systems, LDL 20505, pumped by a Nd:YAG laser, Spectra Physics, GCR 190) through the vibronic levels of the S_1 state while using the fourth harmonic of a Nd:YAG laser at 266 nm (Continuum, Powerlite 7010) for further ionization. In order to separate the different conformational isomers, we performed a UV-UV hole-burning experiment using a third (hole-burning) UV laser (Laser Analytical Systems, LDL 2051, pumped by a Nd:YAG laser, Spectra Physics, GCR 230) fixed on one of the origin bands with a time advance of 20 ns. The hole-burning spectra were obtained by monitoring the difference in the ion signal with and without the hole-burning laser. The two resonant laser beams were set to counterpropagate, while the ionization laser was set to cross the two resonant laser beams at a 5° angle. The light path, the flight tube, and the molecular beam were mutually perpendicular. The relative timing between the laser pulses was controlled by two delay generators (Stanford Research, DG535).

In the two-color ZEKE experiment, the two tunable dye lasers with frequency doubling units were used. The optimal signal was obtained under temporal overlap between the two lasers. Molecules excited to the ZEKE states by the two tunable lasers were allowed to stay for 1-2 μ s in the presence of a spoiling field of ~ 1 V/cm, and ionization and extraction was achieved by a pulsed electric field of ~ 16 V/cm.

In order to assign the observed vibronic structures in both the REMPI and ZEKE spectra, we used the Gaussian 03 suite¹⁹ to perform a series of calculations. For the ground state of the neutral and the cation, density functional theory calculations using the Becke 3LYP functional were carried out with the 6-31G+(d) basis set. The excited state geometry and harmonic frequencies were calculated at the CIS level using the 6-31G(d) basis set. Good agreement between experimental and theoretical results was obtained when a scaling factor of 0.9 for the calculated frequencies of the S_1 state was used.²⁰ No scaling factor for the cationic state was used.

7.4. Results

7.4.1. Two-color 1+1' REMPI and UV-UV hole-burning spectroscopy

The two-color 1+1' REMPI spectrum of MABA is displayed in Figure 2(a). The origin band is a doublet feature, labeled I (30479 cm^{-1}) and II (30506 cm^{-1}). We thus expect two conformational isomers coexisting in the ground state of MABA. Both conformers

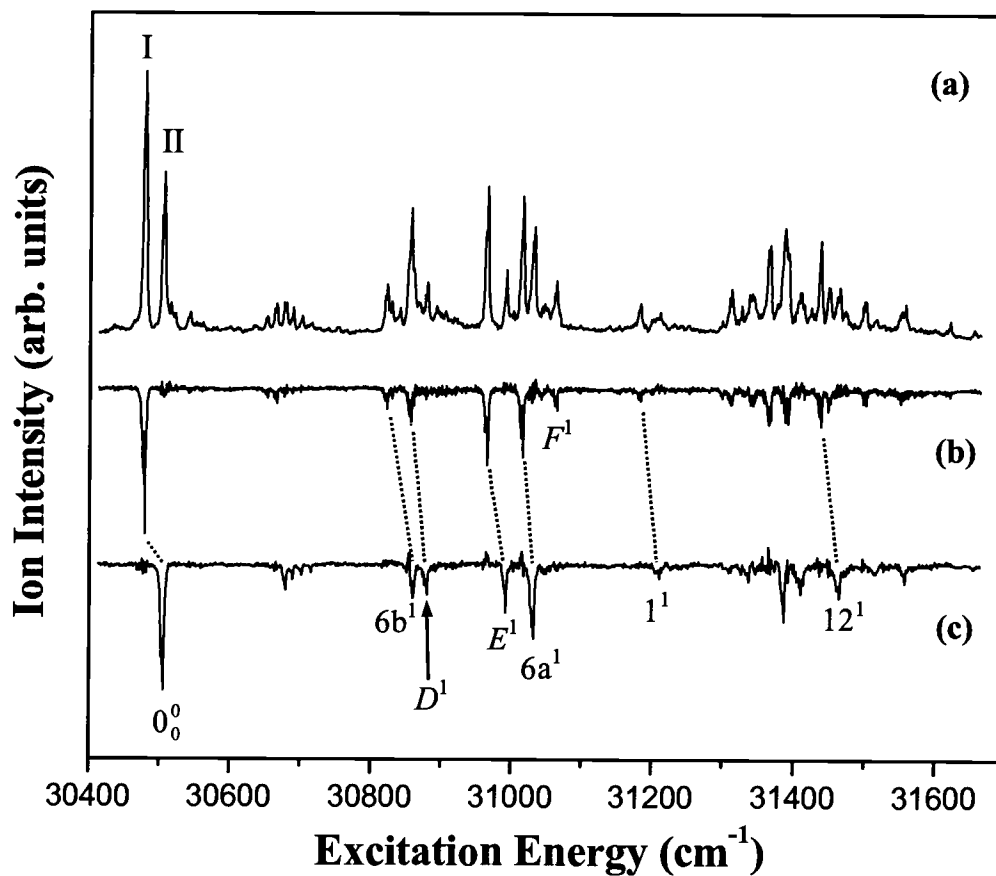


Figure 7.2 Two-color two-photon REMPI spectrum of jet-cooled MABA (a) and UV-UV hole-burning spectra with the hole-burning laser fixed at the I (30479 cm^{-1} , b) and II (30506 cm^{-1} , c) positions.

contribute to the REMPI spectrum, and to identify the features of each conformer, we performed the UV-UV hole-burning experiment as explained earlier. Figure 2(b) and 2(c) show the hole-burning spectra of the two conformers, with the burn laser set to the I (30479 cm^{-1}) or II (30506 cm^{-1}) position respectively. These two conformers are hereafter denoted I and II in keeping with the label of their origin, and conformational assignment to the structures depicted in Figure 1 will be explained in the following discussion section. The REMPI spectra for the two conformers bear close resemblance to each other, which indicates close similarity in structure. The hole-burning spectra exclude the existence of other conformers over the spectral range of the REMPI spectrum, since all the significant features in Figure 2(a) can be associated with either conformer I or II.

The vibronic transitions of the two conformers are listed in Table I. For each conformer, there are 45 normal modes, among which, 30 are associated with the aromatic ring, 6 are associated with the amino moiety, and 9 are associated with the carboxylic acid moiety. The seven stretching modes involving N-H, O-H, and C-H bonds are on the order of 3000 cm^{-1} , and are therefore not observable in Figure 2. To assist assignment, we have performed *ab initio* calculations on the CIS/6-31G(d) level for both conformers and used a scaling factor of 0.9 to compare with the experimental result. Our calculation shows $\pi\pi^*$ character for the S_1 state, and the direction of the transition dipole moment should be in the plane of the aromatic ring. Only in-plane or even quanta of out-of-plane vibrational modes are thus symmetry allowed. In Table I, modes that are associated with the motion of the aromatic ring are labeled using Varsanyi's nomenclature.²¹ Other modes that mainly involve the motion of $-\text{NH}_2$ and $-\text{COOH}$ moieties are named with letters from *A* to *G* in the order of increasing frequency. However, in some instances, strong coupling between the ring and the substituent renders this type of assignment only an approximation. For example, based on the displacement vector from our calculation, mode *E* highly couples with mode 6a, and similarly, mode 1 and mode *F* ($-\text{COOH}$ scissoring motion) also demonstrate strong mixing. Nevertheless, in Table I, the overall agreement between the calculation and the experiment is quite satisfactory.

Similar to PABA, MABA also demonstrate high activities of ring deformation modes (6a, 6b, and 12) and in-plane bending modes that mainly involve motions of either the carboxylic group or the amino group (mode *A* through *G*). Interestingly, neither the

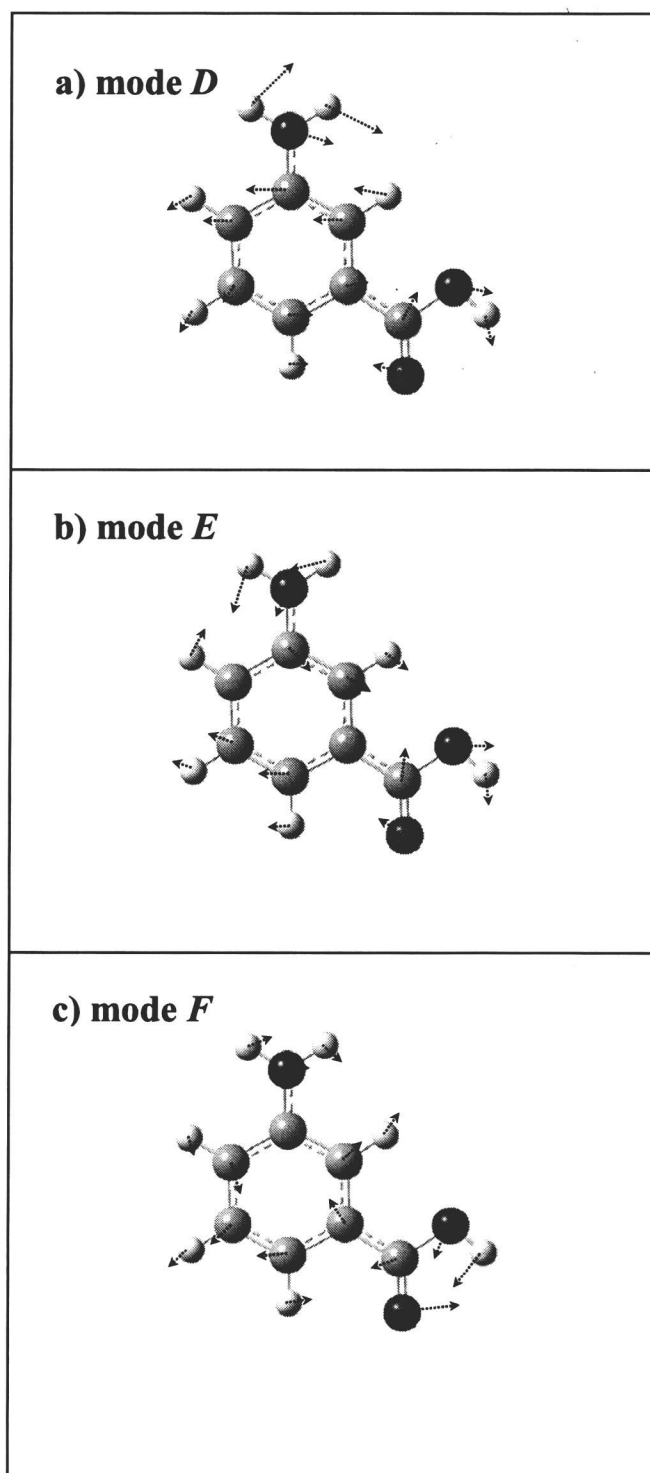


Figure 7.3 Displacement vectors of a) mode *D* at 377 cm^{-1} , b) mode *E* at 486 cm^{-1} , and c) mode *F* at 585 cm^{-1} , of the S_1 state for conformer A.

Table 7.1. Observed vibrational frequencies and assignments for the S_1 state of MABA.

conformer I		conformer II		Assignment and approx. description [#]
Exp.	Calc.*	Exp.	Calc.*	
	91		90	A_0^1 , C-COOH torsion
	95		96	B_0^1 , γ (-COOH)
174	171	171	172	C_0^1 , β (-COOH)
186		183		A_0^2
		195		B_0^2
		208	222	I_0^1 , NH_2 inversion
344	346	354	340	$6b_0^1$, β (ring)
377	369	374	372	D_0^1 , β (-NH ₂)
486	475	486	473	E_0^1 , β (-COOH), β (-NH ₂) and β (ring)
536	513	525	528	$6a_0^1$, β (ring)
585	595			F_0^1 , -COOH scissoring
704	694	699	696	I_0^1 , ring breathing
830				$6b_0^1 E_0^1$
863	872			$19a_0^1$, β (ring)
888		881		$6b_0^1 6a_0^1$
914		905		$D_0^1 6a_0^1$
959	948	960	949	12_0^1 , β (ring)
971		968		E_0^2
1023	1020	1012	1008	G_0^1 , β (N-H)
1074		1052		$6a_0^2$
1141	1148			$8a_0^1$

* The values include a scaling factor of 0.9.

β and γ represent in-plane bending and out-of-plane bending vibrations.

experimental nor the theoretical vibrational frequencies exhibit substantial dependence on the molecular conformation. The distance between the two substituents must be long enough to prevent intramolecular coupling. Consequently, the vibrational frequencies cannot be used for conformational assignments. This insensitivity of the vibrational frequency to the molecular conformation could also partially account for the negligence of the two coexisting conformers in the infrared spectroscopic studies.^{6, 11} The weak progression-like peaks around 180 cm^{-1} in Figure 2(a) looks intriguing at first sight, but they actually belong to the two different conformers based on the hole-burning experiment. The two peaks associated with conformer I are assigned as one quanta of mode *C* (174 cm^{-1}) and two quanta of mode *A* (186 cm^{-1}). The corresponding transitions of conformer II in Figure 2(c) constitute the first two small peaks at 171 cm^{-1} and 183 cm^{-1} , while the other two small peaks on the higher energy side are assigned as two quanta of mode *B* (195 cm^{-1}) and one quanta of mode *I* (208 cm^{-1}). Given a shift of 27 cm^{-1} of the origin band, these six transitions appear as a progression with an average spacing of 12 cm^{-1} .

The displacement vectors for three of the in-plane modes (mode *D*, *E*, and *F*) with high transition intensities for the conformer with structure A are shown in Figure 3, while those for structure B are similar and are therefore not reproduced. All three modes involve distortion of the phenyl ring. Mode *D* mainly involves in-plane bending of the amino group. Mode *E* mainly involves in-plane bending of the carboxylic group and the amino group, but it also couples to the 6a type ring deformation. Mode *F* can be described as the scissoring motion of the carboxylic group. All three modes were chosen as intermediate states in the following ZEKE experiment.

7.4.2. ZEKE spectra

The ZEKE spectra of the two conformers are presented in Figures 4 - 6, and the spectral assignments are summarized in Tables II and III, together with our calculation results at the B3LYP/6-31G+(d) level. No scaling factor for the vibrational frequencies of the cation is used in the list, and the agreement seems to be quite reasonable. Limited by the linewidth of each resonant transition of the S_1 state, unfortunately, the error in the experimental values is 5 cm^{-1} . The same labeling scheme as that of the S_1 state is used in

the assignment of the D_0 state, however, an additional “+” sign in the superscript is used to distinguish the vibrational levels of the cation. The identity of the intermediate level for each ZEKE spectrum is marked on the figure by a black dot. Among the ten ZEKE spectra, each is dominated by a single strong feature, and the identity of this feature is the same as that of the intermediate state. A propensity of $\Delta\nu = 0$ can thus be identified; i.e., the vibrational quantum number ν of each mode is directly transferred from the intermediate state to the cationic state, with little vibrational relaxation or mode mixing. This strong correlation between the intermediate level and the final vibrational level of the cation has also been reported in our previous studies of 4-aminopyridine¹⁵, 2-chloropyrimidine¹⁶ and PABA¹⁷, and the origin of the rigidity of the molecular frame upon photoionization has been discussed.

7.4.2.1. Conformer I

Figure 4 (a) shows the ZEKE spectrum recorded via the origin of conformer I. The most intense peak in the spectrum corresponds to the origin of the cation. The resulting adiabatic ionization potential, including a correction due to field ionization,²² is $64004 \pm 5 \text{ cm}^{-1}$ ($7.9354 \pm 0.0006 \text{ eV}$). In contrast, the *I.P.* value of MABA was first determined to be 8.41 eV in 1973 by Benoit using electron-impact mass spectrometry.¹³ Another report by Meeks, *et al.* using photoelectron spectroscopy listed a value of 8.3 eV.¹⁴ A likely explanation for the higher values from the previous studies is the small Franck-Condon factor at the threshold in single photon ionization or electron-impact ionization. Other transitions in Figure 4(a) with lower intensities correspond to excitations of mode C^+ , $6b^+$, and E^+ . As will be seen in the following, these modes constitute the majority of the active modes in most of the ZEKE spectra.

The other three ZEKE spectra in Figure 4 (the top three panels) are associated with the in-plane bending modes $6b$, E and $6a$. These spectra demonstrate remarkable resemblance to each other and to Figure 4(a), including combinations with modes C^+ , $6b^+$, and E^+ . In the ZEKE spectrum taken via mode $6b$, the activation of other fundamental modes is also observable, including modes C^+ and $16a^+$ (not labeled in the figure to avoid congestion). Ionization via mode E activates the ring deformation mode $6a^+$ (Figure 4(c)). It is interesting to notice that in Figure 4(d), the reverse is also true, i. e., ionization via

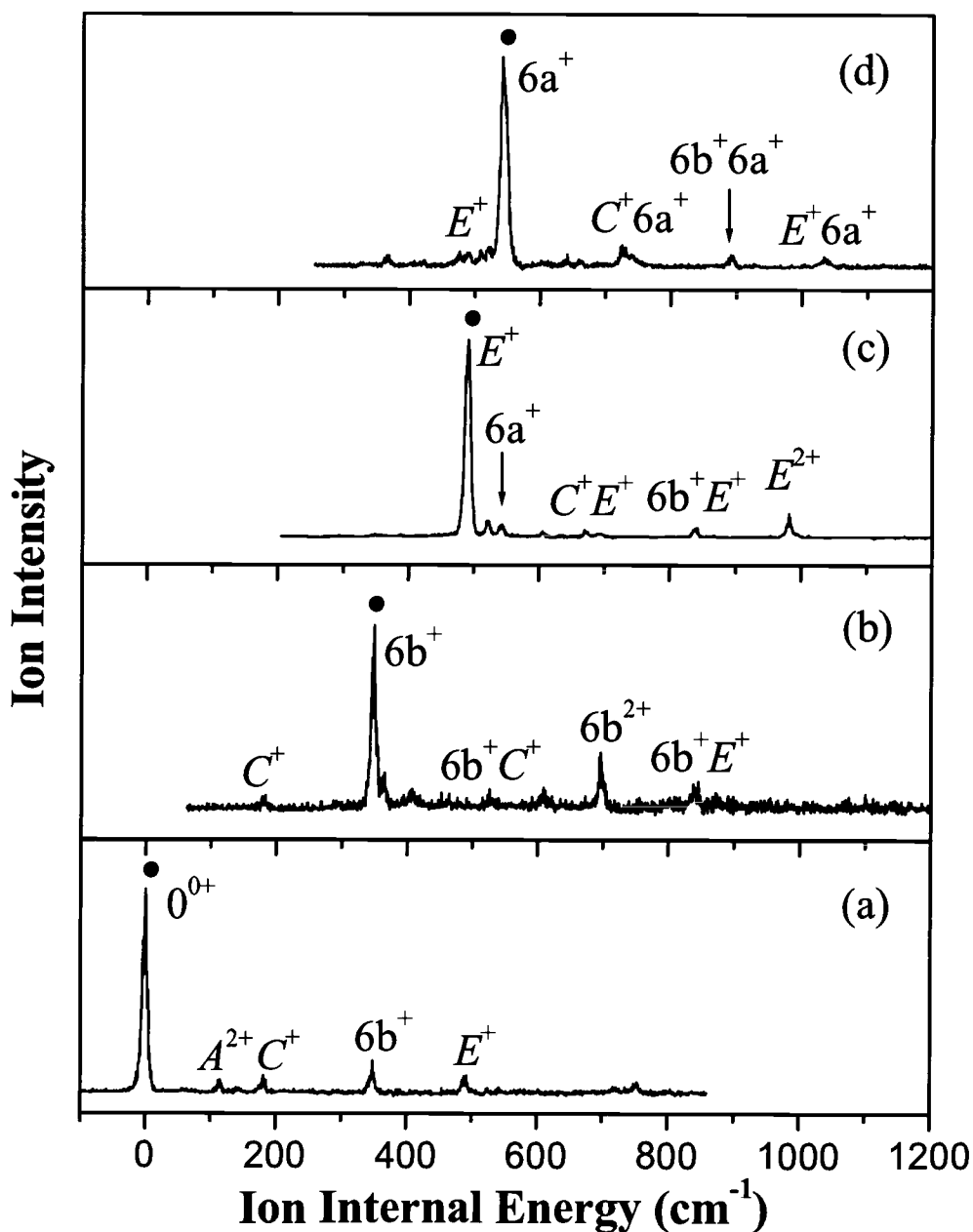


Figure 7.4 Two-color ZEKE spectra of conformer I recorded via the following vibrational levels of the S_1 state as intermediate states: (a) 0^0 , (b) $6b^1$, (c) E^1 , and (d) $6a^1$. The energy in the abscissa is relative to the ionization threshold at 64004 cm^{-1} . The assignment in the figure refers to the vibrational levels of the cation, and the corresponding vibrational level of the intermediate state is labeled by a black dot on each spectrum.

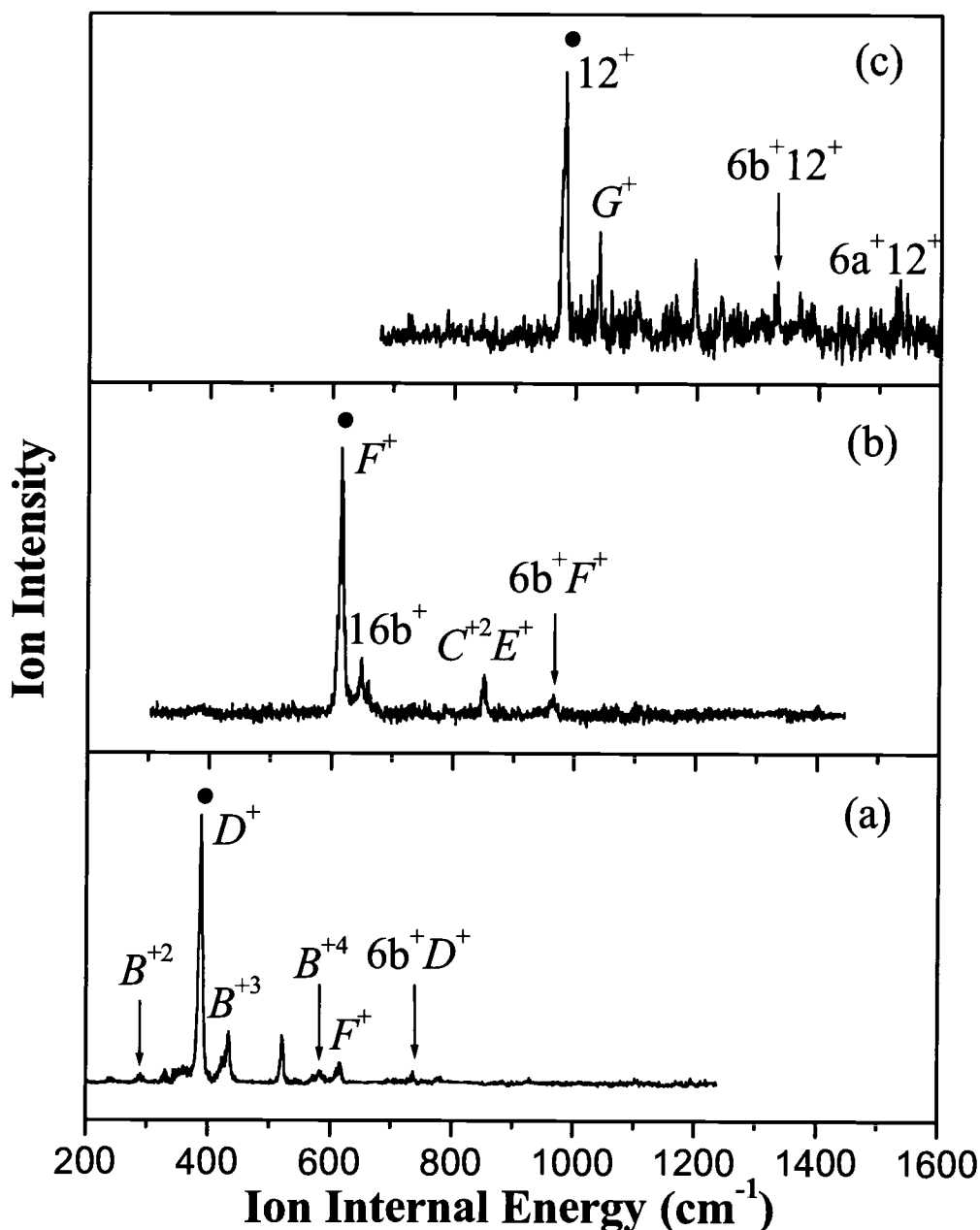


Figure 7.5 Two-color ZEKE spectra of conformer I recorded via the following vibrational levels of the S_1 state as intermediate states: (a) D^1 , (b) F^1 , and (c) 12^1 . The energy in the abscissa is relative to the ionization threshold at 64004 cm^{-1} . The assignment in the figure refers to the vibrational levels of the cation, and the corresponding vibrational level of the intermediate state is labeled by a black dot on each spectrum.

Table 7.2. Observed vibrational frequencies and assignments in the ZEKE spectra of MABA (conformer I).

Intermediate level in the S ₁ state							Calc.	Assignment
0 ₀ ⁰	6b ₀ ¹	D ₀ ¹	E ₀ ¹	6a ₀ ¹	F ₀ ¹	12 ₀ ¹		
115							112	A ⁺²
143							149	B ⁺
182	183						183	C ⁺
		290						B ⁺²
349	349						359	6b ⁺
				368				C ⁺²
		388					387	D ⁺
	407						387	16a ⁺
		434						B ⁺³
				477			472	4 ⁺
492			491				497	E ⁺
		522	521					A ⁺² 16a ⁺
	526							C ⁺ 6b ⁺
			544	542			544	6a ⁺
		583						B ⁺⁴
	608		605					A ⁺² E ⁺
		615			615		633	F ⁺
					650		647	16b ⁺
			669					C ⁺ E ⁺
	696							6b ⁺²
716							728	1 ⁺
				726				C ⁺ 6a ⁺
		736						6b ⁺ D ⁺
753							767	17b ⁺
		780						D ⁺²
	845		840					6b ⁺ E ⁺
					851			C ⁺² E ⁺
				892				6b ⁺ 6a ⁺
					966			6b ⁺ F ⁺
			982					E ⁺²
						982	994	12 ⁺
				1033				E ⁺ 6a ⁺
						1039	1043	G ⁺
						1332		6b ⁺ 12 ⁺
						1527		6a ⁺ 12 ⁺

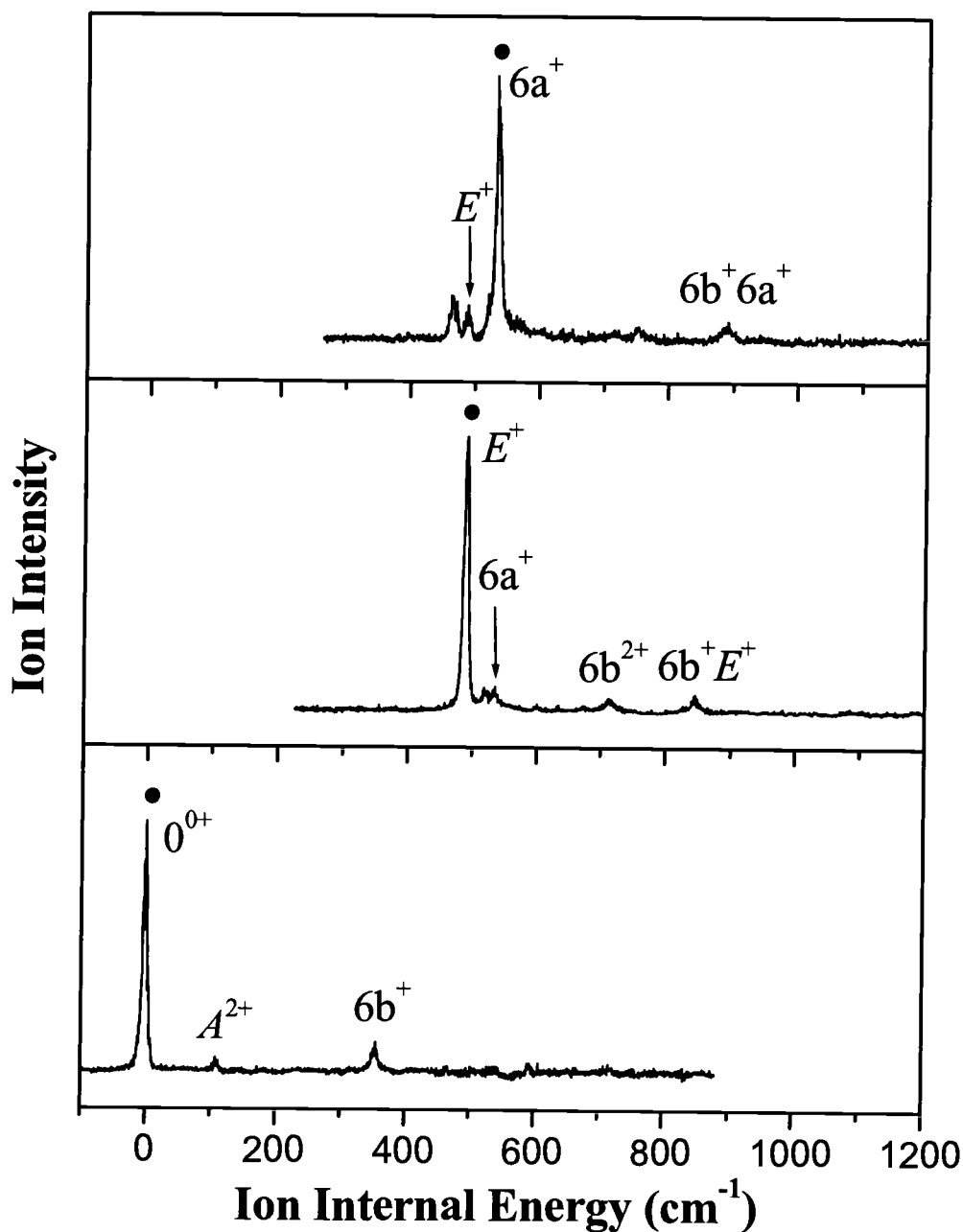


Figure 7.6 Two-color ZEKE spectra of conformer II recorded via the following vibrational levels of the S_1 state as intermediate states: (a) 0^0 , (b) E^1 , and (c) $6a^1$. The energy in the abscissa is relative to the ionization threshold at 64011 cm^{-1} . The assignment in the figure refers to the vibrational levels of the cation, and the corresponding vibrational level of the intermediate state is labeled by a black dot on each spectrum.

Table 7.3. Observed vibrational frequencies and assignments in the ZEKE spectra of MABA (conformer II).

Intermediate level in the S_1 state				Assignment
0_0^0	E_0^1	$6a_0^1$	Calc.	
108			122	A^{+2}
181			182	C^+
355			351	$6b^+$
466		463	470	4^+
485	490	489	498	E^+
	518			$A^{+2}16a^+$
	535	533	550	$6a^+$
593				$A^{+2}E^+$
	634		625	F^+
	672			C^+E^+
	712			$6b^{+2}$
716		715		C^+6a^+
752		752	767	$17b^+$
	845			$6b^+E^+$
		892		$6b^+6a^+$

mode 6a results in the activation of mode E^+ . This observation implies coupling between the two modes.

The ZEKE spectra in Figure 5 demonstrate variations from the consistent pattern shown in Figure 4. All three spectra display a combination band with mode $6b^+$, while the other two bands in Figure 4(a), C^+ and E^+ , are missing, perhaps due to our limited sensitivity. In Figure 5(a), a progression of the out-of-plane bending mode B of the carboxylic group is observable, with up to four vibrational quanta. In Figure 5(b), the two relatively strong features at 650 cm^{-1} and 851 cm^{-1} are tentatively assigned as $16b^+$ and $C^{+2}E^+$. In Figure 5(c), the peak at 1039 cm^{-1} with a medium intensity is tentatively assigned as the -N-H in-plane bending mode G^+ , in reference to our *ab initio* result of 1043 cm^{-1} .

7.4.2.2. Conformer II

Figure 6 (a) shows the ZEKE spectrum of MABA recorded via the origin of the S_1 state of conformer II, and the most intense peak in the spectrum corresponds to the origin of the cation. The resulting adiabatic ionization potential, including a correction due to field ionization, is $64011 \pm 5\text{ cm}^{-1}$ ($7.9363 \pm 0.0006\text{ eV}$). This value is within the error limit of conformer I.

The spectra in Figure 6 are sparse, and in all cases, only combinations with mode $6b^+$ can be clearly identified. Compared with the ZEKE spectra of conformer I in Figure 4(a), modes C^+ and E^+ are even weaker for conformer II. Apparently rotation of the -COOH group by 180° can change its activity, both for the in-plane bending mode C^+ and the coupled bending mode E^+ .

7.5. Discussion

To assign the structures of the two conformers, we performed DFT calculations on the B3LYP level for the S_0 and D_0 states, and *ab initio* calculations at the CIS level for the S_1 state. The two lowest energy conformations in the ground state are shown in Figure 1, and the key geometrical parameters are listed in Table 4. These two conformations differ by a 180° rotation of the carboxylic group, and the resulting differences in the geometric parameters are minor. Structure B is only slightly more stable than structure A, by 0.20

kcal/mol, including corrections due to zero-point energies. The transition energy to S_1 , on the other hand, is 4.9014 eV for structure A and 4.9321 eV for structure B. A blue shift of 0.03 eV (240 cm^{-1}) is therefore expected in the REMPI spectrum of structure B. We thus assign conformer II to be of structure B, and conformer I to be of structure A. Although the energy difference from our calculation is larger than the experimental value, we believe that the theory should be qualitatively reliable in predicting the trend in transition energies. Our calculation also yields ionization potentials of 62749 cm^{-1} and 62760 cm^{-1} for structures A and B. Limited by the uncertainty of the experimental values and the uncertainty of these calculations, however, we cannot use this information to assist with the assignment. Nevertheless, there is no conflict between theory and experiment with respect to the values of *I.P.* for the two conformers. As stated in Section III.A, the values of vibrational frequencies, unfortunately, cannot be used in this assignment due to their insensitivity to molecular conformation.

Photoexcitation to the S_1 state induces changes in the substituents, the aromatic ring, and the bonding between the ring and the substituents. In Table 4, our DFT calculation shows nonplanar geometries for both conformers in their ground state, with the amino group poking out of the plane of the ring at similar angles of $\sim 20^\circ$. This result agrees with the study using X-ray crystallography.⁹ For the S_1 and D_0 states, interestingly, both conformers are found to be planar. Our CIS calculation also implies $\pi\pi^*$ characters for the S_1 state of both conformers. During the $S_1 \leftarrow S_0$ transition, the bond lengths for C1-N7 and C3-C8 decrease, which indicates participation of both polar groups in the conjugation with the aromatic ring. The resulting chemical bonds between the adjacent moieties take on partial double-bond characters. In addition, photoexcitation induces a slight distortion of the aromatic ring. Elongation of the ring along the C2-C5 axis can be observed, resulting in separation between the positive half and the negative half of the ring. These changes are responsible for the activation of the ring deformation modes 6a, 6b and 12, and the in-plane bending modes *A* through *G* for both conformers.

Back donation from an electron rich substituent to the ring upon excitation has been a common theme among our studies of polar substituted aromatic systems.¹⁵⁻¹⁷ In mono-substituted systems, the bond length between the substituent and the ring demonstrates dramatic shortening.^{15,16} In the bi-substituted system PABA,¹⁷ the Mulliken charge²³ on

Table 7.4. Molecular geometry parameters of MABA in the S_0 , S_1 , and D_0 states.

	S_0		S_1		D_0	
	conformer I	conformer II	conformer I	conformer II	conformer I	conformer II
<i>Bond length (Å)</i>						
C1-N7	1.395	1.395	1.339	1.338	1.335	1.335
C1-C2	1.400	1.399	1.409	1.409	1.434	1.432
C2-C3	1.397	1.396	1.405	1.407	1.374	1.375
C3-C4	1.399	1.399	1.435	1.430	1.415	1.414
C4-C5	1.391	1.392	1.394	1.397	1.410	1.413
C5-C6	1.392	1.391	1.389	1.389	1.372	1.371
C6-C1	1.404	1.405	1.437	1.436	1.433	1.434
C3-C8	1.487	1.487	1.440	1.441	1.505	1.508
C=O	1.209	1.210	1.207	1.206	1.201	1.201
C-O(H)	1.360	1.358	1.347	1.346	1.341	1.339
<i>dihedral angle (°)</i>						
H1N7C1C6	24.526	24.826	0	0	0	0
H2N7C1C2	-23.198	-22.426	0	0	0	0

Table 7.5. Mulliken charge distributions of MABA in the S_0 , S_1 , and D_0 states.

	S_0		S_1		D_0	
	conformer I	conformer II	conformer I	conformer II	conformer I	conformer II
-NH ₂	+0.104	+0.104	-0.185	-0.184	+0.372	+0.375
-COOH	-0.117	-0.101	-0.042	-0.042	+0.084	+0.107
Benzene ring	+0.012	0	+0.228	+0.225	+0.545	+0.516
C1	-0.560	-0.534	+0.370	+0.370	-0.373	-0.391
C3	+0.467	+0.469	-0.119	-0.118	+0.470	+0.470

the amino group becomes negative upon excitation to S_1 , while the charge on the carboxylic group becomes positive. We attribute this result to ineffective charge transfer from the amino group to the ring, since in the S_1 state, the amino group is not only out of the plane of the ring, but also twisted around the C-N single bond. As a result, only the planar carboxylic group is available for effective electron back donation. In MABA, the situation is different, since the amino group becomes planar in S_1 , permitting facile electron transfer. However, the Mulliken charge distribution in Table 5 is qualitatively similar to that in PABA, i.e., only the carboxylic group participates in electron back donation, while the amino group seems to be electron withdrawing. This apparent reversal of the role of the two substituents in the electron push-pull scenario of the S_1 state is intriguing. Based on the change in the bond lengths of C1-N7 and C3-O8, we tentatively propose that the lone pair electrons on the amino group indeed become more conjugated with the ring upon excitation, and that there is effective electron back donation in the S_1 state. However, the π^* orbital may contain an important contribution from the atomic orbitals of the amino nitrogen. The resulting π^* cloud therefore preferentially locates at the amino group, resulting in a large net negative charge on the amino group. Some tangible evidence can be seen from the related orbitals obtained from our CIS calculation.

The $D_0 \leftarrow S_1$ ionization process involves the removal of the π^* electron. The resulting major change is the increase of the bond length C3-C8, while the bond length for C1-N7 is essentially unchanged (Table 4). This result implies that there is no change in the degree of electron back donation from the amino group to the ring upon ionization. According to our Mulliken population analysis, the atomic charge on the amino group of conformer I is changed from -0.185 in the S_1 state to +0.372 in the D_0 state, and the change is similar for conformer II (Table 5). Overall, more than 50% of the electron loss upon ionization is from the amino group. This observation further supports our proposal of a high probability of the π^* orbital around the amino group. Effective back donation from the amino group greatly alleviates the electron-deficiency of the ring in the D_0 state, and the resulting positive charge on the ring is only slightly more than +0.5. As a result, the rigidity of the ring structure remains, even during ionization. The normal coordinates

are largely unchanged, and similar to the case of PABA,¹⁷ a strong propensity for $\Delta\nu = 0$ should therefore be obeyed, as evidenced in the ZEKE spectra in Figures 4 - 6.

It is interesting to compare the change in the molecular frame of MABA and PABA upon electronic excitation and ionization. In PABA,¹⁷ the C-N bond length becomes progressively shorter with successive excitation, while in MABA, the C-N bond length essentially reaches its lower limit in the S_1 state, and further ionization has no effect. An interpretation of this difference is that the twist of the amino group in the S_1 state of PABA did not allow effective electron back donation from the amino group to the ring. Only after ionization when the amino group becomes planar can the electron back donation effect achieves its maximum potential. In MABA, the amino group is planar in both the S_1 and D_0 states, and electron back donation reaches its maximum potential in the S_1 state. The change in the C-C(OOH) bond length is similar for MABA and PABA: it first decreases in the S_1 state and then increases to a maximum value in the D_0 state. Conjugation between the carboxylic group and the ring is thus removed upon ionization. In PABA, the electron donating role of the carboxylic group is still sizable in the D_0 state, with a positive charge of +0.307. In MABA, however, the carboxylic group is essentially oblivious to the electron deficiency of the ring, while a significant fraction of the positive charge is located on the amino group.

The distance between the two substituents plays an important role with respect to the stability of the molecular structure. In our work on PABA,¹⁷ we observed a doublet splitting in the ZEKE spectrum obtained via the amino inversion mode. Since the cationic state was shown to be planar from our DFT calculation, the origin of the splitting was puzzling. We tentatively considered the (remote) coupling of the amino group with the carboxylic group. In MAPA, the intramolecular interaction between the two substituents becomes sufficiently strong to manifest as two different conformers in the ground state. Limited by the low transition intensity of the inversion mode in the REMPI spectrum (Figure 2), we were unable to record the ZEKE spectrum via this mode. However, we suspect that the favorable interaction between the two substituents in the planar geometry will only increase the barrier for internal rotation, and no tunneling splitting between the two conformers should therefore be observed. In fact, as evidenced by the hole-burning experiment in Figure 2, even in the non-planar ground state, which is

unfavorable for the formation of a loose internal hydrogen bond, the barrier for internal rotation is sufficiently high to prevent interconversion between the two conformers.

7.6. Conclusion

Spectroscopic properties of the excited and ionic states of both conformers of MABA have been studied using two-color REMPI and ZEKE spectroscopy. Several in-plane and out-of-plane vibrational modes and combination bands in both states have been identified. *Ab initio* and DFT calculations are found to be largely consistent with the experimental observation, and the resulting transition energies to the S_1 state are used to assign the structures of the two observed conformers. The adiabatic ionization energy in the gas phase is determined to be $64004 \pm 5 \text{ cm}^{-1}$ ($7.9354 \pm 0.0006 \text{ eV}$) and $64011 \pm 5 \text{ cm}^{-1}$ ($7.9363 \pm 0.0006 \text{ eV}$) for conformer I and II. The similarity in geometry between the S_1 state and the D_0 state in both conformers results in a strong propensity during ionization; i.e., the ZEKE spectrum obtained via a vibrational level of the S_1 state features a dominant transition to the same vibrational level of the cation. The origin of this rigidity can be traced to electron back donation of the amino group in both the S_1 and D_0 states. The carboxylic group mainly participate in the back donation of the S_1 state, while its contribution in the D_0 state is minimal. This behavior is different from that of PABA where the carboxylic group plays an important role in both S_1 and D_0 . The distance between the two substituents affects not only the structure and stability of the molecular frame but also the tendency of electron back donation upon electronic excitation and ionization.

7.7. Acknowledgements

This work was supported by the National Science Foundation, Division of Chemistry. Acknowledgment is made to the Donors of The Petroleum Research Fund, administered by the American Chemical Society, for partial support of this research. Wei Kong is an Alfred P. Sloan research fellow.

7.8. References

- ¹ A. Yamamoto, T. Sakane, M. Shibukawa, M. Hashida, and H. Sezaki, *J. Pharm. Sci.* **80**, 1067 (1991).
- ² M. Tang, J. Isbell, B. Hodges, and J. Brodbelt, *J. Mass Spectrom.* **30**, 977 (1995).
- ³ T. Ueyama, T. Fujita, A. Yamamoto, and S. Muranishi, *Proceedings of the International Symposium on Controlled Release of Bioactive Materials* **23**, 597 (1996).
- ⁴ K. B. Wiberg, *J. Org. Chem.* **67**, 4787 (2002).
- ⁵ J. Trujillo-Ferrara, L. Montoya Cano, and M. Espinoza-Fonseca, *Bioorg. Med. Chem. Lett.* **13**, 1825 (2003).
- ⁶ L. Gopal, C. I. Jose, and A. B. Biswas, *Spectrochim. Acta* **23A**, 513 (1967).
- ⁷ A. Théorêt, *Spectrochim. Acta* **27A**, 11 (1971).
- ⁸ M. A. Palafox, M. Gil, and J. L. Nunez, *Spectrosc. Lett.* **29**, 609 (1996).
- ⁹ J. Voogd, B. H. M. Verziji, and A. J. M. Duisenberg, *Acta Crystallogr. B* **36**, 2805 (1980).
- ¹⁰ T. Yoshida and S. Sawada, *Bull. Chem. Soc. Jpn.* **49**, 3319 (1976).
- ¹¹ Yu. Ya. Kharitonov, and I. I. Oleinik, *Dokl. Akad. Nauk.* **313**, 384 (1990).
- ¹² A. Pawlukoje and J. Leciejewicz, *Chem. Phys.* **299**, 39 (2004).
- ¹³ F. Benoit, *Org. Mass Spectrom.* **7**, 295 (1973).
- ¹⁴ J. Meeks, A. Wahlborg, and S. P. McGlynn, *J. Electron Spectrosc.* **22**, 43 (1981).
- ¹⁵ Y. He, C. Wu, and W. Kong, *J. Chem. Phys.* **120**, 7497 (2004).
- ¹⁶ Y. He, C. Wu, and W. Kong, *Chem. Phys. Lett.* **391**, 38 (2004).
- ¹⁷ Y. He, C. Wu, and W. Kong, *J. Chem. Phys.* (in press, 2004).
- ¹⁸ Y. He, C. Wu, and W. Kong, *J. Phys. Chem. A* **107**, 5145 (2003).
- ¹⁹ GAUSSIAN 03, Revision A. 7, M. J. Frisch, *et al.*, Gaussian, Inc., Pittsburgh, Pennsylvania, 2003.
- ²⁰ M. E. Casida, C. Jamorski, K. C. Casida, and D. R. Sulahub, *J. Chem. Phys.* **108**, 4439 (1998).
- ²¹ G. Varsanyi, *Assignment of Vibrational Spectra of Seven Hundred Benzene Derivatives* (Wiley, New York, 1974).
- ²² E. W. Schlag, *ZEKE Spectroscopy* (Cambridge University Press, Cambridge, 1998).
- ²³ R. S. Mulliken, *J. Chem. Phys.* **23**, 1833 (1955).

**Cation vibrational energy levels of 1,3-benzodioxole obtained
via zero kinetic energy photoelectron spectroscopy**

Yonggang He, Chengyin Wu, and Wei Kong*

*Department of Chemistry, Oregon State University,
Corvallis, Oregon 97331-4003*

Chemical Physics Letters, **2005**, *402*, 212-216.

* Corresponding author, email: wei.kong@oregonstate.edu, fax: 541-737-2062

8. Cation vibrational energy levels of 1,3-benzodioxole obtained via zero kinetic energy photoelectron spectroscopy

8.1. Abstract

We report vibrational analysis of the cation of 1,3-benzodioxole using two-color zero kinetic energy photoelectron spectroscopy. With the aid of density functional calculations, vibrational modes of the cation have been assigned, and the adiabatic ionization potential has been determined to be $64341 \pm 5 \text{ cm}^{-1}$ ($7.9772 \pm 0.0006 \text{ eV}$). Unlike the ground state and the first electronically excited state of the neutral molecule, the ground state of the cation is proven to be planar. This revelation will help with the vibrational analysis of the excited electronic state.

8.2. Introduction

1,3-benzodioxole (BDO) is an indan-like benzene-fused ring molecule as shown in Figure 1. The five-membered ring contains a double bond, which makes it a pseudo four-membered system, since the double bond is believed to be highly resistant to twisting. Both the puckering (mode 39, P) and the flapping (mode 38, F) modes of the five-membered ring are low in frequency, and consequently, BDO has long served as a model system for the study of potential energy surfaces of low frequency vibrations [1]-[5]. Coupling between the two low frequency modes has challenged the spectroscopic assignment of the vibrational quantum states [6].

The geometry of the ground electronic state (S_0) of BDO is now generally accepted to be puckered with a potential barrier of no more than 200 cm^{-1} . However, the first study by Duckett, *et al.* based on far infrared spectroscopy in the region between 50 and 500 cm^{-1} concluded on a planar geometry [7]. Later, Caminati, *et al.* concluded on a double-minimum potential with a 126 cm^{-1} barrier based on the observed zigzag behavior of the rotational constants upon vibrational excitation [1]. The height of the barrier was revised more recently by Sakurai, *et al.* to 164 cm^{-1} , with the puckering and flapping angles of 24° and 3° at the energy minima [2].

The first excited state (S_1) of BDO remains a challenge as of today. It was first studied by Alves, *et al.* from gas-phase electronic absorption spectroscopy [8]. However, no definitive conclusion on the molecular planarity was made. Based on the assignment of the puckering mode, Hassan and Hollas concluded that the molecular skeleton was planar with respect to CH_2 puckering [9]. Laane, *et al.* attempted a complete assignment of the vibrational energy levels in the S_1 state by combining the observations from absorption and laser induced fluorescence experiments [3]. The authors derived a two-dimensional potential energy surface by including both the puckering and the flapping coordinates. A higher barrier of 264 cm^{-1} than that of the S_0 state was obtained, implying an increased anomeric effect in the S_1 state. Pietraperzia, *et al.* [10], on the other hand, obtained rotational resolutions of a few vibrational levels of the S_1 state, and some of their results seem to contradict the original assignment of Laane *et al.* [3]

So far studies on the cationic state (D_0) of BDO have been rare. To our knowledge, the only published work on BDO^+ is the photoelectron spectroscopy by Anderson, *et*

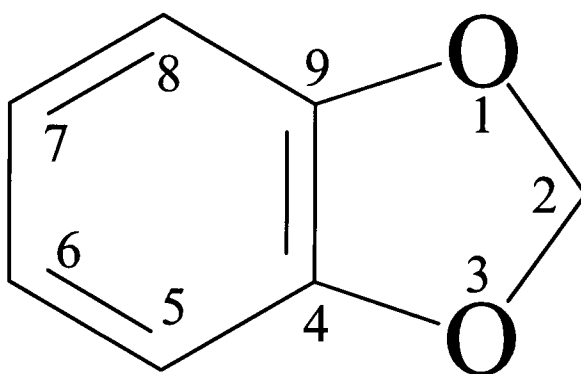


Figure 8.1. Structure of BDO.

al.[11] In this letter, we use two-color two-photon resonantly enhanced multiphoton ionization (REMPI) and two-color zero kinetic energy (ZEKE) photoelectron spectroscopy to investigate the vibrational levels of the ground cationic state. Although we make no formal attempt to resolve the issue with the vibrational energy levels of the S_1 state, as will become clear from our results, we provide evidence that the cationic state is planar. Assignment of the vibrational levels of the cation is therefore independent of the identity of the intermediate level. Moreover, from the ZEKE spectra obtained via different vibrational levels of the S_1 state, we can derive some inspiration with regard to the assignment of the REMPI spectrum.

8.3. Experimental Setup

The experimental apparatus is a standard molecular beam machine with a time of flight mass spectrometer (TOF-MS) [12]. The sample was purchased from Aldrich Co. and the vapor was seeded in argon for supersonic cooling. The REMPI spectra were recorded under two different beam conditions. The ‘cold’ spectrum was recorded under hard expansion conditions with a stagnation pressure of 2.5 atm and a skimmer for differential pumping. The ‘hot’ spectrum was recorded under soft expansion conditions, where the backing pressure was lowered to 0.5 atm, the skimmer was removed, and the nozzle was pushed closer to the detection region. The pump laser was a Nd:YAG (Spectra Physics, GCR 230) pumped dye laser (Laser Analytical Systems, LDL 2051) system equipped with a frequency doubling unit, so was the ionization laser (Laser Analytical Systems, LDL 20505, pumped by Spectra Physics, GCR 190). The absolute wavelength of each laser was calibrated using an iron hollow-cathode lamp filled with neon. The relative timing between the two laser pulses was controlled by a delay generator (Stanford Research, DG535), and the optimal REMPI signal was obtained under temporal overlap between the two lasers. In the UV-UV hole burning experiment, a one-color two-photon REMPI spectrum was first recorded by scanning the pump laser across the vibronic levels of the S_1 state, then a second (hole-burning) UV laser was introduced with a time advance of 100 ns. A hole-burning spectrum was recorded by fixing the second laser on one of the vibronic bands while monitoring the depletion of the ion signal as the pump laser scanned across the REMPI spectrum. In the ZEKE

experiment, molecules excited to ZEKE states were allowed to stay for ~ 1 μ s in the presence of a spoiling field of ~ 1 V/cm, and ionization and extraction was achieved by a pulsed electric field of ~ 16 V/cm.

In order to assign the observed vibronic structures in the ZEKE spectra, we used the Gaussian 03 suite to perform a series of calculations [13]. For the ground state of the neutral and the cation, density functional theory (DFT) calculations using the Becke-Lee-Yang-Parr functional (B3LYP) were carried out with the 6-311G++(d,p) basis set.

8.4. Results

8.4.1. Two-color 1+1' REMPI spectrum

Our two-color 1+1' REMPI spectra of BDO near the origin of the $S_1 \leftarrow S_0$ electronic transition are similar to the fluorescence excitation spectrum reported by Laane, *et al.* [3], and we are currently working on a complete assignment of the REMPI spectrum in collaboration with Laane's group. Figure 2 shows the low energy region of the REMPI spectra recorded under different experimental conditions. The 'cold' spectrum (trace a) has an intense peak at 34796 cm^{-1} , and it is assigned to the band origin of the S_1 state. The full width at half maximum (FWHM) of the observed transition is 1.7 cm^{-1} , and our estimated uncertainty is $\pm 1\text{ cm}^{-1}$. Based on the work of Laane, *et al.* [3], the low energy region of the spectrum is dominated by the flapping and puckering modes, so the other two intense transitions at 102 and 204 cm^{-1} are most likely related to these two modes. As will become clear in the following, the identity of these intermediate states is not crucial to the assignment of the vibrational levels of the cationic state. On the contrary, the assignment of the ZEKE spectra will help to clarify the situation of the S_1 state.

Trace b was recorded under soft expansion conditions. The higher temperature of the molecular beam results in broadening of all the transitions, and the profile of each transition clearly shows two rotational branches [10]. In addition, three new features denoted with '*' at 54 , 93 and 180 cm^{-1} are observable, and these bands are therefore hot bands. In order to resolve the origins of these hot bands, we performed a UV-UV hole-burning experiment, and trace c shows the hole-burning spectrum with the hole-burning laser set at 93 cm^{-1} . The two bands at 93 and 180 cm^{-1} clearly demonstrate that they are from the same vibrational level of the ground state, a conclusion that will be further

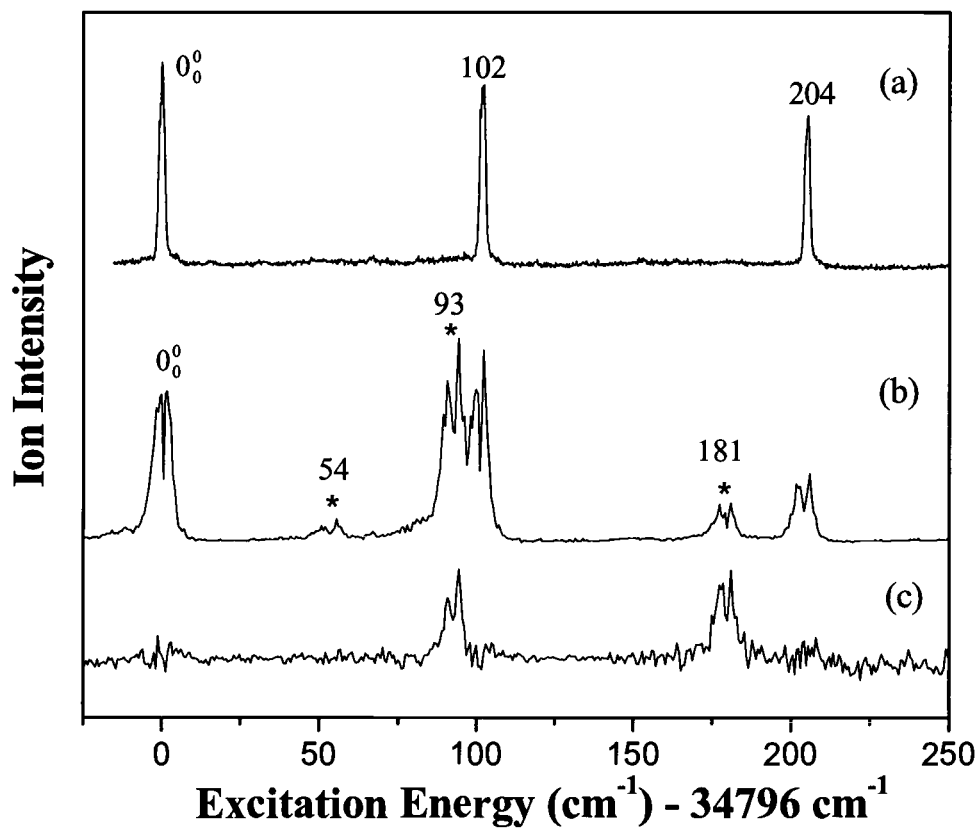


Figure 8.2 Two-color two-photon REMPI spectra of jet-cooled BDO. The spectra were recorded under hard (a) and soft (b) expansion conditions (see text for details). Trace c shows the UV-UV hole-burning spectrum with the hole-burning laser fixed at 93 cm^{-1} .

corroborated in the following ZEKE experiment. Limited by the low intensity of the band at 54 cm^{-1} , trace c cannot definitively confirm the absence of this band. However, as will become clear in the following ZEKE experiment, this band does indeed originate from a different vibrational level from that of the other two hot bands. Overall, the hole-burning experiment alludes to three different vibrational levels of the ground electronic state for the six observed features of trace b.

8.4.2. ZEKE spectra

Using all the features observed in trace b of Figure 2 for resonant excitation, the pulsed field ionization ZEKE spectra are shown in Figure 3. Table 1 summarizes the assignment of the observed vibrational levels of the cation, including our calculation on the B3LYP/6-311G++(d,p) level. No scaling factor for the vibrational frequencies of the cation in the calculation is used. Limited by the linewidth of each resonant transition (all spectra were recorded under soft expansion conditions), the uncertainty in the experimental values is 5 cm^{-1} .

Trace a in Figure 3 shows the ZEKE spectrum recorded via the origin band of the S_1 state. The most intense peak in the spectrum corresponds to the origin of the cationic state. The resulting adiabatic ionization energy, including a correction due to field ionization [14], is $64341 \pm 5\text{ cm}^{-1}$ ($7.9772 \pm 0.0006\text{ eV}$). This value is lower than 8.21 eV determined from vertical ionization [11]. In Figure 3, the abscissa shows the excess total photon energy above our adiabatic ionization energy. Other weaker bands in the spectrum are predominantly associated with the ring puckering and flapping modes. Based on the calculation result listed in Table 1, assignment of these bands is straight forward, and small negative anharmonicities are observable for both modes.

Traces b and c in Figure 3 display the ZEKE spectra recorded via the transition at 102 cm^{-1} and 204 cm^{-1} of Figure 2. The lowest energy bands in both traces coincide with the strongest band in trace a, confirming that these bands are not hot bands. Other than the active participation of the puckering mode, trace b is similar to trace a in that both are dominated by an intense origin band. However, trace c features a dominate transition to the $v^+ = 2$ level of the puckering mode, and it also contains extensive vibrational progressions of both the puckering and flapping modes.

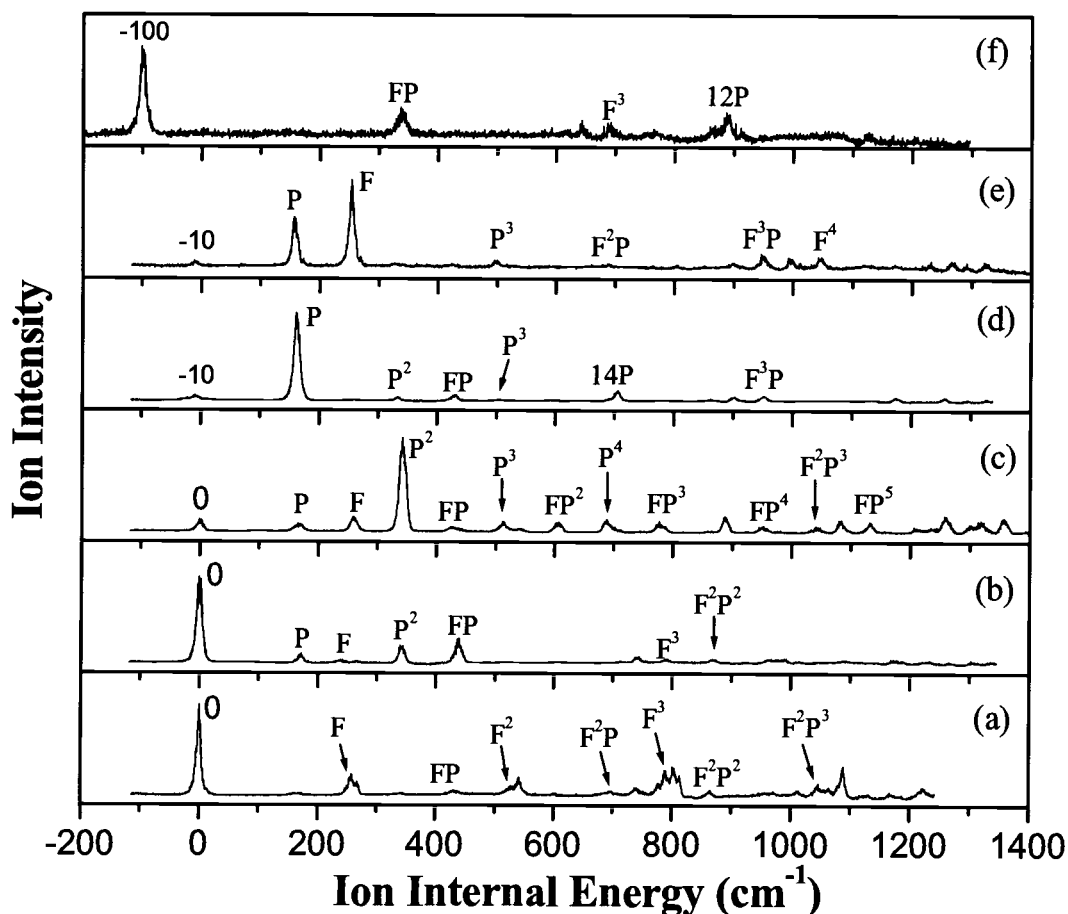


Figure 8.3 Two-color ZEKE spectra of BDO recorded via the following vibronic transitions of Figure 2: (a) 0, (b) 102, (c) 204, (d) 93, (e) 180, and (f) 54 cm^{-1} . The energy in the abscissa is relative to the ionization threshold at 64341 cm^{-1} . The labels “P” and “F” refer to the puckering and flapping modes, respectively.

Table 8.1. Observed vibrational frequencies and assignments in the ZEKE spectra of BDO.

Intermediate level in the S_1 state (cm^{-1})							Assignment*
0	54	93	102	180	204	calc.	
165		171	172	167	168	175	P^1
			238			214	20^1
258		267	267	264	259	276	F^1
340		343	340	337	341		P^2
433	439	442	439	433	425		F^1P^1
		511		510	512		P^3
527							F^2
542						541	14^1
600					608		F^1P^2
					688		P^4
697				698			F^2P^1
		716					14^1P^1
737	743		744			752	13^1
					777		F^1P^3
789	789		787				F^3
801							14^1F^1
814				816		806	12^1
864	865	871	867				F^2P^2
					888		14^1P^2
				956	951		F^1P^4
		962	967				F^3P^1
	987		992				12^1P^1
1047					1041		F^2P^3
1064				1058			F^4
1089					1084		14^2 or 12^1F^1
					1131		F^1P^5 or F^3P^2
1167							12^1P^2

* "P" and "F" refer to the puckering and flapping modes, respectively.

Table 8.2. Molecular geometry parameters of BDO in the ground state of the neutral molecule (S_0) and the cation (D_0).

	S_0	D_0
<i>Bond length (Å)</i>		
O1-C2 (O3-C2)	1.432	1.438
O1-C9 (O3-C4)	1.376	1.331
<i>dihedral angle (°)</i>		
C2O1O3C4	160	180

Traces d and e in Figure 3 show the ZEKE spectra recorded via the hot bands at 93 and 180 cm^{-1} in the REMPI spectrum of Figure 2, trace b. In both traces d and e of Figure 3, the first weak peak is red shifted from the origin band of trace a by 10 cm^{-1} . This result provides further evidence that the origin of these two transitions at 93 and 180 cm^{-1} in the REMPI spectrum of Figure 2 is the same, and that these features are related to the higher energy component of the tunneling doublet of the ground state neutral molecule. Moreover, the amount of shift is consistent with the report on the doublet splitting of 9.6 cm^{-1} in the S_0 state [2]. In Table 2, the listed transition energies have included this additional internal energy of the initial state. The strongest transition in trace d is at 171 cm^{-1} , and in reference to our calculated value of 175 cm^{-1} for the puckering mode, our assignment is unambiguous. The two strong transitions in trace e are assigned to the puckering mode and the flapping mode.

Trace f of Figure 3 shows the ZEKE spectrum recorded via the weak hot band at 54 cm^{-1} in Figure 2. The spectrum is dominated by an intense peak red shifted from the origin band of trace a by 100 cm^{-1} , indicating that the origin of this transition at 54 cm^{-1} in Figure 2 is most likely the third lowest vibrational level of the S_0 state. This level has been reported to be 99 cm^{-1} above the ground vibrational level [3], corresponding to the second overtone of the puckering mode. Other features in the ZEKE spectrum are assigned as combinations of the puckering and flapping modes.

8.5. Discussion

Based on our DFT calculations at the B3LYP level, the D_0 state is planar, while the S_0 [2] and the S_1 states are known to be puckered [3]. Both our REMPI and ZEKE spectra are consistent with this basic conclusion. The vibrational energy levels of the cation reported in Table 1 for both the puckering and the flapping modes are essentially harmonic, and there is no sign of tunneling splitting. In contrast, the hot bands in the REMPI spectrum associated with an energy level 10 cm^{-1} above the ground vibrational level are a clear indication of a puckered geometry in the ground state. The $-\text{CH}_2-$ moiety is displaced out of the aromatic plane, and as a result, there exists a potential barrier between the two equivalent geometries. The puckering mode of the S_0 state is therefore characterized by tunneling splittings and a strong anharmonicity [2]. This lack of

planarity has been ascribed to the anomeric effect by Laane, *et al.* [2][3], and the origin of this effect is suggested to be the interaction between a non-bonded oxygen p orbital and the empty $\sigma^*(\text{C-O})$ orbital on the opposite oxygen atom.

The anomeric effect changes upon electronic excitation and ionization. In the S_1 state, Laane, *et al.* observed an increased tunneling barrier due to a decreased interaction between the benzene π system and the oxygen atoms in the S_1 state [3]. The anomeric effect is therefore enhanced, leading to a more puckered geometry. In our calculation of the D_0 state, the bond lengths for both O1-C9 and O3-C4 are actually decreased compared with those in the S_0 state, as listed in Table 2. The interaction between the benzene π system and the oxygen atoms is therefore enhanced. We thus conclude that the planar geometry of the cationic BDO results from the weakened anomeric effect in the D_0 state.

The planar geometry of the D_0 state greatly simplifies the vibrational assignment of the ZEKE spectra, as evidenced from Table 1. On the other hand, assignment of the ZEKE spectra provides hints to the assignment of the REMPI spectrum and the vibrational levels of the S_1 state. For example, traces a, b, and c all have the same origin band, indicating that the associated transitions in the REMPI spectrum should have the same origin in the S_0 state. In contrast, the onset of the ZEKE spectra for traces d and e is red shifted by 10 cm^{-1} , and the associated transitions at 93 and 180 cm^{-1} should therefore be hot bands. In our previous reports on substituted aromatic systems [12], we observed a propensity of maintaining a one-to-one correlation between the identity of the intermediate vibrational level in the S_1 state and that of the D_0 state. In BDO, however, this propensity no longer exists since the geometry of the molecular frame changes from puckered to planar upon ionization. However, some trends in the ZEKE spectra can still be deduced. For example, the ZEKE spectrum obtained via the origin band of the S_1 state shows relatively high activity of the flapping mode and negligible activity of the puckering mode. However, the ZEKE spectrum via the transition at 93 cm^{-1} displays a clear progression of the puckering mode. We believe that this is an indication that the intermediate state is related to the puckering mode. On the other hand, the ZEKE spectrum via the transition at 180 cm^{-1} shows high activity of both the puckering and the flapping mode, providing evidence that the intermediate state is a combination of these

two modes. This type of exercise will be helpful in solving the assignment problem of the S_1 state.

8.6. Acknowledgement

We express our gratitude to Professor Jaan Laane from Texas A&M University for stimulating discussions on BDO. This work was supported by the National Science Foundation, Division of Chemistry. Acknowledgment is made to the Donors of The Petroleum Research Fund, administered by the American Chemical Society, for partial support of this research. Wei Kong is an Alfred P. Sloan research fellow.

8.7. References

- [1] W. Caminati, S. Melandri, G. Corbelli, L. B. Favero, R. Meyer, *Mol. Phys.* 80 (1993) 1297.
- [2] S. Sakurai, N. Meinander, K. Morris, J. Laane, *J. Am. Chem. Soc.* 121 (1999) 5056.
- [3] J. Laane, E. Bondoc, S. Sakurai, K. Morris, N. Meinander, J. Choo, *J. Am. Chem. Soc.* 122 (2000) 2628.
- [4] J. Laane, S. Sakurai, T. Klots, N. Meinander, K. Morris, W. Y. Chiang, E. Bondoc, *J. Mol. Spectrosc.* 480-481 (1999) 189.
- [5] J. Choo, *J. Mol. Spectrosc.* 597 (2001) 235.
- [6] J. Laane, *J. Phys. Chem.* 104 (2000) 7715.
- [7] J.A. Duckett, T.L. Smithson, H. Weiser, *Chem. Phys. Lett.* 64 (1979) 261.
- [8] A.C.P. Alves, J.M. Hollas, B.R. Midmore, *J. Mol. Spectrosc.* 77 (1979) 124.
- [9] K.H. Hassan, J.M. Hollas, *Chem. Phys. Lett.* 157 (1989) 183.
- [10] G. Pietraperzia, A. Zoppi, M. Becucci, E. Droghetti, E. Castellucci, *Chem. Phys. Lett.* 385 (2004) 304.
- [11] G. M. Anderson III, P. A. Kollman, L. N. Domelsmith, K. N. Houk, *J. Am. Chem. Soc.* 101 (1979) 2344.
- [12] Y. He, C. Wu, W. Kong, *J. Chem. Phys.* 120 (2004) 7497.
- [13] GAUSSIAN 03, Revision A. 7, M. J. Frisch, *et al*, Gaussian, Inc., Pittsburgh, Pennsylvania, 2003.
- [14] E. W. Schlag, *ZEKE Spectroscopy* (Cambridge University Press, Cambridge, 1998).

Structure of gas phase radical cation of 1,3,6,8-tetraazatricyclo[4.4.1.1^{3,8}] dodecane determined from zero kinetic energy photoelectron spectroscopy

Yonggang He[†], Chengyin Wu[†], Wei Kong^{†}, Kevin P. Schultz[†], and Stephen F. Nelsen[†]*

Department of Chemistry, Oregon State University, Corvallis, Oregon 97331-4003, and
Department of Chemistry, University of Wisconsin, 1101 University Avenue, Madison,
Wisconsin 53706-1396.

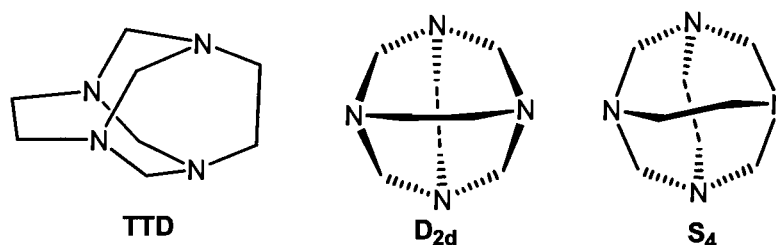
Journal of Physical Chemistry, A
PO Box 3337, Columbus, OH, 43210, USA
2005, 109, 959-961.

* To whom correspondence should be addressed.
E-mail: kongw@chem.orst.edu. Phone: 541-737-6714. Fax: 541-737-2062.

9. Structure of gas phase radical cation of 1,3,6,8-tetraazatricyclo[4.4.1.1^{3,8}] dodecane determined from zero kinetic energy photoelectron spectroscopy

ABSTRACT We report gas phase vibrational spectroscopy of the ground state cation of 1,3,6,8-tetraazatricyclo[4.4.1.1^{3,8}]dodecane (TTD) using two-color two-photon zero kinetic energy photoelectron spectroscopy. From the distribution of active vibrational modes and comparisons between the experiment and theoretical simulation, we offer proof that the cationic state and the first electronically excited state have the same D_{2d} symmetry.

The present study concerns 1,3,6,8-tetraazatricyclo[4.4.1.1^{3,8}]dodecane (TTD), which is designated [1⁴.2²]adz in the "cage adamanzane" nomenclature system introduced by Springborg and coworkers¹ for tricyclic tetraamines having saturated bridging carbon chains. Current interests in cage adamanzanes center upon their importance in biochemistry and coordination chemistry.²⁻⁹ From a fundamental point of view, the basicity and strain energy of these compounds are particularly interesting.¹⁰⁻¹³ TTD was prepared by Bichoff in 1898,¹⁴ but its structure was presumed to contain 1,3-diazacyclopentane units until this structure was proven incorrect by a low temperature proton NMR study.¹⁵ The X-ray structure of TTD verified the structure as shown, and the symmetry of the ground state was believed to be D_{2d} .¹⁶ TTD is one of the very few saturated amines that gives a radical cation persistent enough to show a reversible cyclic voltammogram.¹⁷ Recent gas phase studies based on fluorescence excitation and dispersed emission spectroscopy under supersonic jet expansion conditions concluded that TTD is twisted at its NCCN bonds, so it has static S_4 symmetry, but dynamic D_{2d} symmetry, and the tunneling barrier is only about 0.3 kcal/mol between NCCN twists of opposite sign.¹⁸ The same study also showed that the first excited electronic state (S_1 , the 3s Rydberg state) should be of D_{2d} symmetry.



Our interest in TTD stems from the discussion on the symmetry of the radical cation since the 1970s, particularly regarding the effect of solvent. Nelsen and Buschek first recorded the electron spin resonance spectrum of $\text{TTD}^{+\bullet}$ in the condensed phase.¹⁹ Later, based on semiempirical quantum mechanical calculations, Nelsen, *et al.* proposed unequal $\text{NCH}_2\text{CH}_2\text{N}$ distances caused by a three-electron σ -bond,²⁰ similar to the type demonstrated by Alder in some bicyclic diamine radical cations.²¹ With more advanced technology including Electron-Nuclear Double Resonance (ENDOR) spectroscopy and a variety of deuterated compounds, the most recent work by Zwier, *et al.* concluded that there was a single energy minimum with D_{2d} symmetry.²²

So far all the reports on the symmetry of TTD^{++} were based on indirect evidence:^{18, 22} the gas phase experiment relied on the similarity between a low Rydberg state (3s) and the ground cationic state,¹⁸ while the ENDOR experiment was performed in the solution phase.²² The issue of solvent effects on the symmetry of TTD^{++} has not been fully investigated. Moreover, the limited time resolution of the ENDOR experiment can only provide a time-averaged “effective” symmetry. In this work, we report gas phase studies of TTD^{++} using two-color two-photon zero kinetic energy (ZEKE) photoelectron spectroscopy.²³ From the distribution of active vibrational modes and comparisons between the experiment and theoretical simulation, we offer further proof that the D_0 state and the S_1 state do have the same D_{2d} symmetry.

The experimental apparatus is a standard molecular beam machine with a time of flight mass spectrometer and a pulsed valve heated to $\sim 100^\circ\text{C}$.²⁴ The sample was synthesized in Madison, Wisconsin, using the literature method.¹⁴ Two counter propagating laser beams were used: one for resonant excitation to the different vibrational levels of the S_1 state, and the other for further ionization. By fixing the ionization laser at 328 nm and scanning the resonant laser, we recorded a two-color 1+1' resonantly enhanced multiphoton ionization spectrum. Our result is in excellent agreement with that of Zwier, *et al.*,¹⁸ and the spectrum is provided as part of the supplementary material for reference. By fixing the resonant laser at one of the vibrational levels of the S_1 state, scanning the ionization laser, and detecting only the ZEKE electrons, vibrational spectroscopy of the cation was obtained.

Figure 1 shows the ZEKE spectra of TTD taken via the origin band and eight different levels of mode 20 of the S_1 state. This mode corresponds to rotation of the NR_3 units in opposite directions about the $\text{NCH}_2\text{CH}_2\text{N}$ axes, and its symmetry species is a in the S_4 point group and a_2 in both the D_{2d} and C_{2v} point groups.²⁵ The most remarkable feature of Figure 1 is the dominance of a single transition, and this phenomenon has been documented as a propensity of $\Delta v = 0$,²⁶ while Δv is the change in the vibrational quantum number between the S_1 and D_0 states. The features marked by arrows correspond to transitions with $\Delta v = 2$, and the rest of the weak features correspond to other vibrational modes of the cation, and they are not addressed in this letter. Trace *a* taken via the origin of the electronic transition results in an adiabatic ionization energy of $56343 \pm 3 \text{ cm}^{-1}$ ($6.9856 \pm 0.0004 \text{ eV}$), including a correction due to the detection field.²³

This value is lower than 7.39 eV determined from vertical ionization.¹⁹ Traces $b - i$ provide the energies for the different vibrational levels of mode 20, and the results are listed in Table 1.

To decipher the symmetry of the D_0 state from Figure 1, we attempted to reproduce the experimental observation from a series of calculations. With the Gaussian 03 suite,²⁷ the S_1 state was calculated at the CIS level using the 6-31G basis set. The D_0 state was calculated using the density functional theory (DFT) with the Becke 3LYP functional and the 6-31+G(d) basis set. Similar to the reports by Zwier, *et al.*²² and Nelsen, *et al.*²⁰, our geometry optimization for the radical cation of TTD resulted in two stable structures belonging to D_{2d} and C_{2v} , with the D_{2d} structure more stable by 18.7 kcal/mole. Using the vibrational frequencies and the displacement vectors thus obtained, we then calculated the Franck-Condon (FC) factors from the S_1 to the D_0 state,²⁵ and the results are displayed in Figure 2. The dark grey columns represent intensities obtained by assuming D_{2d} symmetry for the D_0 state, and the light grey columns represent those from C_{2v} symmetry. It is important to note that although the displacement vectors for the S_1 and the D_0 states were obtained from different calculations, the displacement vectors for the D_{2d} and C_{2v} structures were obtained using the same method with the same basis set. Moreover, calculations based on results using different basis sets yielded the same distribution of FC factors. The comparison in Figure 2 should therefore be of considerable credence.

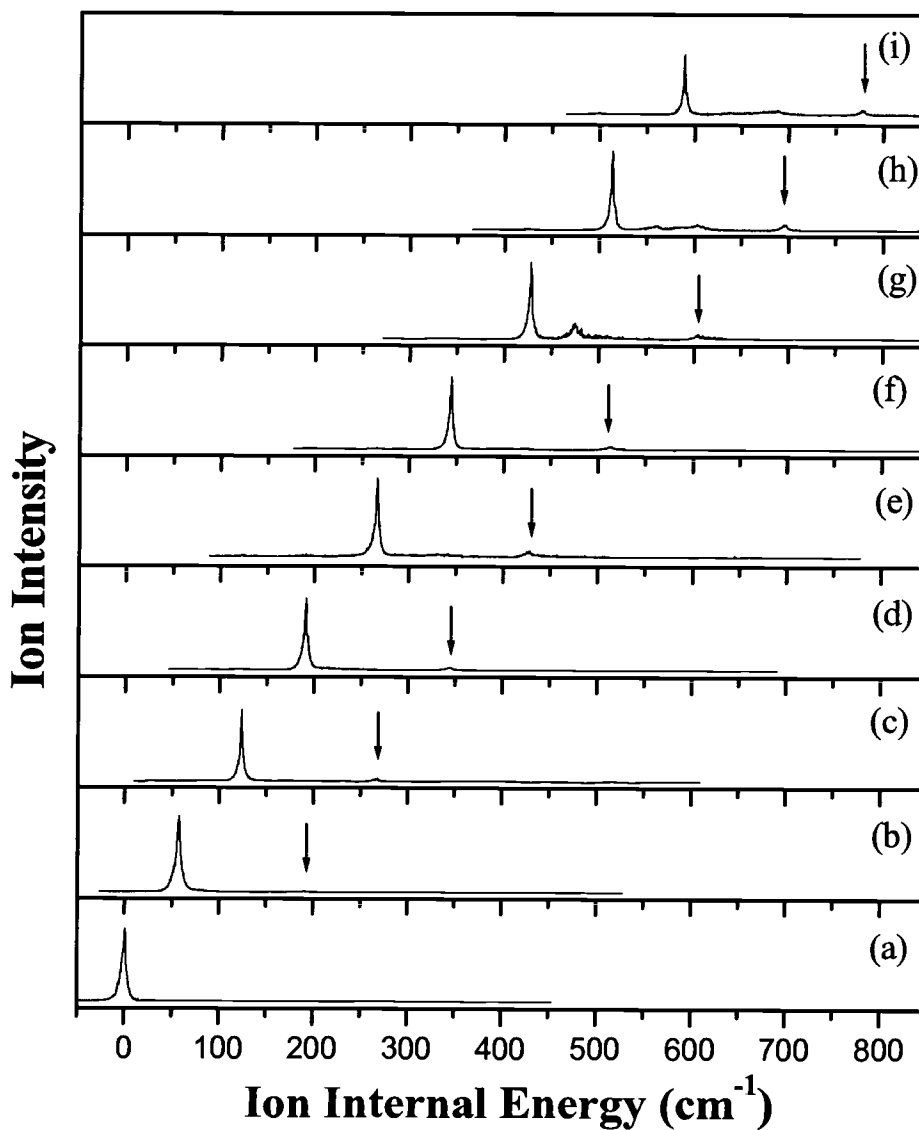


Figure 9.1. ZEKE spectra of TTD taken via the $\nu = 0 - 8$ levels of mode 20 (*a - i*) of the S_1 state. The arrows indicate transitions with $\Delta\nu = 2$. The abscissa is in reference to the adiabatic ionization energy at 56343 cm^{-1} .

Table 9.1. Observed vibrational levels of mode 20 of TTD⁺⁺ (cm⁻¹).

v	0	1	2	3	4	5	6	7	8
E _v	0	57	123	191	266	344	428	513	590
ΔE		57	66	68	75	78	84	85	77

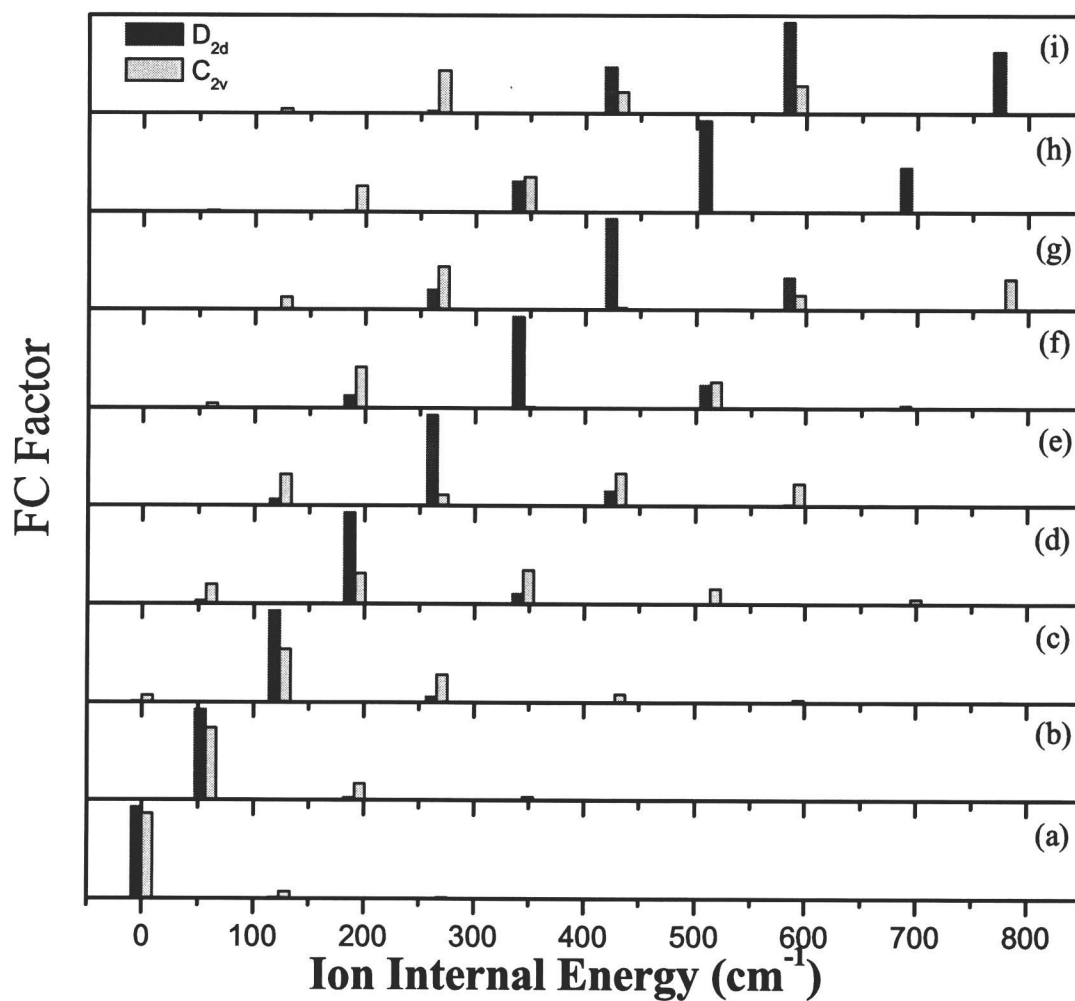


Figure 9.2. Franck-Condon factors from the S_1 to the D_0 state of TTD. The vibrational levels of the S_1 state are $\nu = 0$ (a) – 8 (i). The dark (or light) grey columns were obtained by assuming D_{2d} (or C_{2v}) symmetry for the D_0 state.

From Figure 2, the vibrational distribution obtained based on the D_{2d} symmetry is a far better representation of that in Figure 1, and the symmetry of the D_0 state is thus better described to be D_{2d} than C_{2v} . Although for transitions from the low vibrational levels of the S_1 state, the difference between the two symmetry groups is not obvious, transitions from higher levels are remarkably sensitive to the symmetry assumption of the D_0 state. This result is reasonable since the larger the amplitude of vibration, the broader the space explored by the molecular frame.

The strong propensity of $\Delta v = 0$ demonstrated from both the experiment and the calculation is a natural result of similarity between the S_1 and the D_0 states. The normal modes of the two states have essentially the same displacement vectors, and the vibrational wavefunctions of the two states are almost identical. This result also provides evidence for the assumption that the S_1 state is representative of the D_0 state,¹⁸ even though it is the lowest member of the Rydberg series.

The anharmonicity demonstrated in Table 1 is interesting. The energy gap between adjacent vibrational levels increases with the vibrational quantum number. This result is also consistent with the D_{2d} symmetry of the cation. Since the ground state of the neutral molecule is considered to tunnel between two equivalent S_4 structures, it is therefore natural that the diminished tunneling barrier would result in a flat and wide bottom for the S_1 and the D_0 states. The potential surface of mode 20 thus resembles more to a square well than to a parabola, leading to an increased energy gap for higher vibrational levels.

In summary, from the vibrational spectroscopy of the cation in the gas phase, we offer direct evidence for the D_{2d} symmetry of the ground cationic state of TTD. The previous assumptions regarding the Rydberg nature of the S_1 state and the negligible effect of the solvent on the geometry of the cation are validated.

ACKNOWLEDGMENT This work was supported by the National Science Foundation, Division of Chemistry. Acknowledgment is made to the Donors of The Petroleum Research Fund, administered by the American Chemical Society, for partial support of this research. Wei Kong is an Alfred P. Sloan Research Fellow. S. F. N. thanks the National Science Foundation for partial financial support under Grant CHE-0240197.

References

†Oregon State University.

‡University of Wisconsin.

1. Springborg, J.; Pretzmann, U.; Olsen, C. E. *Acta Chem. Scand.* 1996, 50, 294.
2. Springborg, J. *Dalton Trans.* 2003, 9, 1653.
3. Beilsteins Handbuch der Organischen Chemie, Verlag, Berlin, 1918, Vol. 1, p. 583.
4. Hossain, M. A.; Ichikawa, K. *Tetrahedron Lett.* 1994, 35, 8393.
5. Schmidtchen, F. P.; Gleich, A.; Schummer, A. *Pure Appl. Chem.* 1989, 61, 1535.
6. Nelson, J.; McKee, V.; Morgan, G. *Prog. Inorg. Chem.* 1998, 47, 167.
7. Miyahara, Y.; Tanaka, Y.; Amimoto, K.; Akazawa, T.; Sakuragi, T.; Kobayashi, H.; Kubota, K.; Suenaga, M.; Koyama, H. T.; Inazu, T. *Angew. Chem., Int. Ed.* 1999, 38, 956.
8. Alder, R. W. in *The Chemistry of Amino, Nitroso, and Nitro Compounds and their Derivatives*, ed. Patai, S., Wiley, Chichester, 1982, Ch. 18, p. 763.
9. Stevens, C. D.; Mosteller, R. C. *Cancer Res.* 1969, 29, 1132.
10. Plenio, H.; Diodone, R. *Chem. Ber./Recl.* 1997, 130, 633.
11. Robertson, K. N.; Bakshi, P. K.; Lantos, S. D.; Cameron, T. S.; Knop, O. *Can. J. Chem.* 1998, 76, 583.
12. Howard, S. T.; Fallis, I. A. *J. Org. Chem.* 1998, 63, 7117.
13. Galasso, V. *Chem. Phys.* 2001, 270, 79.
14. Bischoff, C. A. *Chem. Ber.* 1898, 31, 3248.
15. Volpp, G. *Chem. Ber.* 1962, 95, 1493.
16. Murray-Rust, P. J. *Chem. Soc., Perkin Trans. 2* 1974, 1136.
17. Nelsen, S. F.; Hintz, P. J. *J. Am. Chem. Soc.* 1972, 94, 7114.
18. Zwier, J. M.; Brouwer, A. M.; Buma, W. J.; Troisi, A.; Zerbetto, F. J. *Am. Chem. Soc.* 2002, 124, 149.
19. Nelsen, S. F.; Buschek, J. M. *J. Am. Chem. Soc.* 1974, 96, 6424.
20. Nelsen, S. F.; Haselbach, E.; Gschwind, R.; Klemm, U.; Lanyova, S. J. *Am. Chem. Soc.* 1978, 100, 4367.

21. Alder, R. W. *Tetrahedron* 1990, 45, 687.
22. Zwier, J. M.; Brouwer, A. M.; Keszthelyi, T.; Balakrishnan, G.; Offersgaard, J. F.; Wilbrandt, R.; Barbosa, F.; Buser, U.; Amaudrut, J.; Gescheidt, G.; Nelsen, S. F.; Little, C. D. *J. Am. Chem. Soc.* 2002, 124, 159.
23. Schlag, E. W. *ZEKE Spectroscopy*, Cambridge University Press, Cambridge, 1998, pg. 99.
24. He, Y.; Wu, C.; Kong, W. J. *Phys. Chem. A* 2003, 107, 5145.
25. Bernath P. F. *Spectra of Atoms and Molecules*, Oxford University Press, New York, 1994.
26. He, Y.; Wu, C.; Kong, W. J. *Chem. Phys.* 2004, 120, 7497.
27. GAUSSIAN 03, Revision A. 7, Frisch, M. J. et al., Gaussian, Inc., Pittsburgh, Pennsylvania, 2003.

A theoretical and experimental study of water complexes of *m*-aminobenzoic acid $\text{MABA} \cdot (\text{H}_2\text{O})_n$ ($n = 1$ and 2)

*Yonggang He, Chengyin Wu, and Wei Kong**

Department of Chemistry, Oregon State University, Corvallis, Oregon 97331-4003.

Journal of Physical Chemistry, A
PO Box 3337, Columbus, OH, 43210, USA
2005, 109, 748-753.

* To whom correspondence should be addressed.

E-mail: kongw@chem.orst.edu. Phone: 541-737-6714. Fax: 541-737-2062.

10. A theoretical and experimental study of water complexes of *m*-aminobenzoic acid $\text{MABA} \cdot (\text{H}_2\text{O})_n$ ($n = 1$ and 2)

10.1. ABSTRACT

We report studies of supersonically cooled water complexes of *m*-aminobenzoic acid $\text{MABA} \cdot (\text{H}_2\text{O})_n$ ($n = 1$ and 2) using two-color resonantly enhanced multiphoton ionization (REMPI) and UV-UV hole-burning spectroscopy. Density functional theory calculations are also carried out to identify structural minima of water complexes in the ground state. For the most stable isomers of both complexes, water molecules are found to bind to the pocket of the carboxyl group in a cyclic hydrogen bond network. Vibrational frequency calculations for the first electronically excited state (S_1) of these isomers agree well with the experimental observation. The addition of water molecules has a major impact on the normal mode that involves local motion of the carboxyl group, while negligible effects are observed for other normal modes. Based on the hole-burning experiment, two major isomers for each complex are identified, corresponding to the two conformers of the bare compound. Compared with the other two isomers of aminobenzoic acid, the red shifts of the origin bands due to water complexation in MABA are considerably larger. Similar to *p*-aminobenzoic acid and different from *o*-aminobenzoic acid, the existence of the intermolecular stretching mode is ambiguous in the REMPI spectrum of $\text{MABA} \cdot (\text{H}_2\text{O})_n$.

10.2. Introduction

Hydrogen bonding is ubiquitous in chemical and biological systems. Studies of organic chromophores containing competitive multiple hydrogen bonding sites constitute an active area of research.¹⁻⁵ The preference of a solvent molecule for a certain binding site on a solute molecule is of general chemical interest. Such information can be obtained from experiments in the gas phase without the interference of the bulk solvent. Using molecular beam techniques, cold, isolated clusters of different solute-solvent compositions can be prepared, and isomeric molecular complexes with solvent molecules 'frozen' at different binding sites on the solute can be generated.⁶ These complexes can then be interrogated using a variety of high-resolution spectroscopic methods such as mass-resolved resonantly enhanced multiphoton ionization (REMPI). For the identification of different isomeric structures, hole-burning spectroscopy is also routinely employed.

In this paper, we report spectroscopic studies of complexes of *m*-aminobenzoic acid (MABA) containing one or two water molecules. The general interest in aminobenzoic acids and their solvation mechanisms arises from both their biological importance and their chemical properties. They are multifunctional hydrogen bonding molecules, ideal for studies of interactions between water and aromatic chromophores. In protic solvents, they can act both as H acceptors at the O atom of the -C=O group and the N atom of the -NH₂ group, and as H donors at the -OH group and the -NH₂ group. They can also form hydrogen bonds through their aromatic π electrons. In non-polar solvents, MABA exists predominantly as a neutral molecule. In the solid state or in aqueous solutions, it exists as a zwitterion, unlike the other two isomers.^{7,8} On the biological aspect, aminobenzoic acids are antimetabolites of sulfanilamide. MABA is also of great importance in pharmaceutical and chemical industries; it is used in synthesis of analgesics, antihypertensives and vasodilators.⁹

In our previous effort on bare MABA, we observed two conformational isomers, as shown in Figure 1, based on results from resonantly enhanced multiphoton ionization and zero kinetic energy photoelectron spectroscopy (ZEKE).¹⁰ Our hole burning experiment further revealed that the transition energies to the first electronically excited state (S_1) differ by 27 cm⁻¹ for the two conformers. The frequencies of the vibrational modes, however, were found to be independent of the molecular conformation.¹⁰

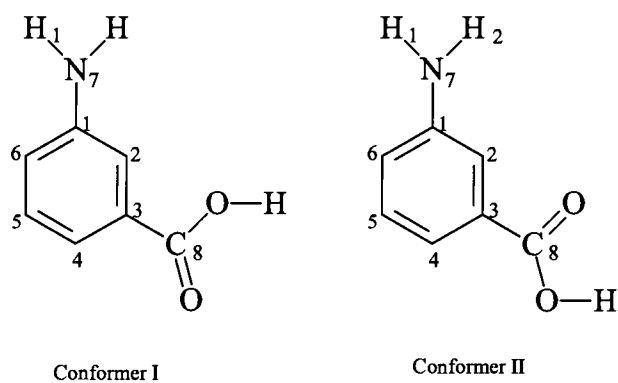


Figure 10.1 Structural conformers of MABA.

In this study, we extend our investigation to the structural and spectroscopic properties of $\text{MABA} \cdot (\text{H}_2\text{O})_n$ complexes with $n = 1$ and 2. We have also performed quantum mechanical calculations to obtain structures and binding energies for a few possible isomers in the ground state, and vibrational frequencies of these species in the first electronically excited state. These results will be discussed in comparison with another study on the water complexes of *p*-aminobenzoic acid (PABA) and *o*-aminobenzoic acid (OABA) from our own group¹¹ and a few other groups.¹²⁻¹⁵

10.3. Experimental Details

The experimental setup has been described elsewhere.^{16,17} Briefly, the apparatus is a standard molecular beam machine with a time-of-flight mass spectrometer (TOF-MS) and a heatable pulsed valve for supersonic cooling. The sample was purchased from Aldrich Co. and used without further purification. The temperature of the nozzle was $\sim 150^\circ\text{C}$, and the carrier gas at 2 atm pressure was a mixture of argon and room temperature water vapor. To optimize for a specific complex, the time delay between the pulsed valve and the laser was adjusted by a delay generator (Stanford Research, DG535).

To resolve the different conformational isomers, we performed UV-UV hole burning experiments. At first, a two-color two-photon REMPI spectrum was recorded by scanning the pump laser (Laser Analytical Systems, LDL 20505, pumped by a Nd:YAG laser, Spectra Physics, GCR 190) across the vibronic levels of the S_1 state while using the fourth harmonic of a Nd:YAG laser at 266nm (Continuum, Powerlite 7010) for further ionization. The intensities of both lasers were minimized so that the ion signal due to either laser was negligible. Then a third (hole-burning) UV laser (Laser Analytical Systems, LDL 2051, pumped by a Nd:YAG laser, Spectra Physics, GCR 230) was introduced with a time advance of 20 ns. By fixing the third laser on one of the origin bands while monitoring the depletion of the ion signal as the pump laser scanned across the REMPI spectrum, vibronic features of the chosen isomer were identified. The two resonant laser beams were set to counterpropagate, while the ionization laser was set to cross the two resonant laser beams at a 5° angle.

10.4. Calculation

Possible structures of MABA and its complexes with one or two water molecules were explored by performing a series of density functional theory (DFT) calculations using the Gaussian 03 suite.¹⁸ The optimized structure of bare MABA was used as the starting point for the complex containing one water molecule (1:1 complex). The water molecule was initially placed alternatively to the different hydrogen bonding sites of MABA, and each structure was then fully optimized using the Becke-Lee-Yang-Parr functional (B3LYP) with a basis set of 6-31+G(d). The convergence of the resulting isomer was confirmed by calculations of vibrational frequencies. The initial structures for complexes with two water molecules (1:2 complex) were generated either with a water dimer bound alternatively to the different hydrogen bonding sites, or with each water molecule bound independently to the available sites. The most stable ground state structures for both the 1:1 and 1:2 complexes were subsequently chosen as the starting point of optimization for the S_1 state at the CIS/6-31G level. Vibrational frequencies of the normal modes at the S_1 state were also calculated at the same level of theory. To obtain a good agreement between theory and experiment in the vibrational assignment, a scaling factor of 0.9 was used.¹⁹

10.5. Results

10.5.1. Theoretical calculations

Our previous UV-UV hole-burning experiment on bare MABA has confirmed the co-existence of two conformational isomers in the gas phase named conformer I and II (Figure 1).¹⁰ Each conformer has six stable structural arrangements with one water molecule. The fully optimized structures together with their relative energies including zero point vibrational energy (ZPVE) corrections are displayed in Figure 2. In the two most stable structures Ia and IIa, the water molecule bridges in between the $-C=O$ and the $-OH$ groups, and the resulting extra stability is about 4 kcal/mol compared with the second set of most stable isomers Ib and IIb.^{11,20} All higher energy isomers have only one H-bond, and those hydrogen bonded at the $-C=O$ group are the most stable, while those bonded at the $-OH$ group are the least stable. The three structures with water hydrogen bonded to the amino group are of similar binding energies, on the order of 5 kcal/mol compared with those of the most stable structures. The molecular conformation, on the other hand, has essentially no effect on water complexation, and

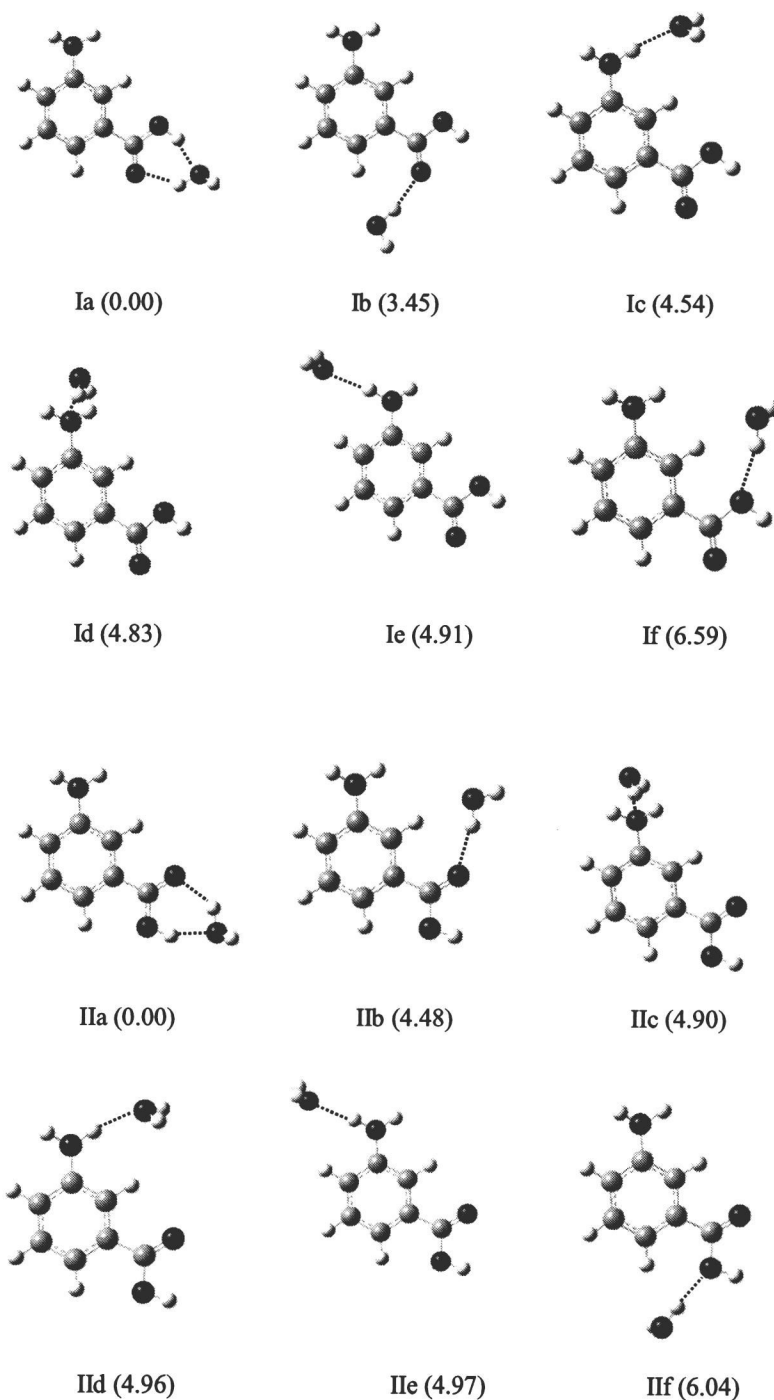


Figure 10.2 Optimized geometries of the 1:1 water complex of the two conformers of MABA at the B3LYP/6-31+G(d) level. The values in parentheses are relative energies in kcal/mol.

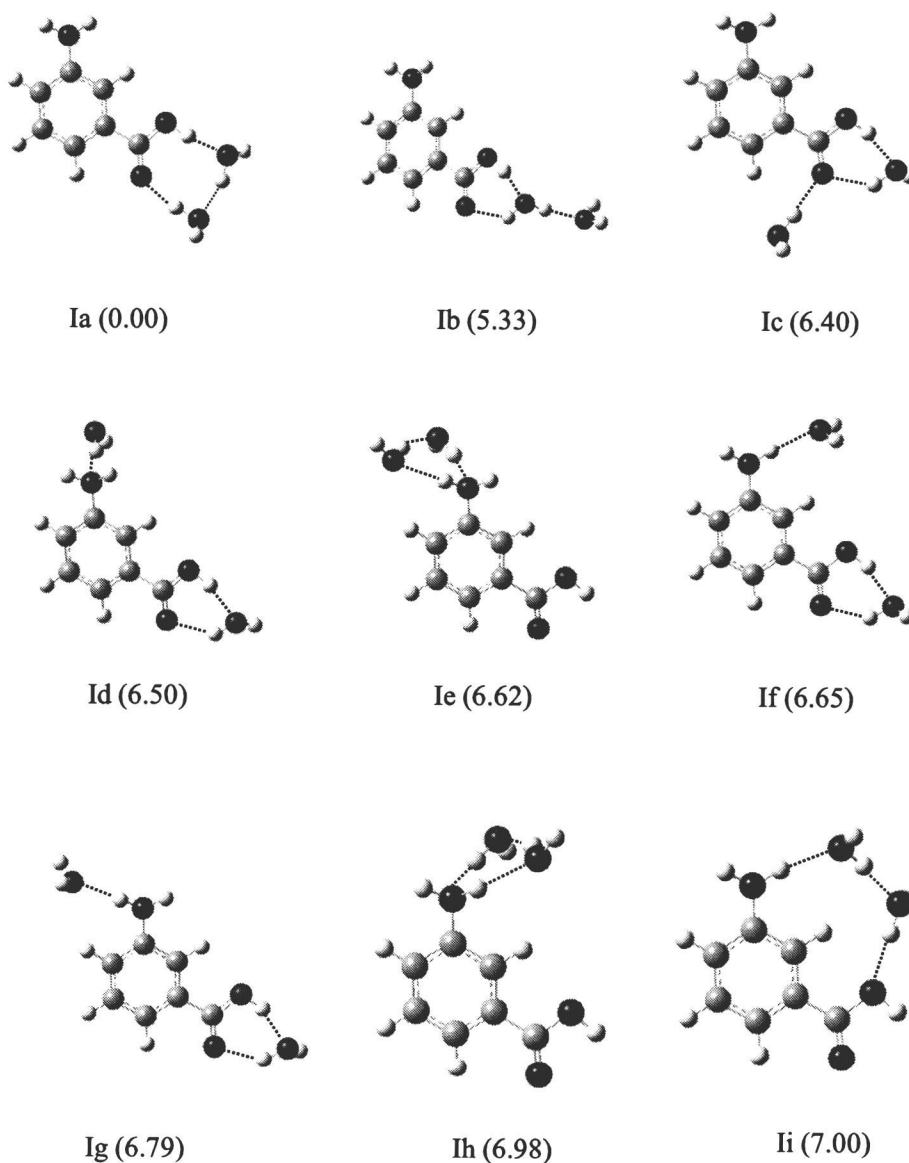


Figure 10.3 Optimized geometries of the 1:2 water complex of conformer I of MABA at the B3LYP/6-31+G(d) level. The values in parentheses are relative energies in kcal/mol.

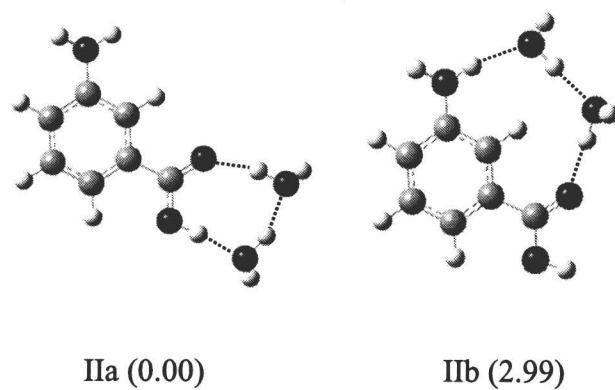


Figure 10.4 Two most stable structures for the 1:2 water complex of conformer II of MABA at the B3LYP/6-31+G(d) level. Higher energy structures are similar to those of Figure 3, Ib – Ih.

except for an order switch between isomers c and d, a one-to-one correlation between the two sets of isomers can be observed.

For each conformer of bare MABA, more than twenty energy minima were found for the 1:2 complex. Nine of the most stable isomers for conformer I are displayed in Figure 3, and the two most stable structures for conformer II are displayed in Figure 4. Other structures for conformer II are similar to those for conformer Ib - Ih, and they are therefore not reproduced for compactness. The energetically most stable structures incorporate three linear hydrogen bonds and allow each molecule to be both a H-bond donor and a H-bond acceptor. In structures Ii and IIb, water dimer bridges are formed between the -NH_2 and the -COOH groups. The energy cost of this bridge, compared with the bridge inside the -COOH group (Isomer Ia and IIa), is about 3 kcal/mol for IIb and 7 kcal/mol for Ii. This difference is consistent with the observation of the 1:1 complex, i.e., the O atom of the -C=O group with a higher electron density is a stronger H acceptor than that of the -OH group. Except for this order switch between structures b and i, similar to the case of the 1:1 complex, a one-to-one correlation between the two sets of isomers are also observed.

10.5.2. Experimental results

The two-color 1+1' REMPI spectrum of the 1:1 water complex of MABA is displayed in Figure 5, trace *a*. The intensities of both laser beams were optimized to avoid interference due to non-resonant ionization, and the ion signal due to any single laser was essentially undetectable. On the low energy side of the spectrum, more than one strong transitions are observable, implying the existence of multiple isomers. Hole-burning experiments are therefore necessary to ascertain the nature and number of isomers.

The hole-burning spectra of the two major isomers of the 1:1 complex are shown in the lower two traces of Figure 5, with the hole-burning laser set at positions Ia (30365 cm^{-1} , trace *b*) and IIa (30373 cm^{-1} , trace *c*) respectively. These two isomers are hereafter denoted as Ia and IIa and are tentatively assigned to the corresponding structures shown in Figure 2. The rationale for this assignment will be presented in the following Discussion section. The small shoulder at 30415 cm^{-1} marked by a number sign in the figure also corresponds to a minor isomer. However, the intensity of this isomer was so

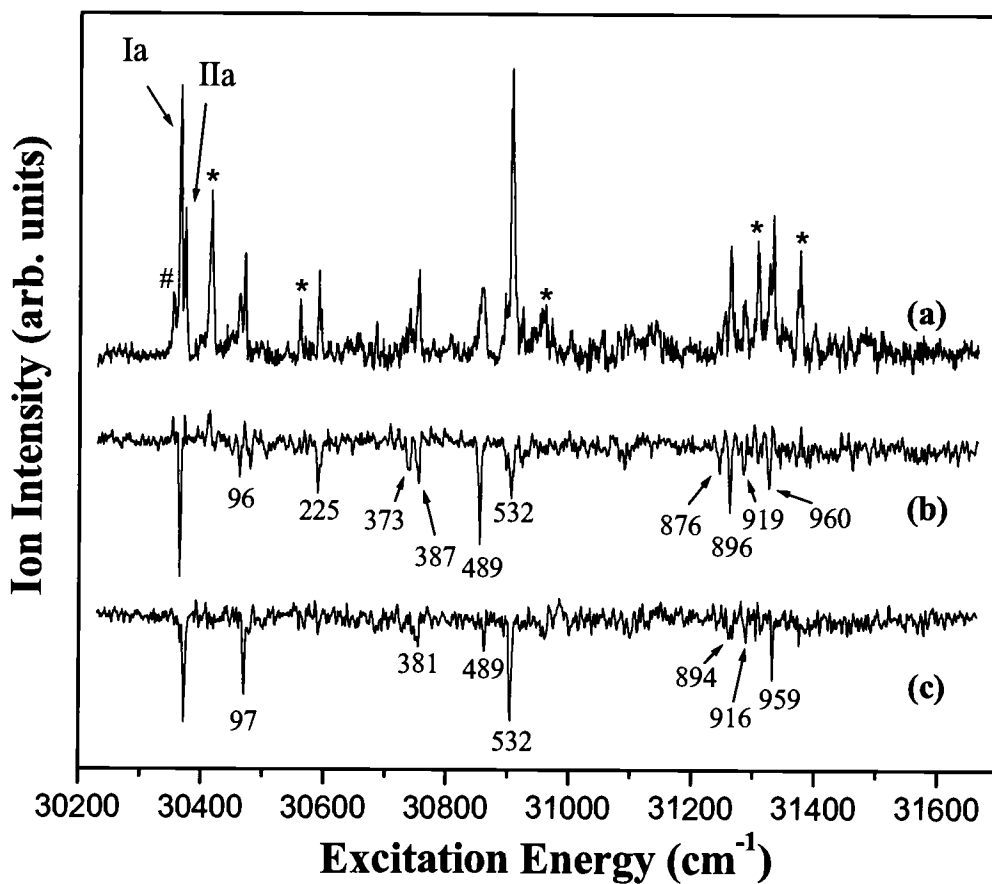


Figure 10.5 Two-color two-photon REMPI spectrum of jet-cooled $\text{MABA} \cdot (\text{H}_2\text{O})_1$ (trace *a*) and UV-UV hole-burning spectra with the hole-burning laser fixed at the Ia (30365 cm^{-1} , trace *b*) and IIa (30373 cm^{-1} , trace *c*) positions. The feature marked by “#” represents a minor isomer, while those marked by “*” are from dissociation of the 1:2 complex (see Figure 7 for further details).

Table 10.1. Observed vibrational frequencies and assignments for the S_1 state of the 1:1 water complex of MABA.

Isomer Ia		Isomer IIa		Assignment & description [#]
Exp.	Calc.*	Exp.	Calc.*	
96	100	97	101	H_0^1 , β (-COOH), β (H ₂ O)
225	225			C_0^1 , β (-COOH)
373	370			$6b_0^1$, β (ring)
387	380	381	376	D_0^1 , β (-NH ₂)
489	492	489	484	E_0^1 , β (-COOH), β (-NH ₂) and β (ring)
532	533	532	527	$6a_0^1$, β (ring)
876				D_0^1 E_0^1
896	877	894	871	$19a_0^1$, β (ring)
919		916		D_0^1 $6a_0^1$
960	967	959	968	12_0^1 , β (ring)

* The values include a scaling factor of 0.9.

β represents in-plane bending vibrations.

low that the hold-burning experiment only produced a single feature at the origin, with no vibrational assignment possible. The features marked by asterisks belong to the 1:2 complex, and they will be discussed later. Taking these considerations into account, all the significant features in trace *a* can then be accounted for. We therefore conclude that there are only two major isomers in the molecular beam within our observation window. The amount of red shift of the origin band in the 1:1 complex compared with the bare compound is considerably larger for MABA than for OABA and PABA. The difference in transition energy between the two isomers of bare MABA or the two isomers of its 1:1 complex, however, is small. The origin band of the two conformers of MABA only differs by 27 cm^{-1} , and the difference for the water complexes Ia and IIa is less than 10 cm^{-1} . The red shifts due to water complexation, on the other hand, are on the order of 100 cm^{-1} for both Ia and IIa. In comparison, the red shift in the 1:1 complex of OABA is 55 cm^{-1} , while a blue shift of 17 cm^{-1} has been observed in PABA.¹¹ Additional stabilization in the excited electronic state is implied in the 1:1 complex of MABA.

Table 1 lists the observed vibronic transitions of the two major isomers. To assist with the assignment, we have performed *ab initio* calculations on the CIS/6-31G level for the vibrational frequencies of the S_1 state. An overall agreement between the calculation and the experiment is obtained when a scaling factor of 0.9 is used with the calculated frequencies. Modes that are associated with the motion of the aromatic ring are labeled using the convention of Varsanyi's nomenclature.²¹ Other modes that mainly involve the motion of the $-\text{NH}_2$ and the $-\text{COOH}$ moieties are named according to the corresponding modes observed in bare MABA.¹⁰ Similar to bare MABA, the spectrum is dominated by in-plane or even quanta of out-of-plane vibrational modes due to symmetry reasons. The normal modes in the 1:1 complex exhibit essentially no dependence on the molecular conformation, and therefore they cannot be used to distinguish between the two isomers Ia and IIa. The transition observed at 96 cm^{-1} (mode *H*) for isomer Ia is assigned as a collective motion of the $-\text{COOH}$ group and H_2O . This mode is also observable in the spectrum of isomer IIa. The feature at 876 cm^{-1} is tentatively attributed to the combination band of modes *D* and *E*, although it is also close to the theoretical value of mode 19a. The rationale for this assignment is that typically for this type of calculation with a scaling factor of 0.9, we only expect a reasonable agreement between theory and experiment for low frequency modes, while at nearly 1000 cm^{-1} , an exact agreement

would be fortuitous. The same argument is also applied in the assignment of the 1:2 complex. It is interesting to note that based on our calculation for isomer Ib in Figure 2, the only low frequency in-plane motion below 200 cm^{-1} is the intermolecular stretching mode at 69 cm^{-1} , and this value is too small to be assigned to the observed transition at $\sim 100\text{ cm}^{-1}$. This result further supports the conclusion that under our experimental conditions, only the most stable isomers Ia and IIa exist in our molecular beam. Normal mode calculations for other structures listed in Figure 2 were considered unnecessary due to the high energies of the corresponding isomers.

Figure 6 shows the two-color 1+1' REMPI spectrum of the 1:2 complex (trace *a*) together with the two hole-burning spectra (traces *b* and *c*). The origins of the hole-burning spectra are 30414 and 30486 cm^{-1} , about 70 cm^{-1} apart. In between the two major isomers, the weak feature marked by an asterisk was confirmed to be a third isomer, but its intensity was too low for vibrational analysis. With the exception of this weak feature, all the significant features of the REMPI spectrum correlate well with the two hole-burning spectra, and we thus conclude that similar to the 1:1 complex, there are only two major isomers and one minor isomer in our molecular beam for the 1:2 complex. These two major isomers are hereafter denoted Ia and IIa, and are tentatively assigned to the corresponding structures shown in Figures 3 and 4. The origins of the two major isomers are red shifted from their respective bare molecules by 65 and 20 cm^{-1} . In contrast, a blue shift of 19 cm^{-1} has been observed in the REMPI spectra of the 1:2 water complexes of both OABA and PABA.¹¹

The observed vibronic transitions of both major isomers of the 1:2 complex are listed in Table 2 together with results from *ab initio* calculations on the CIS/6-31G level. Consistent with Table 1, the scaling factor for the calculated frequencies is also 0.9. Similar mode distributions are observed for both the 1:1 and 1:2 complexes, including mode *H*, which involves a collective motion of the carboxyl group and the two water molecules. Mode *a* represents out of plane vibration of the water dimer relative to the ring.

A recalcitrant problem with experimental studies of weakly bound complexes is the possibility of dissociation.¹⁸ Figure 7 compares the REMPI spectra of the 1:1 (trace *a*) and the 1:2 complex (trace *c*), together with a hole-burning spectrum of each complex.

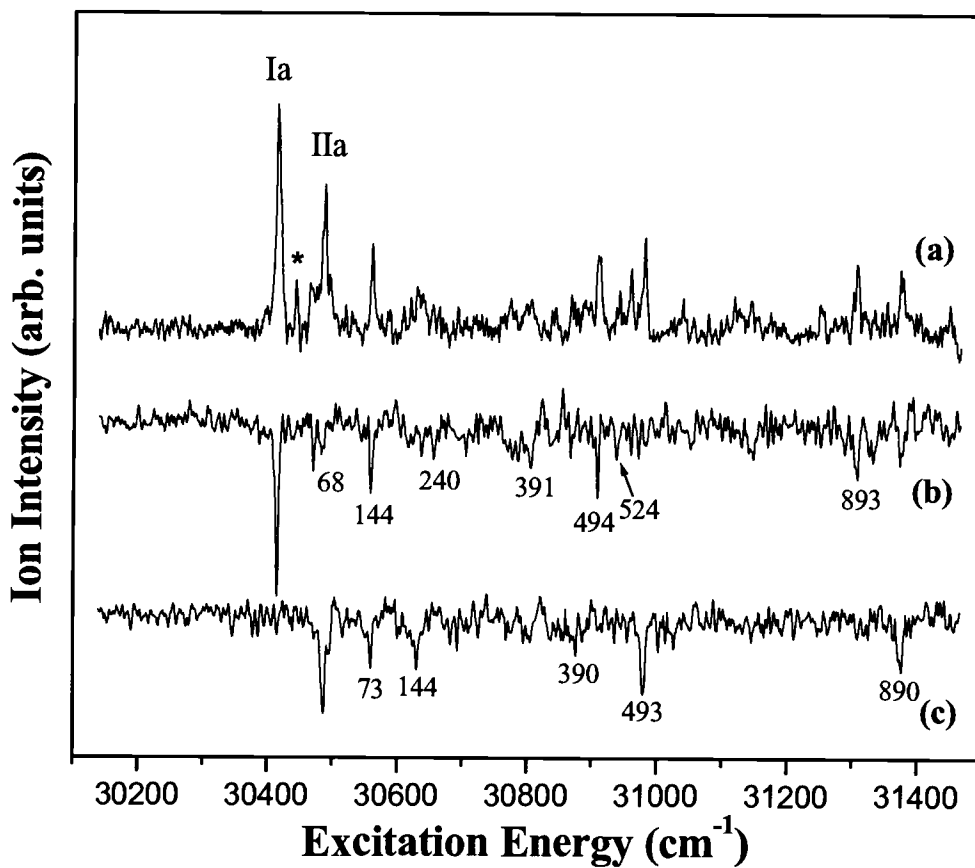


Figure 10.6 Two-color two-photon REMPI spectrum of jet-cooled $\text{MABA} \cdot (\text{H}_2\text{O})_2$ (trace *a*) and UV-UV hole-burning spectra with the hole-burning laser fixed at the Ia (30414 cm^{-1} , trace *b*) and IIa (30486 cm^{-1} , trace *c*) positions.

Table 10.2. Observed vibrational frequencies and assignments for the S_1 state of the 1:2 water complex of MABA.

Isomer Ia		Isomer IIa		Assignment & description [#]
Exp.	Calc.*	Exp.	Calc.*	
68	73	73	72	H_0^1 , β (-COOH), β (H ₂ O)
144	152	144	152	a_0^1 , γ (H ₂ O-ring)
240	235			C_0^1 , β (-COOH)
391	389	390	392	D_0^1 , β (-NH ₂)
494	498	493	497	E_0^1 , β (-COOH), β (-NH ₂) and β (ring)
524	543			$6a_0^1$, β (ring)
893	879	890	874	$19a_0^1$, β (ring)

* The values include a scaling factor of 0.9.

β represents in-plane bending vibrations.

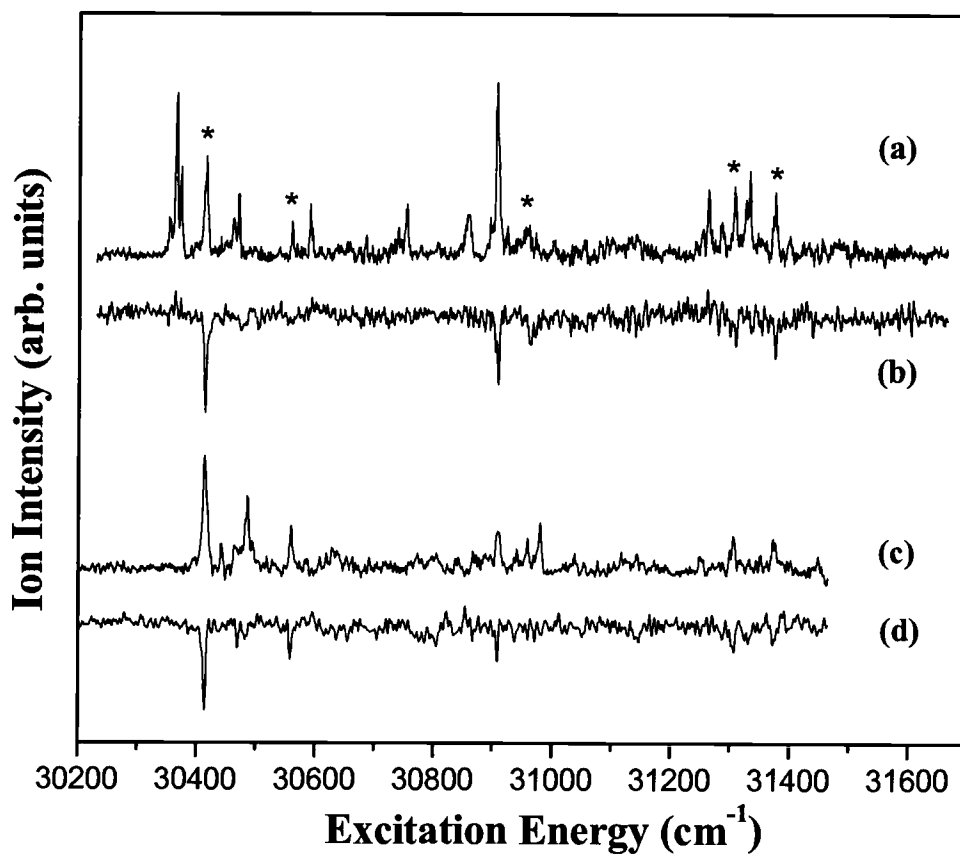


Figure 10.7 REMPI spectra of the 1:1 and 1:2 complexes of MABA. (a) Two-color two-photon REMPI spectrum of jet-cooled $\text{MABA} \cdot (\text{H}_2\text{O})_1$; (b) UV-UV hole-burning spectrum of $\text{MABA} \cdot (\text{H}_2\text{O})_1$ with the hole-burning laser fixed at 30415 cm^{-1} ; (c) two-color two-photon REMPI spectrum of jet-cooled $\text{MABA} \cdot (\text{H}_2\text{O})_2$; (d) UV-UV hole-burning spectrum of $\text{MABA} \cdot (\text{H}_2\text{O})_2$ with the hole-burning laser fixed at 30414 cm^{-1} .

All the features marked by asterisks in trace *a* line up with those in traces *b* – *d*. Trace *b* was obtained by setting the hole-burning laser at 30415 cm^{-1} and the mass gate on the 1:1 complex, while trace *d* was obtained by setting the hole-burning laser at the same origin but the mass gate on the 1:2 complex (isomer Ia). The identical locations of all the marked features allude to the possibility that the species of trace *b* is a dissociation product of the 1:2 complex in trace *d*. Some of the marked features in trace *a* only show up once either in trace *b* or in trace *d*, and we attribute this result to mode dependence during dissociation. For example, mode *H* at 68 cm^{-1} and its second harmonic at 144 cm^{-1} must have a low yield for dissociation, since they are barely observable in the hole-burning spectrum of the 1:1 complex (trace *b*), while they are clearly distinguishable in the spectrum of the 1:2 complex (trace *d*). In contrast, the feature near 30962 cm^{-1} should have a high dissociation yield since it is clearly observable from the spectrum of the 1:1 complex (trace *b*) but not observable in the spectrum of the 1:2 complex (trace *d*). This feature is most likely an intermolecular bending mode with a value of 478 cm^{-1} based on our calculation, and it is not included in Table 2 because of its highly dissociative nature. The feature near 30900 cm^{-1} (trace *a*) contains multiple transitions, including mode 6a of the 1:1 complex, and its intensity is therefore not reproduced in the spectrum of the 1:2 complex.

10.6. Discussion

Structural assignment for the two major isomers of the 1:1 complex is based on the transition energy to the S_1 state. According to our CIS calculation, the transition energy is 4.871 eV for isomer Ia and 4.899 eV for isomer IIa. A blue shift observed in the REMPI spectrum of isomer IIa therefore conforms to the above assignment. Although the energy difference from our calculation is larger than the experimental value, we believe that the theory should be qualitatively reliable in predicting the trend in transition energies. In addition, the relative intensities of the origin bands of the two isomers are similar to those of the two conformers of bare MABA, and this assignment is therefore consistent with the conformational assignment of the bare compound. Our DFT calculation, on the other hand, resulted in a more stable structure for isomer IIa by 37 cm^{-1} , including corrections due to zero-point energies. Given the uncertainty of this type of

calculations, we prefer not to use this information in this assignment. It is worth noting that given the insensitivity of the vibrational frequencies on the molecular conformation and the limited amount of information available at present, this assignment is only tentative.

Similarly, for the 1:2 water complex of MABA, the calculated transition energy is 4.884 eV for isomer Ia and 4.908 eV for isomer IIa. Following the same reasoning as above, the lowest transition at 30414 cm^{-1} in Figure 6a can thus be assigned to the water complex of conformer I of MABA, and *vide infra*. This assignment is also consistent with that of the 1:1 complex and that of the bare compound, i. e., the lower energy transition with a higher intensity corresponds to conformer I in Figure 1 and its water complexes.

For both the 1:1 and 1:2 complexes, traces of a third isomer are observed, although in both cases, the transition intensities of the minor isomer are too low for any vibrational assignment. For the 1:1 complex, structure Ib is more stable than structure IIb by almost 1 kcal/mol in Figure 2, thus this structure is the most logical candidate for the minor isomer. In Figure 4, structure IIb shows substantial stability compared with the rest of the higher energy isomers. We tentatively assign this structure to the minor isomer of the 1:2 complex. This result offers evidence that a ring structure involving both the amino and the carboxyl groups is possible, albeit unfavorable compared with the structure where a water cluster anchors at the carboxyl site. In contrast, our previous observations of water complexes of OABA and PABA only contained one isomer, with no traces of any minor structures.¹¹ This difference might be an indication of the weaker electron induction effect in the meta-substituted compound.

The red shifts of the origin bands of the water complexes compared with the bare compound are considerably larger for MABA than for OABA and PABA.¹¹ For the 1:1 complex of PABA and the 1:2 complexes of PABA and OABA, blues shifts of less than 20 cm^{-1} have been observed. A more tightly bond excited state than the ground state is thus implied in the water complexes of MABA. Based on our DFT and CIS calculations, for the 1:1 complex of MABA, the length of the hydrogen bond $\text{C}=\text{O}\cdots\text{HO}_w$ decreases while that of $\text{O}-\text{H}\cdots\text{O}_w$ increases upon excitation. The observed additional stabilization

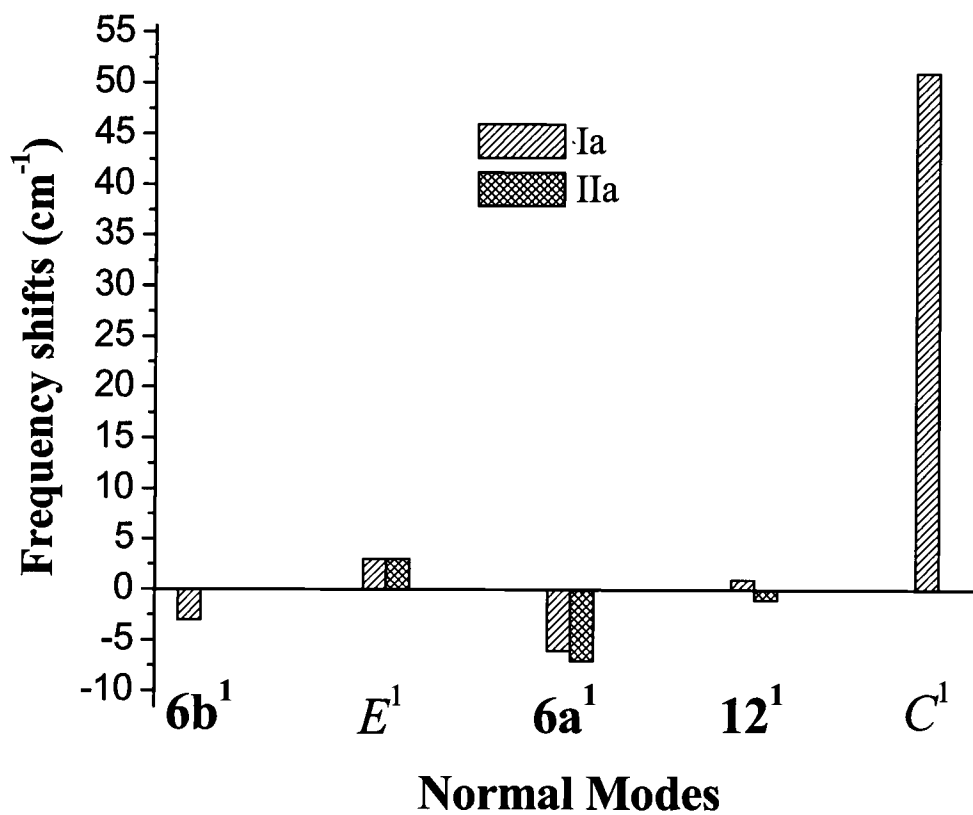


Figure 10.8 Frequency shifts of a few observed normal modes in $\text{MABA} \cdot (\text{H}_2\text{O})_1$ relative to the bare compound. The uncertainty for all the values is 3 cm^{-1} .

in the excited electronic state in the 1:1 water complex is thus a reflection of a stronger hydrogen bonding capability of the carbonyl group than that of the hydroxyl group.

The vibrational spectroscopy of the water complexes offers information on the initial step of water solvation. The site of water addition can be deduced from the frequency shifts with the addition of water molecules. These shifts are displayed in Figure 8 for the two major isomers of the 1:1 complex. Modes 6b, *E*, 6a and 12 mainly involve deformation of the aromatic ring, and with the addition of water molecules, they only undergo slight shifts. On the other hand, a large shift is observable for the in-plane bending mode of the carboxyl group: in Figure 8, mode *C* for the Ia isomer increases by $\sim 50\text{ cm}^{-1}$ with the addition of one water molecule. The site of water addition should therefore be the carboxyl group for conformer I of MABA, in excellent agreement with our DFT calculations. Although mode *C* for isomer IIa is too weak for a definitive assignment, the above conclusion should also be applicable, since the normal modes in the water complexes exhibit essentially no dependence on the molecular conformation. Interestingly, the addition of the second water molecule to the 1:1 complex results in marginal changes in the vibrational frequency. Modes *D*, *E*, and 6a undergo frequency shifts within 10 cm^{-1} of their respective values in the 1:1 complex, and even for the in-plane bending mode *C* of the carboxyl group, the shift is only 15 cm^{-1} . This fact suggests that the second water molecule should be in close proximity to the first water molecule, exerting minimal disturbance to the molecular frame. Limited by available resources, we were unable to perform an IR-UV hole-burning experiment to investigate the vibrational spectroscopy of the ground state of the water complexes. Certainly more information on the frequency shifts of the ground state complexes would be a tremendous addition to this study.

Similar to the cases of PABA and OABA,¹¹ in both the 1:1 and 1:2 complexes of MABA, we believe that it is the hydrogen-bonding site on the carboxyl group that water molecules prefer to occupy. The amino group, although typically considered hydrophilic, loses out in the competition even with the availability of two water molecules. Given the high electron density at the carboxyl group, it is no surprise that the first water molecule prefers the carboxyl site. Somewhat surprising is the essentially hydrophobic behavior of

the amino group. All aminobenzoic acid molecules contain a pair of electron “push-pull” substitutes. In the ground state, a fraction of the electron from the amino group is transferred to the carboxyl group. According to the Mulliken population analysis, the amino group has a positive charge of $\sim +0.1$ and the carboxyl group has a negative charge of ~ -0.1 for both conformers of MABA. Although the electron-attracting inductive effect of the carboxyl group in MABA is slightly smaller than that in PABA and OABA due to the resonance effect, it is still sufficient to hold on to both water molecules, at least for the major isomers formed in our molecular beam.

Similar to PABA but different from OABA,¹¹ the assignment of the intermolecular stretching mode in the REMPI spectra of the water complexes of MABA remains ambiguous, although mode *H* and mode *C* both contain contributions from intermolecular bending vibration. Based on our calculation, the stretching mode should appear at 178 cm^{-1} above the origin of the 1:1 complex. Given the signal-to-noise ratio of the experimental spectrum (Figure 5), it is difficult to definitively identify this transition.

10.7. Conclusions

Spectroscopic properties of the excited state of MABA water complexes have been studied using two-color resonantly enhanced multiphoton ionization and UV-UV hole-burning spectroscopy. Structures and binding energies for several of the most possible isomers in the ground state have been explored based on DFT calculations. The overall analysis of the experimental and theoretical data has led to the identification of two major isomers for both the 1:1 and 1:2 complexes. With the aid of *ab initio* calculations, vibrational modes of the S_1 state of the observed isomers have been assigned, and a reasonable agreement between theory and experiment has been obtained. From the frequency shifts of some of the observed normal modes upon water addition, we conclude that it is the hydrogen-bonding site on the carboxyl group that water molecules prefer to occupy. Different from the water complexes of the other two isomers of aminobenzoic acid, both the 1:1 and 1:2 complexes of MABA show signs of a minor isomer, and in the 1:2 complex, a water bridge between the carboxyl group and the amino group might have been formed. We attribute this result to the weaker electron “push-pull” effect in MABA. Mode dependent dissociation of the 1:2 complex are also observed, but the assignment of the intermolecular stretching mode remains ambiguous.

10.8. ACKNOWLEDGMENT

This work was supported by the National Science Foundation, Division of Chemistry. Acknowledgment is made to the Donors of The Petroleum Research Fund, administered by the American Chemical Society, for partial support of this research. Wei Kong is an Alfred P. Sloan research fellow.

10.9. REFERENCES

- 1 Bernstein, E. R., *Atomic and Molecular Clusters*, Elsevier, Amsterdam, 1990.
- 2 Jeffrey, G. A.; Saenger, W., *Hydrogen Bonding in Biological Structures*, Springer, Berlin, 1991.
- 3 Castleman, A. W., Jr.; Wei, S., *Annu. Rev. Phys. Chem.* 1994, 45, 685-719.
- 4 Zwier, T. S., *Annu. Rev. Phys. Chem.* 1996, 47, 205-241.
- 5 Wolfenden, R.; Snider, M. J., *Acc. Chem. Res.* 2001, 34, 938-945.
- 6 *Atomic and Molecular Beam Methods*, Volume 1, edited by Scoles, G., Oxford University Press, Inc., New York, 1988.
- 7 Gopal, L.; Jose, C. I.; Biswas, A. B., *Spectrochim. Acta* 1967, 23A, 513-518.
- 8 Théorêt, A., *Spectrochim. Acta* 1971, 27A, 11-18.
- 9 Palafox, M. A.; Gil, M.; Nunez, J. L., *Spectrosc. Lett.* 1996, 29, 609-629.
- 10 He, Y.; Wu, C.; Kong, W., *J. Chem. Phys.* 2004, 121, 8321-8328.
- 11 He, Y.; Wu, C.; Kong, W., *J. Phys. Chem. A* (in preparation, 2004).
- 12 J.A. Stearns, A. Das, T.S. Zwier, *Phys. Chem. Chem. Phys.* 2004, 6, 2605-2610.
- 13 He, Y.; Wu, C.; Kong, W., *J. Chem. Phys.*, 2004, 121, 3533-3539.
- 14 Wu, C.; He, Y.; Kong, W., *Chem. Phys. Lett.* 2004, 398, 351-356.
- 15 C.A. Southern, D.H. Levy, G.M. Florio, A. Longarte, T.S. Zwier, *J. Phys. Chem. A* 2003, 107, 4032-4040.
- 16 He, Y.; Wu, C.; Kong, W., *J. Phys. Chem. A*, 2003, 107, 5145-5148.
- 17 He, Y.; Wu, C.; Kong, W., *J. Phys. Chem. A*, 2004, 108, 943-949.
- 18 GAUSSIAN 03, Revision A. 7, Frisch, M. J., *et al.*, Gaussian, Inc., Pittsburgh, Pennsylvania, 2003.
- 19 Casida, M. E.; Jamorski, C.; Casida, K. C.; Sulahub, D. R., *J. Chem. Phys.*, 1998, 108, 4439-4449.
- 20 Stearns, J. A.; Das, A.; Zwier, T. S., *Phys. Chem. Chem. Phys.*, 2004, 6, 2605-2610.
- 21 Varsanyi, G., *Assignment of Vibrational Spectra of Seven Hundred Benzene Derivatives*, Wiley, New York, 1974.
- 22 *Cluster Ions*, edited by Ng, C.-Y.; Baer, T.; Powis, I., Chichester; New York : J. Wiley & Sons, c1993.

Theoretical and experimental studies of water complexes of *p*- and *o*-aminobenzoic acid

*Yonggang He, Chengyin Wu, and Wei Kong**

Department of Chemistry, Oregon State University, Corvallis, Oregon 97331-4003.

Journal of Physical Chemistry, A
PO Box 3337, Columbus, OH, 43210, USA
2005, *In press*.

* To whom correspondence should be addressed.
E-mail: kongw@chem.orst.edu. Phone: 541-737-6714. Fax: 541-737-2062.

11. Theoretical and experimental studies of water complexes of *p*- and *o*-aminobenzoic acid

11.1. ABSTRACT

We report studies of supersonically cooled water complexes of *p*- and *o*-aminobenzoic acid with one or two water molecules using two-color resonantly enhanced multiphoton ionization spectroscopy. Density functional theory calculations are carried out to identify structural minima of water complexes in the ground state. According to the calculation, water molecules are bound to both the C=O and –OH groups to form a cyclic hydrogen bond network in the most stable isomer. Vibrational frequency calculations for the first electronically excited state (S_1) of the most stable isomer agree well with the experimental observation. Based on this agreement, we believe that only one isomer exists in our molecular beam. The frequency shifts of a few normal modes caused by the water molecules further confirm the site of water addition. A surprising observation is that for OABA(H₂O)_{*n*} complexes, abundant intermolecular vibrational modes are clearly observable in the REMPI spectra, while for PABA(H₂O)_{*n*} complexes, these modes are conspicuously missing. A red shift in the transition energy is observed for OABA(H₂O)₁, while blue shifts are observed for the rest of the complexes. This difference alludes to the relative stabilities of the water complexes of the two aminobenzoic acids in both the ground and excited electronic state. These observations will be discussed in comparison with those from the meta isomer.

11.2. Introduction

Studies of water solvated organic chromophores containing competitive multiple hydrogen bonding sites constitute an active area of research.¹⁻⁸ The importance of such studies lies in not only the fundamental nature of hydrogen bonding itself but also the understanding of the role of water in related processes such as catalysis, molecular recognition and biochemical regulation.

Although the largest body of today's experimental data comes from studies in the condensed phase,⁹ work in the gas phase can achieve investigations of hydrogen bonding interactions in the absence of bulk solvent effects. Thus gas phase studies can provide microscopic models in understanding a variety of interactions between the solute and solvent molecules. Molecular beam technology has proven an efficient way to prepare cold, isolated clusters of different sizes through supersonic jet expansion.¹⁰ During the expansion, the vibrational and rotational degrees of freedom of the complexes are cooled. Interrogation with a variety of high-resolution spectroscopic methods such as resonantly enhanced multiphoton ionization (REMPI) and laser induced fluorescence (LIF) can be achieved.

Interests in aminobenzoic acids arise from both their biological importance and their chemical properties. *O*-aminobenzoic acid (OABA), also named anthranilic acid, has been used as a convenient fluorescence probe in internally quenched fluorescent peptides due to its high quantum yield and small size.^{11,12} *P*-aminobenzoic acid (PABA) is an antimetabolite of sulfanilamide and was once widely used as an active ingredient in sunscreen and a photodegradation inhibitor. PABA and OABA are both multifunctional hydrogen bonding molecules. In protic solvents, they can act both as hydrogen atom acceptors at the O atom of the C=O group and the N atom of the -NH₂ group, and as hydrogen atom donors at the -O-H and the H-N-H sites. They can also form a hydrogen bond through the aromatic π electrons. The existence of multiple hydrogen bonding sites makes these molecules ideal models for studying the interaction between water and aromatic chromophors. The effect of water on the photophysical behaviors of these species is crucial in interpreting the message of the fluorescence probe.

Gas phase spectroscopic investigations of PABA, OABA, and their water complexes have been carried out to a limited extent.¹³⁻¹⁹ Using laser desorption, Meijer, *et al.* have recorded the REMPI spectra of bare PABA and its complexes with argon, methanol and

water.¹³ However, no detailed vibrational assignment has been carried out. Southern, *et al.* have recorded the electronic and infrared spectra of bare OABA in a supersonic jet,¹⁴ and later, Stearns, *et al.* have extended the investigation to the corresponding water complexes.¹⁵ The emphasis of the work on OABA has been the dislocation of the hydrogen atom in the first electronically excited state (S_1), and the effect of the intramolecular hydrogen bond on water complexation. Our group has recently investigated the ground cationic state (D_0) of all three isomers of aminobenzoic acid using two-color zero kinetic energy (ZEKE) photoelectron spectroscopy.^{16,17,18} We have achieved complete vibrational assignment of both the S_1 and the D_0 states. Our studies of the water complexes of the meta isomer (MABA) using REMPI and UV-UV hole-burning spectroscopy techniques have revealed the existence of multiple isomers of the bare molecule and the corresponding water complexes.¹⁹ From the comparison between the observed vibrational frequency and our DFT calculation, structural assignment and vibrational spectroscopy of the S_1 state have been achieved. Our observation of the change in the vibrational frequency and ionization threshold with the addition of water molecules has revealed a basic road map of water solvation.

The present report is a continuation of our study on water complexes of the different isomers of aminobenzoic acid.¹⁹ Following the same procedure as used in our previous report, we present detailed vibrational assignment of the REMPI spectra of PABA(H_2O) $_n$ and OABA(H_2O) $_n$ complexes with n from 0 to 2. We have also performed quantum mechanical calculations to obtain structures and binding energies for possible isomers in the ground state, and vibrational frequencies of these species in the first electronically excited state. These results will be discussed in comparison with our results on MABA, and the uniqueness of each isomer reflected from the spectroscopy of the solvent/solute complex will be explored.

11.3. Experimental setup and calculation method

The experimental setup has been described elsewhere,^{20,21} and the conditions for forming the water complexes of OABA and PABA are similar to those in the case of MABA.¹⁹ Both one color ($1 + 1$) and two color ($1 + 1'$) REMPI experiments were performed to obtain vibrational information of the first excited state and the ionization potential (IP) of each complex. Mass-selected, one-color two-photon REMPI spectra of

PABA(H₂O)₀₋₂ were recorded by scanning an OPO laser (Continuum, Panther, pumped by Continuum, Powerlite 7010) near the region of the S₁ state. The two-color two-photon REMPI spectra of OABA(H₂O)₀₋₂ were recorded by scanning a dye laser (Laser Analytical Systems, LDL 2051, pumped by Spectra Physics, GCR 230) through the vibronic levels of the S₁ state while another dye laser (Laser Analytical Systems, LDL 20505, pumped by Spectra Physics, GCR 190) was set at 285 nm for further ionization. To determine the ionization potential, we recorded the photoionization efficiency spectra (PIE) by fixing the OPO or one of the dye lasers at the origin of the S₁ state while scanning the second dye laser through the ionization threshold. In all two laser experiments, the laser beams were set to counterpropagate, while the light path, the flight tube, and the molecular beam were mutually perpendicular. The resulting ions were accelerated by an extraction field of ~130 V/cm and detected by a chevron multichannel plate detector.

Possible structures of PABA, OABA and their complexes with one or two water molecules were explored by performing a series of density functional theory (DFT) calculations using the Gaussian 98 and Gaussian 03 suites.^{22,23} The procedure for generating and optimizing different water complexes was the same as that used in the case of MABA.¹⁹ To obtain a good agreement between theory and experiment in the vibrational assignment, a scaling factor of 0.95 was used for bare OABA, and a scaling factor of 0.9 was used for the rest of the compounds.²⁴

11.4. Results

11.4.1. Theoretical calculations

PABA(H₂O)₀₋₂

Our DFT optimization for the ground state of bare PABA at the B3LYP/6-31+G(d) level shows that PABA is non-planar with an angle of 25.69° between the amino group and the plane of the ring. Exploration of isomer space minimum for the 1:1 complex at the B3LYP/6-31+G(d) level has led to the discovery of six stable isomers. The optimized structures together with their relative energies including zero point vibrational energy (ZPVE) corrections are displayed in Figure 1. In general, these structures are similar to those of MABA, with the water molecule bound to the carboxyl pocket in the most stable isomer (I) to form a cyclic hydrogen bond network. This isomer is lower in energy than

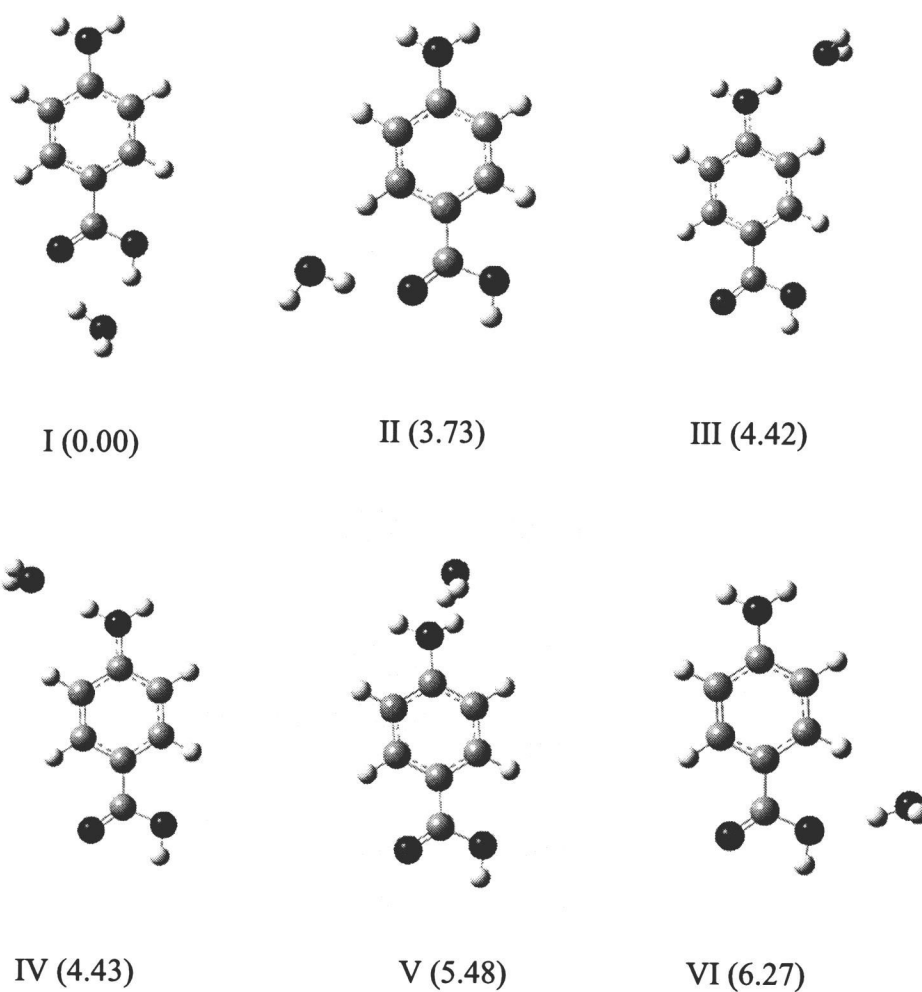


Figure 11.1 Optimized geometries of 1:1 water complex of PABA at the B3LYP/6-31+G(d) level. The values in parentheses are relative energies in kcal/mol.

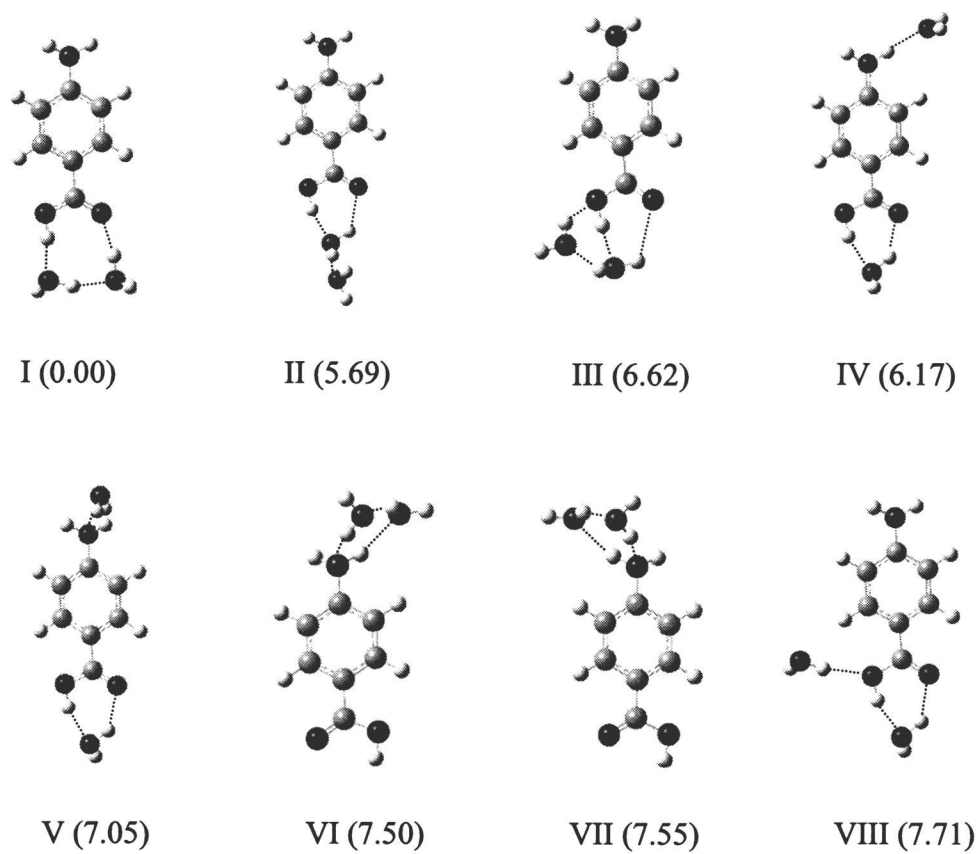


Figure 11.2 Optimized geometries of 1:2 water complex of PABA at the B3LYP/6-31+G(d) level. The values in parentheses are relative energies in kcal/mol.

the second most stable isomer (II) by 3.73 kcal/mol. This large energy difference implies that isomer I should be the dominant species in a supersonic jet. In the other higher energy isomers II to VI, only one hydrogen bond is formed, and based on our previous experience, these structures are irrelevant to our experimental measurement.

Figure 2 shows four of the most stable structures for the 1:2 complexes of PABA. Similar to the case of MABA, the energetically most stable structure incorporates three linear hydrogen bonds and allows each molecule to be both a donor and an acceptor. This structure can be viewed as a water dimer hydrogen bonded to the C=O and the -OH group. Compared with the second most stable structure in which only one water molecule interacts with the -COOH group, this structure is stable by 5.69 kcal/mol in energy. It should thus be the only possible species in our supersonic jet. It is interesting to notice that structure III has the maximum number of hydrogen bonds, but its bonding energy is much higher than structure I, even higher than structure IV with the two water molecules independent of each other.

OABA(H₂O)₀₋₂

Our DFT calculation on bare OABA at the B3LYP/6-31+G(d) level has resulted in two stable conformers, which agrees with the calculation by Southern, *et al.*¹⁴ According to the hole-burning experiment by the original authors and our later experiment on both the S₁ and the D₀ state,¹⁸ however, only the more stable isomer exists in a supersonic jet. In this structure, an intramolecular hydrogen bond is formed between one of the amino hydrogen atoms and the carbonyl group.

Adding one water molecule to the more stable structure of OABA has resulted in five stable structures, as depicted in Figure 3. In the most stable isomer I, water resides in Pocket I according to Stearns, *et al.*,¹⁵ similar to the case of PABA(H₂O)₁. Based on the resonant ion-dip infrared spectroscopy (RIDIR) experiment,¹⁵ this isomer should be the only species in the molecular beam. In isomer II, the water molecule bridges between the amino group and the carboxyl group. The formation of this isomer involves breaking of the intramolecular hydrogen bond between the two substituents and creation of two intermolecular bonds. Interestingly, the stability of isomer II and III is similar, although the number of hydrogen bonds are quite different. This is an indication of a high energy cost in breaking the intramolecular hydrogen bond.

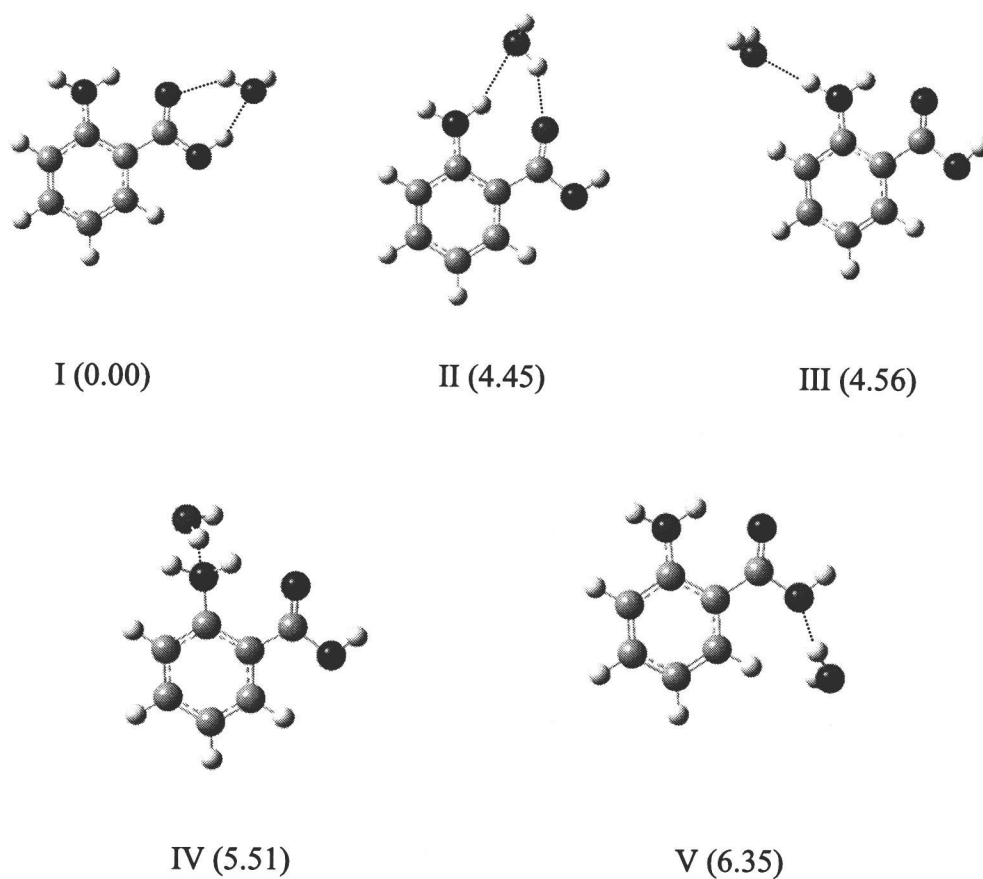


Figure 11.3 Optimized geometries of 1:1 water complex of OABA at the B3LYP/6-31+G(d) level. The values in parentheses are relative energies in kcal/mol.

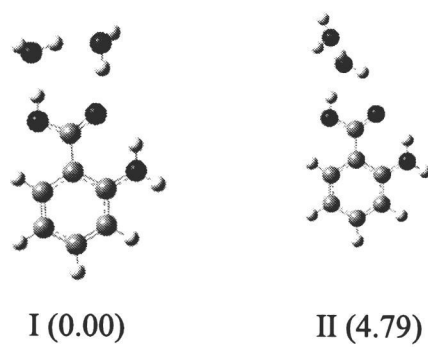


Figure 11.4 Two most stable geometries of the 1:2 water complex of OABA at the B3LYP/6-31+G(d) level. The values in parentheses are relative energies in kcal/mol.

The two most stable water complexes of OABA(H₂O)₂ shown in Figure 4 have similar structures as those in Figure 2. The most stable structure containing a six member ring in a cyclic hydrogen bonding network has an additional binding energy of 4.79 kcal/mole than the next most stable isomer.

Summary of theoretical results

In summary, the bonding structures for PABA and OABA with water molecules are similar, and in all cases, only one dominant structure has been found. In the 1:1 complex, the water molecule resides in the pocket of the carboxyl group, and the stability of this structure is around 4 kcal/mol more than that of the next most stable one. In the 1:2 complex, a cyclic ring structure involving three hydrogen bonds is the most stable motif, with both water molecules bonded to the carboxyl group. Bonding at the amino site has proven costly in energy, even with the formation of a cyclic structure. The intermolecular hydrogen bond between two water molecules is stronger than that between a water molecule and the amino group. The intramolecular hydrogen bond in OABA does not seem to impose any influence on the intermolecular bond with water, at least for the most stable structure.

11.4.2. Experimental results

PABA(H₂O)₀₋₂

Figure 5 shows the one-color two-photon REMPI spectra of PABA(H₂O)₀₋₂ plotted with respect to the origin of the S₁ ← S₀ transition of bare PABA at 34185 cm⁻¹. All three spectra demonstrate discrete narrow-band structures. The one-color REMPI spectrum of bare PABA was first obtained by Meijer, *et al.* using laser desorption,¹³ and later, a complete vibrational assignment was achieved by our group based on *ab initio* and DFT calculations and in correlation with two-color zero kinetic energy photoelectron (ZEKE) spectroscopy.¹⁶ For both the 1:1 and 1:2 complexes, only one single strong transition near the origin is observable. This result is very different from those of water complexes of MABA where multiple origin bands were observed. Moreover, a striking similarity exists between the vibrational progression of both complexes as well as that of bare PABA; i.e., essentially all the major transitions observed in bare PABA are repeated in the spectra of the water complexes. These facts suggest that we are only observing a

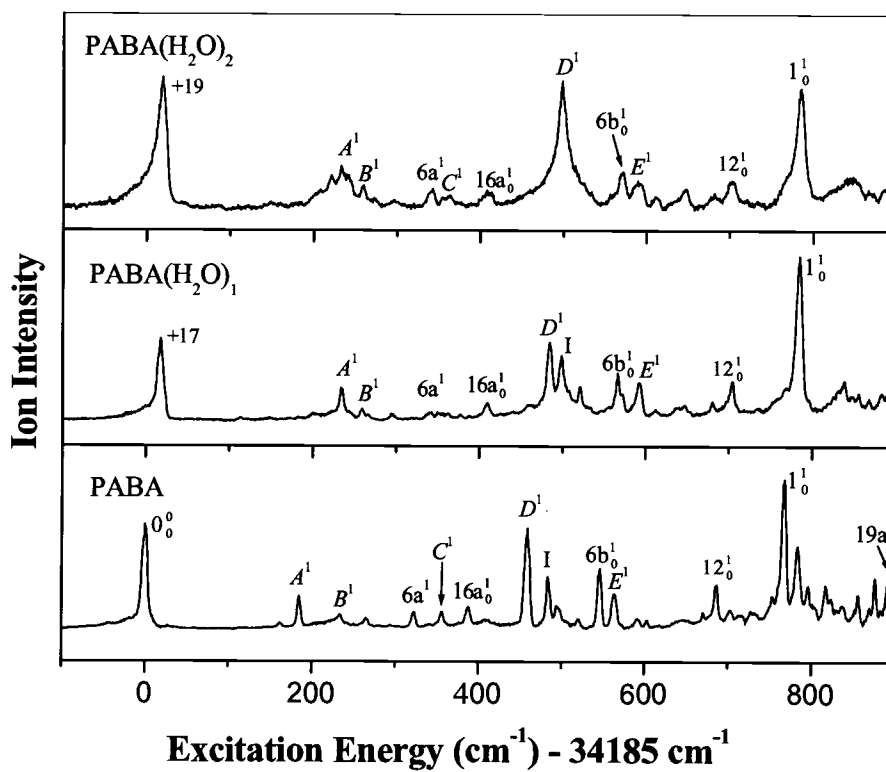


Figure 11.5 (1+1) REMPI spectrum of jet-cooled PABA(H₂O)_n ($n = 0 - 2$) plotted with respect to the origin of the $S_1 \leftarrow S_0$ transition of bare PABA at 34185 cm⁻¹.

Table 11.1. Observed vibrational frequencies and assignments for the S_1 state of PABA(H_2O)₀₋₂.

PABA		PABA(H_2O) ₁		PABA(H_2O) ₂		Assignment and approx. description [#]
Exp.	Calc.*	Exp.	Calc.*	Exp.	Calc.*	
185	149	217	228	214	234	A_0^1 , β (-COOH)
233	209	242	267	240	266	B_0^1 , C-NH ₂ torsion, β (-COOH)
322	323	323	343	323	351	$6a_0^1$, β (ring)
357	329			345	361	C_0^1 , β (-NH ₂)
388	376	392	389	389	389	$16a_0^1$, γ (ring)
459	466	467	480	479	483	D_0^1 , β (-COOH), β (-NH ₂)
483	512	481	484			I_0^1 , NH ₂ inversion
546	543	549	575	553	577	$6b_0^1$, β (ring)
564	564	576	584	570	585	E_0^1 , -COOH scissoring,
592		595				$B_0^1 C_0^1$
687	694	687	707	684	709	12_0^1 , β (ring)
768	767	767	772	766	773	l_0^1 , ring breathing
784	762					$17b_0^1$, γ (ring)
796		838				$B_0^1 E_0^1$
817						$C_0^1 D_0^1$
857	906					$17a_0^1$, γ (ring)
876						$A_0^1 12_0^1$
893	936					$19a_0^1$, β (ring)

* The values include a scaling factor of 0.9.

β and γ represent in-plane bending and out-of-plane bending vibrations, respectively.

single conformation for each complex in the molecular beam, in agreement with our own calculation. Based on our hole-burning experiment on water complexes of MABA, even for an isomer with an additional instability of 3 kcal/mol, its contribution in our supersonic molecular beam was negligible. We therefore concluded that a hole-burning experiment on the water complexes of PABA was unnecessary.

The shifts of the origin band for both water complexes are small. The origin band of the 1:1 complex is blue shifted by 17 cm^{-1} with respect to bare PABA, while the blue shift of the 1:2 complex is 19 cm^{-1} . These small spectral shifts indicate that the complexes are only slightly more stable in the S_0 state than in the S_1 state. In contrast, the shifts of the origin bands in water complexes of MABA were much larger, on the order of 100 cm^{-1} for the 1:1 complex.

A complete assignment of the observed vibronic transitions for all three species is listed in Table 1. Modes that are associated with the motion of the aromatic ring are labeled using the convention of Varsanyi's nomenclature.²⁵ Other modes that mainly involve the motion of the $-\text{NH}_2$ and $-\text{COOH}$ moieties are named with letters from *A* to *E* in the order of increasing frequency. An overall agreement between the calculation and the experiment is obtained when a scaling factor of 0.9 is used.²⁴

The observed frequency shifts for the water complexes compared with bare PABA are displayed in Figure 6. The $16a_0^1$ transition is observed at 388 cm^{-1} for bare PABA, while it occurs at 392 and 389 cm^{-1} for the 1:1 and 1:2 complexes respectively. For modes 6b, 12, and 1, the frequencies in both complexes are also within a few wavenumbers of their respective values in the bare molecule. These modes mainly involve deformation of the aromatic ring, and with the addition of water molecules, they only undergo slight shifts. On the other hand, a large shift is observed for the in-plane bending mode of the carboxyl group: in Figure 6, mode *A* increases by $\sim 30\text{ cm}^{-1}$ in both complexes. These experimental observations are also born out from the theoretical calculations, as shown in Table 1, although the exact amount of frequency shift is even more dramatic in the calculation. The site of water addition should therefore be the carboxyl group for both $n = 1$ and 2, in excellent agreement with our DFT calculations. The shifts in other modes of the substituents are moderate, mainly because of their close coupling with the ring. For example, modes *D* and *E* involve collective motions of the whole molecular frame, while the displacement vectors of modes *B* and *C* undergo dramatic changes upon

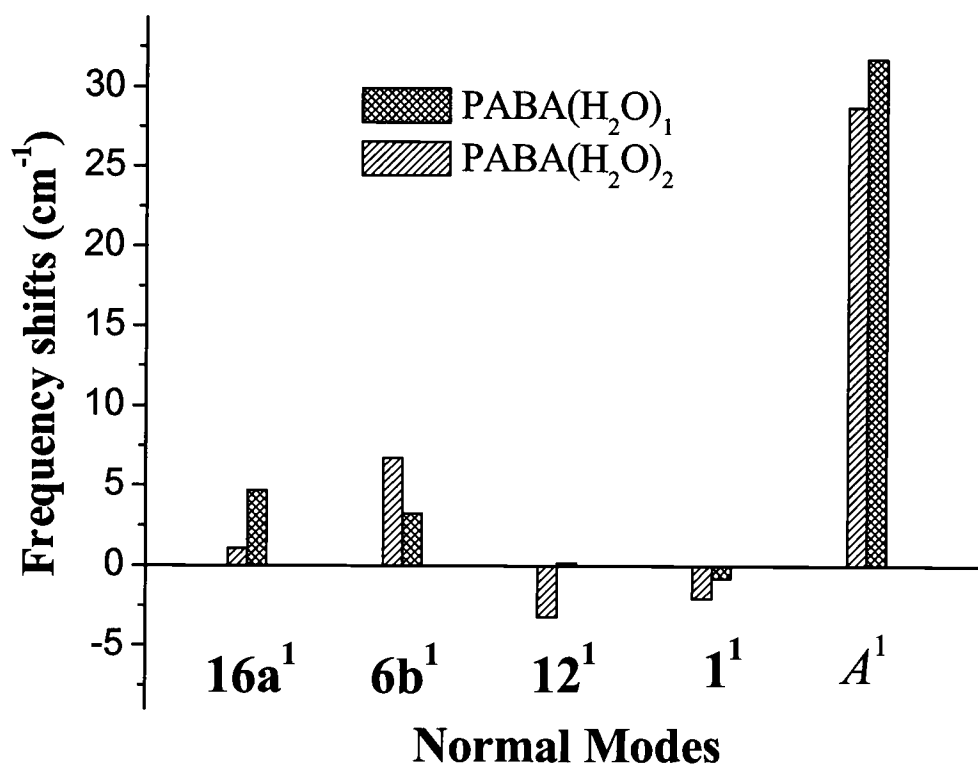


Figure 11.6 Frequency shifts of a few observed normal modes in PABA(H₂O)_n ($n = 1$ and 2) relative to the bare compound. The uncertainty in the shift of mode D for PABA(H₂O)₂ is $\sim 10 \text{ cm}^{-1}$ due to the unresolved broad feature, while the uncertainty for the rest of the values is 3 cm^{-1} .

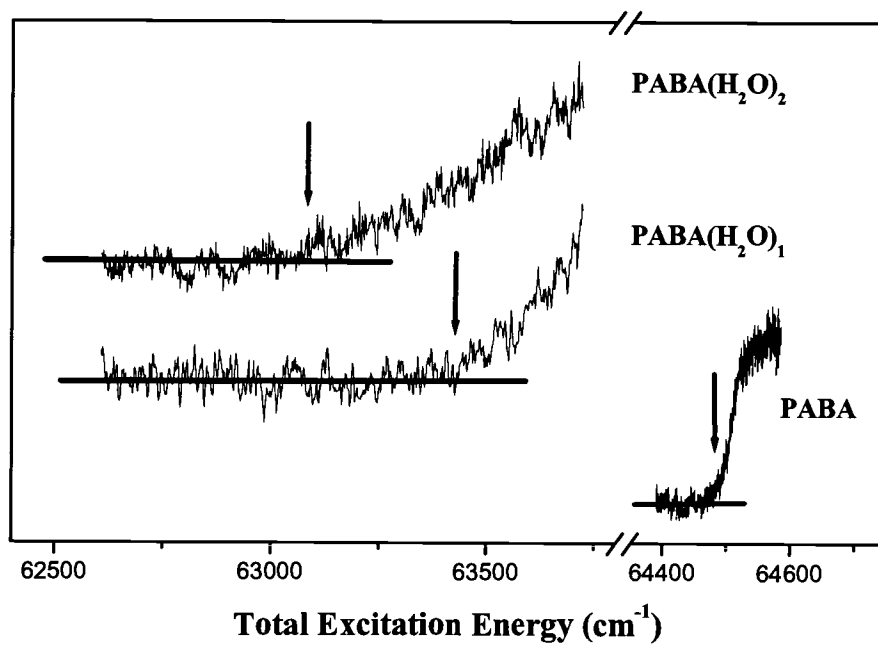


Figure 11.7 Two-color PIE spectra of jet-cooled PABA(H₂O)_n ($n = 0 - 2$). The IP values are marked by an arrow on each trace.

complexation. The in-plane bending motion of the -COOH moiety in mode B is frozen upon complexation. In mode C , the in-plane bending motion of the -NH_2 moiety extends to the water molecule(s) in the complex(es). Interestingly, the addition of the second water molecule to the 1:1 complex results in marginal changes in the vibrational frequency. This fact suggests that the second water molecule should be in close proximity to the first water molecule, exerting minimal disturbance to the molecular frame.

In order to determine the ionization potential, we have recorded the photoionization efficiency spectra for all three complexes in a two-color two-photon ionization experiment. Figure 7 shows the threshold portion of the PIE spectrum obtained by pumping to the origin of the S_1 state of each species and scanning the probe laser. The ionization potential has been obtained by linearly extrapolating the post-threshold portion to the baseline of the ion signal. Taking into account the field ionization effect in the ion collection region,²⁶ the threshold for bare PABA has been determined to be 8.001 eV, in good agreement with our own value obtained from a ZEKE experiment.¹⁶ In contrast to the sharp onset of ion signal at the threshold of bare PABA, ions with $n = 1$ and 2 have shallow slopes near the threshold, typical for water complexes of aromatic molecules. Using the same linear extrapolation method, the IPs for the 1:1 and the 1:2 complexes have been determined to be 7.871 eV and 7.823 eV respectively. Due to the shallow slopes around the ionization threshold in Figure 7, the uncertainty in these values is estimated to be 0.01 eV. The shallow slopes also indicate substantial geometry changes of the complex upon ionization. Limited by the signal-to-noise ratio and the small FC factors at the threshold, unfortunately, we were unsuccessful in recording the ZEKE spectrum of the complexes. The vibrational information from such an experiment would shed more light on the change in geometry upon ionization. On the other hand, the state selection offered in the first step of excitation has eliminated contributions from hot bands, the threshold obtained from the current extrapolation method is therefore of a higher precision compared with that from single photon ionization.

OABA(H₂O)₀₋₂

Figure 8 displays the two-color two-photon REMPI spectra of OABA(H₂O)₀₋₂ plotted with respect to the origin of bare OABA at 28594 cm⁻¹. These spectra are similar to those

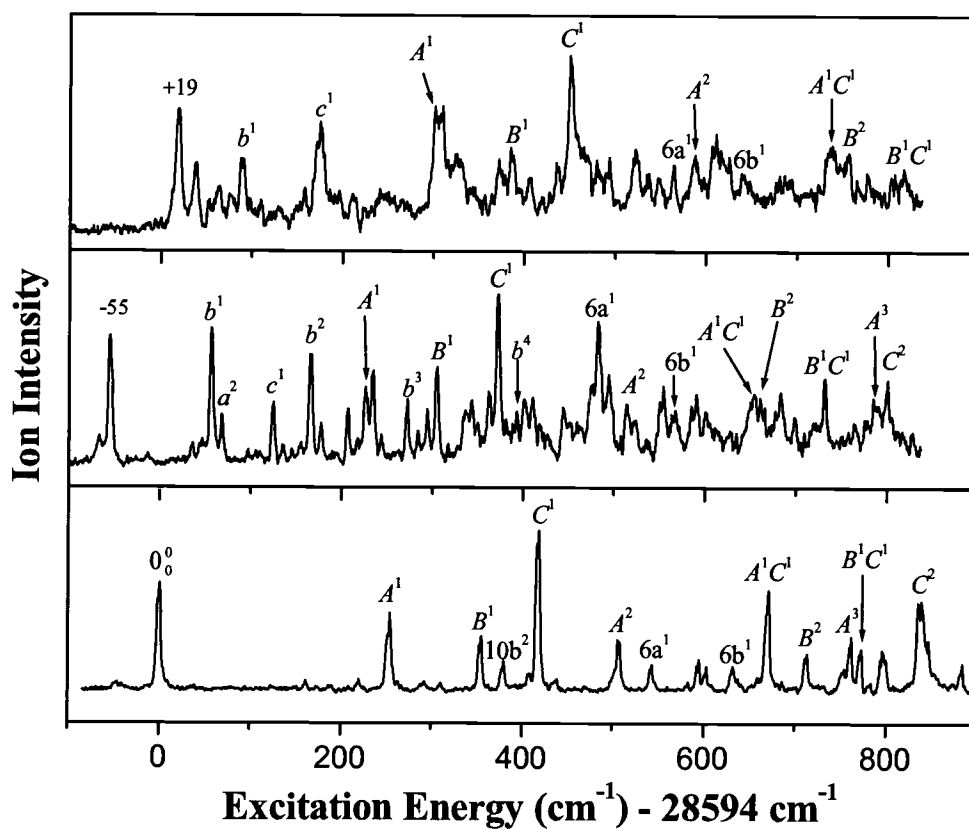


Figure 11.8 (1+1') REMPI spectrum of jet-cooled OABA(H₂O)_n (*n* = 0 - 2) plotted with respect to the origin of the S₁ ← S₀ transition of bare OABA at 28594 cm⁻¹.

reported by Stearns, *et al.*¹⁵ in terms of the shift in origin for both complexes and the distribution of active vibrational modes. In this work, we have extended the measurement more than 400 cm^{-1} beyond that reported by Stearns, *et al.*,¹⁵ and we have also attempted at a complete assignment of all the observed vibronic features for both complexes. In Figure 8, all three spectra demonstrate discrete narrow-band structures, and the similarities among them are marginal. Both observations indicate that the smaller complexes are not a product of dissociation from the larger complexes. The lowest energy transition for the 1:1 complex is red shifted by 55 cm^{-1} with respect to the bare molecule, and this band is assigned as the origin band. In contrast, a blue shift of 19 cm^{-1} is observed in the REMPI spectrum of the 1:2 complex. Using resonant ion-dip infrared spectroscopy,¹⁵ Stearns, *et al.* have established that there is only one dominant isomer in the 1:1 complex, thus a UV-UV hole burning experiment is deemed unnecessary. Although a small shoulder to the red edge of the origin band in trace b is observable in our spectrum, perhaps due to the higher temperature of our molecular beam compared with that of Stearns, *et al.*,¹⁵ given its low intensity and based on our experience with hole-burning spectroscopy in water complexes of MABA, a hole-burning experiment could, at best, only identify the existence of a minor isomer, with no vibrational information. For the 1:2 complex, both our calculation result on the binding energy difference among the possible isomers (Figure 4) and the assignment of the observed vibrational modes as listed in Table 2 imply the existence of only one isomer. Limited by the signal strength of the spectrum, we were unable to perform a hole-burning experiment to confirm this assumption.

A complete assignment of the observed vibronic transitions for all three species is listed in Table 2. Also listed in the table are our own calculations at the CIS/6-31G(d) level for the monomer and at the CIS/6-31G level for the water complexes. Due to the different levels of calculation, we have used different scaling factors: 0.95 for the bare molecule and 0.9 for the complexes. The same nomenclature as that applied for PABA(H₂O)₀₋₂ is used in this table. For the intramolecular modes, we use lower case alphabets in the order of increasing frequency for the 1:1 complex, and to make the comparison intuitive between the two complexes, we use the same name for those in the 1:2 complex if the displacement vectors are similar in the two complexes. Other observed intermolecular modes that are unique to the 1:2 complex are only listed in Table

Table 11.2. Observed vibrational frequencies and assignments for the S_1 state of OABA(H₂O)₀₋₂.

OABA		OABA(H ₂ O) ₁		OABA(H ₂ O) ₂		Assignment and approx. description [#]
Exp.	Calc. [§]	Exp.	Calc. *	Exp.	Calc. *	
				20	24	$\gamma(\text{H}_2\text{O-ring})$
				45	46	$\gamma(\text{H}_2\text{O-ring})$
		111	118	70	83	$b_0^1, \beta(\text{H}_2\text{O-ring})$
		123	112			$a_0^2, \gamma(\text{H}_2\text{O-ring})$
		180	180	156	171	$c_0^1, \nu(\text{H}_2\text{O-ring})$
220		210				$A_0^2, \text{C-COOH torsion}$
		221		139		b_0^2
		232				$a_0^2 b_0^1$
254	258	281	282	287	298	$B_0^1, \beta(-\text{COOH})$
		288				$b_0^1 c_0^1$
		299				$a_0^2 c_0^1$
				306		c_0^2
		328				b_0^3
		339	334			$16a_0^1, \gamma(\text{ring})$
		349				$a_0^2 b_0^2$
355	371	360	371	366	380	$C_0^1, \beta(-\text{NH}_2)$
		391		353		$b_0^1 B_0^1$
379	416	398	430	388	430	$10b_0^2, \gamma(\text{ring})$ and NH_2 wag
418	415	427	432	431	414	$D_0^1, \beta(-\text{NH}_2), \beta(-\text{COOH})$
		448				b_0^4
		466	467	475	481	$d_0^1, \beta(\text{H}_2\text{O-ring})$
		499				$b_0^2 B_0^1$

				503		$b_0^1 D_0^1$
				518		$c_0^1 C_0^1$
		549				$a_0^2 D_0^1$
506		569		569		B_0^2
544	560	537	548	546	548	$6a_0^1, \beta(\text{ring})$
595						$A_0^2 10b_0^2$
602	603	579	586	592	585	$16b_0^1, \gamma(\text{ring})$
		610				$b_0^3 B_0^1$
632	626	622	608	620	606	$6b_0^1, \beta(\text{ring})$
		646				$B_0^1 C_0^1$
		656				$b_0^2 D_0^1$
672		709		719		$B_0^1 D_0^1$
713		716		737		C_0^2
		738				$B_0^1 a_0^2 b_0^3$
		753				$b_0^3 D_0^1$
762		840				B_0^3
772		787		798		$C_0^1 D_0^1$
797		818				$B_0^1 6a_0^1$
884	875	831	842			$19a_0^1, \beta(\text{ring})$
839		856				D_0^2

§ The values include a scaling factor of 0.95.

* The values include a scaling factor of 0.9.

ν , β , and γ represent stretching, in-plane bending, and out-of-plane bending vibrations, respectively.

II. Our assignment is in overall agreement with that of Stearns, *et al.*,¹⁵ except for the in-plane bending mode *B* of the -COOH moiety. Stearns, *et al.* assigned the transition at 288 cm^{-1} in $\text{OABA}(\text{H}_2\text{O})_1$ as mode *B* based on its similar position and intensity as that of the monomer.¹⁵ We believe that this peak belongs to the combination of mode *b* and *c*. We assign the peak at 281 cm^{-1} as mode *B*, consistent with the value of 282 cm^{-1} from the CIS calculation. Moreover, this assignment makes it more reasonable to assign the transitions at 569 and 840 cm^{-1} to overtones of mode *B*, and peaks at 391 , 646 , 709 , and 818 cm^{-1} to its combination bands. It is worth noting that for both complexes, there are many more low frequency modes than listed in Table 2 based on our calculation. The two features at 20 and 46 cm^{-1} in the spectrum of the 1:2 complex are most likely out of plane intermolecular vibrations among the three constituents as listed in Table 2. Although indirect, this assignment of all the major features in the low frequency region of the spectrum further confirms the assumption that there are no other isomers in the molecular beam for the water complexes of OABA.

Unlike the REMPI spectra of PABA complexes shown in Figure 5, Figure 8 displays rich activities of intermolecular vibration for both the 1:1 and 1:2 complexes. In the spectrum of the 1:1 complex, a strong transition at 111 cm^{-1} is assigned as the in-plane bending mode *b*. This mode is so active that a clear vibrational progression with ν up to four is observable, where ν is the vibrational quantum number. Two other strong features at 123 cm^{-1} and 180 cm^{-1} are assigned as the out-of-plane bending mode *a* with $\Delta\nu = 2$ and the fundamental transition of a stretching mode *c*. Modes *b* and *c* are also observed for the 1:2 complex of OABA at 70 and 156 cm^{-1} respectively. The obvious shifts in both the intermolecular and the intramolecular vibrational modes among the three species further reinforce the assessment that the smaller complexes are not dissociative products of the larger complexes.

The shifts in frequency for some of the observed modes in the water complexes of OABA are displayed in Figure 9. Similar to the case of PABA, the ring deformation mode 6a changes by less than 10 cm^{-1} , while the in-plane bending mode *B* of the carboxyl group increases by $\sim 30\text{ cm}^{-1}$. The site of water addition should therefore be the carboxyl group, in excellent agreement with our theoretical predictions. Modes *C* and *D* involve collective motions of the whole molecular frame, and are therefore not as sensitive as mode *B* to the addition of water.

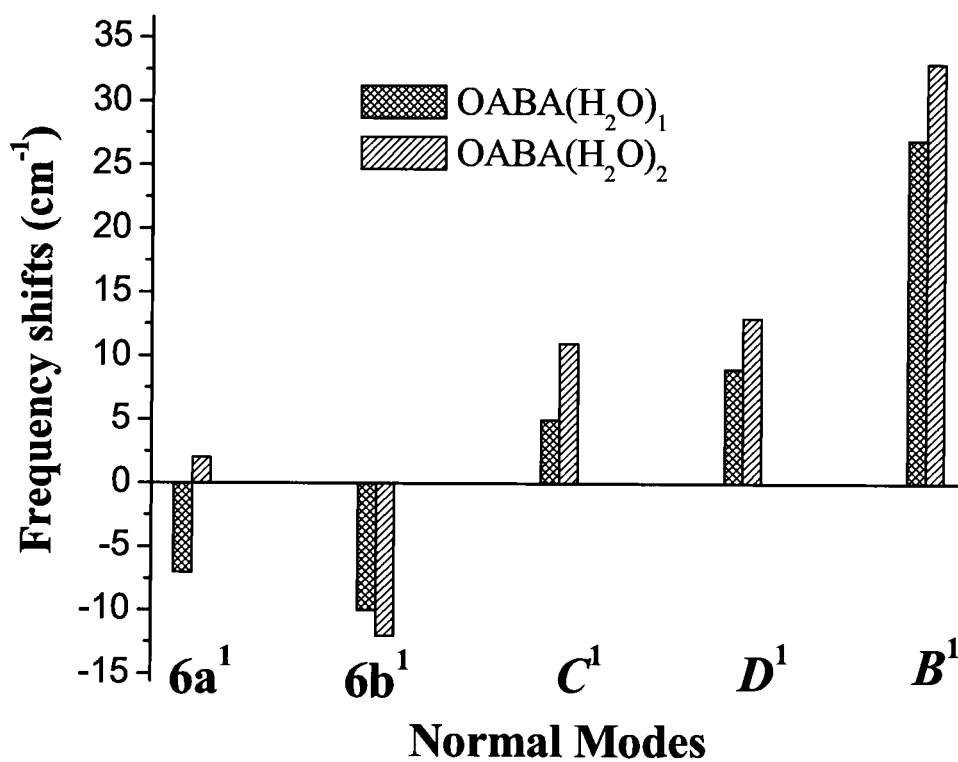


Figure 11.9 Frequency shifts of a few observed normal modes in OABA(H₂O)_n ($n = 1$ and 2) relative to the bare compound. The uncertainty for all the values is 3 cm⁻¹.

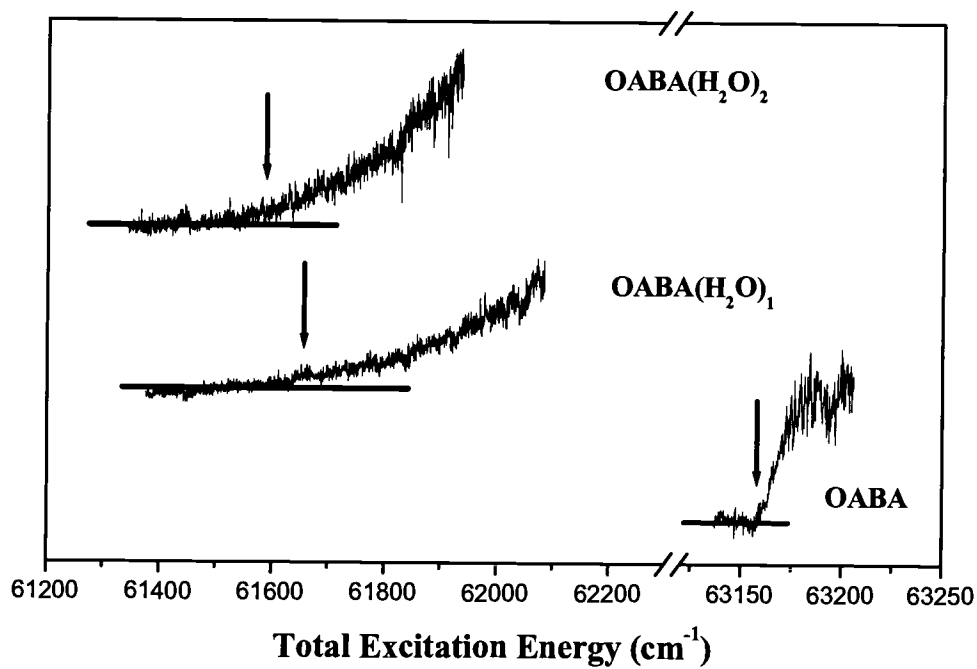


Figure 11.10 Two-color PIE spectra of jet-cooled OABA(H₂O)_n ($n = 0 - 2$). The IP values are marked by an arrow on each trace.

Figure 10 shows the threshold portion of the PIE spectra for all three species. The threshold for bare OABA has been determined to be 7.836 eV from this procedure, and this value is in good agreement with our own report from a ZEKE experiment.¹⁸ The IPs for the 1:1 and the 1:2 complexes have been determined to be 7.644 eV and 7.635 eV respectively. Similar to the situation of the water complexes of PABA, the onset of the ion signal for the water complexes of OABA is also quite slow with the increase of excitation energy.

11.5. Discussion

The above experimental and theoretical results provide a consistent picture with regard to the initial step of water solvation of aminobenzoic acids. All aminobenzoic acids can be viewed as electron “push-pull” molecules, and in the ground state, a fraction of the electron from the amino group is transferred to the carboxyl group. The lack of electrons on the amino group and the ready availability of extra electrons on the carboxyl group therefore result in an amphipathic behavior in both molecules. For MABA,¹⁹ due to the weaker electron induction effect in meta substitution, minor isomers in both the 1:1 and the 1:2 complexes were observed, while for PABA and OABA, our observation and that of Stearns, *et al.*¹⁵ both allude to the existence of only one isomer in all cases. We therefore conclude that it is the hydrogen-bond site on the carboxyl group that the water molecules prefer to occupy. The amino group loses out in the competition even with the availability of two water molecules.

Unique to OABA is the intramolecular hydrogen bond between the two substituents, and based on our results, this hydrogen bond has minimal effect on the water complexes. In the study of Stearns, *et al.*,¹⁵ the “free” NH stretching vibration in the S_1 state of $\text{OABA}(\text{H}_2\text{O})_1$ was the same as that of bare OABA. The authors thus concluded that water complexation exerts only a minor perturbation to the molecular frame. Our study is sensitive to the in-plane-bending mode C of the amino group, and based on Table 2, only a slight shift of this mode, on the order of 10 cm^{-1} , is observable. This result is in agreement with the study of Stearns, *et al.*¹⁵

One of the intriguing results from the above measurement is that except for the 1:1 complex of OABA, the 1:2 complex of OABA and both water complexes of PABA demonstrate blue shifts. The spectra of the water complexes of MABA, interestingly, all

Table 11.3. Calculated hydrogen bond lengths in the 1:1 complex of PABA and OABA upon electronic excitation.

	C=O...HO _w (Å)		O-H...OH _w (Å)	
	S ₀	S ₁	S ₀	S ₁
PABA(H ₂ O) ₁	1.914	2.018	1.803	1.942
OABA(H ₂ O) ₁	1.943	1.902	1.790	1.798

demonstrated sizable red shifts.¹⁹ These shifts reflect the difference of the ground and the excited state in water complexation. Typically, a blue shift implies a more tightly bond ground state than the excited state, and *verse versa*. It would thus be instructive to compare the geometry changes upon excitation. The location of the water molecules is the same for OABA and PABA in both water complexes. Table 3 lists the hydrogen bond lengths for the 1:1 complexes. Upon electronic excitation, the lengths for both hydrogen bonds $\text{C}=\text{O}\cdots\text{HO}_w$ and $\text{O}-\text{H}\cdots\text{O}_w$ *increase* in the 1:1 complex of PABA, implying a decrease in bond strength. In contrast, the bond length for $\text{C}=\text{O}\cdots\text{HO}_w$ *decreases* in $\text{OABA}(\text{H}_2\text{O})_1$, indicating a slight enhancement of the hydrogen bond. This additional stability in the S_1 state of $\text{OABA}(\text{H}_2\text{O})_1$ may be the reason for the red shift of the origin band. Unfortunately, the precision from our calculation on the binding energy is insufficient to confirm the above assessment with regard to the relative strength of the hydrogen bonding.

Another intriguing result is the missing intermolecular modes in the spectra of the water complexes of PABA in Figure 5. Based on our calculation, these modes should appear within 200 cm^{-1} above the origin band. Our initial suspicion is small Franck-Condon factors near the origin of the electronic transition, since upon excitation, one of the OH bond in water rotates into the plane of the aromatic ring. However, the existence of the large origin band dismisses this possibility. An opposite extreme is that there is no change in the displacement vector upon ionization from the S_1 state to the cationic state, and the only non-vanishing vibrational band is thus the origin band. It is interesting to note that our spectroscopic assignment of the water complexes of MABA did not reveal the existence of intermolecular vibrational modes either. The prevalence of the rich intermolecular features in the spectra of the water complexes of OABA is therefore unique to the ortho isomer.

11.6. Conclusion

Spectroscopic properties of the excited state of PABA and OABA water complexes have been studied using two-color resonantly enhanced multiphoton ionization spectroscopy. Structures and binding energies for several of the most possible isomers in the ground state have been explored based on DFT calculations. In all cases, only the most stable isomer exists in the supersonic molecular beam, and the intramolecular

hydrogen bond in OABA has minimal effect on water complexation. With the aid of *ab initio* calculations, vibrational modes of the S_1 state of the most stable complexes have been assigned, and a reasonable agreement between theory and experiment has been obtained. From the frequency shifts of some of the observed normal modes upon water addition, we conclude that it is the hydrogen-bond sites on the carboxyl group that the water molecules prefer to occupy. The ionization thresholds of both bare molecules and their water complexes have been determined, although with a larger uncertainty for the water complexes than for the bare molecules due to the shallow slop in the corresponding PIE spectra.

11.7. Acknowledgements

This work was supported by the National Science Foundation, Division of Chemistry. Acknowledgment is made to the Donors of The Petroleum Research Fund, administered by the American Chemical Society, for partial support of this research. Wei Kong is an Alfred P. Sloan research fellow.

11.8. References

1. Bernstein, E. R., *Atomic and Molecular Clusters*, Elsevier, Amsterdam, 1990.
2. G Jeffrey, G. A.; Saenger, W., *Hydrogen Bonding in Biological Structures*, Springer, Berlin, 1991.
3. Castleman, A. W., Jr.; Wei, S., *Annu. Rev. Phys. Chem.*, 1994, 45, 685-719.
4. Zwier, T. S., *Annu. Rev. Phys. Chem.*, 1996, 47, 205-241.
5. Wolfenden, R.; Snider, M. J., *Acc. Chem. Res.*, 2001, 34, 938-945.
6. Robertson, E. G.; Simons, J. P., *Phys. Chem. Chem. Phys.*, 2001, 3, 1-18.
7. Neusser, H. J.; Siglow, K., *Chem. Rev.*, 2000, 100, 3921-3942.
8. Brutschy, B., *Chem. Rev.*, 2000, 100, 3891-3920.
9. Jeffrey, G. A., *An Introduction to Hydrogen Bonding*, Oxford University Press, New York, 1997.
10. *Atomic and Molecular Beam Methods*, Volume 1, edited by Scoles, G., Oxford University Press, Inc., New York, 1988.
11. Turchilleo, R. F.; Lamy-Freund, M. T.; Hirata, I. Y.; Juliano, L.; Ito, A. S., *Biophys. Chem.*, 1998, 73, 217-225.
12. Ito, A. S.; Turchilleo, R. F.; Hirata, I. Y.; Cezari, M. H. S.; Meldal, M.; Juliano, L., *Biospectroscopy*, 1998, 4, 395-402.
13. Meijer, G.; de Vries, M. S.; Hunziker, H. E.; Wendt, H. R., *J. Chem. Phys.*, 1990, 92, 7625-7635.
14. Southern, C. A.; Levy, D. H.; Florio, G. M.; Longarte, A.; Zwier, T. S., *J. Phys. Chem. A*, 2003, 107, 4032-4040.
15. Stearns, J. A.; Das, A.; Zwier, T. S., *Phys. Chem. Chem. Phys.*, 2004, 6, 2605-2610.
16. He, Y.; Wu, C.; Kong, W., *J. Chem. Phys.*, 2004, 121, 3533-3539.

17. He, Y.; Wu, C.; Kong, W., *J. Chem. Phys.*, 2004, 121, 8321-8328.
18. Wu, C.; He, Y.; Kong, W., *Chem. Phys. Lett.*, 2004, 398, 351-356.
19. He, Y.; Wu, C.; Kong, W., *J. Phys. Chem. A* (in press, 2004).
20. He, Y.; Wu, C.; Kong, W., *J. Phys. Chem. A*, 2003, 107, 5145-5148.
21. He, Y.; Wu, C.; Kong, W., *J. Phys. Chem. A*, 2004, 108, 943-949.
22. GAUSSIAN 98, Revision A. 7, Frisch, M. J., et al., Gaussian, Inc., Pittsburgh, Pennsylvania, 1998.
23. GAUSSIAN 03, Revision A. 7, Frisch, M. J., et al., Gaussian, Inc., Pittsburgh, Pennsylvania, 2003.
24. Casida, M. E.; Jamorski, C.; Casida, K. C.; Sulahub, D. R., *J. Chem. Phys.*, 1998, 108, 4439-4449.
25. Varsanyi, G., *Assignment of Vibrational Spectra of Seven Hundred Benzene Derivatives*, Wiley, New York, 1974.
26. Duncan, M. A.; Dietz, T. G.; Smalley, R. E., *J. Chem. Phys.*, 1981, 75, 2118-2125.

**Observing microsolvation by adding one water molecule at a time:
Electronic spectroscopy of water complexes of *p*-aminobenzoic acid**

Yonggang He, Chengyin Wu, and Wei Kong*

*Department of Chemistry, Oregon State University,
Corvallis, Oregon 97331-4003*

2005, to be submitted.

* Corresponding author, email: wei.kong@oregonstate.edu, fax: 541-737-2062

12. Observing microsolvation by adding one water molecule at a time: Electronic spectroscopy of water complexes of *p*-aminobenzoic acid

12.1. Abstract

The solvation mechanism of *p*-aminobenzoic acid is investigated based on vibrational analysis of the first electronically excited state of the neutral complex and the shift of ionization thresholds with increasing water content. A large change in the vibrational frequency of the carboxylic group upon water addition alludes to the site of water addition. The similarity of the observed vibrational modes implies the formation of a water cluster attached to the carboxylic group. The gradual decrease of ionization thresholds with water addition suggests that the eventual closure of the solvation shell is unidirectional, and that the amino group remains on the surface of the complex even with forty surrounding molecules.

12.2. Introduction

The microscopic process of solvation has captured the fascination of scientists for decades (1 - 4). In the solution phase, thermodynamics can explain the chemical composition of a steady state at equilibrium, and kinetics theory can predict the relaxation process when deviated from equilibrium. In the gas phase, spectroscopy provides an insightful look at the ensemble average of isolated species, being either the solute or the solvent. Studies of complexes of atoms or molecules with solvent molecules provide the bridge between the two limits. In particular, observations on the change in physical and chemical properties of the solute as a function of the number of solvent molecules can provide the ultimate information for this linkage. Since the first experiment on ion solvation in water complexes using high pressure mass spectrometry (5), experimental techniques, both in terms of cluster generation and spectroscopic detection, have been greatly improved. Molecular beam technology has proven an efficient way to prepare cold, isolated complexes of different sizes (4, 6 - 11). As a result, solvation of atomic species, such as alkali metal atoms (6, 7), halogen anions (8 - 10), or electrons (4, 11), have been reported. The generation of neutral complexes involving medium sized species, such as heteroaromatic and benzene derivatives, is still technically challenging (12). Attachment of rare gas atoms or water molecules has been limited to just a few solvent molecules, thus the scope of these investigations is far from the regime of bulk phase solution. On the other hand, the solvation of medium sized species is particularly important in biological reactions (13 - 16). The effect of water on the chemical and physical properties of nucleic acids and amino acids has proven critical in our understanding of molecular evolution (17 - 19).

In this work, we investigate the microsolvation mechanism of *p*-aminobenzoic acid (PABA) in water. The biological activities of PABA range from sulfanilamide antimetabolite to photodegradation inhibitor (20). From a chemistry point of view, it is an electron "push-pull" species with a donor (-NH₂) and an acceptor (-COOH) connected by a π -ring. In protic solvents, both groups can act as proton donors and acceptors simultaneously, and the π electrons on the aromatic ring can also form a hydrogen bond with a proton donor. The existence of multiple hydrogen bonding sites makes PABA a fascinating model for studies of interactions between water and aromatic species.

Our investigation method is electronic spectroscopy, including vibrational mode analysis of the first excited electronic state (S_1) and size dependence of ionization thresholds to the ground cationic state (D_0) of the complexes. Using two lasers in a two-color resonantly enhanced multiphoton ionization (REMPI) experiment, we can derive information on the existence of structural isomers and their geometry. This can be achieved by scanning the resonant laser and fixing the ionization laser high above the ionization threshold. For complexes that are too large to provide this type of information, we look into the ionization thresholds using two-photon ionization. This is achieved by fixing the resonant laser to an intermediate state and scanning the ionization laser for the appearance energy of the threshold ions or electrons. All experiments were performed using a standard molecular beam machine with a time of flight mass spectrometer (TOF-MS) and a pulsed valve heated to 140°C. Water complexes were generated by seeding the heated vapor of PABA in a mixture of room temperature water vapor and argon gas at a stagnation pressure of 3 atm. The size range of this study is $n = 0 - 40$, where n represents the number of water molecules in a PABA complex. Evidence from our experimental results suggests that this range is large enough to reach the regime of macroscopic water droplets.

12.3. Results

12.3.1. REMPI spectroscopy

Figure 1 shows the REMPI spectra of the water complexes of PABA with $n = 0 - 6$. Details of the spectroscopic assignment will be published elsewhere (21). Except for the in plane twist modes ($ip\beta$) of the carboxylic acid group, the rest of the observed vibrational modes are related to in-plane ring deformation. All seven spectra in Figure 1 look similar, and the addition of water molecules does not seem to have changed the distribution of the observed vibrational modes. This result implies that the addition of water molecules exerts minimal disturbance to the molecular frame of PABA.

The origin band demonstrates frequency shifts and shape changes, and transitions to excited vibrational levels are also shifted in frequency and broadened in linewidth. These signatures are telltales of the microsolvation mechanism. The shifts in frequency for the observed modes in complexes with $n \leq 2$ are illustrated in Figure 3. While the ring

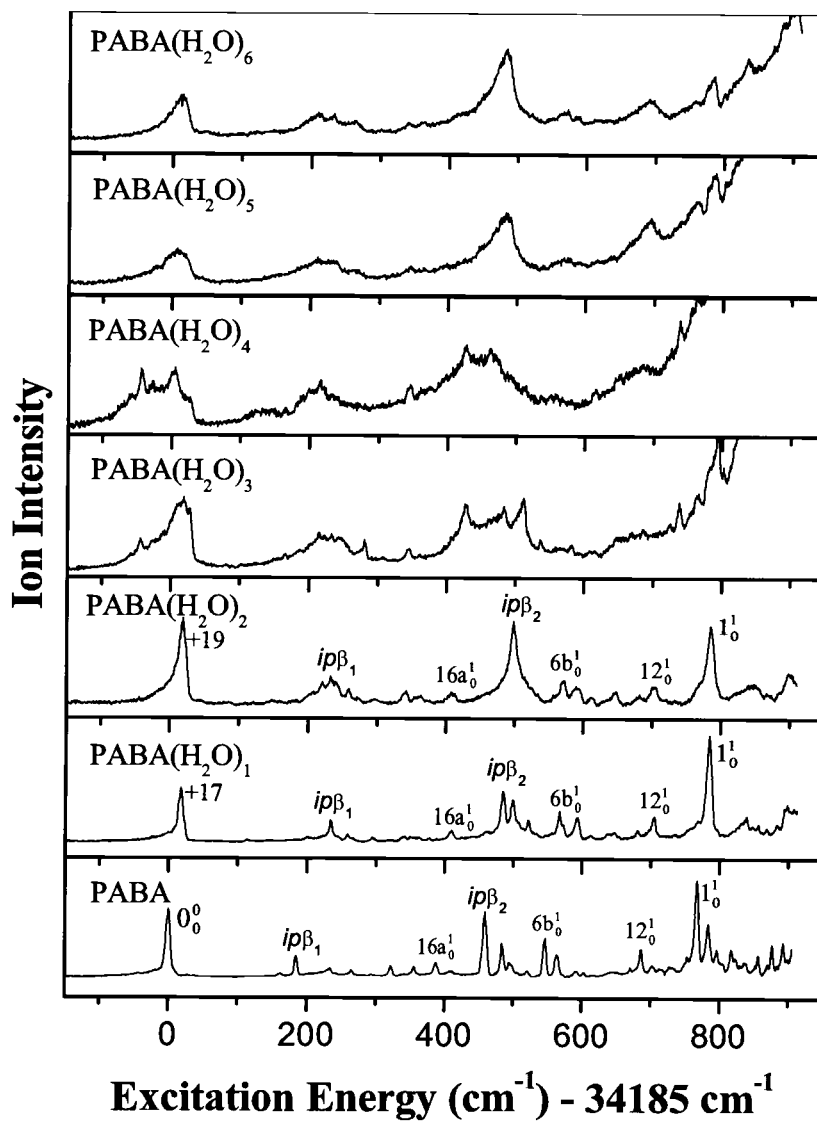


Figure 12.1. REMPI spectra of PABA•water complexes.

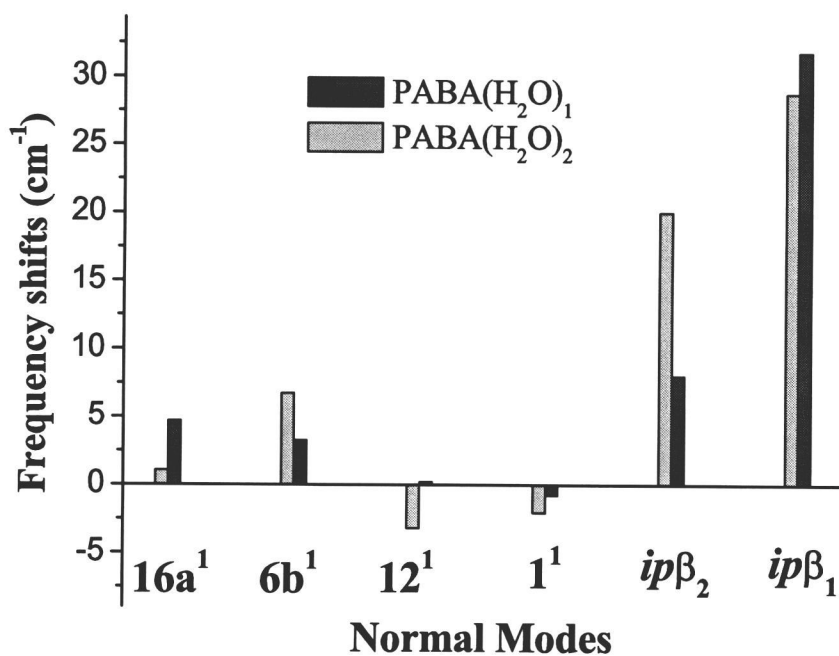


Figure 12.2. Frequency shifts of a few observed normal modes in $\text{PABA}(\text{H}_2\text{O})_n$ ($n = 1$ and 2) complexes. The uncertainty in the shift of the $ip\beta_2$ mode for $\text{PABA}(\text{H}_2\text{O})_2$ is $\sim 10 \text{ cm}^{-1}$ due to the unresolved broad feature, while the uncertainty for the rest of the values is 3 cm^{-1} .

deformation modes change by less than 10 cm^{-1} , the twist mode $ip\beta_1$ of the carboxylic acid group increase by $\sim 30\text{ cm}^{-1}$. The site of addition of the water molecules should therefore be the carboxylic acid group for $n = 1$ and 2. This deduction is in line with our intuition since the acidic group is hydrophilic, and therefore intermolecular hydrogen bonds are easily formed. It also fits in the picture of this "push-pull" molecule: since the amino group acts as an electron donor within the molecular frame of PABA, its ability to form intermolecular hydrogen bonds with water is weakened. Yang, *et al.* reported even-odd alternation in the changes of the adiabatic electron detachment energy with in water complexes of *p*-benzene-dicarboxylate and suberate dianions (22). The authors attributed this phenomenon to alternative solvation of the two carboxylic groups. Replacing one of the carboxylic groups with an amino group in our experiment eliminates the even-odd alternation. The amino group on PABA loses out to the carboxylic group in the competition. It is worth noting that mode $ip\beta_2$ involves a collective motion of the whole molecular frame, including twist of the amino group. This mode is therefore not particularly sensitive to the addition of water. Moreover, for $\text{PABA}(\text{H}_2\text{O})_2$, this mode cannot be resolved from a nearby vibration (not assigned in Figure 1), and the plotted shift for this mode has a large uncertainty.

Figure 1 provides the basic road map of microsolvation in PABA: the addition of water molecules is initiated at the carboxylic acid group, and further growth of the water complex is also centered on the same site. In other words, the intermolecular hydrogen bonds among water molecules supercede the intermolecular bonds between PABA and water. The $\text{PABA}\cdot\text{water}$ complex is thus initially a surface cluster, in contrast to an interior cluster where the solvent molecules maximize the contact with the solute molecule (23). This structure of $\text{PABA}\cdot\text{water}$ is similar to that proposed for the sodium $\cdot\text{water}$ (24) and halogen anion $\cdot\text{water}$ complexes (25), except for $\text{F}^-\cdot\text{water}$ (26), which is known to have an interior structure. It is interesting to notice that PABA has a bulky frame and contains multiple functional groups, yet its solvation in water is similar to that of a small compact sodium atom.

The uniqueness of the above mechanism can be tested from the distribution of energetically accessible isomers. In our experimental setup, the water complexes were formed during supersonic expansion. The temperature of the pulsed valve was 140°C ,

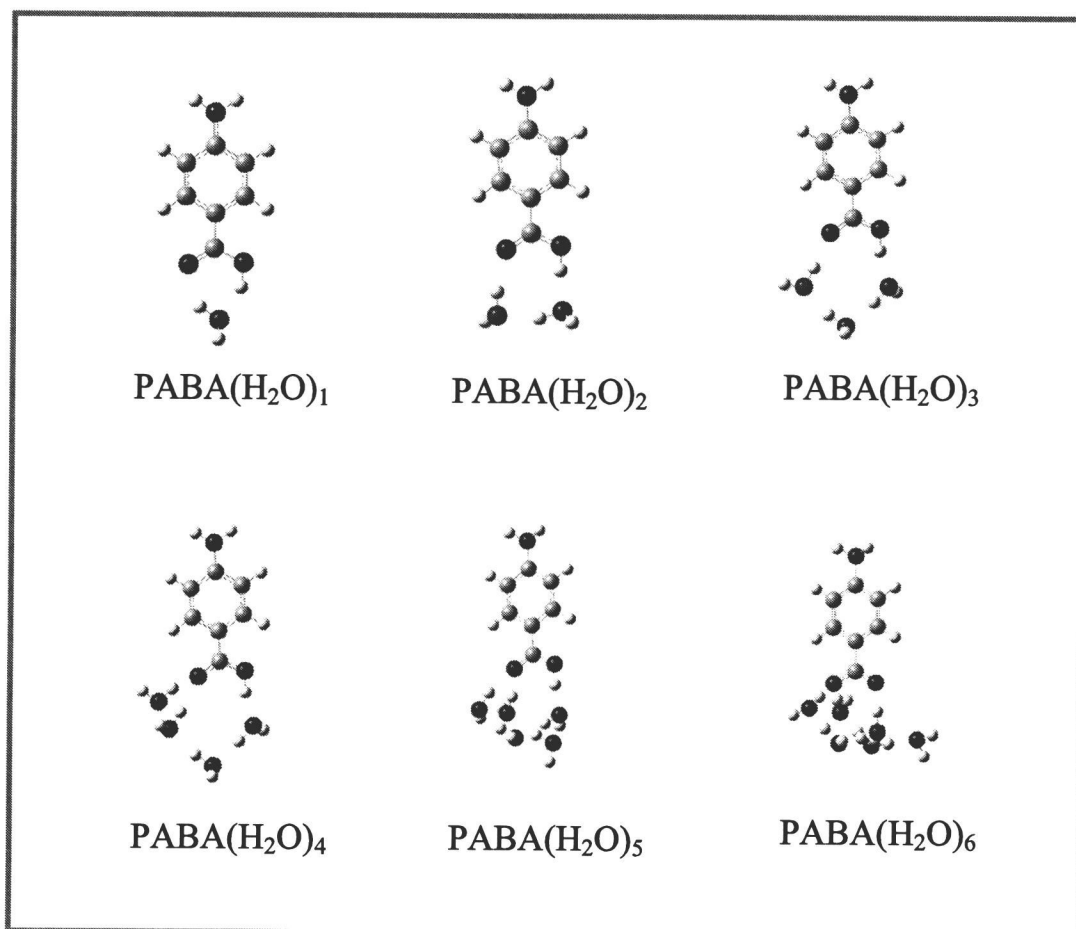


Figure 12.3. The most stable structures of PABA(H₂O)_n ($n = 1 - 6$) complexes obtained from our density functional calculation at the B3LYP/6-31g* level.

and the temperature of the complexes should be around 50 - 100 K. Energetically accessible isomers are therefore limited to those within 300 cm^{-1} (40 meV) above the most stable structure. The origin band for complexes with $n \leq 2$ bears no fine structures, albeit slightly asymmetric in lineshape, while for $n > 2$, two or more closely spaced bands overlap. We performed *ab initio* calculations on the HF/6-31g* level and density functional calculations on the B3LYP/6-31g* level to search for stable ground state structures of these water complexes. Limited by our computer resources, it was only practical to investigate complexes with $n \leq 6$. Figure 3 shows the most stable structures obtained from our calculation. In agreement with the experimental observation, for clusters with $n \leq 2$, essentially no other energetically competitive isomers are obtained. The isomers with a water molecule hydrogen bonded to the amino group is $2000\text{-}3000\text{ cm}^{-1}$ higher in energy than those in Figure 3. Moreover, our calculation further reveals that among the isomers with $n = 3$ and 4, all the water molecules are located in the proximity of the carboxylic acid group, and the isomeric structures only reflect the different ways of forming intermolecular hydrogen bonds among the water molecules. It is only at $n = 6$ that the amino group shows some probability of hydrogen bonding with the surrounding water molecules, with an energy cost of 700 cm^{-1} .

Based on this result, we further propose that the closure of the solvation shell is unidirectional, i.e., the “polar cap” from the carboxylic side would eventually engulf the whole molecule. In contrast, a bidirectional process would require the formation of a second polar cap around the opposite amino group, and eventually the two caps would merge to form a closed shell. Based on Figure 1, the water-water hydrogen bond dwarfs the intermolecular hydrogen bond between the carboxylic group and water, so the possibility of forming the initial amino-water hydrogen bond would be extremely low.

A missing piece of spectroscopic information from Figure 1 is the intermolecular vibration between a water molecule and PABA, particularly for the $\text{PABA}(\text{H}_2\text{O})_1$ complex. Based on our calculation, this transition should occur between the origin band and the first observed intramolecular vibrational mode of PABA at 185 cm^{-1} . However, after an extensive search, we failed to locate this vibrational mode. Our tentative explanation is that this mode is highly disfavored by the Franck-Condon factor during the

electronic transition: in the ground state, the water molecule is in the plane of the benzene ring, while in the S_1 state, one of the OH bonds swings out of the plane.

12.3.2. Photoionization spectroscopy

Figure 4 shows the time of flight mass spectra of PABA(H_2O) $_n$ ($n = 0 - 40$) complexes at six different photon energies. Based on the dependence of the signal strength on the power of the excitation laser, the nature of the process was confirmed to be non-resonant coherent two photon ionization. For complexes with $n < 20$, smaller ions disappear faster than larger ions with the decreasing photon energy. This fact indicates that the ionization thresholds of PABA(H_2O) $_n$ from $n = 0$ to $n \approx 20$ decrease monotonically with the number of attached solvent molecules. However, for complexes with $n > 20$, the mass spectra show a uniform drop of all sized ions with the decreasing photon energy. This observation suggests that complexes with $n > 20$ have essentially one common ionization threshold, independent of the number of solvent molecules.

In order to determine the ionization potential, we recorded the photoionization efficiency spectra (PIE) for a few size selected complexes. By linearly extrapolating the post-threshold portion to the baseline of the ion signal, and taking into account the field ionization effect in the ion collection region, we obtained a value of 8.001 eV for the threshold of bare PABA molecules. This result is in good agreement with our own report based on a zero kinetic energy photoelectron spectroscopy (ZEKE) experiment (27). Hydration by a single water molecule reduces the threshold by about 0.13 eV. Addition of more water molecules decreases the threshold further but by a smaller magnitude. When the number of attached water molecules reaches 20, the ionization threshold approaches a constant value of 7.754 eV, about 0.25 eV lower than that of a bare molecule.

Figure 5 shows the dependence of the ionization thresholds on the number of solvent molecules. As far as the ionization threshold is concerned, the complex reaches bulk phase property with twenty surrounding water molecules. The smooth drop in the ionization threshold with increasing water content for $n < 20$ indicates a unidirectional closure process for the solvation shell. If another polar cap were formed around the amino group, we would expect some discontinuity in the change of the ionization

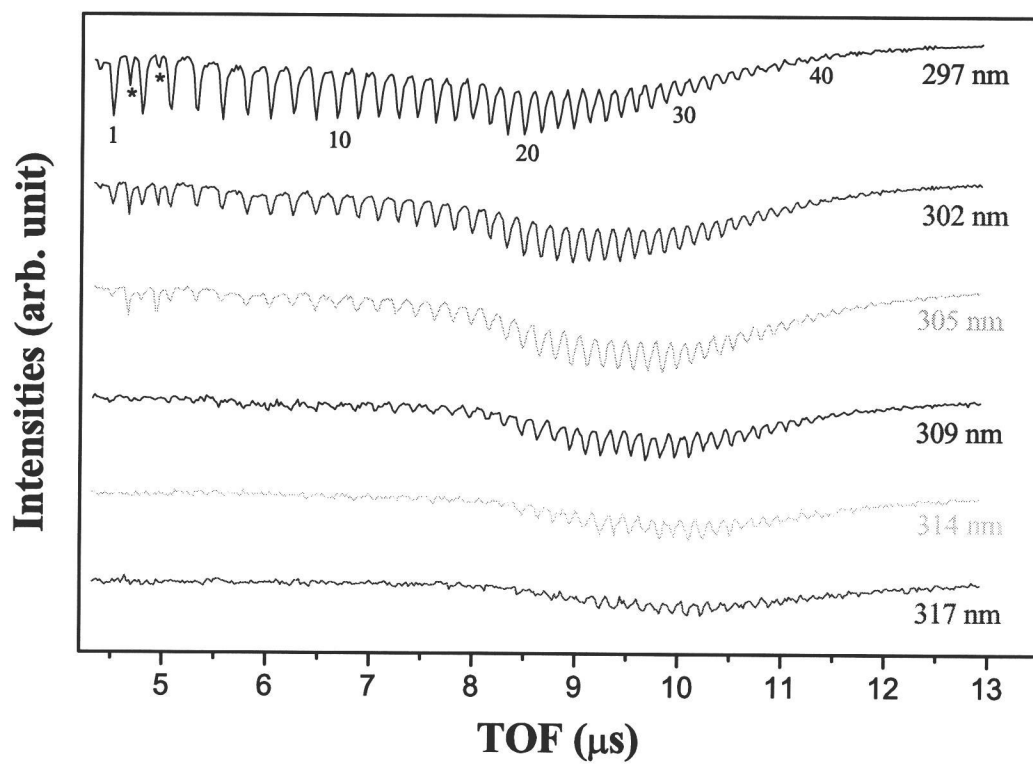


Figure 12.4. Time-of-flight mass spectra of PABA(H₂O)_n ($n = 0 - 40$) at six different excitation wavelengths. The peaks marked “*” are fragments from dissociation of large clusters.

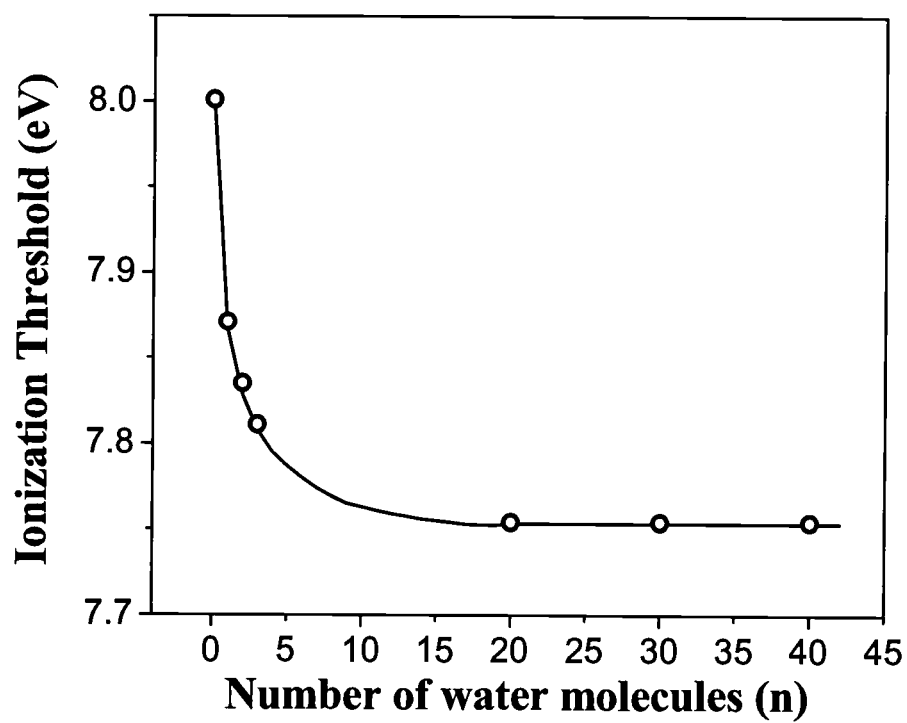


Figure 12.5. Ionization thresholds of PABA•water complexes.

threshold when the first water molecule attached to the amino group. Given the limitation of the data, however, we mention this latter point with caution.

12.4. Discussion

The experimental results on vibrational spectroscopy of the first excited electronic state and on the ionization threshold provide information on the formation, growth, and asymptotic behavior of PABA•water complexes. The initiation step is similar to that of sodium (24) and halogen anion (25) where the solute molecule is located on the outside of the solvent cluster. At first sight, this conclusion may seem difficult to comprehend. However, in this “push-pull” molecule, a fraction of the electron from the amino group is transferred to the carboxylic group. According to Mulliken population analysis, the amino group has a positive charge of +0.108 and the carboxylic group has a negative charge of -0.121 in the ground state. The lack of electrons on the amino group and the ready availability of extra electrons on the carboxylic group therefore result in an amphipathic behavior of PABA. It would be interesting to measure the surface structure of water solutions of PABA, since based on this assessment, we would predict that the amino group should be on the surface of the liquid-vacuum interface. In the work of Wang, *et al.* on hydrated sulfate and oxalate anions, the authors reported that once the surrounding water molecules reached nanometer size, emission of photoelectron from the solute disappeared due to solvent entrapment (28). In our case, photoionization occurs even with 40 surrounding water molecules. This fact further supports the surface structure of PABA•water complexes.

It is known for anions that the detachment energy should be linearly dependent on the reverse of the radius of the cluster (29). Extrapolation of this straight line should yield the ionization energy of the solute in the bulk medium. In the case of PABA, the availability of experimental points is limited, but it is clear from Figure 5 that the bulk limit should be 7.75 eV, since no change in the ionization energy is observable for $n > 20$. This value is substantially lower than the ionization energy of pure water, which is known to be 10.06 eV (28). This comparison further confirms the surface structure of PABA•water complexes, since the ejection of a photoelectron should be limited to a surface component of the droplet.

The stability of zwitterions in the gas phase has been a fascinating issue (30 - 33). Although we believe that with more than twenty surrounding water molecules, a full solvation shell is complete, the species in our system is still not zwitterionic. The equilibrium constant between the zwitterion and the neutral species is 0.09 at room temperature for PABA in a pure water solution (34), thus even in the bulk solution, the solute exists mostly as a neutral species. In fact, the concentration of the neutral species amounts to 0.82 in mole fraction. Contributions from protonated and deprotonated PABA are therefore also negligible.

In summary, this experiment provides hints on the microsolvation process of PABA in water. The shifts in the observed vibrational frequencies of the S_1 state for $n = 1$ and 2 provide the evidence that solvation in water begins with the carboxylic group. The similarity among all the REMPI spectra with $n \leq 6$ further suggests that addition of more water molecules simply expands the water cluster within the complex, without a major modification of the PABA molecular frame. The smooth drop in the ionization threshold with increasing solvent molecules further demonstrates that closure of the solvation shell is unidirectional. When there are more than twenty solvent molecules in the vicinity, the ionization threshold of the complexes approaches the value of the corresponding liquid solution.

12.5. References and Notes

- 1 H. Ohtaki, T. Radnai, *Chem. Rev.* **93**, 1157 (1993).
- 2 N. Nandi, K. Bhattacharyya, B. Bagchi, *Chem. Rev.* **100**, 2013 (2000).
- 3 Q. Zhong, A. W., Jr. Castleman, *Chem. Rev.* **100**, 4039 (2000).
- 4 J. V. Coe, *Int. Rev. Phys. Chem.* **20**, 33 (2001).
- 5 P. Kebarle, *Annu. Rev. Phys. Chem.* **28**, 445 (1977).
- 6 I. V. Hertel, C. Hüglin, C. Nitsch, C. P. Schulz, *Phys. Rev. Lett.* **67**, 1767 (1991).
- 7 R. Takasu, F. Misaizu, K. Hashimoto, K. Fuke, *J. Phys. Chem. A* **101**, 3078 (1997).
- 8 G. Markovich, S. Pollack, R. Giniger, O. Cheshnovsky, *J. Chem. Phys.* **101**, 9344 (1994).
- 9 P. Ayotte, G. H. Weddle, M. A. Johnson, *J. Chem. Phys.* **110**, 7129 (1999).

- 10 L. Lehr, M. T. Zanni, C. Frischkorn, R. Weinkauff, D. M. Neumark, *Science* **284**, 635 (1999).
- 11 K. H. Bowen, H. Haberland, in *Solvated Electron Clusters*, edited by H. Haberland (Springer-Verlag, Berlin, 1995).
- 12 H. J. Neusser, K. Siglow, *Chem. Rev.* **100**, 3921 (2000).
- 13 C. Desfrancois, S. Carles, J. P. Schermann, *Chem. Rev.* **100**, 3943 (2000).
- 14 M. Orozco, F. J. Luque, *Chem. Rev.* **100**, 4187 (2000).
- 15 T. S. Zwier, *J. Phys. Chem. A* **105**, 8827 (2001).
- 16 S. K. Pal, A. H. Zewail, *Chem. Rev.* **104**, 2099 (2004).
- 17 R. Weinkauff, J.-P. Schermann, M. S. de Vries, K. Kleinermanns, *Z. Phys. D: At., Mol. Clusters* **20**, 309 (2002).
- 18 Y. He, C. Wu, W. Kong, *J. Phys. Chem. A* **108**, 943 (2004).
- 19 C. E. Crespo-Hernandez, B. Cohen, P. M. Hare, B. Kohler, *Chem. Rev.* **104**, 1977 (2004).
- 20 A. Kluczyk, T. Popek, T. Kiyota, P. de Macedo, P. Stefanowicz, C. Lazar, and Y. Konishi, *Curr. Med. Chem.* **9**, 1871 (2002).
- 21 Y. He, C. Wu, W. Kong, *J. Chem. Phys.* (Manuscript in preparation, 2004).
- 22 X. Yang, Y.-J. Fu, X.-B. Wang, P. Slaviček, M. Mucha, P. Jungwirth, and L.-S. Wang, *J. Am. Chem. Soc.* **126**, 876 (2004).
- 23 K. Hashimoto, K. Morokuma, *J. Am. Chem. Soc.* **117**, 4151 (1995).
- 24 K. Hashimoto, K. Morokuma, *J. Am. Chem. Soc.* **116**, 11436 (1994).
- 25 L. Perera, M. L. Berkowitz, *J. Chem. Phys.* **99**, 4222 (1993).
- 26 L. Perera, M. L. Berkowitz, *J. Chem. Phys.* **100**, 3085 (1994).
- 27 Y. He, C. Wu, W. Kong, *J. Chem. Phys.* (In press, 2004).
- 28 X.-B. Wang, X. Yang, J. B. Nicholas, L.-S. Wang, *Science* **294**, 1322 (2001).
- 29 R. N. Barnett, U. Landman, C. L. Cleveland, J. Jortner, *Chem. Phys. Lett.* **145**, 382 (1988).
- 30 W. D. Price, R. A. Jockusch, E. R. Williams, *J. Am. Chem. Soc.* **119**, 11988 (1997).
- 31 C. J. Chapo, J. B., Paul, R. A. Provencal, K. Roth, R. J. Saykally, *J. Am. Chem. Soc.* **20**, 12956 (1998).
- 32 R. R. Julian, R. Hodyss, J. L. Beauchamp, *J. Am. Chem. Soc.* **123**, 3577 (2001).

- 33 X.-B. Wang, J. E. Dacres, X. Yang, L. Lis, V. M. Bedell, L.-S. Wang, S. R. Kass, *J. Am. Chem. Soc.* **125**, 6814 (2003).
- 34 J. J. Christensen, D. P. Wrathall, R. M. Izatt, D. O. Tolman, *J. Phys. Chem.* **71**, 3001 (1967).
- 35 We thank Dr. J. V. Coe and Dr. L.-S. Wang for valuable discussions. This work was supported by the National Science Foundation, Division of Chemistry.
- Acknowledgment is made to the Donors of The Petroleum Research Fund, administered by the American Chemical Society, for partial support of this research.
- Wei Kong is an Alfred P. Sloan research fellow.

13. Concluding Remarks and Future Work

13.1 Summary

Using a variety of multiphoton techniques, we have investigated the structural stability of substituted aromatic systems, the cage adamenzane system, and fused ring systems. We have also obtained decay mechanisms of the unstable system of pyrimidine bases. Our work demonstrates that although for many large molecular systems, the information content in a spectroscopic investigation is limited, useful dynamical information can be derived, and a general conclusion with regard to the photochemical and photophysical behaviors of a series of compounds can be obtained.

Although gas phase investigations are related to isolated system, from the progressive formation of water complexes of solute molecules, we have obtained spectroscopic information about the interaction between the solute and solvent molecules. Our observations on the changes of physical and chemical properties as a function of the number of solvent molecules have also provided a way to bridge our observation from the gas phase to the solution phase.

13.2 Future Work

Vaporization via direct heating is limited to thermally stable species, while many biomolecules are thermally labile. Recently, laser desorption (LD) has been used to circumvent this problem.^{1,2} When combined with jet cooling, it can be used to obtain both mass and energy information of complex molecules with extremely low vapor pressures.

A laser desorption source is currently under construction in our laboratory. So far, we have finished some preliminary work and proved the feasibility of the new design. Data from the testing experiment are shown in Figures 1 and 2. These two figures display one-color two-photon REMPI spectra of laser desorbed jet-cooled guanine and *p*-amino benzoic acid (PABA) respectively. Although calibration of vibrational temperature has not been performed yet, the sharp vibrational structures in the figures indicate that

sufficient cooling has been achieved. In addition, the weak hot band in Figure 2 further indicates that the vibrational temperature of the molecular beam is lower than 30 K.³

Further improvements including the shot-to-shot stability and effective supersonic cooling are needed to achieve better spectroscopic sensitivity and resolution. Our ultimate goal is to combine the versatile laser-desorption source with our REMPI and ZEKE spectrometer to investigate photophysics of relatively large biologically relevant species, such as polynucleotides and polypeptides.

13.3 References

- ¹ Nir, E., Brauer, B., Grace, L., and de Vries, M. 1999, *J. Am. Chem. Soc.* 121, 4896.
- ² Mons, M., Dimicoli, I., Piuze, F., Tardivel, B., and Elhanine, M. 2002, *J. Phys. Chem. A* 106, 5088.
- ³ G. Meijer, M. S. de Vries, H. E. Hunziker, and H. R. Wendt, *J. Chem. Phys.* **92**, 7625 (1990).

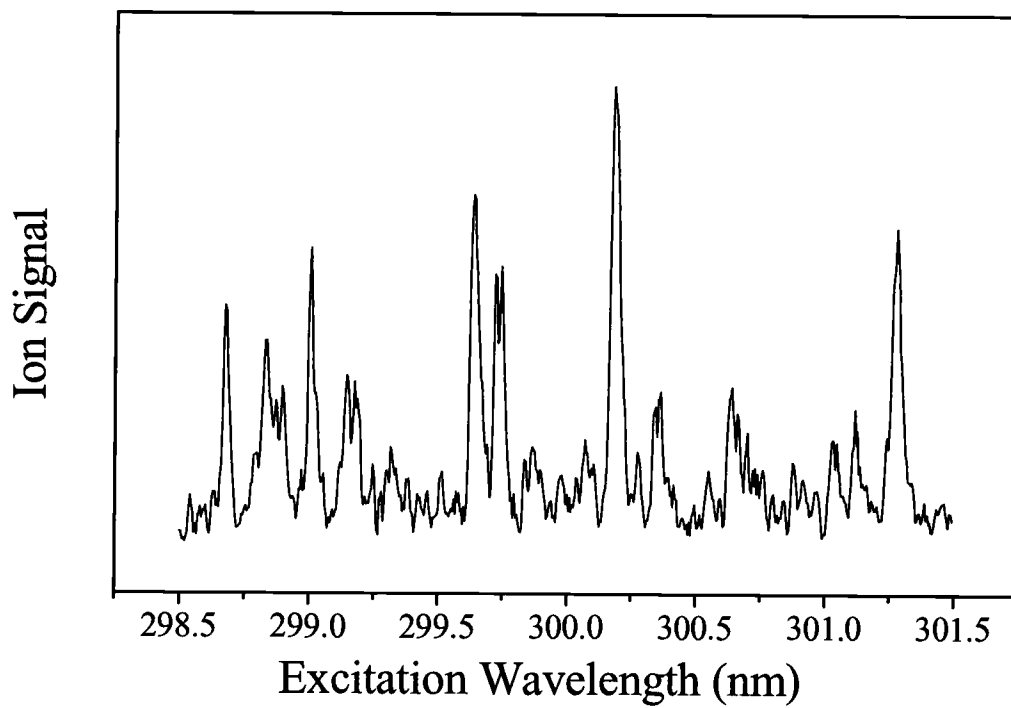


Figure 13.1. 1+1 REMPI spectrum of laser-desorbed and jet-cooled guanine.

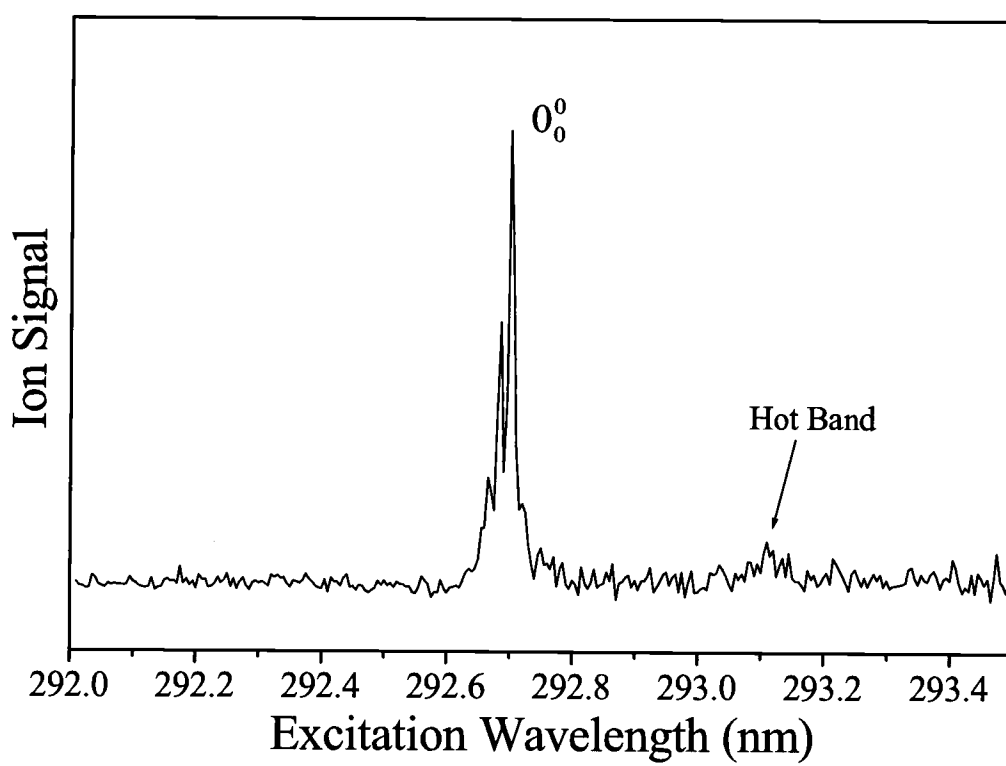


Figure 13.2. 1+1 REMPI spectrum of laser-desorbed and jet-cooled PABA near the origin of the S_1 state.